Experiments to Understand the Impact of Local and Global Slenderness on the Inelastic Deformation Capacity of Square and Round HSS Braces

Lily Ana Swanson

A thesis

submitted in partial fulfillment of the

requirements for the degree of

Master of Science in Civil Engineering

University of Washington

2025

Committee:

Jeffrey W. Berman

Dawn E. Lehman

Program Authorized to Offer Degree:

Civil and Environmental Engineering

University of Washington

Abstract

Experiments to Understand the Impact of Local and Global Slenderness on the Inelastic Deformation Capacity of Square and Round HSS Braces

Lily Ana Swanson

Co-Chairs of the Supervisory Committee:
Dawn E. Lehman
Civil and Environmental Engineering

Jeffrey W. Berman
Civil and Environmental Engineering

Concentrically braced frames (CBFs) are widely used as seismic force-resisting systems in low- to mid-rise buildings. In these systems, the braces serve as the primary yielding components. Ordinary CBFs (OCBFs) are intended to achieve a moderate level of ductility, while special CBFs (SCBFs) are intended to achieve a high level of ductility. Hollow structural sections (HSS) are commonly used as the brace component in CBFs and limits on their local slenderness (i.e., width-to-thickness or diameter-to-thickness) defined in the AISC Seismic Provisions (AISC 341-22) are used to achieve a target ductility and drift range capacity for OCBF and SCBF systems. To evaluate these limits, a comprehensive experimental program on the inelastic deformation capacity of HSS was conducted at the University of Washington. The test program was comprised of HSS braces with square and circular cross-sections covering a wide range of local and global slenderness ratios. The selected brace cross-sections include those

that meet the high ductility and/or moderate ductility limits of the AISC Seismic Provisions and those that do not meet the current limits. The test setup enabled testing braces with various lengths, allowing for the examination of the effect of global slenderness, and its interaction with local slenderness, on brace inelastic deformation capacity. The experimental results demonstrate that the current AISC 341-22 local slenderness limits are overly conservative for square braces at moderate ductility and for circular braces at both moderate and high ductility. Findings also suggest that local slenderness limits could be more efficiently expressed as a function of global slenderness. It is clear from the experiments that braces with larger global slenderness can have larger local slenderness and still meet deformation capacity targets for braces in SCBFs and OCBFs, and braces with small global slenderness require smaller local slenderness to meet the deformation capacity targets.

Table of Contents

List of Figures

List of Tables

Acknowledgements

I'd first like to thank my advisors, Professors Dawn Lehman, Jeffrey Berman, Charles Roeder, and Andrew Sen for giving me the amazing opportunity to work on such an impactful project. Your insight and guidance were essential in the success of this research. Thank you for your support and sharing your advice and knowledge throughout the past two years.

This research was only possible due to the efforts of a team of people while this project was in the testing phase. Lab manager, Vince Chaijaroen, thank you for showing me how to think outside the box in order to solve difficult problems and reminding me that if things go wrong, it's part of the process and there is always a solution to be found. A huge thank you to all the undergraduate research assistants that spent numerous hours in the lab contributing to this project. Special thanks to undergraduate assistant Grace Zhang for managing the material testing for this research.

Thank you to the American Institute of Steel Construction for funding this research and thank you to Nucor Tubular Products and Searing Industries for providing materials for experimental testing. Also, thank you to the Steel Tube Institute for facilitating the procurement of testing materials and for helping articulate the notable findings presented in this research.

Last, I would like to thank my family and friends. Your love and encouragement even when many of you were over a thousand miles away meant the world.

Chapter 1. Introduction

1.1 Background and Motivation

Braced frame systems are commonly used as seismic force-resisting systems in buildings. Ordinary (OCBFs) and Special Concentrically Braced Frames (SCBFs) are two types of Concentrically Braced Frame (CBFs) systems offering moderate and high ductility, respectively. SCBFs are designed with more stringent brace geometry and connection design requirements which maximize drift capacity when subjected to high seismic loads. The selection of the diagonal brace members has a significant impact on the performance of all CBF systems because they act as the primary source of lateral strength and stiffness. HSS sections are often used as the brace member to provide this lateral resistance.

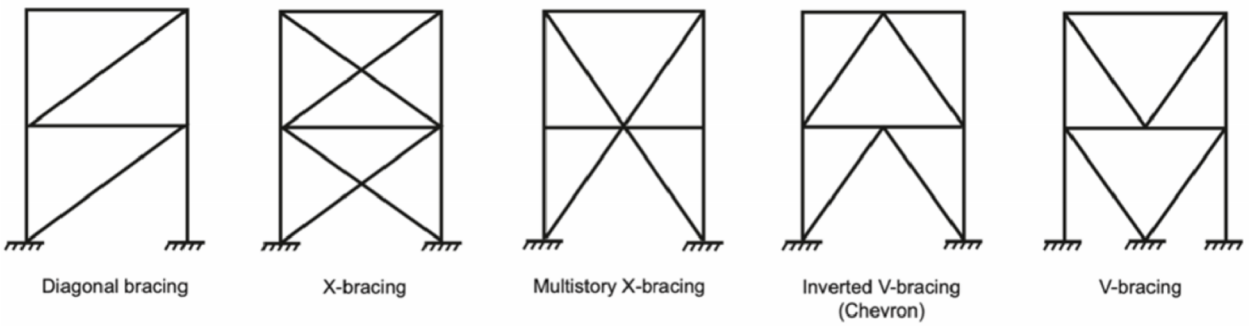

Figure 1.1 Concentrically Braced Frame Configurations (Sabelli et al., 2013)

HSS braces are designed to be the fuse elements in CBF systems and are expected to go through inelastic yielding in tension and buckling in compression. Large axial compressive deformations lead to the formation of a plastic hinge at the midspan of the brace. With increasing deformation, local deformations at the plastic hinge occurs, referred to as cupping, and highly localized strains develop. Local deformations seen in Figure 1.2 and Figure 1.3 show the progression of local deformation of square and round HSS starting at cupping. Cupping is the onset of damage that indicates that the brace is now susceptible to tearing and fracturing in tension. Tearing of the cupping region typically initiates at the top and bottom corners of the brace in tension after cupping. Fracture occurs after tearing. Under earthquake loading, a favorable brace is one that has the ability to withstand large inelastic axial deformations before the formation of cupping and subsequent tearing and fracture at the plastic hinge.

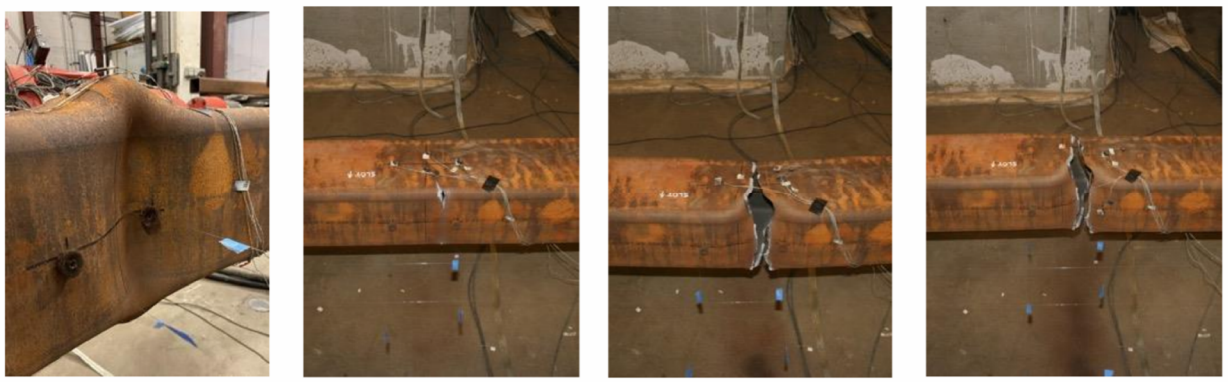

Figure 1.2 Progression of Brace Deformation and Damage at Brace Midspan – Square HSS (Kaldestad, 2022)

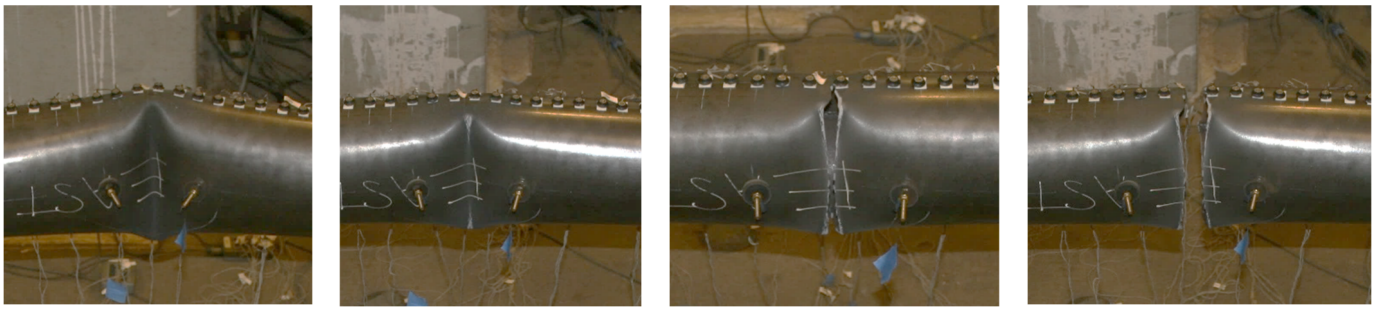

Figure 1.3 Progression of Brace Deformation and Damage at Brace Midspan – Round HSS

Two geometric properties are known to affect brace response and inelastic deformation capacity: brace global slenderness, L_c/r and local slenderness, b/t (square) or D/t (round). L_c is the effective brace length, r is the radius of gyration, b is the flat wall width for square HSS, D is the outside diameter, and t is the wall thickness. The current limiting width/diameter-to-thickness (local slenderness) ratios for HSS braces from Table D1.1a of AISC 341-22 (AISC, 2022) are summarized below in Table 1.1. The moderately ductile limit provides the maximum width/diameter-to-thickness ratio for braces in OCBFs and the highly ductile limit provides the maximum width/diameter-to-thickness ratio for braces in SCBFs. The current limits have no dependence on global slenderness. They are dependent on modulus of elasticity, E, ratio of the expected yield stress to the specified minimum yield stress, R_y, and nominal yield stress, F_y.

Table 1.1 AISC Limiting Width/Diameter-To-Thickness Ratios

HSS Type	AISC 341-22 Limits
Moderately Ductile - Square	$\lambda_{md} = 0.76\sqrt{\frac{E}{R_y F_y}}$
Highly Ductile - Square	$\lambda_{hd} = 0.65\sqrt{\frac{E}{R_y F_y}}$
Moderately Ductile - Round	$\lambda_{md} = 0.062\frac{E}{R_y F_y}$
Highly Ductile - Round	$\lambda_{hd} = 0.053\frac{E}{R_y F_y}$

Since the AISC limits depend on material properties, the limits will change depending on the selected material specification. ASTM A500 grade C is the most common grade of HSS steel used. A500 Gr. C steel has a specified nominal yield stress of 50 ksi and a yield strength ratio, R_y, of 1.3. The limiting width/diameter-to-thickness ratios and other material properties can be found in Table 1.2. It is important to note that the current AISC limits have not changed from the previous versions of the specification, but specified material strengths have increased for round HSS leading to a decrease in the allowable *D/t* for both moderately and highly ductile specimens.

Table 1.2 HSS Specifications for A500 Gr. C Steel

Property	ASTM A500 Gr. C
Yield Strength Ratio, Ry	1.3
Yield Stress	50 ksi (min)
Tensile Stress	62 ksi (min)
Wall Thickness Tolerance	-10%
Design Thickness	$0.93*t_{min}$
Moderately Ductile Limit - Square	16.1
Highly Ductile Limit - Square	13.7
Moderately Ductile Limit - Round	27.7
Highly Ductile Limit - Round	23.6

Other material specifications such as ASTM A1085 are available. This specification requires tighter control of the yield stress which results in a lower yield strength ratio. This material specification was not selected to be tested as a focus in this research. Previous research in the University of Washington Structural Research Laboratory (UW SRL) by Kaldestad (2022) focused on the comparison between A1085 and A500 steel. A summary of this research can be found in Chapter 2.

To understand the behavior of a large range of square and round HSS sizes and lengths, large scale experimental testing of full-size braces subjected to cyclic loading were performed. Thirty A500 HSS braces of various shapes, sizes, and lengths were selected for testing based on their local and global slenderness. Previous research on square A500 HSS specimens performed in the UW SRL by Bergendahl (Bergendahl, 2021) and Kaldestad (Kaldestad, 2022) tested a large number of square HSS braces with *b/t* ratios near the AISC 341-16 high and moderate ductility limits. As such, only one square brace with a *b/t* ratio larger than 20 was tested and there remained a need to test additional square sections with *b/t* ratios between 20 and 30. Nine square braces with b/t ratios larger than 20 were tested as the first test series in the research presented here.

The second test series presented here consisted of twenty-one round HSS braces. Experimental data for circular HSS braces are much more limited in the literature in comparison to square HSS braces. There was a need for the study of local and global slenderness on brace response of round HSS with modern steel. The purpose of this test series was to examine the effect of *D/t* and L_c/r on drift range for a large range of round braces. This included braces with *D/t* ratios near and outside of the AISC 341-22 high and moderate ductility limits.

1.2 Research Objectives

The goal of this research is to evaluate the performance of square and round A500 HSS braces through large-scale experimental testing. The specific research objectives are to:

- Investigate the behavior of square HSS sections with *b/t* ratios greater than 20 using large-scale experiments.
- Investigate the behavior of round HSS sections with a full range of *D/t* ratios using large-scale experiments.
- Document the material and geometric properties through material testing and precise measurements.
- Examine the effects of local slenderness and global slenderness on brace behavior.
- Study the impact of local and global slenderness on the concentration of deformation and strain at the plastic hinge location.
- Determine the appropriate local slenderness limits for AISC 341 or verify that current limits are satisfactory.

1.3 Document Overview

In this thesis, the following chapters were used to address the objectives and goals of this research project:

- Chapter 2: This chapter introduces the background for the performance requirements of CBFs, including its dependence on brace ductility. It also reviews existing literature on previous experimental research focusing on the inelastic response of round HSS under cyclic loading.
- Chapter 3: The test setup, specimen design, and loading protocol are described in detail. This chapter also details the instrumentation used during testing.
- Chapter 4: The results from both test series are presented in a short summary of observations during testing and each braces force-displacement response.
- Chapter 5: This chapter analyzes experimental data. Brace response metrics such as axial deformation, local forces, and local deformations are recorded and compared to examine the influence of various test parameters.
- Chapter 6: Evaluation of design provisions in AISC 341-22 using experimental results and AISC 342-22 backbone curves for round HSS braces.
- Chapter 7: A summary of research findings are provided with key conclusions and recommendations for future work.

Chapter 2. Literature Review

2.1 Introduction

This chapter will provide an overview of CBF design intent and requirements, as well as a review of prior research projects to establish the motivation for this research. The evolution of CBF purpose and design are explained in Section 2.2. Section 2.3 and 2.4 will review relevant prior research on round HSS, general brace behavior, and previous phases of research performed by Bergendahl (2021) and Kaldestad (2022) that act as the motivation for this testing. The same test frame at the UW SRL that was designed and utilized by Bergendahl (2021) and Kaldestad (2022) was used for this phase of testing. For detailed literature on square HSS brace response see Bergendahl (2021) and Kaldestad (2022).

2.2 Design and Requirements for Braces in CBFs

In CBFs, the brace is designed as the fuse element to sustain the damage from an earthquake while the other elements in the structure remain elastic; this is the successful result of capacity-based design which was a design principle introduced in the 1988 Uniform Building Code (ICBO, 1988). It's important to understand brace behavior and performance in order to design these systems efficiently and ensure the intended seismic performance. Braces must withstand cyclic yielding in tension and buckling in compression through a story drift large enough to ensure the structure does not collapse in the risk-adjusted maximum earthquake shaking (MCE_R) as intended by modern building codes. Non-seismic CBFs, OCBFs, and SCBFs have different design requirements for the system's intended purpose. The design requirements are summarized below in Table 2.1. Non-seismic CBFs cannot be utilized in areas classified in ASCE 7-22 (ASCE, 22) as Seismic Design Category C and D but have no seismic limits on global or local slenderness. OCBFs and SCBFs can be used in Seismic Design Category C and D but have additional design requirements and limits to ensure brace ductility and system performance.

Table 2.1 Brace Requirements in Braced Frames (Hsiao, 2012)

Component	Non-Seismic CBFs (R = 3)	OCBFs (R = 3.25)	SCBFs (R = 6)
Brace Global Slenderness	No limit	$L_c/r < 4\sqrt{E/F_y} \approx 100$	$L_c/r < 200$
Brace Local Slenderness	No limit	Compactness ratio < λ_{md}	Compactness ratio < λ_{hd}
Net Section	Design for factored loads	Design for factored loads	Design for $R_yF_yA_g$ of brace
Brace Connection Design	Design for factored loads	Design for minimum of $R_yF_yA_g$ of brace or amplified seismic load	Design for $R_yF_yA_g$ and $1.1R_yP_n$ of brace & permit end rotation of brace

Prior to capacity-based design, braced frames were designed to resist expected seismic loads without accounting for the fact that brace capacity is often larger than the minimum required to resist design loads. This approach resulted in less ductile systems prone to failure connections, beams and columns at low deformation where such failure occurs before inelastic brace deformation. This is why the current design requirements intend to ensure ductile systems behavior, which starts with ductile brace behavior. Limits on brace geometry were set to ensure ductile brace behavior, which are now formalized as local and global slenderness limits. Previous research by Fell et al. (2009) showed that when braces exceeded width-to-thickness ratio limits they are unlikely to withstand the drift demands in a large earthquake (Fell et al., 2009). They confirmed that braces with high local slenderness ratios tend to develop local damage and fracture at much lower drifts.

Brace global slenderness also affects the deformability of braces. Increasing the global slenderness decreases the brace compressive capacity, but it generally provides more ductility because the curvature at the plastic hinge is reduced for a given level of axial ductility demand. The current requirements in AISC 341-22 for global slenderness are upper bounds intended to ensure that the compressive braces contribute adequately to the lateral strength and are ~100 and 200 for OCBFs and SCBFs respectively; However, there is not a lower limit that accounts for the relationship between global slenderness and ductility capacity. Instead, the current upper bound limits are there to prevent large, unbalanced forces and to avoid tension-only braced frame response.

Section 2.3 will review previous experimental research programs that influenced the research in this thesis. Section 2.4 and 2.5 summarize the findings by Bergendahl (Bergendahl, 2021) and Kaldestad (Kaldestad, 2022) that provided the basis for the research in this thesis.

2.3 Cyclic Testing and Behavior of Steel Bracing Members

2.3.1 *Tests of Cold-Formed Circular Tubular Braces under Cyclic Axial Loading (Elchalakani et al., 2003)*

In this research program, twenty circular hollow sections (CHS) were tested to better understand the inelastic cyclic behavior of CHS struts using cyclic tests. The braces were made from AS1163 (1991) grade 350L0 steel, an Australian designation. The CHS had diameter-to-thickness ratios from 32 to 55 and a global slenderness between 30 and 55. The braces had fixed-end conditions which allowed no end rotation. These braces are likely stockier than is typical in an OCBF and SCBF. The braces were tested with one of three different loading protocols in the test setup shown in Figure 2.1. The first test procedure consisted of a large compression-tension cycle followed smaller cycles. This is denoted in Figure 2.2 (a) as series A. The second test procedure, noted as series B, subjected the specimens to a displacement amplitude that uniformly increased up to fracture. The third loading history is similar to the second procedure, but the oscillations were repeated three times at each amplitude. This is noted as series C in Figure 2.2 (b).

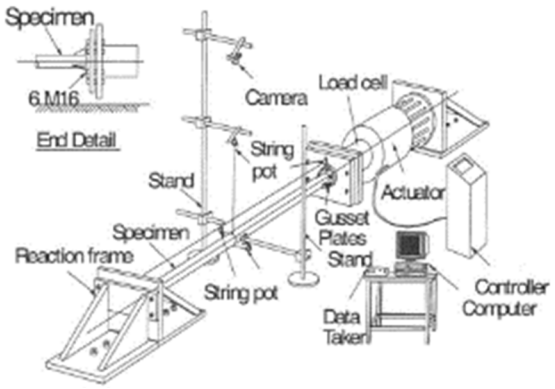

Figure 2.1 Test Setup

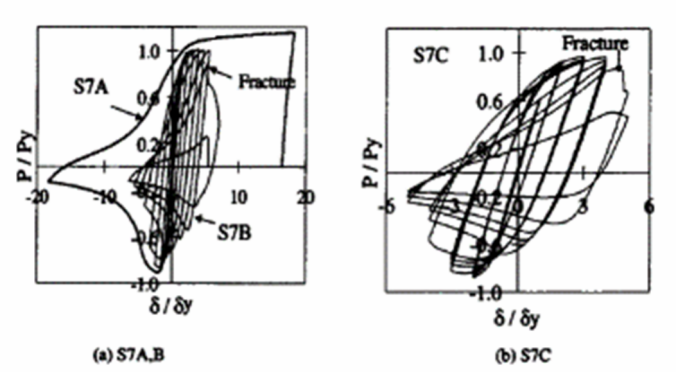

Figure 2.2 P – δ Hysteresis Curves for (a) S7A, B, and (b) S7C

The ratio of peak deformation to yield deformation was defined as the specimen's ductility capacity ratio, δ_u/δ_y. The results of the tests show that the specimens ductility capacity ratio was between 1.4 and 2.7 prior to brace fracture. They also summarized that the fracture life depends heavily on the occurrence of local buckling. Fracture was noted to occur two or three cycles after the central hinge formed. They last identified that more testing is needed for braces with global slenderness larger than 55. In addition, it is common for SCBFs to have end connections that allow end rotation. The fixed end conditions in this research were not representative of braces designed with such connections.

2.3.2 *Cumulative Cyclic Deformation Capacity of Circular Tubular Braces under Local Buckling (Takeuchi and Matsui, 2011)*

In this research, study, ten circular tube brace specimens of different local and global slenderness were tested. Specimen local slenderness (D/t) ranged from 21 to 32 and global slenderness ranged from 53 to 121. Braces were connected via pin ends into the test frame depicted in Figure 2.3. The braces were made from SK400 (JIS G344) steel. Each brace was subjected to increasing normalized axial displacement of 0.5%, 1.0%, 2.0%, and 3.0%. Braces were subjected to each displacement step for three cycles until the 3.0% step where the brace was cycled until fracture.

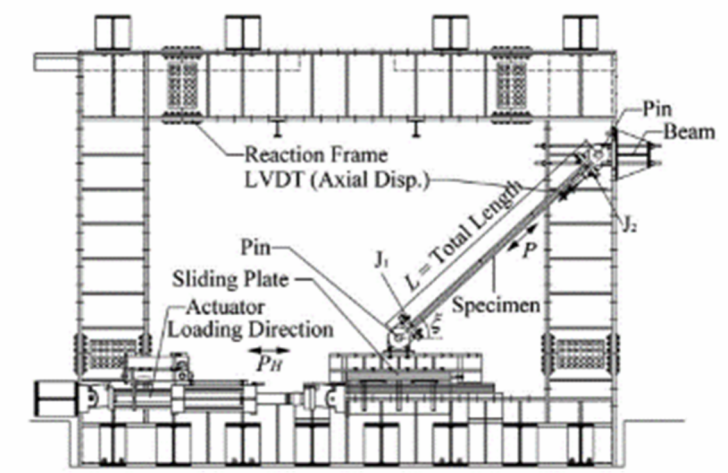

Figure 2.3 Test Setup

All specimens exhibited global buckling when normalized axial deformation was in the range of 0.3-0.8% and local buckling in the range of 0.6%-2.0%. At a normalized deformation in the range of 1.0%-2.6%, all specimens fractured. This data showed that local buckling occurs earlier in braces as the diameter-to-thickness ratio increased and the slenderness ratio decreases. This relationship is similarly reflected in the brace's cumulative deformation capacity.

Another goal of this research study was to investigate the relationship between local and global slenderness on the strain concentration of the locally deformed region of the brace. A simplified hinge zone model for circular tube braces was utilized to develop a relationship between the length and diameter of the brace to the strain at the hinge region, ε_h. The strain concentration ratio is defined as the ratio between the hinge region strain and the average strain along the brace, $\varepsilon_h/\varepsilon_n$. The strain concentration was plotted versus the normalized deformation amplitude and is shown in Figure 2.4. The first number in the specimen notation identifies specimen length; 5 corresponds to braces 1,622mm in length. 7 corresponds to braces 2,219mm in length. 10 corresponds to braces 3,135mm in length. The last two numbers denote the brace diameter-to-thickness ratio. As local slenderness increases, so does the strain concentration ratio. As global slenderness increases, the strain concentration ratio decreases.

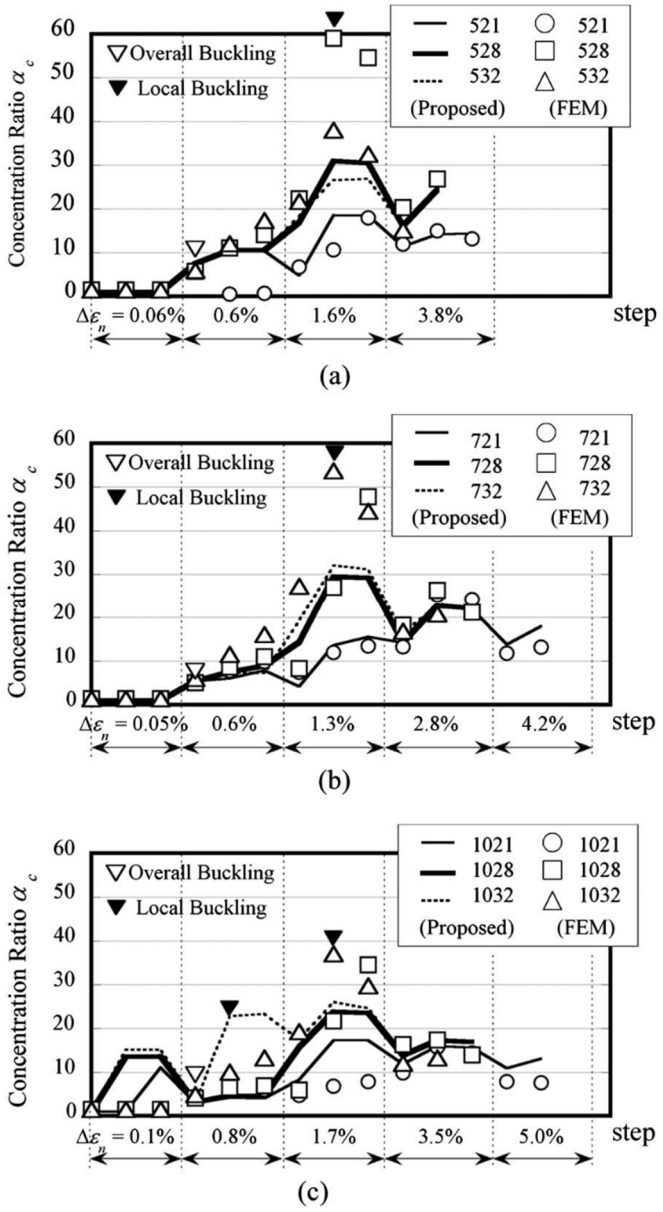

Figure 2.4 Estimated Strain Concentration Ratios (a) Specimens 521, 528, 532; (b) Specimens 721, 728, and 732; (c) Specimens 1021, 1028, and 1032

It was proposed that the strain concentration ratio is a valid method for fracture prediction. The strain concentration ratio might also be used to assess the cumulative deformation capacity of braces until fracture. The local strain in the buckling zone increases more significantly than that in other parts of the brace, which leads to fracture. Based on the results presented in Takeushi and Matsui (2011) it seems there is a need to test braces with larger D/t ratios and explore the variation of strain concentration ratio for D/t around and above the AISC 341-22 limit.

2.3.3 *Experimental Investigation of Foam-Filled CHS Braces under Cyclic Loading (Ammons et al., 2021)*

The goal of this experimental program was to examine the effect of foam infill of circular hollow sections (CHS) under cyclic loading. Two experimental programs undertaken. The first experimental program consisted of six cold-formed CHS braces fabricated from JIS G3444 STK400 steel – a Japanese standard. Three different section sizes were tested with and without foam infill. These braces had local slenderness values ranging from 27.8 to 32.7 and global slenderness ranging from 54.4 to 70.1. The second experimental program was made up of an additional six cold-formed CHS braces which were fabricated from ASTM A500 Gr. B steel. These braces had local slenderness values ranging from 34.7 to 44.4 and global slenderness ranging from 77.3 to 97.4. Three A500 braces were filled and the other three braces were empty. The JIS and ASTIM braces were subjected to a displacement-controlled loading protocol with displacement steps in terms of story drift (%). A diagonal brace frame testing system was used for both test series. The A500 braces were tested in the frame in Figure 2.5.

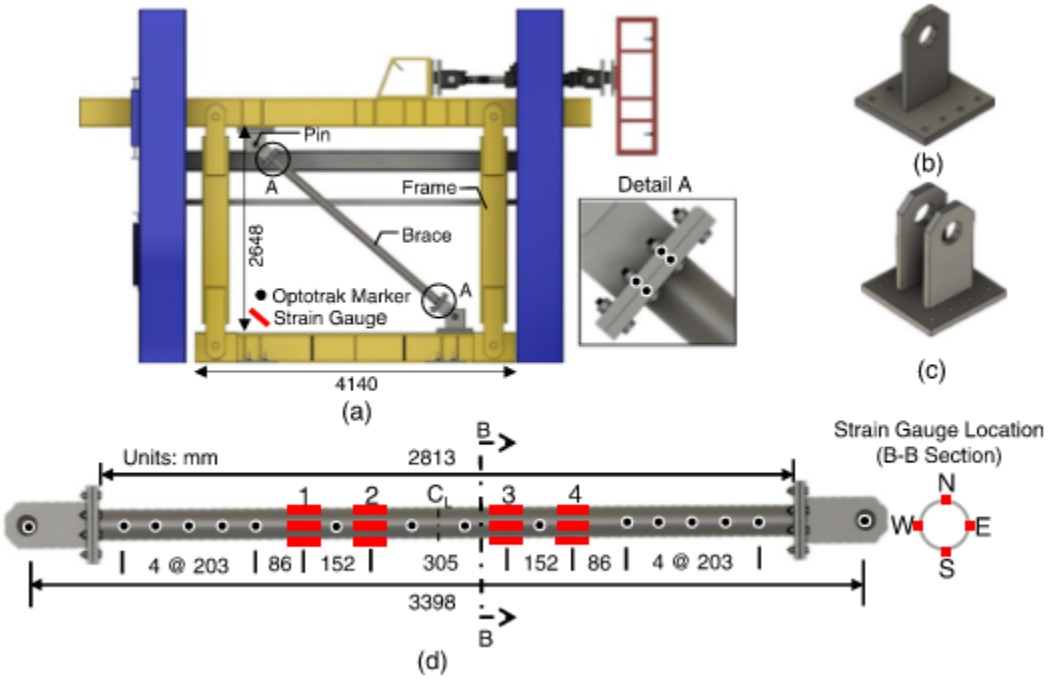

Figure 2.5 Test setup for A500 Gr. B braces: (a) load frame; (b) single plate pin connection; (c) double plate pin connection; (d) brace instrumentation and strain gauge locations.

The positive effect of the foam infill was most evident during cycles when local cupping initiated. Local cupping initiated during later cycles in braces with foam infill and the severity of cupping was less than that of empty braces. The buckling shape was different in filled and empty

braces - Figure 2.6. The empty braces buckled inward in a shape that reflects round HSS buckling behavior. Filled braces buckled outward due to the foams ability to prevent inward deformation of the steel. This change in local buckling mode led to reduced strains in the local cupping region as can be seen in Figure 2.7. The foam caused the strain to be dispersed over a larger length so the demand at the middle of the brace was reduced. The strain dispersion in the foam filled braces led to an increase in brace ductility which can be seen in the brace hysteretic response in Figure 2.8. The foam infill was the most effective in increasing brace inelastic deformation capacity in the 101.6 mm diameter specimens.

Figure 2.6 Midlength local buckling at the end of the first cycle to a specified story drift for braces: (a) E1013, −1.5%; (b) F1013, −3%; (c) E1143, −1.5%; (d) F1143, −2%; (e) E1273, −1%; and (f) F1273, −1%.

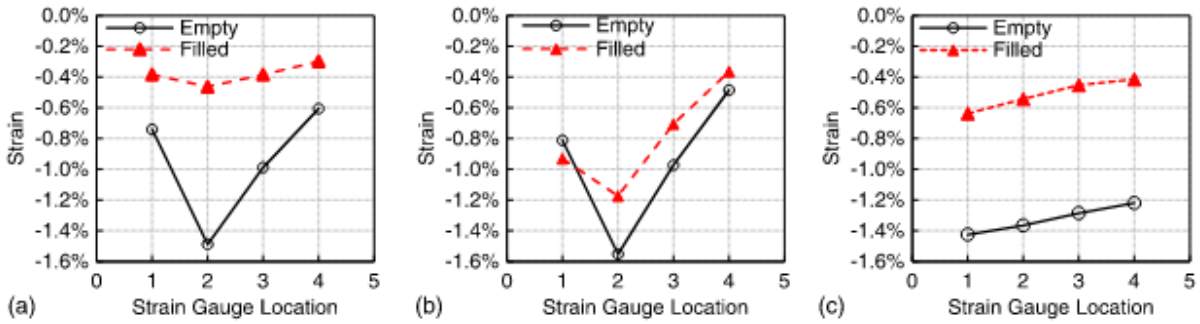

Figure 2.7 Strain distribution in the plastic hinge region of the ASTM A500 Gr. B braces: (a) 101.6-mm-diameter specimens; (b) 114.3-mm-diameter specimens; and (c) 127-mm-diameter specimens.

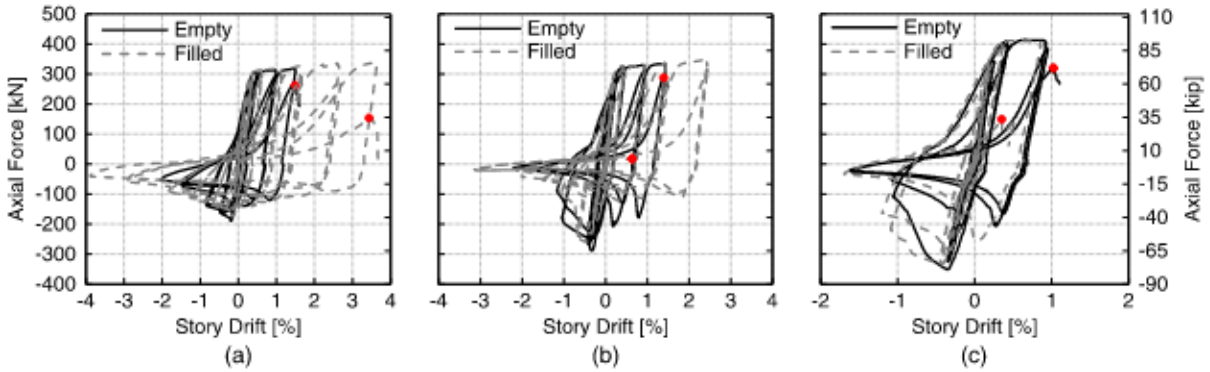

Figure 2.8 Empty and filled ASTM A500 Gr.B brace axial force–story drift response for the (a) 101.6-mm-diameter specimens; (b) 114.3-mm-diameter specimens; and (c) 127-mm-diameter specimens.

Based off the results from this experimental study, the authors recommended using foam infill for moderatly ductile braces. Compared to emtpy braces, filled braces delay the onset of cupping and fracture at least one cycle. Foam fill significatly delays the onset of cupping for moderetly ductile braces - In some cases, up to four cycles later. The difference in tensile and compressive axial capcity between empty and filled braces was small and the bond between the steel and foam was weak. This would suggest that typical sysmic design practices can still be followed with foam filled braces. While the authors do recommend foam infill for moderatly ductile braces, it's important to note that only two braces with moderate ductility (according to AISC 341-16) were tested. The test matrix was selected to focus around braces close but not meeting the moderatly ductile limit.

2.4 Experimental Investigation to Compare the Cyclic Response of A500 and A1085 Braces (Bergendahl, 2021)

The tests performed by Bergendahl (2021) are a part of the same research effort as this thesis. The main goal of Bergendahl's tests were to compare the performance of A500 HSS to A1085 HSS. Ten different section sizes of HSS were tested with A500 material and A1085 material, totaling 20 braces. The summary of these specimens can be found below in Figure 2.9. Green indicates HSS that meet the criteria for highly ductile braces, orange represents HSS that meet the standards for moderately ductile braces, and red signifies HSS that fail to meet either of the limits specified in the ASIC seismic provisions.

HSS Shape	Nominal Width-to-Thickness Ratio	
	A500 Gr. C	A1085
10x10x3/8	25.7	23.7
8x8x1/2	14.2	13
8x8x3/8	19.9	18.3
7x7x1/2	12.1	11
7x7x3/8	17.1	15.7
7x7x5/16	21.1	19.4
6x6x1/2	9.9	9
6x6x3/8	14.2	13
6x6x5/16	17.6	16.2
5x5x3/8	11.3	10.3

(a)

HSS Shape	Nominal Global Slenderness Ratio	
	A500 Gr. C	A1085
10x10x3/8	60.6	60.9
8x8x1/2	78.1	78.6
8x8x3/8	76.6	76.9
7x7x1/2	90.3	91.0
7x7x3/8	88.3	88.6
7x7x5/16	87.3	87.6
6x6x1/2	106.5	107.5
6x6x3/8	104.2	104.6
6x6x5/16	102.8	103.3
5x5x3/8	127.0	127.7

(b)

Figure 2.9 Summary of the Local (a) and Global (b) Slenderness of Test Specimens – Series 1

The test setup was designed by Bergendahl (2021) and is also used for testing all specimens mentioned in this current thesis. Braces were designed with slotted ends and welded gusset plates which were bolted into the test setup at the UW SRL. The gusset plates were bolted into large plates at the ends but clearance was provided for gusset plate rotation consistent with the end conditions for braces in SCBFs. The twenty braces in series 1 were 237.5” long and were all subjected to a symmetric displacement protocol. Two cycles were executed at each displacement step. The protocol began at 1/8” and increased in additional 1/8” steps to 3/4". The magnitude of steps increased to 1/2" increments until brace fracture.

The performance of each brace is noted below in Table 2.2 Summary of Test Specimen PerformanceTable 2.2. The peak compressive and tensile forces, $P_{T,max}$ and $P_{C,max}$, are noted for each specimen. Measured yield stress, F_{ym}, and measured cross-sectional area, $A_{g,m}$, are used to calculate measured values of theoretical peak yield load, P_y, and peak compressive load, P_{Cr}. The ratio of experimental to theoretical loads are noted below their respective experimental tensile or compressive load. The maximum axial deformation in tension, $\Delta_{T,max}$, and compression, $\Delta_{C,max}$, are used to calculate an approximate drift based on assumptions and calculations explained in Section 4.2. The maximum axial deformation range, Δ_{range}, is equal to the difference between the maximum tensile and compressive deformations and the accumulated axial deformation, Δ_{Acc}, is equal to the sum of all axial deformation. The deformation range was normalized by brace length and plotted versus normalized nominal width-to-thickness ratio, $\lambda_{nom}/\lambda_{HD}$, below in Figure 2.10.

The last column in the table presents the energy dissipation capacity, $\sum E_{Diss}$, normalized by the measured cross-sectional area ($A_{g,m}$) and the measured yield strength (F_{ym}).

The summary of the test specimen performance shows that there is a minimal difference between the performance of A500 and A1085 braces of the same cross-section. For six of the ten HSS shapes tested, the A1085 had a larger deformation range, whereas for the remaining four HSS shapes, the A500 had a greater deformation range.

Table 2.2 Summary of Test Specimen Performance – Test Series 1

HSS Section	$P_{T,max}$ (kips) ($P_{T,max}/P_y$)	$P_{C,max}$ (kips) ($P_{C,max}/P_{Cr}$)	$\Delta_{T,max}$ (in.) (Drift %)	$\Delta_{C,max}$ (in.) (Drift %)	Δ_{range} (in.) (Drift %)	Δ_{Acc} (in.) (Drift %)	$\frac{\sum E_{Diss}}{A_{g,m}F_{y,m}}$
5x5x3/8 A500 Y	432.50 *(1.04)*	-95.30 *(0.96)*	5.13 *(4.28)*	4.89 *(4.07)*	10.02 *(8.35)*	119.54 *(99.65)*	20.57
5x5x3/8 A1085 Y	443.60 *(1.02)*	-98.38 *(0.97)*	5.25 *(4.38)*	5.50 *(4.59)*	10.75 *(8.96)*	132.02 *(110.05)*	21.74
6x6x5/16 A500 R	409.70 *(1.06)*	-125.75 *(0.79)*	3.06 *(2.55)*	3.26 *(2.71)*	6.31 *(5.26)*	52.34 *(43.63)*	13.29
6x6x5/16 A1085 Y	456.40 *(1.07)*	139.80 *(0.87)*	3.13 *(2.61)*	3.12 *(2.60)*	6.25 *(5.21)*	51.33 *(42.79)*	12.57
6x6x3/8 A500 R	511.00 *(1.05)*	-168.70 *(0.92)*	3.74 *(3.12)*	3.72 *(3.10)*	7.46 *(6.22)*	65.80 *(54.85)*	16.45
6x6x3/8 A1085 Y	547.90 *(1.01)*	-180.00 *(0.97)*	3.52 *(2.93)*	3.52 *(2.93)*	7.04 *(5.87)*	56.61 *(47.19)*	13.63
6x6x1/2 A500 R	646.20 *(1.02)*	-218.70 *(0.98)*	4.45 *(3.71)*	4.06 *(3.39)*	8.51 *(7.10)*	80.64 *(67.22)*	17.25
6x6x1/2 A1085 Y	727.20 *(1.06)*	-218.60 *(1.00)*	4.67 *(3.89)*	5.12 *(4.27)*	9.79 *(8.16)*	97.41 *(81.21)*	22.36
7x7x5/16 A500 Y	496.60 *(1.05)*	-209.80 *(0.89)*	1.73 *(1.44)*	1.83 *(1.53)*	3.56 *(2.97)*	20.29 *(16.91)*	5.82
7x7x5/16 A1085 Y	478.10 *(1.05)*	-201.50 *(0.84)*	1.99 *(1.66)*	2.31 *(1.92)*	4.29 *(3.58)*	27.94 *(23.30)*	8.01
7x7x3/8 A500 Y	570.90 *(1.06)*	-231.80 *(0.87)*	2.51 *(2.09)*	2.79 *(2.33)*	5.30 *(4.42)*	35.26 *(29.40)*	10.49
7x7x3/8 A1085 Y	615.90 *(1.07)*	-254.90 *(0.90)*	2.36 *(1.97)*	2.85 *(2.38)*	5.21 *(4.35)*	37.42 *(31.20)*	9.76
7x7x1/2 A500 B	710.40 *(1.06)*	-278.80 *(0.83)*	3.59 *(2.99)*	4.16 *(3.47)*	7.75 *(6.46)*	70.86 *(59.08)*	19.31
7x7x1/2 A1085 Y	805.10 *(1.04)*	-305.70 *(0.86)*	3.48 *(2.90)*	4.41 *(3.68)*	7.89 *(6.58)*	70.13 *(58.46)*	18.21
8x8x3/8 A500 W	702.70 *(1.02)*	359.98 *-(0.92)*	1.24 *(1.04)*	1.90 *(1.58)*	3.14 *(2.62)*	18.10 *(15.09)*	4.97
8x8x3/8 A1085 Y	672.60 *(1.02)*	-328.80 *(0.84)*	2.18 *(1.82)*	2.18 *(1.82)*	4.36 *(3.63)*	27.43 *(22.87)*	9.18
8x8x1/2 A500 W	905.97 *(1.03)*	-434.72 *(0.89)*	2.71 *(2.26)*	2.80 *(2.34)*	5.51 *(4.60)*	38.25 *(31.89)*	12.66
8x8x1/2 A1085 Y	921.90 *(1.02)*	-418.20 *(0.83)*	2.96 *(2.46)*	3.32 *(2.77)*	6.28 *(5.23)*	44.07 *(36.74)*	13.29
10x10x3/8 A500 W	785.40 *(1.01)*	-480.10 *(0.85)*	2.10 *(1.75)*	2.48 *(2.07)*	4.58 *(3.81)*	25.71 *(21.43)*	5.96
10x10x3/8 A1085 Y	812.80 *(1.01)*	-507.60 *(0.87)*	1.60 *(1.33)*	1.84 *(1.53)*	3.44 *(2.87)*	15.66 *(13.05)*	4.67

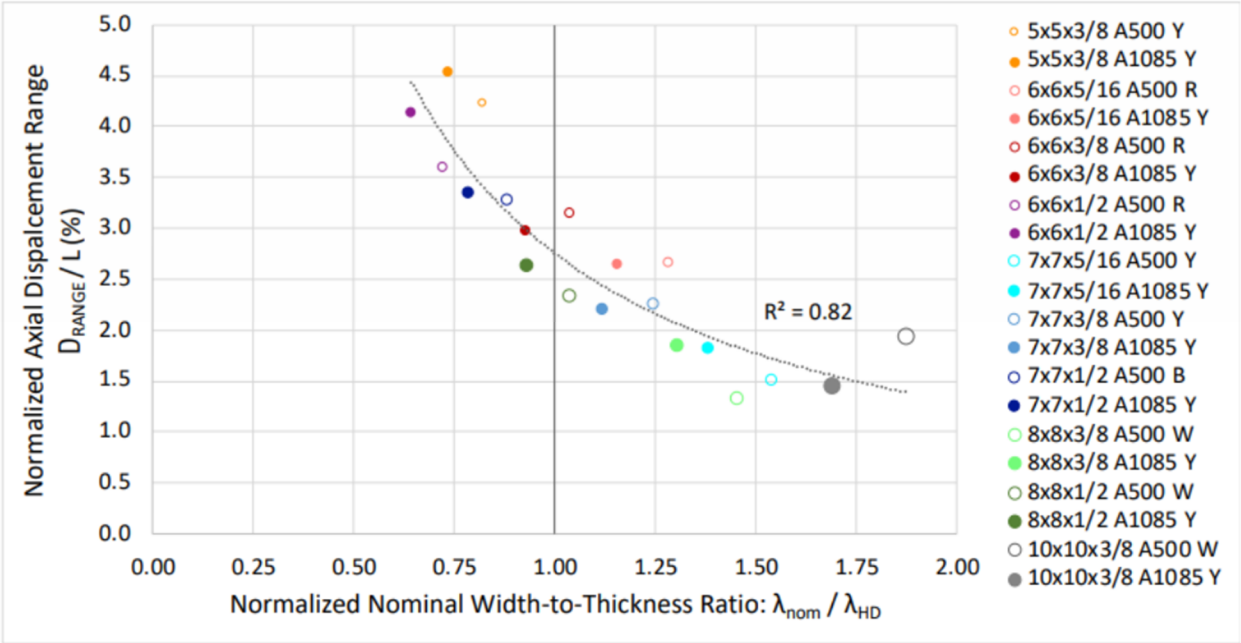

Figure 2.10 Axial Displacement Range vs. Local Compactness (Bergendahl, 2021)

The plot above, Figure 2.10, plots the normalized axial displacement range versus the normalized brace local slenderness, where the axial displacement range is the difference the maximum tensile and compressive displacements achieved during each test. The axial displacement range is normalized by the brace length and the local slenderness, λ_{nom}, is normalized the AISC highly ductile limit, λ_{HD}. Values on the x-axis smaller than one meet the requirements for a highly ductile brace. There is a clear relationship that as the local slenderness increases, the axial displacement range decreases. Normalized brace axial displacement range was also plotted against brace nominal global slenderness below in Figure 2.11. There is an evident relationship that as the global slenderness increases, the axial displacement range increases.

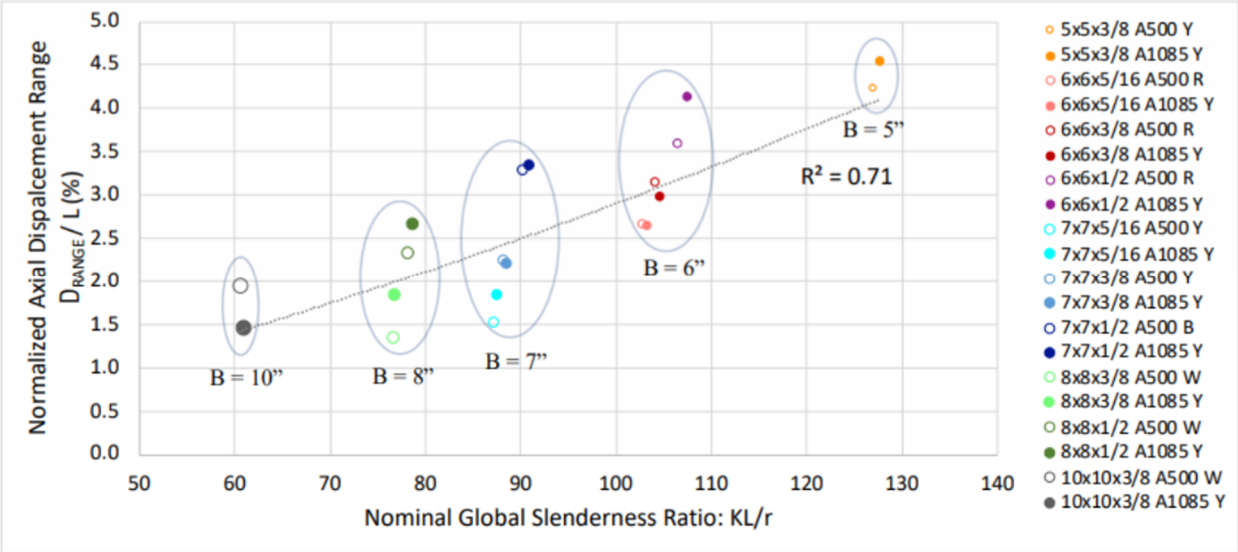

Figure 2.11 Axial Displacement Range vs. Global Slenderness (Bergendahl, 2021)

It was concluded that ASTM material grade had negligible effect on the axial displacement capacity of the specimens. While the A1085 specification has stricter tolerances for certain geometric and material properties, many of the A500 specimens either met or were close to meeting the A1085 specification. There is a large influence on axial displacement range due to the brace local slenderness, *b/t*, and brace global slenderness, *KL/r*. Variables that were not studied in Bergendahl's thesis were the effects of loading protocol and steel producer. These variables will be the focus of study in Kaldestad's thesis in the following section.

2.5 Experimental Investigation into the Cyclic Response of A1085 HSS Braces (Kaldestad, 2022)

The tests performed by Kaldestad (2022) are a part of the same research effort as this thesis. The two main research goals were to identify the impact of steel producer and loading protocol on the performance of square HSS braces. The braces for testing were obtained from four different steel producers. Each steel producer was assigned a color: red (R), white (W), yellow(Y), and blue (B). The test setup detailed in Chapter 3 of this thesis was used to perform tests on these braces. The braces were subjected to one of three loading protocols: symmetric, near fault, or chevron. The symmetric loading protocol was identical to the symmetric loading protocol used by Bergendahl (2021). The braces tested under this loading protocol were known as Series 2. The chevron loading protocol was compression dominant and intended to represent the behavior of a brace within an SCBF with a chevron configuration where vertical beam

deformation occurs. The near fault loading protocol was tension dominant and intended to represent the pulse demands of a near fault ground motion. The braces tested under the chevron and near fault protocols were known as series 3. In the last series, series 4, additional symmetric loading protocol tests were performed on braces 4.5' shorter in length than the braces tested in series 1 and 2. The magnitude of the displacement steps from the loading protocol in series 1 and 2 was scaled down based on proportional brace length. The goal of the series 4 tests were to explore the effects of brace length and global slenderness.

The nominal and measured geometric properties of the braces tested are summarized in Table 2.3. The name of each brace indicates the section size, producer color, and load protocol. Where no load protocol is noted, it can be assumed that it is part of the series 2 symmetric loading protocol. The nominal *b/t* ratios are color coded to indicate compliance with the AISC-341 *b/t* limits. Green indicates HSS that meet the criteria for highly ductile braces, orange represents HSS that meet the standards for moderately ductile braces, and red signifies HSS that fail to meet either of the limits specified in The Seismic Provisions. Kaldestad (2022) tested braces with local slenderness ranging 10.3 – 18.3 and global slenderness ranging 68.5 – 127.7.

Table 2.3 Summary of Nominal and Measured Geometric Properties - Test Series 2, 3, and 4

			Wall Thickness		Brace Compactness		
Test Specimen	**Nominal Area, A_g (in²)**	**Moment of Inertia, I (in⁴)**	**Nominal, t_{nom} (in)**	**Measured, t_{meas} (in)**	**Nominal, b/t_{nom}**	**Measured, b/t_{meas}**	**Global Slenderness, KL/r**
5x5x3/8 A1085 R	6.58	22.8	0.375	0.375	10.30	9.23	127.7
5x5x3/8 A1085 W	6.58	22.8	0.375	0.374	10.30	9.50	127.7
5x5x3/8 A1085 B	6.58	22.8	0.375	0.381	10.30	9.27	127.7
6x6x3/8 A1085 R	8.08	41.6	0.375	0.371	13.00	12.30	104.6
6x6x3/8 A1085 W	8.08	41.6	0.375	0.376	13.00	11.74	104.6
6x6x3/8 A1085 B	8.08	41.6	0.375	0.380	13.00	11.41	104.6
8x8x3/8 A1085 R	11.1	106.0	0.375	0.368	18.30	17.43	76.9
8x8x3/8 A1085 W	11.1	106.0	0.375	0.374	18.30	17.26	76.9
8x8x3/8 A1085 B	11.1	106.0	0.375	0.375	18.30	16.77	76.9
8x8x1/2 A1085 R	14.4	131.0	0.500	0.465	13.00	12.82	78.6
8x8x1/2 A1085 W	14.4	131.0	0.500	0.499	13.00	12.20	78.6
8x8x1/2 A1085 B	14.4	131.0	0.500	0.501	13.00	11.68	78.6
5x5x3/8 A1085 Y Chevron	6.58	22.8	0.375	0.376	10.3	9.42	127.7
5x5x3/8 A1085 Y Near Fault	6.58	22.8	0.375	0.376	10.3	9.42	127.7
7x7x3/8 A1085 Y Chevron	9.58	68.7	0.375	0.365	15.7	14.21	88.6
7x7x3/8 A1085 Y Near Fault	9.58	68.7	0.375	0.365	15.7	14.21	88.6
8x8x3/8 A1085 Y Chevron	11.1	106.0	0.375	0.370	18.3	15.89	76.9
8x8x3/8 A1085 Y Near Fault	11.1	106.0	0.375	0.370	18.3	15.89	76.9
5x5x3/8 A1085 Y Short	6.58	22.8	0.375	0.376	10.3	9.42	98.7
7x7x3/8 A1085 Y Short	9.58	68.7	0.375	0.365	15.7	14.21	68.5
8x8x3/8 A1085 Y Short	11.1	106.0	0.375	0.370	18.3	15.89	59.4

The performance of each brace is noted below in Table 2.4. The table includes the same information that was summarized in Section 2.4 for Table 2.2. The first main focus of the research done by Kaldestad (2022) was to investigate the consistency of brace response among steel producers. Figure 2.12 compares the normalized axial deformation range for four different section sizes. For the 8x8x3/8 and 8x8x1/2 sections, there is very little variation in axial deformation range. For the 5x5x3/8 and 6x6x3/8 sections, the steel from the blue producer

performed slightly behind the other produces. Kaldestad (2022) notes that this could be due to differences in material properties. The blue producer had the highest yield strength for each of the four sizes of HSS tested.

Table 2.4 Summary of Test Specimen Performance – Test Series 2, 3, and 4

HSS Section	$P_{T,max}$ (kips) ($P_{T,max}/P_y$)	$P_{C,max}$ (kips) ($P_{C,max}/P_{Cr}$)	$\Delta_{T,max}$ (in.) (Drift %)	$\Delta_{C,max}$ (in.) (Drift %)	Δ_{range} (in.) (Drift %)	Δ_{Acc} (in.) (Drift %)	$\frac{\sum E_{Diss}}{A_{g,m}F_{y,m}}$
5x5x3/8 A1085 R	456.59 *(1.01)*	-114.23 *(1.13)*	4.91 *(4.09)*	5.14 *(4.29)*	10.05 *(8.38)*	*120.09 (100.11)*	18.79
5x5x3/8 A1085 W	468.27 *(1.03)*	-110.19 *(1.09)*	4.72 *(3.93)*	5.27 *(4.39)*	9.99 *(8.32)*	*109.31 (91.13)*	17.64
5x5x3/8 A1085 B	538.20 *(1.03)*	-126.44 *(1.25)*	3.93 *(3.28)*	5.07 *(4.23)*	9.00 *(7.51)*	*98.28 (81.93)*	15.50
6x6x3/8 A1085 R	521.04 *(1.08)*	-178.82 *(0.97)*	3.96 *(3.30)*	4.14 *(3.45)*	8.09 *(6.75)*	*73.05 (60.89)*	17.30
6x6x3/8 A1085 W	549.55 *(1.00)*	-185.84 *(1.00)*	3.66 *(3.05)*	4.04 *(3.37)*	7.70 *(6.42)*	*65.74 (54.81)*	14.62
6x6x3/8 A1085 B	581.67 *(1.03)*	-177.88 *(0.96)*	2.97 *(2.48)*	3.26 *(2.72)*	6.23 *(5.19)*	*50.27 (41.91)*	10.74
8x8x3/8 A1085 R	660.41 *(0.99)*	-323.69 *(0.80)*	2.68 *(2.23)*	1.77 *(1.48)*	4.45 *(3.71)*	*25.76 (21.48)*	8.17
8x8x3/8 A1085 W	711.95 *(1.02)*	-361.03 *(0.89)*	2.31 *(1.93)*	2.28 *(1.90)*	4.59 *(3.83)*	*26.46 (22.06)*	8.30
8x8x3/8 A1085 B	763.00 *(1.01)*	-363.94 *(0.90)*	1.74 *(1.45)*	2.55 *(2.12)*	4.29 *(3.57)*	*24.55 (20.47)*	6.71
8x8x1/2 A1085 R	819.18 *(1.04)*	-425.29 *(0.83)*	3.31 *(2.76)*	2.95 *(2.46)*	6.26 *(5.21)*	*47.25 (39.39)*	11.77
8x8x1/2 A1085 W	964.72 *(1.01)*	-446.26 *(0.87)*	2.83 *(2.36)*	3.28 *(2.73)*	6.10 *(5.09)*	*45.42 (37.86)*	13.10
8x8x1/2 A1085 B	938.58 *(0.98)*	-478.57 *(0.94)*	3.03 *(2.53)*	3.05 *(2.55)*	6.08 *(5.07)*	*39.67 (33.07)*	10.93
5x5x3/8 A1085 Y Chevron	409.06 *(0.94)*	-93.31 *(0.92)*	3.64 *(3.03)*	7.82 *(6.52)*	11.46 *(9.55)*	*229.47 (191.30)*	23.12
5x5x3/8 A1085 Y Near Fault	464.24 *(1.07)*	-95.36 *(0.94)*	7.88 *(6.57)*	4.34 *(3.62)*	12.22 *(10.19)*	*152.72 (127.32)*	24.92
7x7x3/8 A1085 Y Chevron	258.35 *(0.45)*	-257.40 *(0.88)*	1.16 *(0.97)*	4.24 *(3.54)*	5.41 *(4.51)*	*34.04 (28.37)*	5.81
7x7x3/8 A1085 Y Near Fault	670.92 *(1.16)*	-255.17 *(0.87)*	4.08 *(3.40)*	1.50 *(1.25)*	5.57 *(4.65)*	*42.55 (35.47)*	12.78
8x8x3/8 A1085 Y Chevron	332.92 *(0.50)*	-320.72 *(0.79)*	1.10 *(0.92)*	3.58 *(2.98)*	4.68 *(3.90)*	*25.74 (21.46)*	5.32
8x8x3/8 A1085 Y Near Fault	716.32 *(1.08)*	-308.41 *(0.76)*	3.95 *(3.29)*	1.03 *(0.86)*	4.98 *(4.15)*	*32.37 (26.98)*	11.43
5x5x3/8 A1085 Y Short	438.58 *(1.01)*	-140.80 *(0.83)*	3.64 *(3.93)*	3.45 *(3.73)*	7.10 *(7.66)*	*76.29 (63.60)*	15.94
7x7x3/8 A1085 Y Short	617.53 *(1.07)*	-327.91 *(0.84)*	1.56 *(1.68)*	1.74 *(1.88)*	3.30 *(3.57)*	*19.88 (16.57)*	7.10
8x8x3/8 A1085 Y Short	666.42 *(1.01)*	-393.60 *(0.78)*	1.61 *(1.74)*	1.65 *(1.78)*	3.27 *(3.52)*	*19.70 (16.42)*	6.98

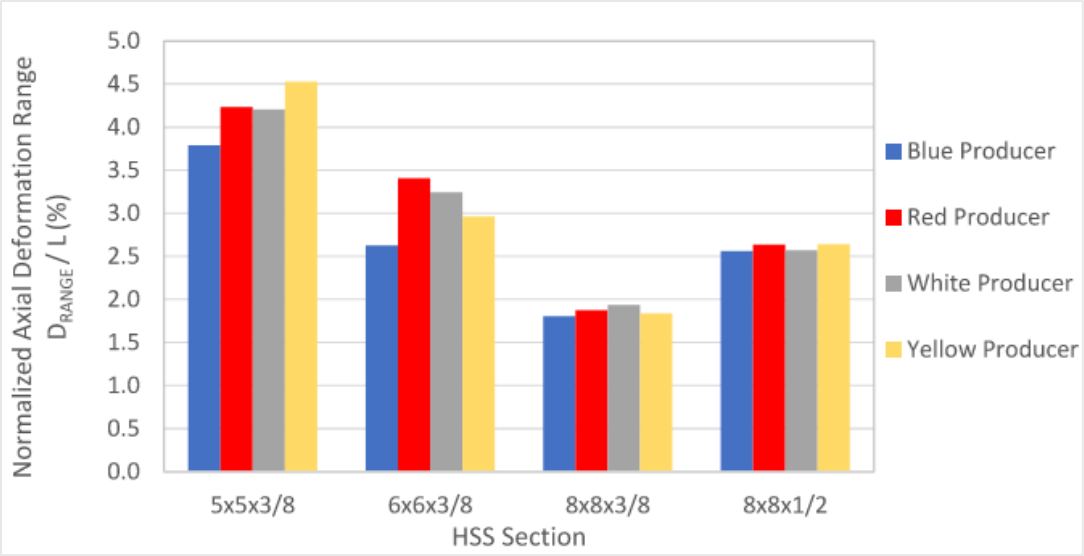

Figure 2.12 Producer Comparison of Normalized Axial Displacement Range

The second main focus of the research done by Kaldestad (2022) was the effect of displacement protocol on brace response. Below, Figure 2.13 compares the normalized axial deformation ranges for the 5x5x3/8, 7x7x3/8, and 8x8x3/8 test specimens subjected to the three different displacement protocols. There is minimal variation in axial deformation capacity seen between the loading protocol types. The symmetric loading protocol produces marginally smaller values for axial displacement range compared to the other protocol types. This suggests that the symmetric loading protocol is more damaging to the specimens and produces a conservative estimate for axial deformation range.

The columns in Figure 2.13 are stacked to show the maximum tensile and compressive range for each specimen. As shown, the chevron protocol applied more deformation in compression, and the near fault protocol applied more deformation in tension. While the peak tensile and compressive deformations were very dependent on the loading protocol, the total displacement range is not significantly impacted. This indicates that the deformation range serves as a more reliable measure of brace deformation capacity than using either the tensile or compressive deformation capacities alone.

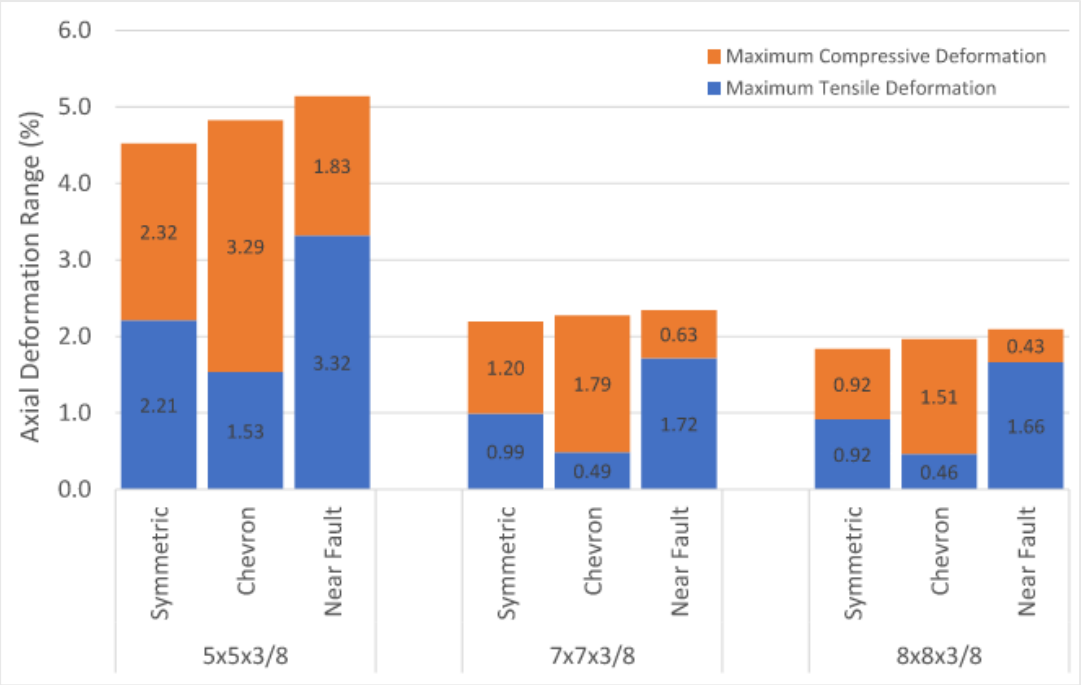

Figure 2.13 Effect of Displacement Protocol on Normalized Axial Deformation Range

The effect of steel producer and loading protocol types on brace response was determined to be negligible. However, when looking to characterize the seismic response of OCBFs and SCBFs, story drift range (computed from brace deformation range) should be used rather than maximum drift in a single direction due to its dependence on loading protocol. Similar to prior research results by Bergendahl (2021), test results indicated that ductility and energy dissipation capacity of HSS bracing members are most significantly impacted by the local and global slenderness ratios. The drift range of brace members was shown to increase with increased global slenderness and decreased local slenderness. Kaldestad (2022) recommended a re-evaluation of the ASIC 341-16 limits due to results indicating the moderately-ductile limit being conservative. It was also recommended that future work be performed on the cyclic performance of stocky braces with high and moderate ductility with *KL/r* ratios between 40 and 90.

2.6 Summary of Findings

The research summarized above emphasizes that brace ductility and performance is most strongly affected by local slenderness, *b/t* or *D/t*, and global slenderness, L_c/r. This behavior is present for both round and square HSS and is not dependent on loading protocol. As the brace global slenderness increases and local slenderness decreases, brace ductility increases. No significant evidence was found to suggest that square HSS sections conforming to A1085

provided much more additional deformation capacity than those conforming to A500. Material testing and measured dimensions showed that A500 HSS sections are being produced very close to HSS A1085 specification requirements. The focus of research efforts summarized in this thesis are to expand the available data sets for square and round A500 HSS tested under a symmetric loading protocol. A more detailed investigation into the effects of local and global slenderness was undertaken to properly re-evaluate the AISC 341-22 ductility limits for HSS used as braces in CBFs.

Chapter 3. Test Setup and Specimen Design

3.1 Introduction

This chapter provides descriptions of the following: (1) design and construction of the test setup, (2) design and construction of the test specimens, (3) instrumentation and (4) the loading protocols. A total of nine A500 square HSS and twenty-one A500 round HSS were tested to evaluate the impact of local and global slenderness on the cyclic response of HSS braces used in concentrically braced frames.

3.2 Test Setup

This section summarizes the overall layout and design of the test setup. The setup was designed and constructed in previous research (Bergendahl 2021 and Kaldestad 2022). Bergendahl (2021) contains a detailed description of the test setup which is referenced in this section. Thus, a general overview of the test setup and its design is provided here. This section will provide the following information: Layout (Section 3.2.1), Loading System (Section 3.2.2), Sliding Beam Design (Section 3.2.3), and End Reaction Block and End Connection Plate Design (Section 3.2.4).

3.2.1 *Layout and Overview of Test Setup*

The test frame was designed to test different HSS sizes and lengths. The maximum size of the HSS sections was determined by the tensile capacity of the actuators. The lengths were determined by the tie downs in the strong floor (3 ft. on center). Two lengths were used. The test setup in Figure 3.1 tests 219.5” long specimens. The adjusted test setup in Figure 3.2, accommodated the 183.5” specimens using a spacer. The end reaction block (Figure 3.13) on the south side of the test setup remained in the same location for both brace lengths. An additional 36” deep spacer block was added to the north side of the end reaction block as can be seen in Figure 3.2 to test the short brace length.

Two hydraulic actuators operated in parallel with maximum combined actuator force of 1000 kips in tension and 700 kips in compression. The load-carrying capacity of each component of the test setup was designed to meet these maximum loads. The south end reaction blocks and actuator reaction blocks are fixed to the strong floor using post tensioned anchor rods while the

actuator forces are applied to move the sliding beam. Each block was anchored to the strong floor with six 1-3/4” diameter 150 ksi threaded bars and a layer of hydrostone to create a monolithic surface between the block and floor. The sliding beam is able to slide on a near frictionless surface to apply the full actuator force through the connection plates to the specimen

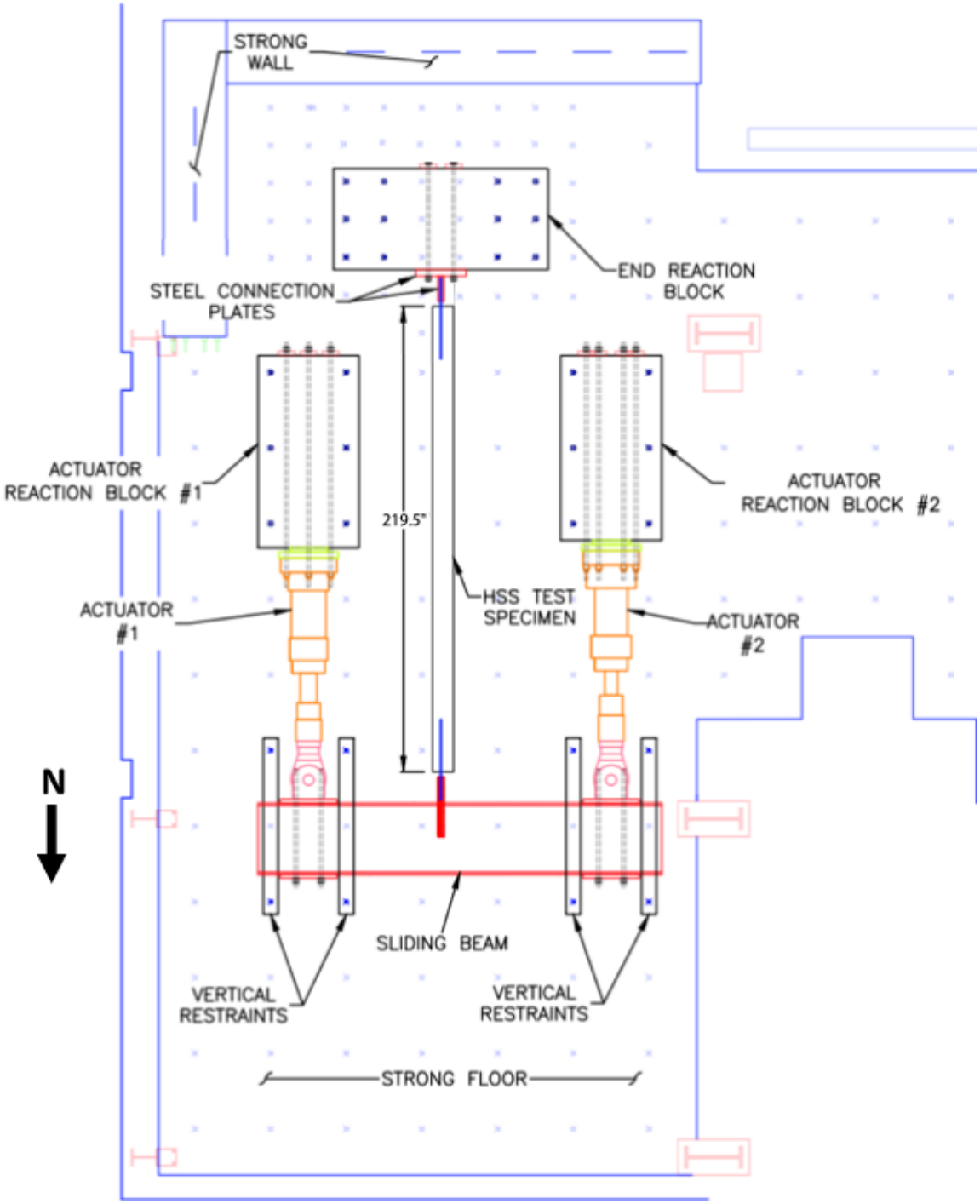

.

Figure 3.1. Overview of Test Frame for 219.5” Long Specimens

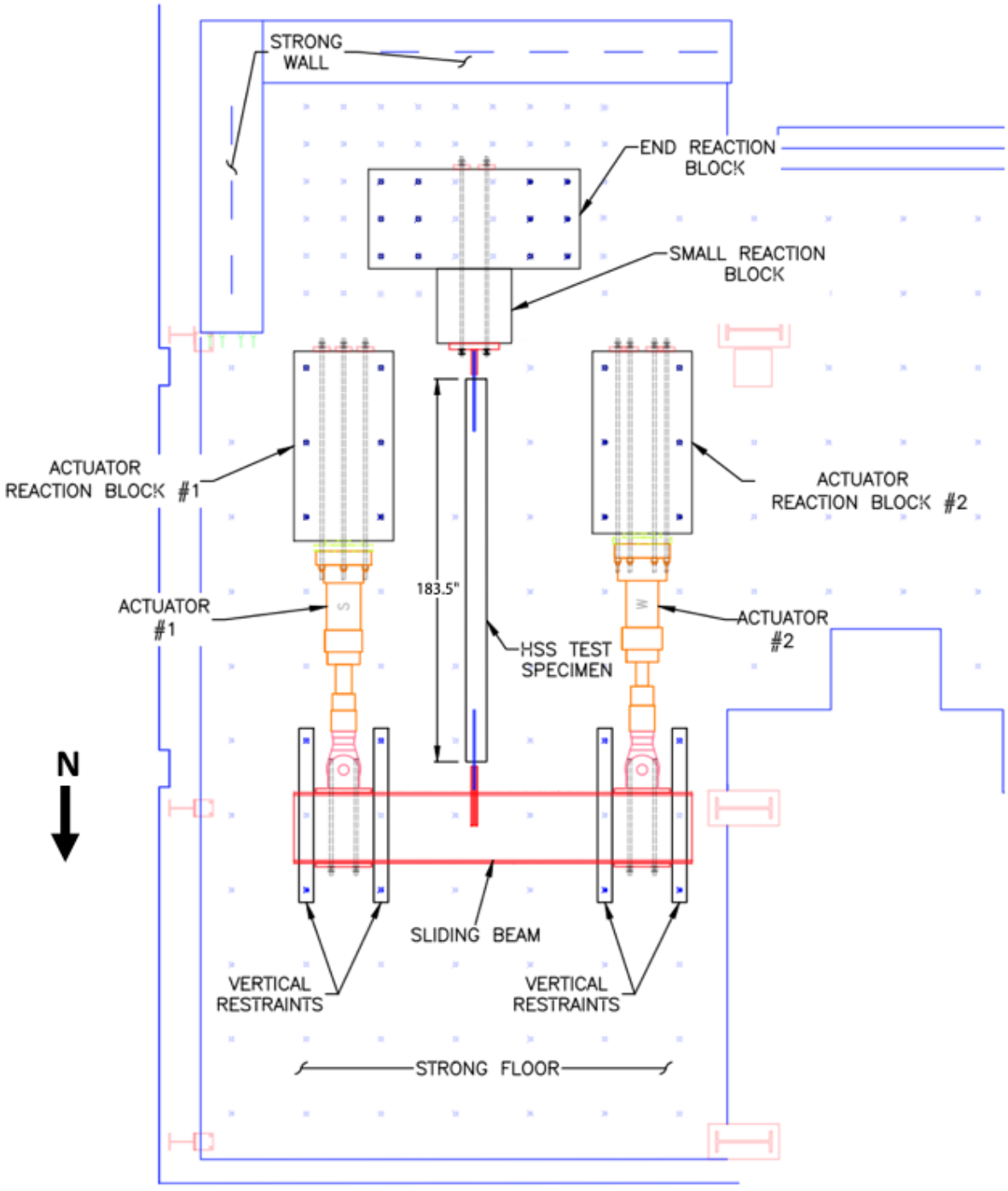

Figure 3.2. Overview of Test Frame for 183.5” Long Specimens

3.2.2 *Horizontal Loading System*

Two hydraulic actuators were used in parallel to apply axial forces to the test specimens. These actuators were positioned 12 feet apart horizontally, measured center-to-center of each actuator, and aligned parallel to the test specimen in the north-south direction. This spacing provided adequate room for the out-of-plane buckling displacements of the test specimens.

Figure 3.3 Orientation of Actuators and Sliding Beam

The two hydraulic actuators had different capacities corresponding to a capacity ratio of 9:7. At a hydraulic pressure of 3000 psi, the larger actuator (Actuator 1, Figure 3.1) had a capacity of 450 kips in compression and 375 kips in tension, while the smaller actuator (Actuator 2, Figure 3.1) had a capacity of 350 kips in compression and 275 kips in tension. The orientation of the test setup resulted in the actuators' compressive capacity corresponds to the tensile capacity of the brace, and vice versa. To accommodate larger specimens, the hydraulic pump pressure was increased, resulting in a system capacity of almost 1000 kips when the brace is subjected to tension (actuator pushing) and 700 kips when the brace is subjected to compression (actuator pulling).

Due to their different capacities, the actuators were positioned asymmetrically to optimize performance. As shown in Figure 3.4, the larger actuator was placed 63 inches from the specimen's center, and the smaller actuator 81 inches away. This spacing ratio allowed the setup to fully utilize the maximum compressive capacities of both actuators and ensured the axial

forces were applied to the specimen without a bending moment, preventing rotation of the sliding beam.

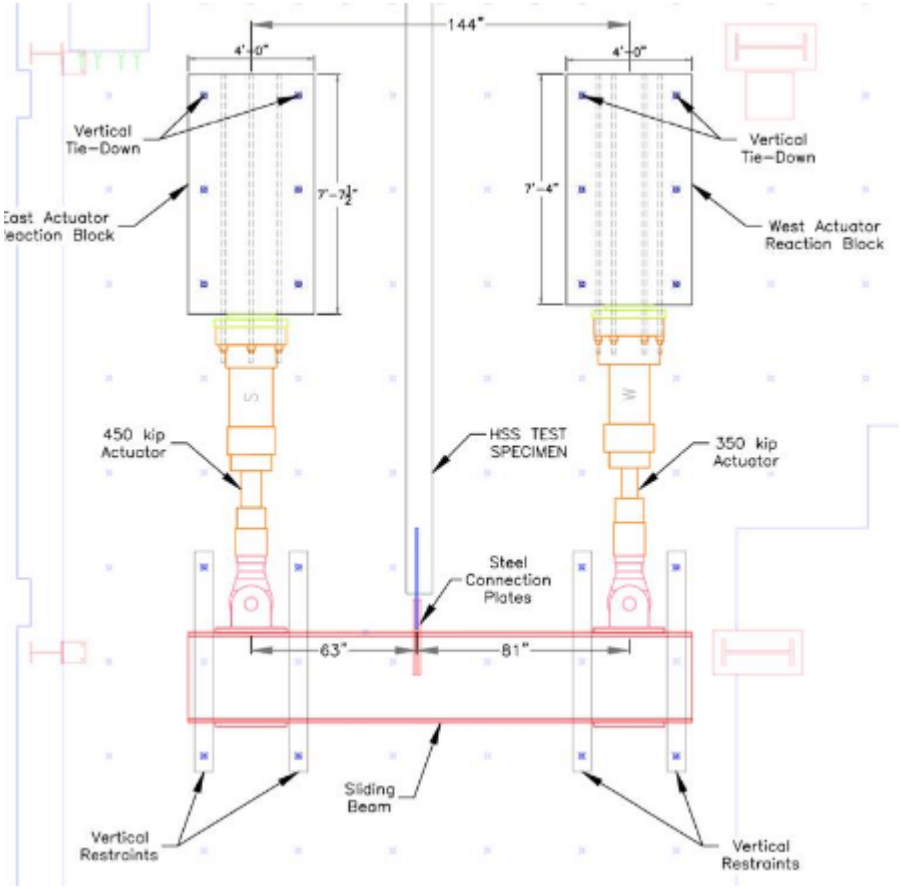

Figure 3.4 Layout of Actuators and Sliding beam

The actuators were anchored to the strong floor through stationary concrete reaction blocks. Each block was anchored to the strong floor with six 1-3/4 in diameter 150 ksi threaded bars and a layer of hydrostone to create a monolithic surface between the block and floor. The bars were post-tensioned to 200 kips.

The actuators were connected to the concrete reaction blocks via a connection assembly that consisted of six 1-1/4 in diameter 150 ksi threaded bars, a 3 in thick steel plate, and 2 in thick elastomeric cotton duct bearing pad. The threaded bars were post tensioned to 100 kips

each to prevent fatigue of the rods while the actuators were loaded to capacity in tension. The steel plate provided a solid bearing surface at the base of the actuator. Between the steel plate and the reaction block, the cotton duck bearing pad permitted small actuator rotation to ensure the actuators were not damaged during testing. This assembly and base plate layout can be seen below in Figure 3.5 and Figure 3.6.

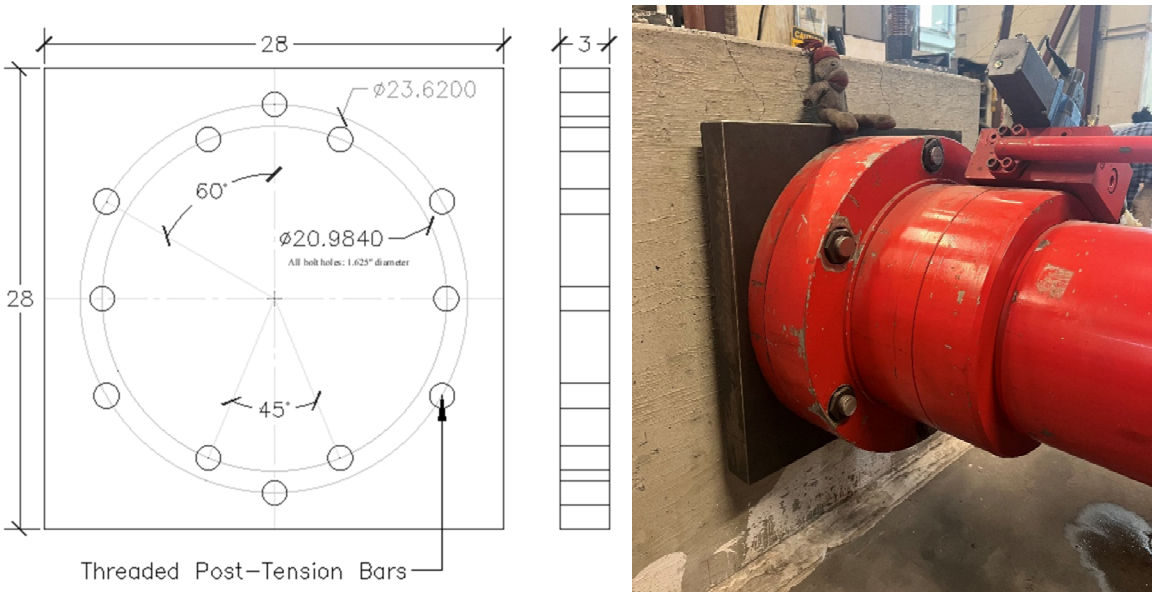

(a) (b)

Figure 3.5 Actuator Base Plate Design (a) and Layout (b)

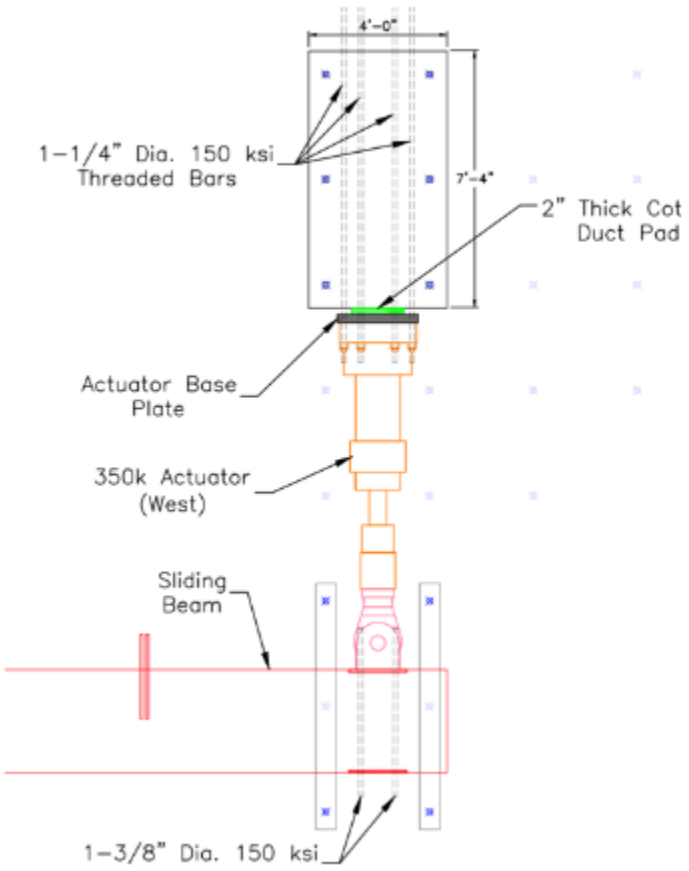

Figure 3.6 Actuator Assembly and Connections

3.2.3 *Sliding Beam Design*

The sliding beam was designed to be very stiff and strong to minimize flexural and shear deformations withstand the large bending and shear demands while the applied actuator loads were being transferred to the specimen. The high stiffness made it so that the actuator displacements were approximately equal to brace axial displacements. The sliding beam was a concrete filled steel beam built up of a 16-foot-long W33x201 beam with ¾ in thick steel plates welded to its flanges. The box section in Figure 3.7 was filled with concrete to increase the bending stiffness.

Figure 3.7 Sliding beam

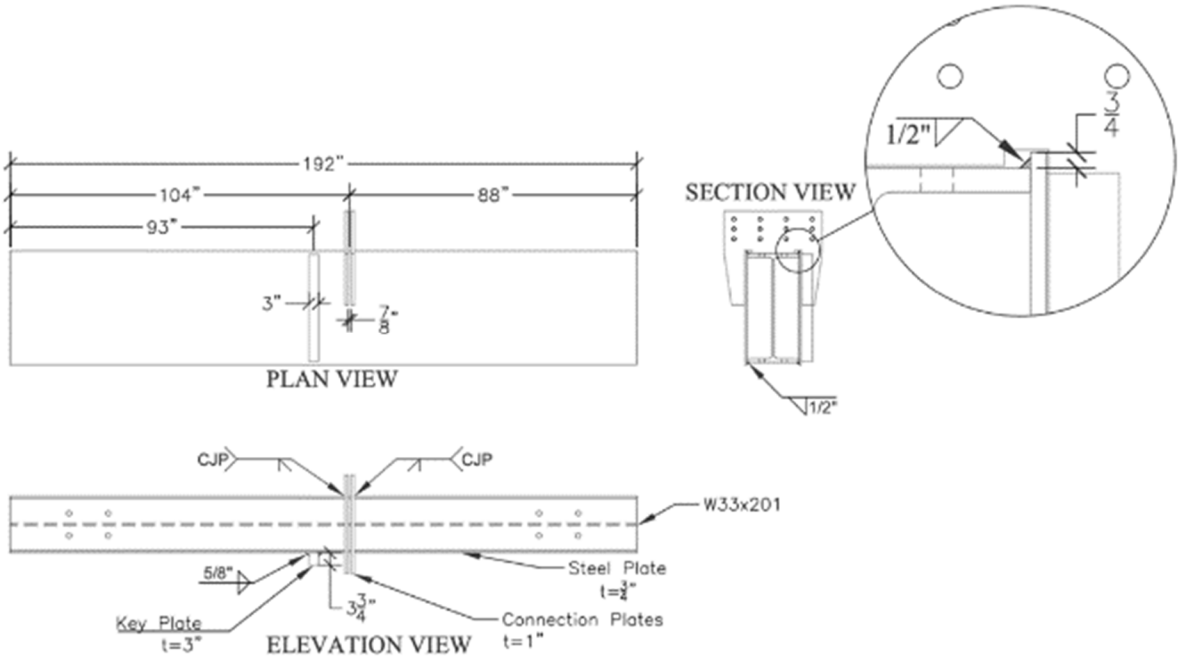

Figure 3.8 Sliding Beam Dimensions

Four vertical restraints were used to support the sliding beam and resist any vertical movement. The bottom support was made up of a 4x4x3/8 HSS welded to the top of a 14-inch deep wide-flange beam, which was anchored to the strong floor with 1-inch diameter steel threaded rods. A 6x6x1/4 HSS served as the top restraint and was connected to the bottom support using 1-inch poet-tensioned threaded rods. 1-1/4-inch diameter holes were drilled through the top HSS, bottom HSS, and wide-flange beam to allow the threaded rods to pass from the top of the top HSS through to the bottom of the wide-flange's upper flange. A greased Polytetrafluoroethylene (PTFE) and stainless-steel interface created a nearly frictionless sliding

surface for the sliding beam to move. The resistance due to friction was less than 1 kip. This assembly can be seen below in Figure 3.9.

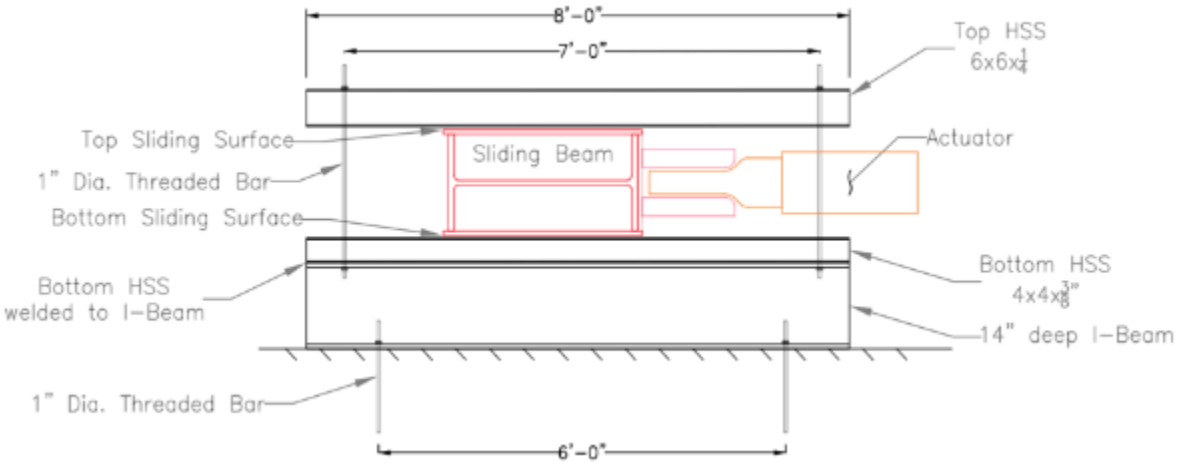

Figure 3.9 Cross-Sectional View of Sliding Beam and Vertical Restraint System

The key and keyway system, illustrated in Figure 3.10, was designed to prevent lateral movement. The "key" was a 3-inch thick, 3.5-inch-deep rectangular steel section welded to the underside of the sliding beam. The "keyway" consisted of a 4-inch-thick steel plate welded to a 3-inch-thick floor plate, which was anchored to the strong floor with four 1-3/4-inch diameter, 150 ksi threaded bars, each prestressed to 200 kips. This setup allowed the key to move freely in the north-south direction through the keyway, with a 3/8-inch gap on each side to reduce friction. However, if the sliding beam shifted laterally in the east-west direction, the key would engage the keyway to prevent any lateral movement.

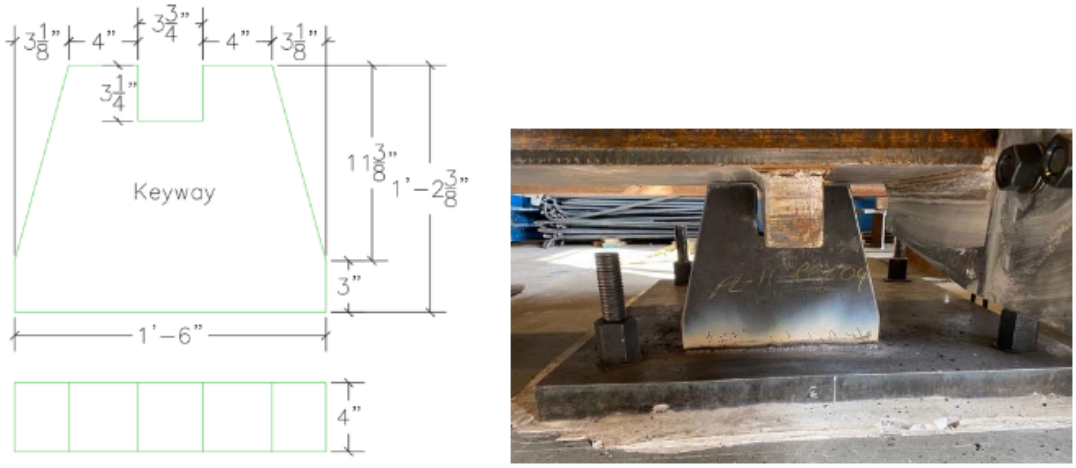

(a) (b)

Figure 3.10 Keyway Plate Dimensions (a) and Keyway Plate Welded in Place (b)

The gusset plate of the test specimens were bolted to the connection plates detailed below in Figure 3.11. The connection plates consisted of two 1-inch-thick plates welded along the top, side, and bottom to the sliding beam. A 7/8-inch gap was between the connection plates to accommodate various sized gusset plates. Any additional space was filled using steel shim plates for a tight connection. Each connection plate had twelve 1-1/8-inch diameter bolt holes, aligned to match the bolt pattern of the gusset plate.

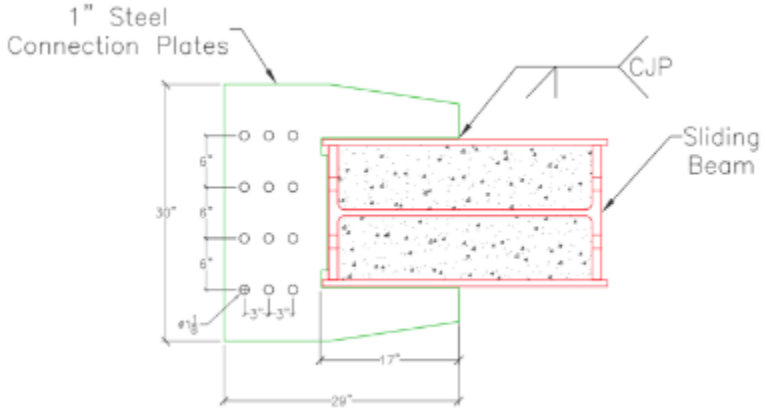

Figure 3.11 Sliding Beam Connection Plate

3.2.4 *End Reaction Block and End Connection Plate Design*

The end reaction block shown in Figure 3.12 needed to resist the combined actuator force of 1000 kips. On the south end of the strong floor, there is a smaller spacing (18 in.) of anchor

holes which provided locations for twelve tie-down rods. To resist the combined actuator force, twelve 1-3/4-inch diameter 150 ksi tie down rods were stressed to 200 kips each. Prior to stressing, the reaction blocks were placed over a layer of hydrostone to create a uniform bearing surface between the block and the floor.

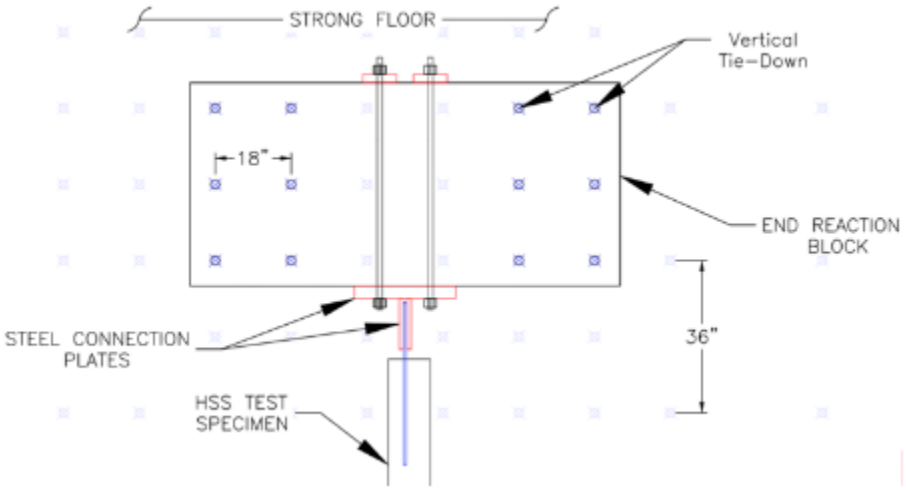

Figure 3.12. Layout of South End of Test Frame

The long brace length specimens used the configuration shown in Figure 3.12 and Figure 3.13. A small reaction block was added to the test setup to accommodate the short brace length. Figure 3.14 below shows the short brace length configuration. The small reaction block was 36-inches wide by 36-inches long and 41-inches tall. Eight horizontal rods ran through the steel connection plate, small reaction block, and south reaction block. The eight horizontal rods were 1-3/8-inch diameter 150 ksi treaded bars stressed to 180 kips each. This provided a prestressing force of 1440 kips which exceeded the maximum demand of 1000 kips. This also prevented movement of the connection plate relative to the block to prevent fatigue in the threaded bars during cyclic loading.

Figure 3.13. End Reaction Block, Long Brace Length Configuration

Figure 3.14. End Reaction Block with Added Spacer Block, Short Brace Length Configuration

The steel end connection plate used to connect the gusset plate of the specimen to the test setup consisted of two 1-inch connection plates welded to a 3-inch steel plate as seen in Figure 3.15. The two connection plates were spaced 7/8-inches apart for the gusset plate connection. The connection plates had the same twelve bolt hole layout as the north connection plates. Eight 1-3/8-inch diameter 150 ksi threaded rods were used to connect the steel connection plate to the south reaction block.

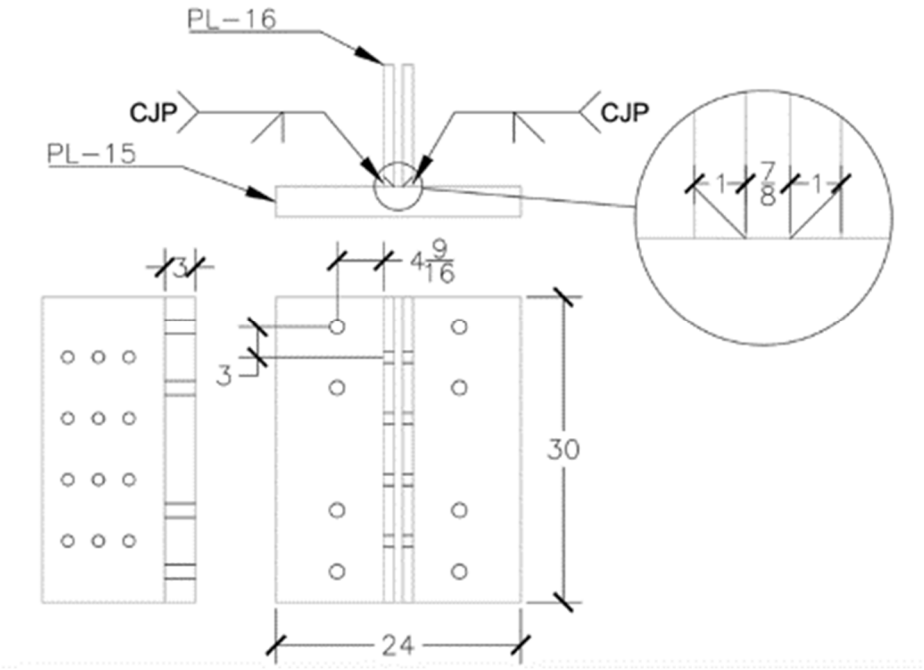

Figure 3.15. End Connection Plate Details

3.3 Test Matrix and Specimen Design

3.3.1 *Overview*

Thirty tests were completed at the University of Washington Structural Research Lab (UW SRL) in two test series. This test program built on previous research completed by Bergendahl (Bergendahl, 2021) and Kaldestad (Kaldestad, 2022). That research focused on the differences in behavior for A500 and A1085 square HSS braces from different manufactures and consisted of ten and twenty-five tests, respectively.

The focus of this research effort was to: (1) expand the dataset for A500 square HSS braces to include a larger range of local slenderness values and (2) to develop a new dataset for

round A500 HSS braces. All the braces tested were fabricated from A500 B/C steel (i.e., dual certified for both Grade B and C). Various HSS sections were selected based on their local compactness ratio, global slenderness ratio, and availability from producers. The expected brace tensile capacity had to be less than 1000 kips – the capacity of the actuators in the test setup.

The focus of previous test data was square HSS specimens with local slenderness values less than 20. Test series 1 shown in Table 3.1 was selected to extend the dataset to include *b/t* values up to 31.5. The length of specimens was selected based on test set-up geometric limitations and lobal slenderness ratios expected to be used in design of SCBFs and OCBFs. The specimens in this test series included braces at the 183.5" and 219.5" brace lengths which resulted in L_c/r values of 93.6 or less. The braces were subjected to a symmetric cyclic loading protocol with increasing displacements.

Table 3.1 Square Specimens - Test Series 1

Section	b/t	L_c/r
HSS5x5x3/16	25.7	93.6
HSS6x6x3/16	31.5	70.1
HSS6x6x3/16	31.5	77.4
HSS6x6x1/4	22.8	78.4
HSS6x6x1/4	22.8	79.8
HSS7x7x1/4	27.0	66.7
HSS7x7x1/4	27.0	93.8
HSS8x8x5/16	24.5	58.3
HSS8x8x5/16	24.5	92.6

Table 3.2 lists the Round HSS specimens that comprise Test Series 2, which included braces at the short and long brace length. The overall goal of this test series was to establish a new dataset for round HSS over a large range of *D/t* and L_c/r to update local and global slenderness limits in AISC 341. The selected brace sections resulted in a range of *D/t* values from 14.2 to 46.1. The *D/t* of the braces were selected so that there was a range of *D/t* that spanned and extended beyond the current limits in AISC 341-22 Table D1.1a. Similarly, the specimen lengths provided a range of L_c/r values that reasonably bounded the values expected in practice for SCBFs and OCBFs.

Table 3.2 Round Specimens - Test Series 2

Section	D/t	L_c/r
HSS6x3/16	34.5	89.1
HSS6x3/16	34.5	106.6
HSS6x1/4	25.8	90.0
HSS6x1/4	25.8	107.6
HSS6.625x3/16	38.1	96.3
HSS6.625x1/4	28.4	81.2
HSS6.625x1/4	28.4	97.1
HSS6.625x3/8	19.0	82.7
HSS6.625x3/8	19.0	98.9
HSS6.625x1/2	14.2	84.2
HSS6.625x1/2	14.2	100.7
HSS8.625x3/16	49.6	61.4
HSS8.625x3/16	49.6	73.4
HSS8.625x1/4	37.0	61.8
HSS8.625x1/4	37.0	73.9
HSS8.625x3/8	24.7	62.6
HSS8.625x3/8	24.7	74.9
HSS10.750x1/4	46.1	49.3
HSS10.750x1/4	46.1	59.0
HSS10.750x0.365	31.7	49.9
HSS10.750x0.365	31.7	59.6

The expected yield and critical buckling loads of all the tested specimens are listed below in Table 3.3. While the expected yield force does not depend on the brace length, the critical buckling load does vary with brace length. The values shown for the expected critical buckling force are for the short brace length – 183.5”, while the values shown in parentheses are the critical buckling force for the long brace length – 219.5”. The forces calculated in this table were found using nominal values of cross-sectional area, yield strength, and the ratio of expected to nominal strength, R_y, as defined in ASIC 341-22 (AISC 2022).

Table 3.3 Test Specimen Expected Tensile and Compressive Capacity

HSS Shape	Expected Yield Force, $P_{y,e}$ (kips)	Expected Critical Buckling Force, $P_{cr,e}$ (kips)
5x5x3/16	213	106
6x6x3/16	259	167 (131)
6x6x1/4	341	217 (168)
7x7x1/4	401	300 (250)
8x8x5/16	569	468 (407)
6x3/16	207	111 (80)
6x1/4	274	145 (104)
6.625x3/16	229	(108)
6.625x1/4	304	185 (142)
6.625x3/8	447	266 (201)
6.625x1/2	585	340 (254)
8.625x3/16	300	239 (205)
8.625x1/4	399	317 (271)
8.625x3/8	590	463 (394)
10.750x1/4	501	453 (410)
10.750x0.365	722	650 (587)

3.3.2 *Layout and Connection Design*

The test specimens were cut to length from the stock length tube using a horizontal band saw and slotted at both ends using a plasma cutter. The cut-to-length specimens were welded to gusset plates which were connected to the reaction block and sliding beam through steel connection plates and twelve 1-inch diameter A490 bolts. The test specimen detailed in Figure 3.16 is the final layout before testing. The length noted in this figure is the end-to-end brace length that was equal to the 183.5” and 219.5” test specimen lengths.

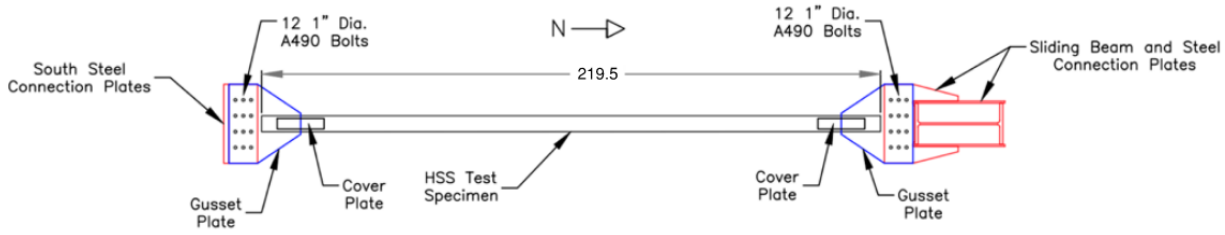

Figure 3.16 Test Specimen Layout

To control the direction of out-of-plane buckling, the gusset plate was placed a distance of 3/16 in. from the center of the brace. The eccentricity was intended to control the direction of buckling without compromising the compressive strength. Control of the buckling direction was necessary to prevent the brace from hitting the actuator reaction blocks with large out-of-plane buckling deformation and to provide a more efficient use of instrumentation. In previous testing, a ratio of slot eccentricity to radius of gyration (e/r) equal to 0.1 was used as the slot eccentricity (Bergendahl, 2021). After reviewing the data, it became apparent that specimens with larger radius of gyration and larger eccentricity had a more substantial reduction in buckling strength. The smallest eccentricity used in previous testing that still forced the direction of buckling was 3/16”. Initial imperfections of the tube could also affect the buckling direction so a measurement of the imperfection at midspan was taken as shown below in Figure 3.17. A thin wire was connected to the top and bottom of the specimen. The perpendicular distance from the wire to the outer face of the tube was summarized for each specimen in Table 3.4. The brace was slotted on both ends perpendicular to the face of the brace with the largest imperfection such that the imperfection was essentially additive with the eccentricity to promote buckling in the desired direction.

Figure 3.17 Measurement of Imperfection at Midspan

Table 3.4 Summary of Midspan Imperfections

	Imperfection (in.)	
HSS Shape	**183.5" Brace Length**	**219.5" Brace Length**
5x5x3/16	0.10	-
6x6x3/16	0.05	0.10
6x6x1/4	0.02	0.06
7x7x1/4	0.02	0.03
8x8x5/16	0.05	0.03
6x3/16	0.02	0.05
6x1/4	0.22	0.27
6.625x3/16	-	0.12
6.625x1/4	0.06	0.10
6.625x3/8	0.20	0.30
6.625x1/2	0.05	0.10
8.625x3/16	0.05	0.10
8.625x1/4	0.05	0.05
8.625x3/8	0.02	0.08
10.750x1/4	0.05	0.05
10.750x0.365	0.02	0.05

The trapezoidal shaped gusset plate was designed considering the following limit states: yielding on the gross area, tensile rupture, block shear, bearing and tear out, and buckling. The summary of gusset plate and gusset plate-to-brace weld design for each brace size can be found in Table 3.5. The gusset plates were designed to create pinned ends to allow for rotation at the ends while the brace buckles. The clearance between the end of the brace and the steel connection plates is equal to three times the gusset plate thickness. The gusset plates were fit into the test setup with thin steel shim plates to create a tight fit before bolting. Twelve 1" A490 tension-controlled bolts were used to connect the specimen the fixed reaction block and the sliding beam. The bolt layout is shown in Figure 3.18. The prestressed bolted connection was designed to be slip-critical; however, significant cyclic axial loads caused the bolts to slip during each test. Generally, the connection slipped only once under tension, but for some of the larger members, it experienced multiple slips due to the substantial forces in both tension and compression.

Table 3.5 Summary of Gusset Plate and Weld Design

	Gusset Plate		**Fillet weld**	
HSS Shape	**Length (in.)**	**Thickness (in.)**	**Length (in.)**	**Size (in.)**
5x5x3/16	27.75	0.25	15.0	3/8
6x6x3/16	27.75	0.25	15.0	3/8
6x6x1/4	30.125	0.375	17.0	3/8
7x7x1/4	30.125	0.375	17.0	3/8
8x8x5/16	31.5	0.5	18.0	3/8
6x3/16	25.75	0.25	13.0	3/8
6x1/4	25.75	0.25	13.0	3/8
6.625x3/16	25.75	0.25	13.0	3/8
6.625x1/4	25.75	0.25	13.0	3/8
6.625x3/8	30.125	0.375	17.0	3/8
6.625x1/2	31.5	0.5	18.0	3/8
8.625x3/16	30	0.313	17.0	3/8
8.625x1/4	30.125	0.375	17.0	3/8
8.625x3/8	34.5	0.5	21.0	3/8
10.750x1/4	34.5	0.5	21.0	3/8
10.750x0.365	35.875	0.625	22.0	3/8

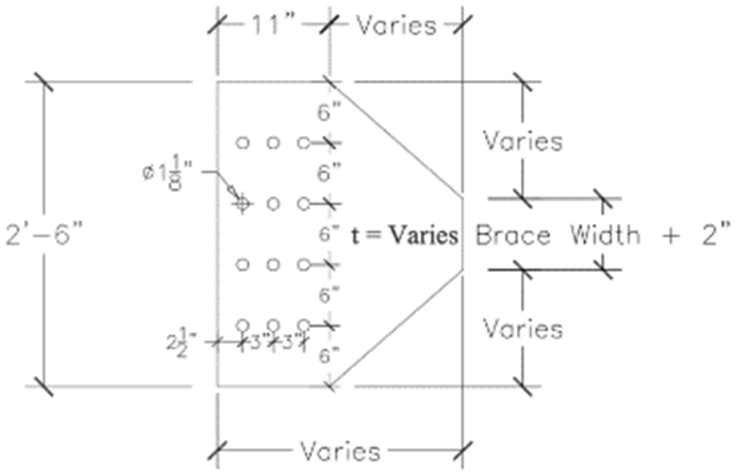

Figure 3.18 Gusset Plate Design

To prevent net section rupture at the reduced slotted cross-section, net section plates were designed and welded to the HSS. The net section plate was 3/8" thick and welded to the brace with ¼" fillet welds. These welds were designed to have a capacity equal to that of the reinforcement plate on each side of the end of the slot. The dimensions of the net section reinforcement plates are shown in Table 3.6.

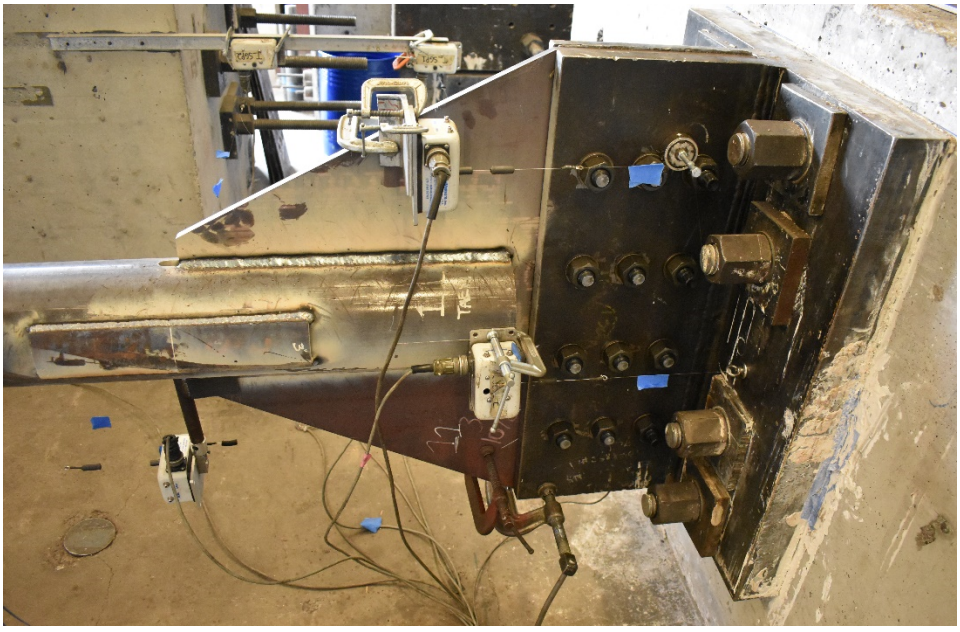

Figure 3.19 Connection Region Before Testing

Table 3.6 Summary of Net Section Reinforcement Design

	Net Section Reinforcement Plate	
HSS Shape	**Length (in.)**	**Width (in.)**
5x5x3/16	12	2.5
6x6x3/16	16	3.5
6x6x1/4	16	3.5
7x7x1/4	17	4.0
8x8x5/16	17	4.0
6x3/16	14	3.0
6x1/4	14	3.0
6.625x3/16	14	3.0
6.625x1/4	14	3.0
6.625x3/8	14	3.0
6.625x1/2	14	3.0
8.625x3/16	16	3.5
8.625x1/4	16	3.5
8.625x3/8	16	3.5
10.750x1/4	18	4.0
10.750x0.365	18	4.0

3.4 Test Specimen Properties

The ductility of a brace refers to its capacity to withstand inelastic deformations while maintaining sufficient strength. Previous research has shown that the inelastic behavior of HSS is mainly affected by the section's local width-to-thickness and global slenderness ratio (Kaldestad, 2022). With the objective to evaluate the current ductility limits in AISC 341-22, these two parameters were the basis of how HSS sections were selected in this research.

The nominal width-to-thickness ratios of the square specimens are summarized in Table 3.7. The nominal width-to-thickness ratios in Table 3.7 and Table 3.8 are color-coded based on what limits they do, or do not satisfy in AISC 341-22 Table D1.1a. Green indicates HSS that meet the criteria for highly ductile braces, orange represents HSS that meet the standards for moderately ductile braces, and red signifies HSS that fails to meet either of the limits specified in The Seismic Provisions. The current moderately ductile limit in accordance with the seismic

provisions with an F_y = 50ksi and R_y = 1.3 is 16.1. Since all the sections in this test series had a b/t greater than this limit, they are highlighted red. Previous research focused on investigating sections with b/t less than 20.

Table 3.7 Nominal Width-to-Thickness Ratio - Test Series 1

Section	b/t
HSS5x5x3/16	25.7
HSS6x6x3/16	31.5
HSS6x6x1/4	22.8
HSS7x7x1/4	27.0
HSS8x8x5/16	24.5

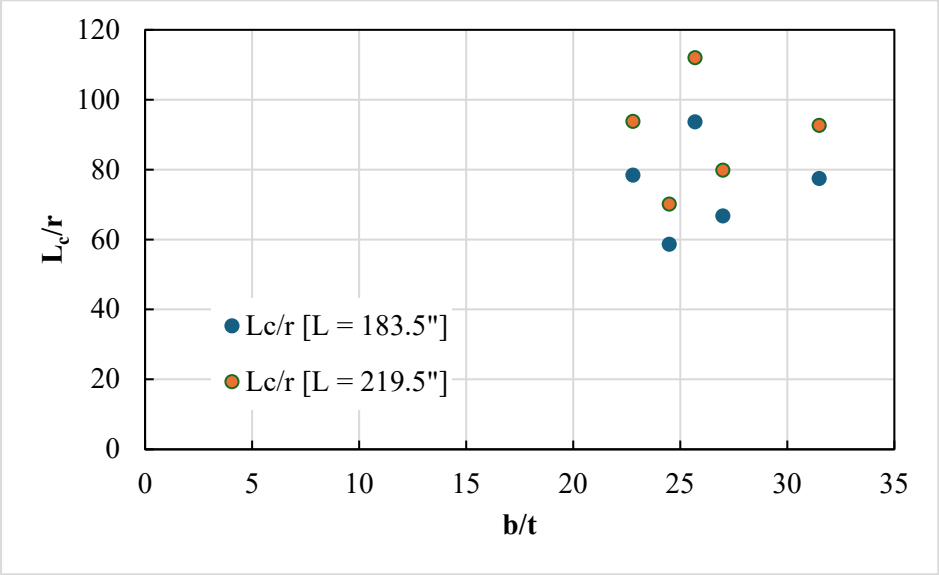

Figure 3.20 Global Slenderness, Lc/r versus Local Slenderness, b/t - Test Series 1

Below in Table 3.8, the width-to-thickness ratios of test series 2 are summarized. Because of the lack of previous test data on round HSS, the *D/t* of the braces were selected so that there was a range of *D/t* that spanned and extended beyond the current limits. A wide range of global slenderness ratios were selected to get data to explore the effect of L_c/r on the performance of the brace. The relationship between the local and global slenderness ratios of the selected test sections can be seen below in Figure 3.21.

Table 3.8 Nominal Diameter-to-Thickness Ratio - Test Series 2

Section	D/t
HSS6x3/16	34.5
HSS6x1/4	25.8
HSS6.625x3/16	38.1
HSS6.625x1/4	28.4
HSS6.625x3/8	19.0
HSS6.625x1/2	14.2
HSS8.625x3/16	49.6
HSS8.625x1/4	37.0
HSS8.625x3/8	24.7
HSS10.750x1/4	46.1
HSS10.750x0.365	31.7

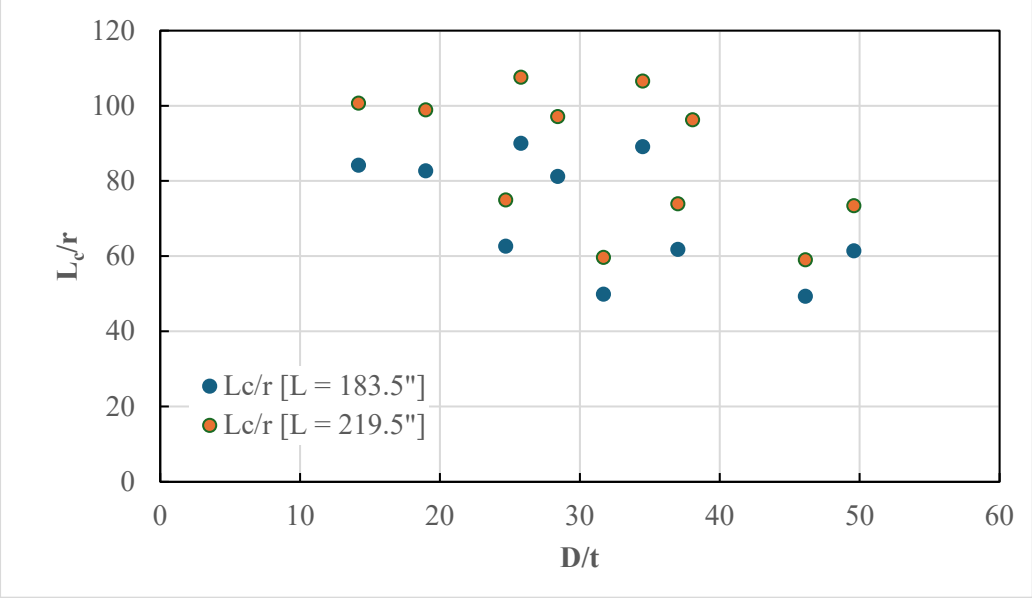

Figure 3.21 Global Slenderness, Lc/r versus Local Slenderness, D/t - Test Series 2

3.4.1 *Geometric Properties*

The geometric properties of all the test specimens were measured and summarized in Table 3.9 which included a comparison of measured and nominal properties. The width and thickness of each specimen was measured using a dial caliper at multiple locations along the specimen. The nominal thickness of the braces was used for the comparison between t_{meas}/t_{nom}.

The design thickness is used in AISC calculations for *b/t* and *D/t* that are shown below. Almost all the ratios between measured and nominal values for thickness and width-to-thickness are within ±5%. All the square specimens had a larger measured width-to-thickness ratio than nominal values; However, almost all the round specimens had a smaller diameter

Table 3.9 Summary of Nominal and Measured Geometric Properties

Test Specimen	Nominal Area, A_g (in^2)	Nominal, t_{nom} (in)	Measured , t_{meas} (in)	t_{meas}/t_{nom}	Nominal, b/t_{nom}, D/t_{nom}	Measured, b/t_{meas}, D/t_{meas}	$b/t_{meas}/b/t_{nom}$, $D/t_{meas}/D/t_{nom}$
5x5x3/16 Short	3.28	0.174	0.190	1.09	25.7	26.5	1.03
6x6x3/16 Short	3.98	0.174	0.181	1.04	31.5	33.2	1.05
6x6x3/16 Long	3.98	0.174	0.187	1.07	31.5	32.2	1.02
6x6x1/4 Short	5.24	0.233	0.231	0.99	22.8	26.1	1.14
6x6x1/4 Long	5.24	0.233	0.240	1.03	22.8	25.1	1.10
7x7x1/4 Short	6.17	0.233	0.232	1.00	27.0	30.3	1.12
7x7x1/4 Long	6.17	0.233	0.239	1.03	27.0	29.4	1.09
8x8x5/16 Short	8.76	0.291	0.287	0.99	24.5	27.9	1.14
8x8x5/16 Long	8.76	0.291	0.310	1.07	24.5	25.8	1.05
6x3/16 Short	3.18	0.174	0.195	1.12	34.5	30.8	0.89
6x3/16 Long	3.18	0.174	0.176	1.01	34.5	34.1	0.99
6x1/4 Short	4.22	0.233	0.245	1.05	25.8	24.5	0.95
6x1/4 Long	4.22	0.233	0.243	1.04	25.8	24.7	0.96
6.625x3/16 Long	3.53	0.174	0.181	1.04	38.1	36.7	0.96
6.625x1/4 Short	4.68	0.233	0.237	1.02	28.4	28.0	0.99
6.625x1/4 Long	4.68	0.233	0.242	1.04	28.4	27.4	0.96
6.625x3/8 Short	6.88	0.349	0.353	1.01	19.0	18.8	0.99
6.625x3/8 Long	6.88	0.349	0.351	1.01	19.0	19.0	1.00
6.625x1/2 Short	9.00	0.465	0.473	1.02	14.2	14.1	0.99
6.625x1/2 Long	9.00	0.465	0.462	0.99	14.2	14.5	1.02
8.625x3/16 Short	4.62	0.174	0.187	1.07	49.6	46.1	0.93
8.625x3/16 Long	4.62	0.174	0.199	1.14	49.6	43.4	0.88
8.625x1/4 Short	6.14	0.233	0.233	1.00	37.0	37.1	1.00
8.625x1/4 Long	6.14	0.233	0.243	1.04	37.0	35.6	0.96
8.625x3/8 Short	9.07	0.349	0.345	0.99	24.7	25.0	1.01
8.625x3/8 Long	9.07	0.349	0.354	1.01	24.7	24.4	0.99
10.750x1/4 Short	7.15	0.233	0.232	1.00	46.1	46.4	1.01
10.750x1/4 Long	7.15	0.233	0.249	1.07	46.1	43.2	0.94
10.750x0.365 Short	11.1	0.339	0.339	1.00	31.7	31.8	1.00
10.750x0.365 Long	11.1	0.339	0.349	1.03	31.7	30.8	0.97

3.4.2 *Material Properties*

Tension tests were performed in the UW SRL to compare measured, nominal, and provided mill certification data. A laser extensometer and YFLA strain gauges were applied to each coupon specimen to collect data. A 2" gauge length was used for the laser extensometer to calculate percent elongation. Data processed from the coupon tests can be found in Table 3.10. A nominal value of 50 ksi and 62 ksi were used for yield stress and tensile stress respectively to calculate measured yield and tensile overstrength. For comparison, AISC 341-22 Table A3.2 specifies values of R_y equal to 1.3 and R_t equal to 1.2 for A500 Gr. C steel. The average ratio of over all the tested sections is similar to the AISC specified values the ratio of expected to nominal strength. All the measured yield strengths were at least ten percent higher than the specified nominal value.

Table 3.10 Summary of Material Testing Properties

HSS Shape	Measured Yield Strength, $F_{y,m}$ (ksi)	Measured Yield Strength Ratio, $R_{y,m}$	Measured Tensile Strength, $F_{u,m}$ (ksi)	Measured Tensile Strength Ratio, $R_{t,m}$	Percent Elongation (%)
5x5x3/16	71.6	1.4	83.1	1.3	31.6
6x6x3/16	58.9	1.2	80.5	1.3	30.2
6x6x1/4	64.7	1.3	78.6	1.3	31.3
7x7x1/4	64.1	1.3	78.8	1.3	30.3
8x8x5/16	64.3	1.3	75.8	1.2	34.2
6x3/16	53.6	1.1	73.4	1.2	33.2
6x1/4	54.2	1.1	71.6	1.2	40.5
6.625x3/16	56.5	1.1	76.8	1.2	34.8
6.625x1/4	59.0	1.2	74.6	1.2	36.2
6.625x3/8 *	58.3	1.2	63.7	1.0	-
6.625x1/2	63.7	1.3	66.0	1.1	36.7
8.625x3/16	69.5	1.4	81.6	1.3	29.5
8.625x1/4	67.0	1.3	79.5	1.3	30.3
8.625x3/8	65.7	1.3	75.2	1.2	36.0
10.750x1/4	62.7	1.3	74.8	1.2	34.2
10.750x0.365	60.4	1.2	77.0	1.2	35.6

*Percent elongation gauge length varies from standard 2"

3.5 Loading Protocol

As mentioned in Section 3.2.2, two hydraulic actuators, working in parallel, were used to apply cyclic axial displacements to the sliding beam while the opposite end remained fixed in place. These actuators operated under a displacement-controlled loading protocol using MTS MultiPurpose TestWare (MPT) Software. Under the displacement control of the actuators, this setup prevented rotational movement at the end of the brace.

Before each test, two cycles of ±1/16" displacements were applied to the specimen. Data was collected in the data acquisition system and reviewed to ensure proper functioning of the instrumentation prior to the actual displacement procedure. During testing, one of the displacement-controlled load histories detailed in this section was followed until specimen failure. The loading protocol was paused throughout testing to take pictures and make observations.

Previous test data by Kaldestad (Kaldestad, 2022) included test series that were subjected to displacement protocols which mimicked near fault and chevron loading conditions in addition to a symmetric based loading protocol. For the same brace, minimal variance in axial deformation range was seen between loading protocols. The symmetric displacement protocol was developed based on previous research at the UW SRL and recommendations for testing components of steel structures (ATC, 1992, Krawinkler, 2009). All braces in this research were subjected to a symmetric loading protocol.

Figure 3.22 and Figure 3.23 show the two loading protocols utilized in this research. Cycles started by pulling the brace into tension until the target displacement and then reversed into compression to the same magnitude of target displacement. Two full cycles were conducted for each target displacement. The first six target displacements were small steps of 1/8" to observe the elastic behavior of the brace, initial global buckling, and yielding. The small steps increased until 0.75" after which target displacement steps increased to 0.5" every change in target displacement until brace failure. The 183.5" braces were subjected to this displacement protocol which is noted below in Figure 3.22.

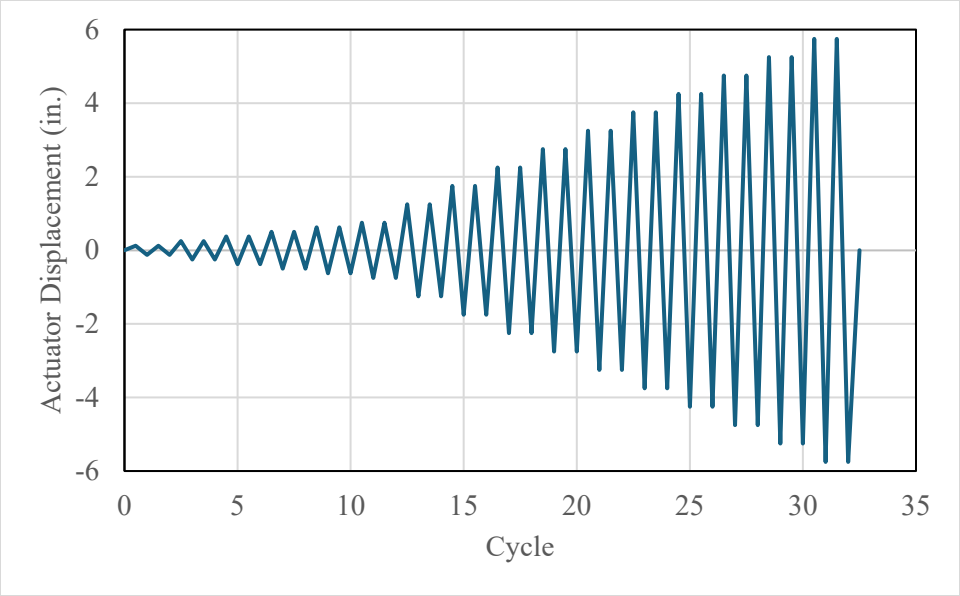

Figure 3.22 Symmetric Displacement Protocol – Type 1

To adjust for the variation in brace length, the type 2 protocol depicted in Figure 3.23 was created. This adjustment was used halfway through testing the 219.5” specimens. In previous research by Kaldestad (Kaldestad, 2022), a long brace length of 237.5” was used instead of 219.5”. To compare previous data to data in this research phase, the ratio between 219.5 and 237.5 was used to scale down the loading protocol found in Figure 3.22. Table 3.11 provides a summary of which loading protocol each specimen was subjected to.

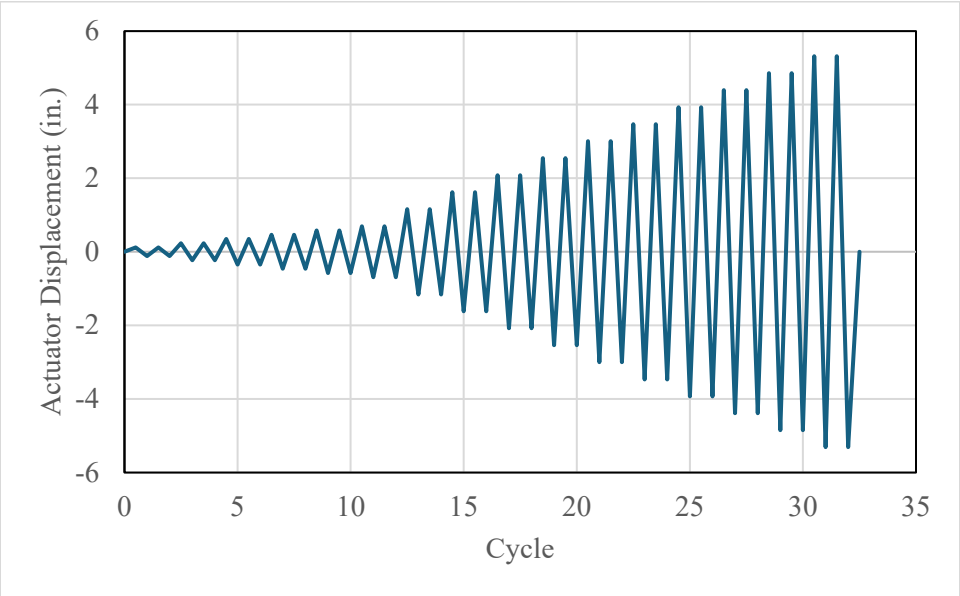

Figure 3.23 Symmetric Displacement Protocol - Type 2

Table 3.11 Summary of Test Procedure Types

Test Specimen	Test Procedure Type
5x5x3/16 Short	1
6x6x3/16 Short	1
6x6x3/16 Long	2
6x6x1/4 Short	1
6x6x1/4 Long	2
7x7x1/4 Short	1
7x7x1/4 Long	2
8x8x5/16 Short	1
8x8x5/16 Long	2
6x3/16 Short	1
6x3/16 Long	2
6x1/4 Short	1
6x1/4 Long	2
6.625x3/16 Long	2
6.625x1/4 Short	1
6.625x1/4 Long	2
6.625x3/8 Short	1
6.625x3/8 Long	2
6.625x1/2 Short	1
6.625x1/2 Long	2
8.625x3/16 Short	1
8.625x3/16 Long	1
8.625x1/4 Short	1
8.625x1/4 Long	1
8.625x3/8 Short	1
8.625x3/8 Long	1
10.750x1/4 Short	1
10.750x1/4 Long	1
10.750x0.365 Short	1
10.750x0.365 Long	2

3.6 Test Instrumentation

Multiple instruments were utilized to collect data on forces, displacements, and strains during testing. The devices used during testing included string potentiometers, Duncan potentiometers, strain gauges, load cells, Linear Variable Differential Transformers (LVDTs), and Optotrak sensors. LabVIEW, a software by National Instruments, was used to collect data from the potentiometer, strain gauges, load cells, and LVDTs. Northern Digital Inc. First

Principles software was used to collect data from the Optotrak sensors. This section provides further details on the instruments and their specific locations during testing.

3.6.1 *Load Cells and LVDTs*

The loads applied by the two actuators were monitored by internal load cells. The load cell data was used to determine the axial brace forces in the test specimens. The actuator displacement was controlled by LVDTs to verify the effective operation of the dual actuator displacement control. Individual actuator displacements were monitored during testing to ensure that the two actuators were moving in sync.

3.6.2 *Potentiometers*

Testing utilized two types of potentiometers to measure critical displacements of the test specimens and components of the test frame: UniMeasure P510 string potentiometers and BEI Duncan 600 Series linear conductive potentiometers. The string potentiometers shown in Figure 3.24 and Figure 3.25 were used where displacements were generally expected to exceed 2". The Duncan potentiometers were used for small displacements of the components of the test setup, with their locations depicted in Figure 3.26.

(a)

(b)

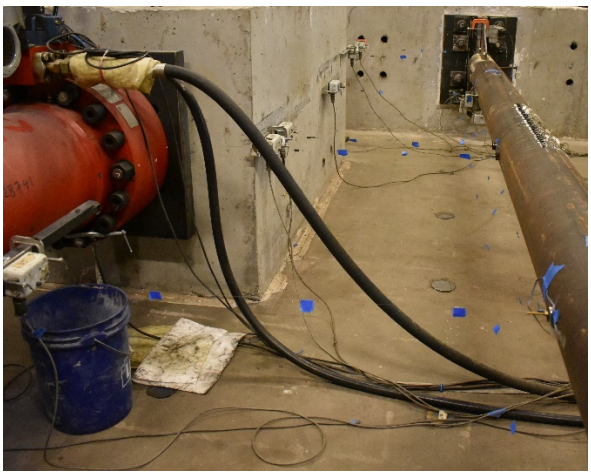

(c)

(d)

Figure 3.24 String Potentiometers (a, b, and c) and Duncan Potentiometers (d)

Numbers in Figure 3.25 and Figure 3.26 identify the location of the corresponding potentiometer. String Potentiometers (SPs) 10 and 11 measured axial brace deformation. SP 10 was connected from gusset plate to gusset plate while SP 11 was attached from connection plate to connection plate which captured displacements that included bolt slip and deformation of the gusset plates. SPs 6, 7, 8, 9, 16, and 17 record lateral deformations of the test specimen. SPs 6 and 16 measured rotation of the south gusset plate and are spaced a distance, x, that varied by gusset plate size. SP 6 was located above the brace-gusset weld at the end of the brace and SP 16 was located above the brace-gusset weld at the end of the brace-gusset connection. This data assisted in correcting for the effects of rigid body rotation in the axial deformation data of SP 10. Halfway through testing, SP 22 was added which collected brace axial deformation data in addition to SP 10 but was able to collect data independently of the gusset plate rotations removing the need for the correction script detailed in Chapter 5

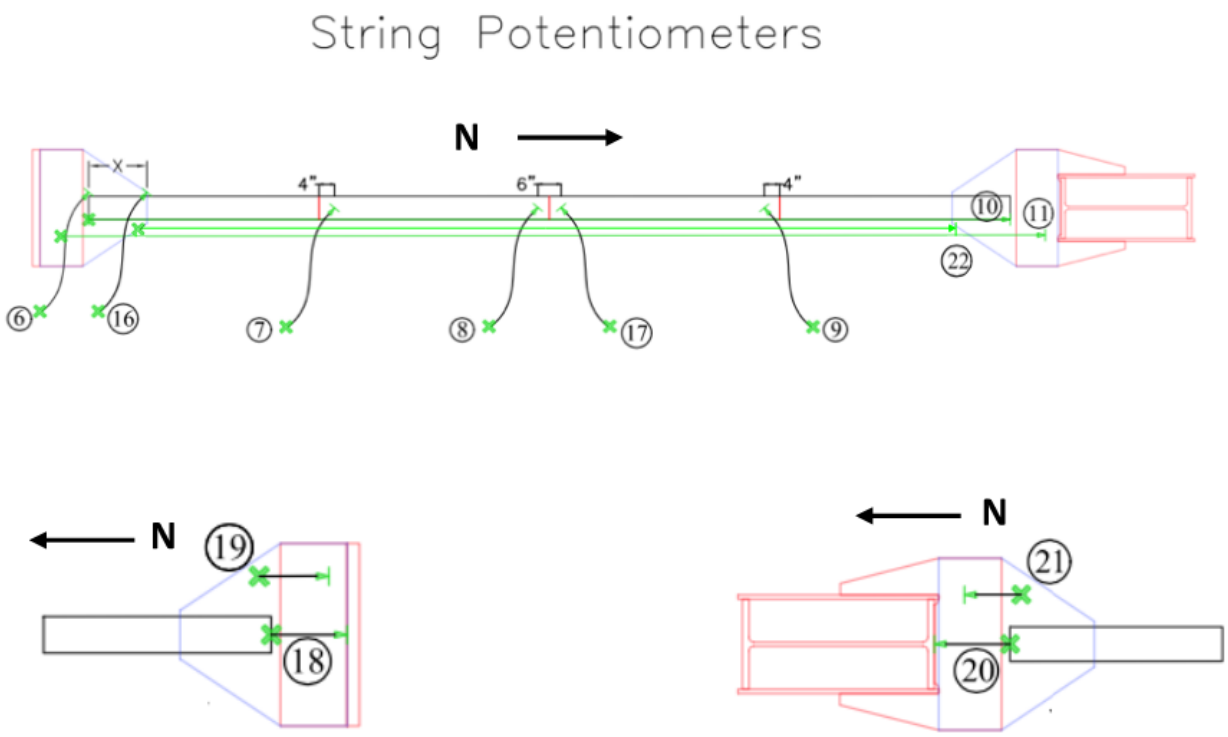

Figure 3.25 String Potentiometer Layout

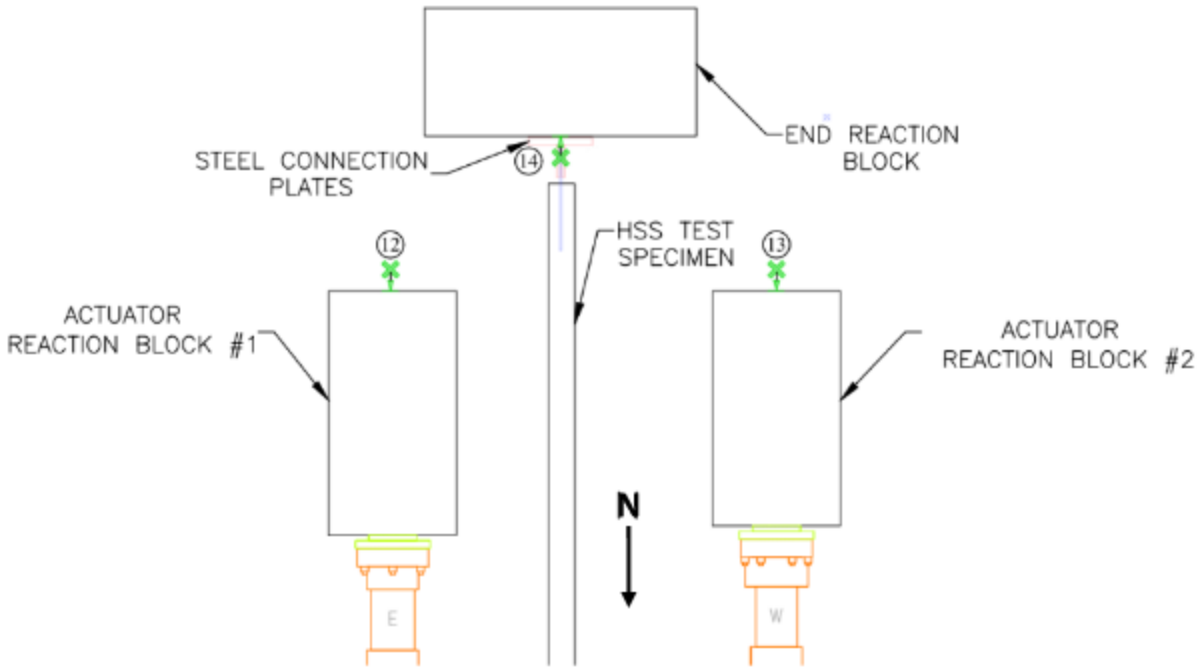

Figure 3.26 Duncan Potentiometer Layout

The components of the test frame were monitored during testing using Duncan Potentiometers (DPs) ensuring there was no significant unintended movement. Each reaction block had a string potentiometer as detailed in Figure 3.26 to monitor block movement. An additional string potentiometer was attached to the west side of the sliding beam against the stationary column to monitor minimal rotations of the sliding beam during cycles.

3.6.3 *Strain Gauges*

Four YFLA strain gauges were placed at a quarter of the brace length on the north and south end oriented longitudinally. For the square braces, one gauge was placed on the center of each face like pictured in Figure 3.27. For the round braces, four gauges were placed at each increment of 90 degrees centered on the top of the brace. The strain gauge data provided redundancy for the LVDT load data.

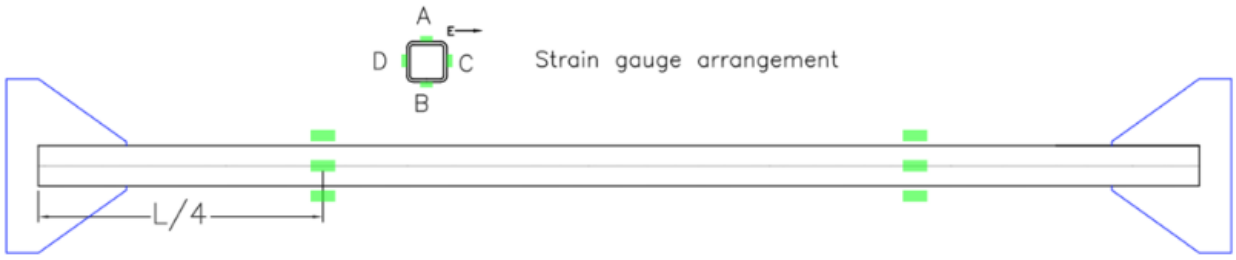

Figure 3.27 Strain Gauge Layout

3.6.4 *Optotrak*

The Optotrak system utilizes a set of three cameras to capture 3-dimensional displacements at LED sensor locations, with measurements accurate to within one millimeter. The camera was positioned on the east side of the test frame, and 30 LED sensors were placed according to Figure 3.28. This setup enabled the system to capture data for local cupping region to further characterize the deformability of this high strain region.

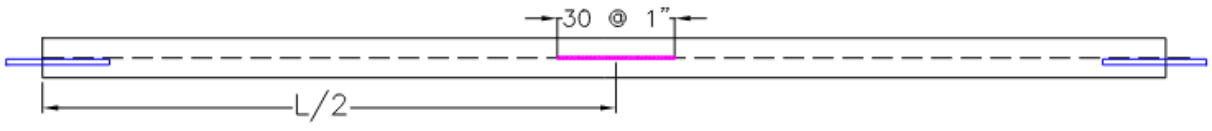

Figure 3.28 Optotrak LED Layout

Figure 3.29 Pre-Test Optotrak Layout

3.7 Pre-Testing Procedure

The specimen was fabricated and prepared for testing using the following procedure. Initially, the HSS was cut to the desired brace length with a horizontal band saw, as the tubes that were provided were supplied in 40-foot or 42-foot sections. After being cut to length, an imperfection check was performed as noted in section 3.3.2. With the information from this check, the specimens were slotted on both ends using a plasma cutter.

Next, the braces were tack welded, utilizing the testing rig as a jig. The gusset plates were temporarily bolted into the connection plates while the slotted brace was dropped down with the overhead crane. The tack welds ensured that the components stay stable until a certified structural welder completed the full welds. The two steps in the welding process can be seen below in Figure 3.30.

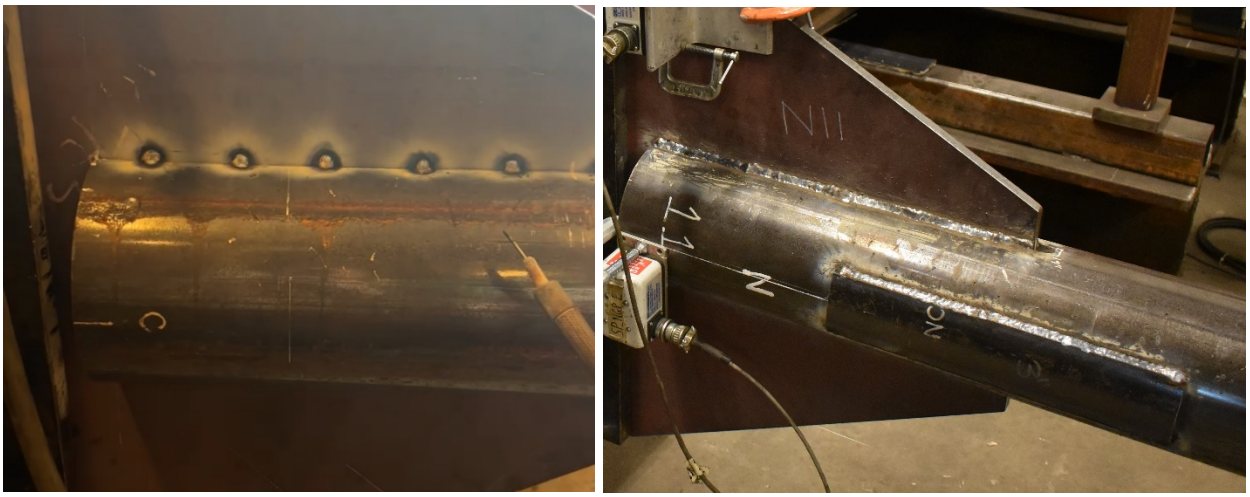

(a) (b)

Figure 3.30 Test Specimen Tack Welded (a) and Fully Welded (b)

After the fabrication process was complete, the brace was connected to the fixed reaction block and sliding beam via twelve 1” A490 tension-controlled bolts. The bolts were tightened using a shear wrench to achieve the intended bolt tension.

The instrumentation process began with attaching eight strain gauges to locations as detailed in Figure 3.27. The SPs were attached and connected along with the strain gauges into the data acquisition system. Three digital cameras were used during testing. Two were setup at two locations around the specimen – one on top of the south reaction block capturing the out-of-plane displacements of the entire specimen, and one on the east side of the specimen capturing the local deformations at the center of the brace. The third camera was used to take pretest photos and capture instances during testing that the stationary cameras did not capture.

Chapter 4. Experimental Results

4.1 Introduction

This chapter summarizes the experimental results. As described in Chapter 3, this experimental program consisted of two testing series: Test Series 1, square HSS braces and Test Series 2, Round HSS sections. Braces were subjected to the symmetrical loading protocol detailed in Section 3.5. Chapter 4 will provide the following information:

- Force-deformation plots and a summary of the response are provided for each test in Sections 4.2.1 through 4.2.30. More extensive summaries that include additional tables, plots, and photos can be found in Appendix E.
- Summary tables which detail material properties, expected and measured forces, damage states, and axial deformations provided in Section 4.2.

4.1.1 *Damage States*

Damage states observed during testing are defined in Table 4.1. The damage states focus only on the brace; damage states for the gusset plate or weld are not included. These were adopted from previous research on SCBFs with a focus on the brace alone (Swatosh, 2016). This chapter uses the damage states to describe the damage progression for each brace test. As shown in prior testing of square braces, the sequence of damage is similar regardless of local and global slenderness ratios. Therefore, it is helpful to title and describe the states and use that nomenclature when describing the results of each test, in particular to correlate the study parameters with the onset of each damage state. Figure 4.1 shows the legend used to indicate each damage state on the force-displacement response curves for each brace specimen. The initiation of each performance state is indicated by the symbol on the hysteretic curve.

Table 4.1 Summary of Damage States

Damage State	Abbreviation	Illustration/Photo of Damage State	Description
Initial Global Buckling	B1	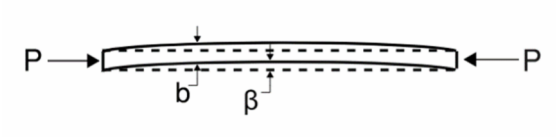	Brace mid-span deflection, β, is visible but less than the brace depth b. Begins when the maximum compressive load is reached.
Moderate Global Buckling	B2	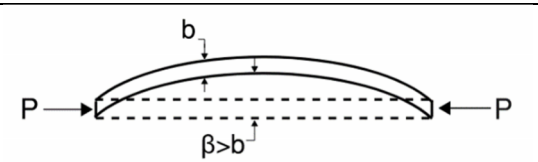	Brace mid-span deflection, β, is greater than the brace depth, b.
Local Cupping Deformations	B3 - C	 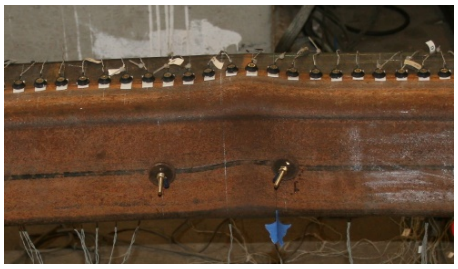	Visible local cupping deformations near or at the midpoint of the brace (plastic hinge/cupping region).
Striations and Initial Tearing	B3 - T	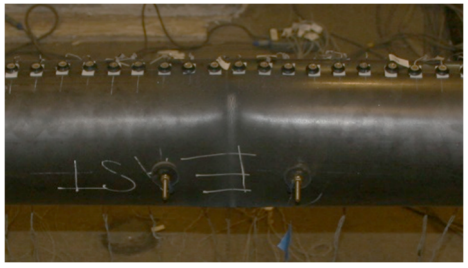 	Striation lines forming at the middle of the cupping region.

50% Tearing	B4 - T	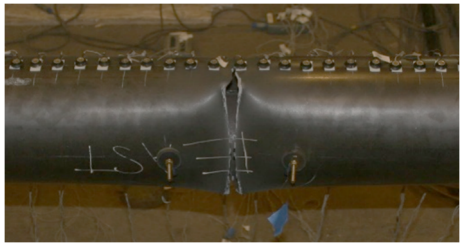		Approximately half of the cross-section torn.
Brace Fracture	B4 - F			Brace fractures through the entire cross-section.

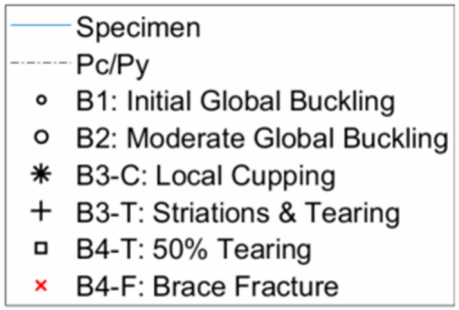

Figure 4.1 Common Legend for Brace Hysteretic Response

Summary tables and brace axial force versus deformation curves are provided in Section 4.2. The summary tables detail material properties, expected and measured forces, damage states, and axial deformations. The hysteretic plots are shown along with a brief summary of observations from each test in Sections 4.2.1 through 4.2.30. More extensive summaries that include additional tables, plots, and photos can be found in Appendix E.

4.2 Test Results

This section provides key, tabulated values for the nominal (specified) and measured properties for the test specimens. It also provides a brief summary of each specimen test and tables that compile brace data at each damage state. The tables and figures are as follows.

Nominal and measured properties are provided in Table 4.2. The tabulated values include nominal width-to-thickness ratios (*b/t* for square sections and *D/t* for round sections). These cells are shaded to indicated their compliance with the Seismic Provisions, AISC 341-22 (AISC 2022) moderate and highly ductile width-to-thickness limits as provided in Table D1.1. The shading indicates the following: values less than or equal to the highly ductile limit are shaded green, values less than or equal to the moderately ductile limit but larger than the highly ductile limit are shaded orange, and all others (which exceed the moderately ductile limit) are shaded red.

Table 4.3 summarizes the expected and measured brace forces corresponding to tensile yielding and critical buckling. The nominal brace forces are calculated using the specified yield stress, $F_{y,e}$, the specified area, A_g, and the over-strength factor for the steel grade of A500C, R_y The nominal brace forces are calculated using nominal yield stress, $F_{y,e}$, nominal area, A_g, and over strength factor, R_y. The measured brace forces substitute measured yield stress, $F_{y,m}$ for $R_yF_{y,e}$. The expected critical buckling stress was calculated using expected yield stress, $R_yF_{y,e}$ and measured buckling stress was determined using measured yield stress, $F_{y,m}$.

Sections 4.2.1 through 4.2.30 provide the normalized force-displacement response and a brief test summary. The force is normalized to the expected yield force and the brace axial deformation is normalized to the initial length of the brace. The damage state symbols are plotted to indicate the onset of damage.

Table 4.4 provides the engineering demand parameters corresponding the damage states provided in Table 4.1. Specifically, the target axial displacement, and measured brace axial deformation for each damage state. Additionally, it summarizes brace yielding and peak tensile force where brace yielding is the point where the applied axial load first equals the predicted measured yield force. The target displacement corresponds to the target actuator displacement step of the cycle in the loading protocol. The value in parenthesis below indicates the first or second cycle at that target displacement cycle. The force at each damage state is the combined actuator load when the damage state first occurs. The value in parentheses is a ratio of the force

to either the yield load or the critical buckling load. Tensile forces are shown as a ratio of the yield load and compressive forces are shown as a ratio of the critical buckling load. The listed axial deformations represent the values observed at the onset of each specified performance state.

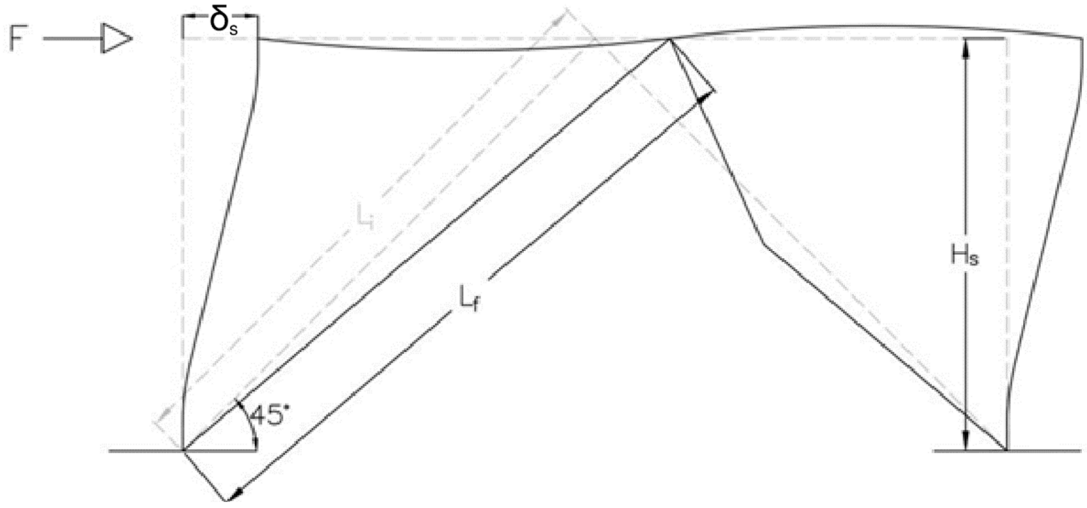

Figure 4.2 Assumed Chevron Brace Configuration

Provided in the parenthesis in Table 4.4 is an approximate drift range at the specified axial deformation. Using the geometric relationship in the chevron configuration above assuming a brace angle of 45 degrees, an approximate drift ratio can be calculated. L_i, denoted the initial brace length and L_f denotes the deformed brace length assuming small angles and neglecting any movement of the beam. The corresponding story height, H_s is:

$$H_s = \sqrt{\frac{{L_i}^2}{2}} \tag{1}$$

The story drift, ρ_s, that is summarized for each brace axial deformation in Table 4.4 and Table 4.5 is approximated as a percentage of story height:

$$\rho_s = \frac{\delta_s}{H_s} = \frac{2*\cos(45°)*(L_f - L_i)}{H_s} * 100 \tag{2}$$

Table 4.5 highlights the maximum tensile and compressive axial deformations with their corresponding drift ratios below in parentheses. The sum of the compressive and tensile maximum story drifts is the drift range.

Table 4.2 Summary of Nominal and Measured Material Properties

			Wall Thickness		Brace Compactness		
Test Specimen	**Nominal Area, A_g (in^2)**	**Moment of Inertia, I (in^4)**	**Nominal, t_{nom} (in)**	**Measured, t_{meas} (in)**	**Nominal, b/t_{nom}, D/t_{nom}**	**Measured, b/t_{meas}, D/t_{nom}**	**Global Slenderness, L_c/r**
5x5x3/16 Short	3.28	12.6	0.174	0.190	25.7	26.5	93.6
6x6x3/16 Short	3.98	22.3	0.174	0.181	31.5	33.2	77.4
6x6x3/16 Long	3.98	22.3	0.174	0.187	31.5	32.2	92.6
6x6x1/4 Short	5.24	28.6	0.233	0.231	22.8	26.1	78.4
6x6x1/4 Long	5.24	28.6	0.233	0.240	22.8	25.1	93.8
7x7x1/4 Short	6.17	46.5	0.233	0.232	27.0	30.3	66.7
7x7x1/4 Long	6.17	46.5	0.233	0.239	27.0	29.4	79.8
8x8x5/16 Short	8.76	85.6	0.291	0.287	24.5	27.9	58.6
8x8x5/16 Long	8.76	85.6	0.291	0.310	24.5	25.8	70.1
6x3/16 Short	3.18	13.5	0.174	0.195	34.5	30.8	89.1
6x3/16 Long	3.18	13.5	0.174	0.176	34.5	34.1	106.6
6x1/4 Short	4.22	17.6	0.233	0.245	25.8	24.5	90.0
6x1/4 Long	4.22	17.6	0.233	0.243	25.8	24.7	107.6
6.625x3/16 Long	3.53	18.4	0.174	0.181	38.1	36.7	96.3
6.625x1/4 Short	4.68	23.9	0.233	0.237	28.4	28	81.2
6.625x1/4 Long	4.68	23.9	0.233	0.242	28.4	27.4	97.1
6.625x3/8 Short	6.88	34.0	0.349	0.353	19.0	18.8	82.7
6.625x3/8 Long	6.88	34.0	0.349	0.351	19.0	19.0	98.9
6.625x1/2 Short	9.00	42.9	0.465	0.473	14.2	14.1	84.2
6.625x1/2 Long	9.00	42.9	0.465	0.462	14.2	14.5	100.7
8.625x3/16 Short	4.62	41.3	0.174	0.187	49.6	46.1	61.4
8.625x3/16 Long	4.62	41.3	0.174	0.199	49.6	43.4	73.4
8.625x1/4 Short	6.14	54.1	0.233	0.233	37.0	37.1	61.8
8.625x1/4 Long	6.14	54.1	0.233	0.243	37.0	35.6	73.9
8.625x3/8 Short	9.07	77.8	0.349	0.345	24.7	25.0	62.6
8.625x3/8 Long	9.07	77.8	0.349	0.354	24.7	24.4	74.9
10.750x1/4 Short	7.15	85.3	0.233	0.232	46.1	46.4	49.3
10.750x1/4 Long	7.15	85.3	0.233	0.249	46.1	43.2	59
10.750x0.365 Short	11.1	150	0.339	0.339	31.7	31.8	49.9
10.750x0.365 Long	11.1	150	0.339	0.349	31.7	30.8	59.6

Table 4.3 Expected and Measured Loads

Test Specimen	Yield Load		Critical Buckling Load	
	Expected, $P_{y,e}$ (kips)	Measured, $P_{y,m}$ (kips)	Expected, $P_{cr,e}$ (kips)	Measured, $P_{cr,m}$ (kips)
5x5x3/16 Short	213	235	106	107
6x6x3/16 Short	259	234	167	160
6x6x3/16 Long	259	234	131	128
6x6x1/4 Short	341	339	217	216
6x6x1/4 Long	341	339	168	168
7x7x1/4 Short	401	395	300	297
7x7x1/4 Long	401	395	250	248
8x8x5/16 Short	569	563	468	465
8x8x5/16 Long	569	563	407	405
6x3/16 Short	207	170	111	104
6x3/16 Long	207	170	80	80
6x1/4 Short	274	229	145	137
6x1/4 Long	274	229	104	104
6.625x3/16 Long	229	199	108	106
6.625x1/4 Short	304	276	185	178
6.625x1/4 Long	304	276	142	140
6.625x3/8 Short	447	401	266	255
6.625x3/8 Long	447	401	201	199
6.625x1/2 Short	585	573	340	338
6.625x1/2 Long	585	573	254	254
8.625x3/16 Short	300	321	239	250
8.625x3/16 Long	300	321	205	211
8.625x1/4 Short	399	411	317	323
8.625x1/4 Long	399	411	271	275
8.625x3/8 Short	590	596	463	466
8.625x3/8 Long	590	596	394	396
10.750x1/4 Short	465	448	453	440
10.750x1/4 Long	465	448	410	400
10.750x0.365 Short	722	670	650	614
10.750x0.365 Long	722	670	587	558

4.2.1 *5x5x3/16 A500 Short*

The 5x5x3/16 short specimen reached a max tensile load of 243 kips at a brace displacement of 1.07” and a max compressive load of 87 kips (0.81 of the expected critical buckling load) at a brace axial displacement of -0.18”. Moderate global buckling occurred at a brace axial displacement of -0.43” during the first 0.625” target displacement cycle. Minor local cupping initiated about 3” south of center at a brace axial displacement of -0.69”. Local damage increased for the next two compression cycles which led into 50% tearing. Striations and tearing appeared during the same tension cycle as 50% tearing (1.25 T2). The axial load at 50% tearing was 207 kips.

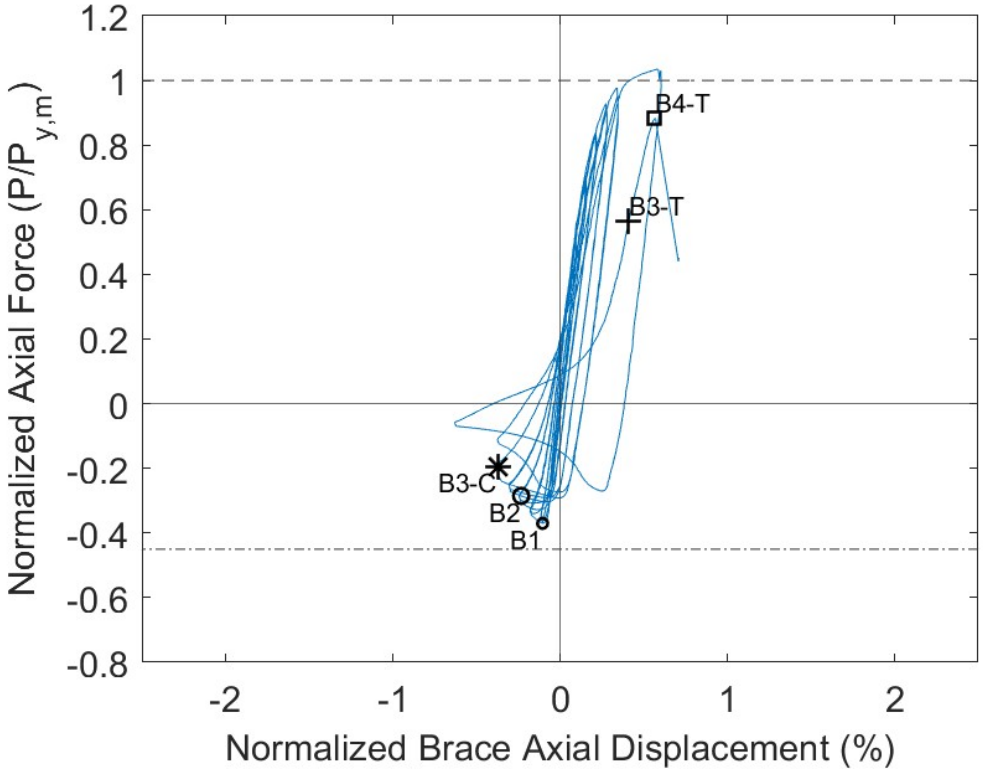

Figure 4.3 Normalized Force-Displacement Response: 5x5x3/16 Short

4.2.2 *6x6x3/16 A500 Short*

Global buckling of the 6x6x3/16 short specimen was observed at a compressive deformation of 0.18". At the peak of this cycle, the brace reached a peak compressive load of 118 kips (0.74 of the expected critical buckling load). The first sign of local cupping was at a compressive axial brace deformation of 0.59". The initial cupping was approximately ½" deep and occurred 6.75" north of center. The severity of local cupping proceeded to increase in subsequent compression cycles. Moderate global buckling occurred at a brace axial deformation of -0.66" after cupping had first been observed. The tension cycle before fracture, the brace reached its peak tensile load of 256 kips at a brace deformation of 0.61". Striations and tearing developed during the same tension cycle as 50% tearing (1.25 T1). At a brace axial displacement of 0.76" and a force of 227 kips, the brace reached 50% tearing.

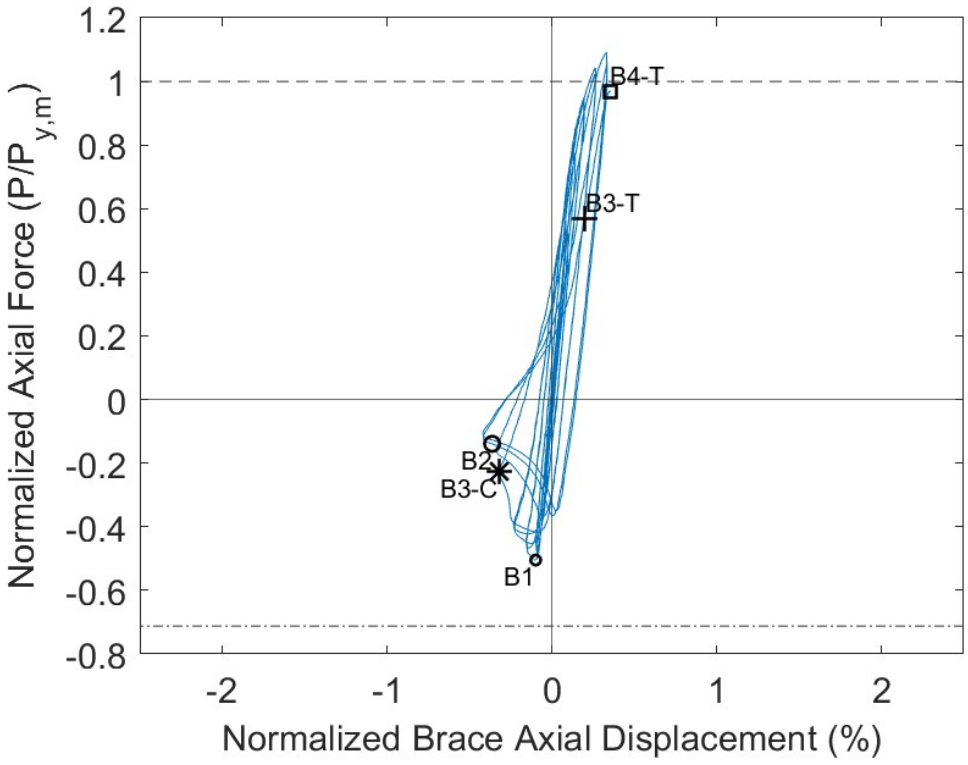

Figure 4.4 Normalized Force-Displacement Response: 6x6x3/16 Short

4.2.3 *6x6x1/4 A500 Short*

The 6x6x1/4 short specimen reached a maximum compressive force of 180 kips (0.83 the expected critical buckling load), at which point the specimen exhibited global buckling. Moderate buckling occurred at an axial brace deformation of -0.59". Local cupping was first observed when the compressive axial deformation of the brace reached 1.19". Local cupping developed about 7.75" north of center and was approximately 0.8" deep. The severity of local cupping proceeded to increase in subsequent compression cycles. In the first tension cycle of 1.25 target displacements, the brace reached a peak tensile load of 364 kips at a brace axial displacement of 1.25". Striation initialized the tension cycle before 50% tearing. The braced reached 50% tearing at an axial displacement of 1.25".

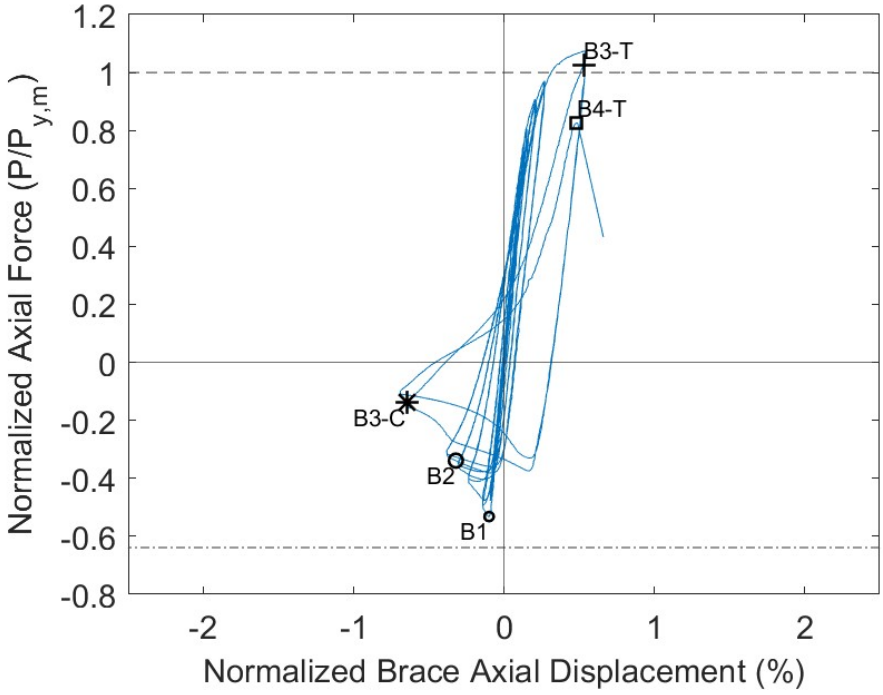

Figure 4.5 Normalized Force-Displacement Response: 6x6x1/4 Short

4.2.4 *7x7x1/4 A500 Short*

Global buckling of the 7x7x1/4 short specimen occurred at an axial deformation of -0.22" while the compressive force was 244 kips (0.82 the expected critical buckling load). The out-of-plane deformation of the brace was never equal to or greater than the brace width so B2, Moderate Global Buckling did not occur. Local cupping deformations became visible at a brace axial deformation of -0.60". Cupping deformations were centered 3" north of center. The magnitude of cupping started at 0.6" and progressed to 1.25" at the last compression cycle before 50% tearing. The tension cycle before 50% tearing, the peak tensile load was 357 kips. Initial striations and tearing occurred during the same tension cycle as 50% tearing. The brace reached 50% tearing at a brace axial deformation of 0.94".

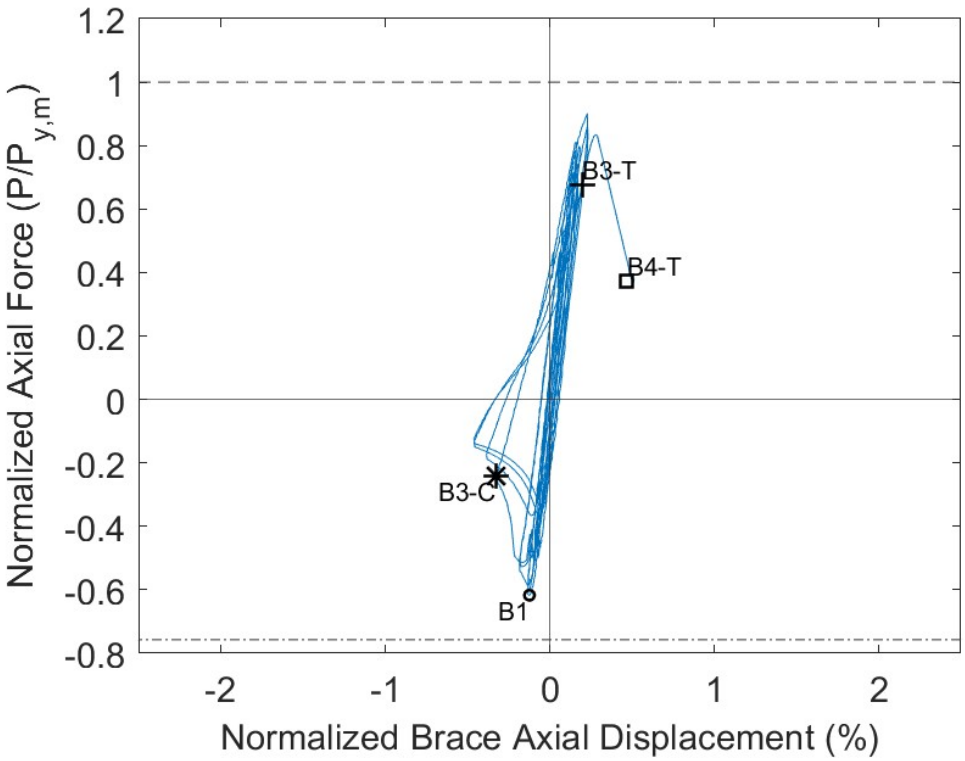

Figure 4.6 Normalized Force-Displacement Response: 7x7x1/4 Short

4.2.5 *8x8x5/16 A500 Short*

The 8x8x5/16 short specimen had a peak compressive load of 379 kips (0.82 of the expected critical buckling load) at a brace axial displacement of -0.36”. Large bolt slip took place at many of the peaks during tension cycles. Cupping was first observed when the axial brace deformation was -0.6” and the axial load was -291 kips. Local cupping initiated about 4” north of center. Moderate global buckling occurred two compressive cycles after initial cupping. The peak tensile load of 579 kips occurred when the brace axial deformation was 0.72”. Striations and tearing and 50% tearing took place in the last tension cycle at a brace axial displacement of 446 kips.

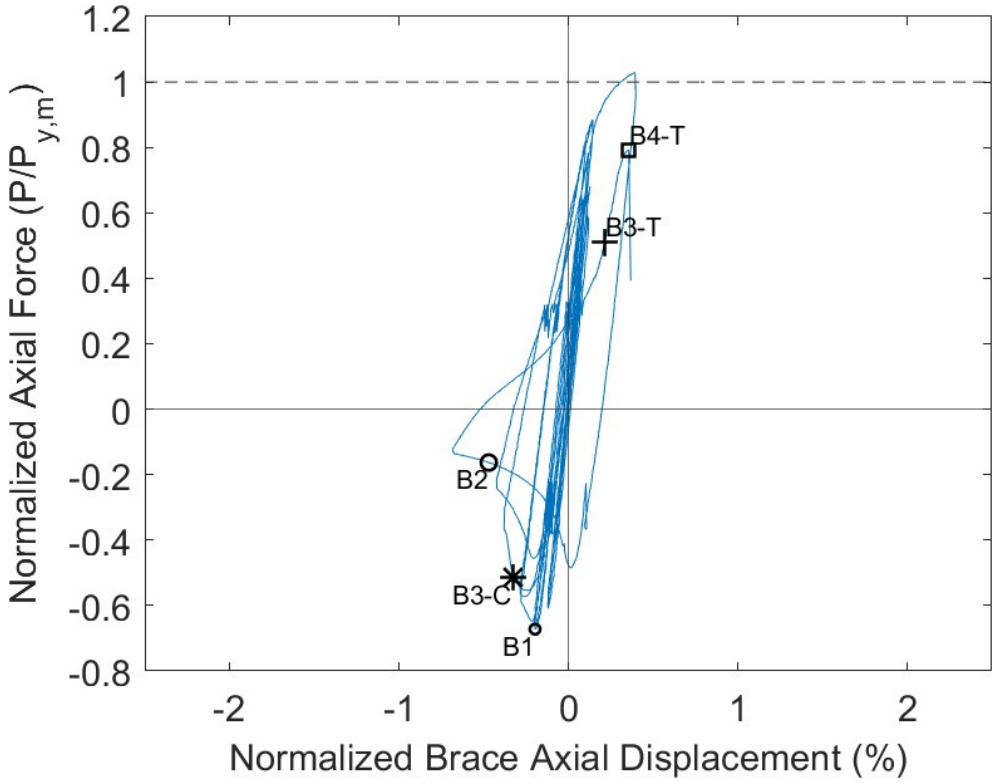

Figure 4.7 Normalized Force-Displacement Response: 8x8x5/16 Short

4.2.6 *6x3/16 A500 Short*

Initial Global Buckling occurred at a compressive load of 74 kips (0.71 of the expected critical buckling load) when the axial displacement was -0.13”. Moderate Global Buckling appeared at an axial load of -47 kips and an axial displacement of -0.48”. Local cupping was first observed at a brace axial displacement of -1.53”. The cupping was estimated to be 0.5” deep when cupping first ensued and it progressed to about 1.4” deep the compression cycle before 50% tearing. A peak tensile load of 186 kips occurred the tension cycle before 50 % tearing. Striations and tearing and 50% tearing took place in the last tension cycle. The brace reached 50% tearing at an axial displacement of 2.48”.

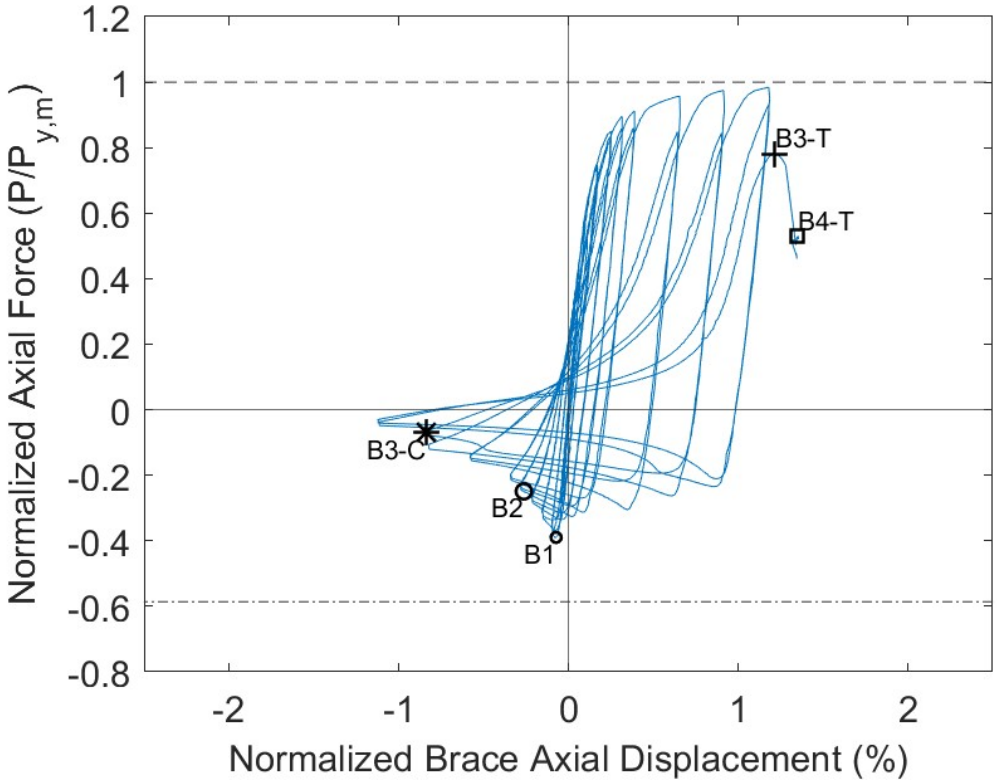

Figure 4.8 Normalized Force-Displacement Response: 6x3/16 Short

4.2.7 *6x1/4 A500 Short*

Global buckling of the 6x1/4 short specimen occurred at the first 0.25” compression target displacement cycle while the compressive force was 92 kips (0.67 the expected critical buckling load). Moderate Global Buckling appeared during the first compression cycle of 0.625” target displacements. The brace switched buckling directions during the first compression cycle of 1.25” target displacements. Local cupping deformations became visible at a target compressive displacement of 2.75”. The magnitude of cupping started at 0.8” and progressed to 1.5” at the last compression cycle before 50% tearing. Two tension cycles before 50% tearing, the peak tensile load was 241 kips. Initial striations and tearing occurred during the tension cycle before 50% tearing. The brace reached 50% tearing at a 74 kip force during the first 3.75” target tension cycle. Figure 4.9 is based off of actuator displacement data instead of string potentiometer data. String potentiometer data was inaccurate due to the switch in buckling directions.

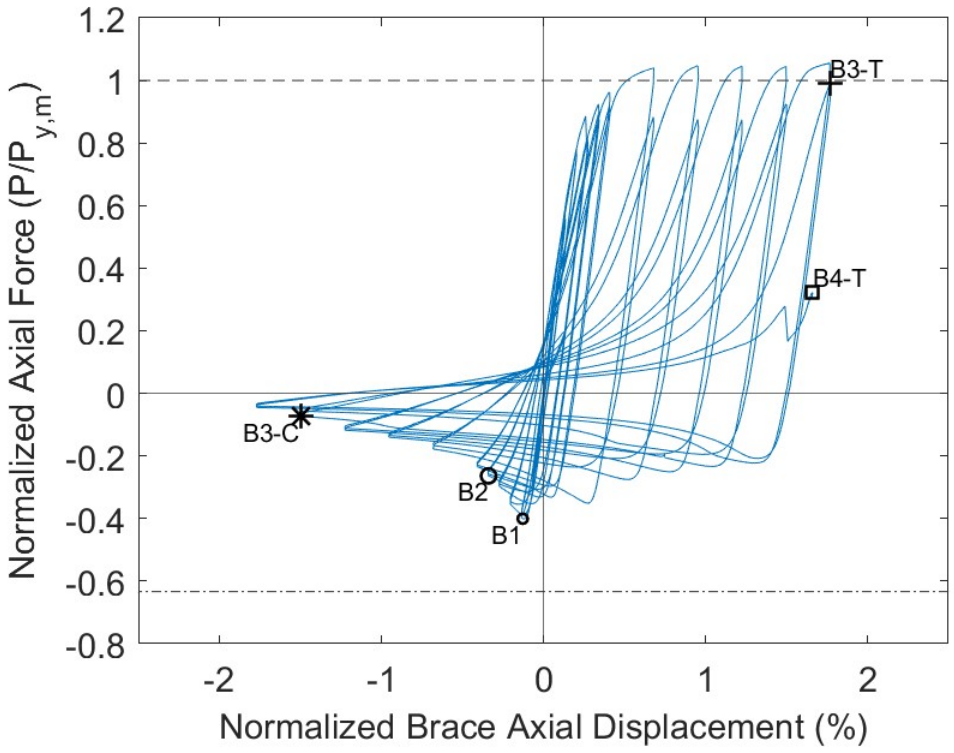

Figure 4.9 Normalized Force-Displacement Response: 6x1/4 Short

4.2.8 *6.625x1/4 A500 Short*

The 6.624x1/4 short specimen reached a maximum compressive force of 131 kips (0.74 the expected critical buckling load), at which point the specimen exhibited global buckling. Moderate buckling occurred during the first compression cycle of the 0.75 target displacements. Local cupping was first observed when the compressive axial deformation of the brace reached 2.09". Local cupping was approximately 0.6" deep when this damage state first appeared. The severity of local cupping proceeded to increase in subsequent compression cycles. In the first tension cycle of 2.75 target displacements, the brace reached a peak tensile load of 284 kips at a brace axial displacement of 2.54". Striation initialized two tension cycles before 50% tearing. The braced reached 50% tearing at an axial displacement of 2.21".

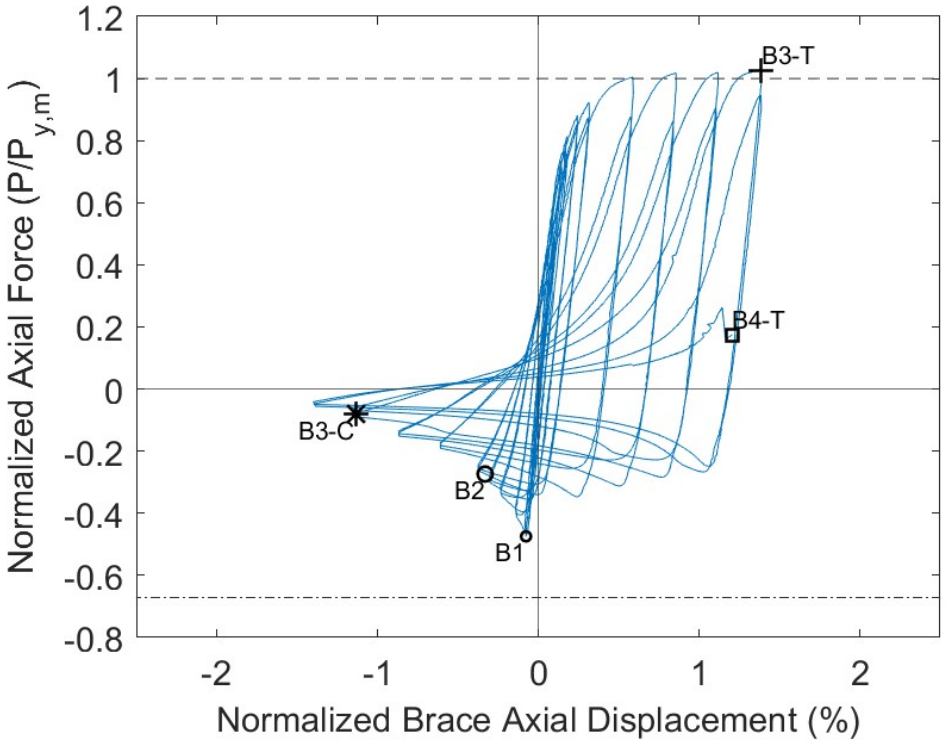

Figure 4.10 Normalized Force-Displacement Response: 6.625x1/4 Short

4.2.9 *6.625x3/8 A500 Short*

Global buckling of the 6.625x3/8 specimen occurred at a compressive axial deformation of 0.18” while the compressive force was 197 kips (0.77 the expected critical buckling load). Moderate Global Buckling occurred at a 112 kip compressive load when the axial brace deformation was 0.75”. Local cupping deformation became visible during the second compression cycle of the 2.25 target displacements. The magnitude of cupping started at 0.5” and progressed to 1.7” at the last compression cycle before 50% tearing. Initial striations and tearing occurred the tension cycle before 50% tearing. The brace reached 50% tearing during the second tension cycle of 3.25” target displacements when the brace axial deformation was equal to 3.15”. The load at 50% tearing was 194 kips.

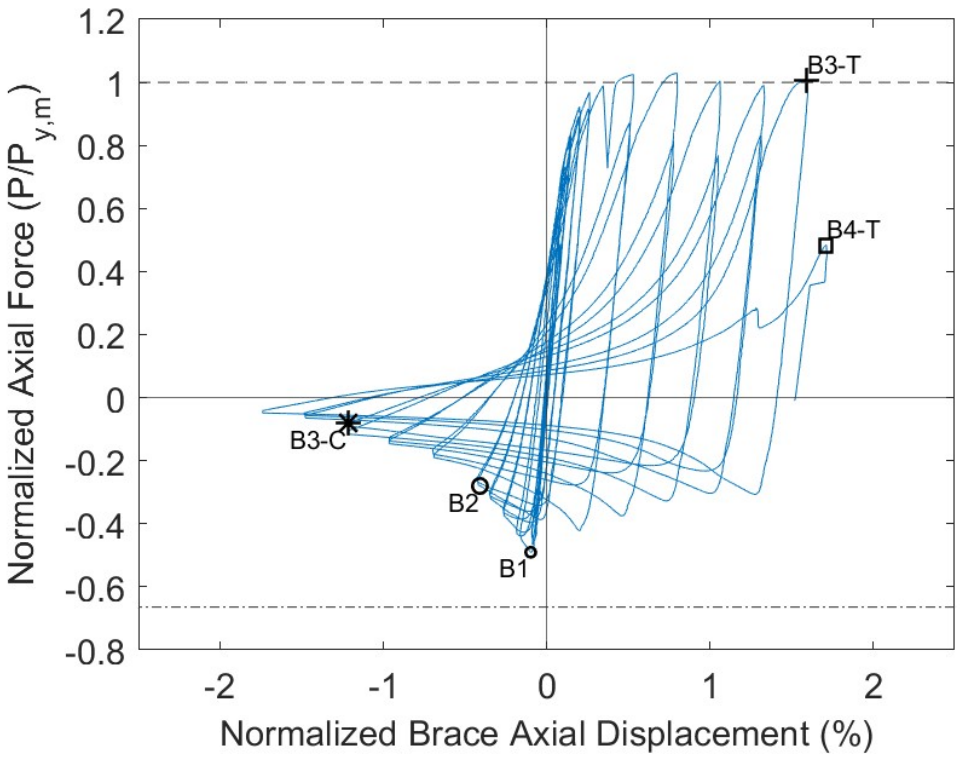

Figure 4.11 Normalized Force-Displacement Response: 6.625x3/8 Short

4.2.10 *6.625x1/2 A500 Short*

The 6.625x1/2 short specimen reached a maximum compressive force of 296 kips (0.88 the expected critical buckling load), at which point the specimen exhibited global buckling. Moderate buckling occurred during the first compression cycle of the 0.50 target displacements. Local cupping was first observed when the compressive axial deformation of the brace reached 3.05". Local cupping was approximately 0.2" deep when this damage state first appeared. The severity of local cupping proceeded to increase in subsequent compression cycles up to 1.6" deep at the compression cycle before 50% tearing. In the first tension cycle of 1.25 target displacements, the brace reached a peak tensile load of 550 kips at a brace axial displacement of 0.81". Striations initialized one tension cycle before 50% tearing. The braced reached 50% tearing at an axial displacement of 3.95". The load at 50% tearing was 200 kips.

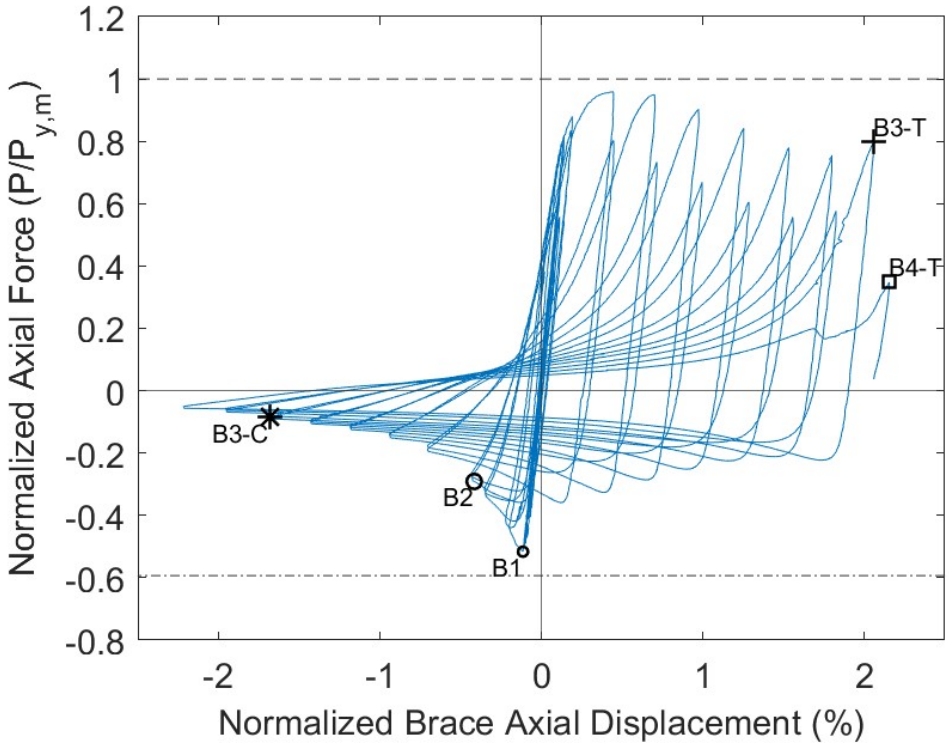

Figure 4.12 Normalized Force-Displacement Response: 6.625x1/2 Short

4.2.11 *8.625x3/16 A500 Short*

The 8.624x3/16 short specimen reached a maximum compressive force of 201 kips (0.80 the expected critical buckling load), at which point the specimen exhibited global buckling. Moderate buckling occurred during the first compression cycle of the 1.25 target displacements. Local cupping was first observed when the compressive axial deformation of the brace reached 0.99". Local cupping was approximately 1.4" deep when this damage state first appeared. The local cupping region had multiple centers of cupping: a large main center of cupping present in other tests, and two smaller lobes. See Appendix E for photos of this damage state. The severity of local cupping proceeded to increase in subsequent compression cycles. In the first tension cycle of 1.25 target displacements, the brace reached a peak tensile load of 337 kips at a brace axial displacement of 1.45". Striations and tearing appeared at a tensile force of 337 kips a tension cycle before fracture. The brace fractured at an axial displacement of 1.72" and an axial load of 134 kips.

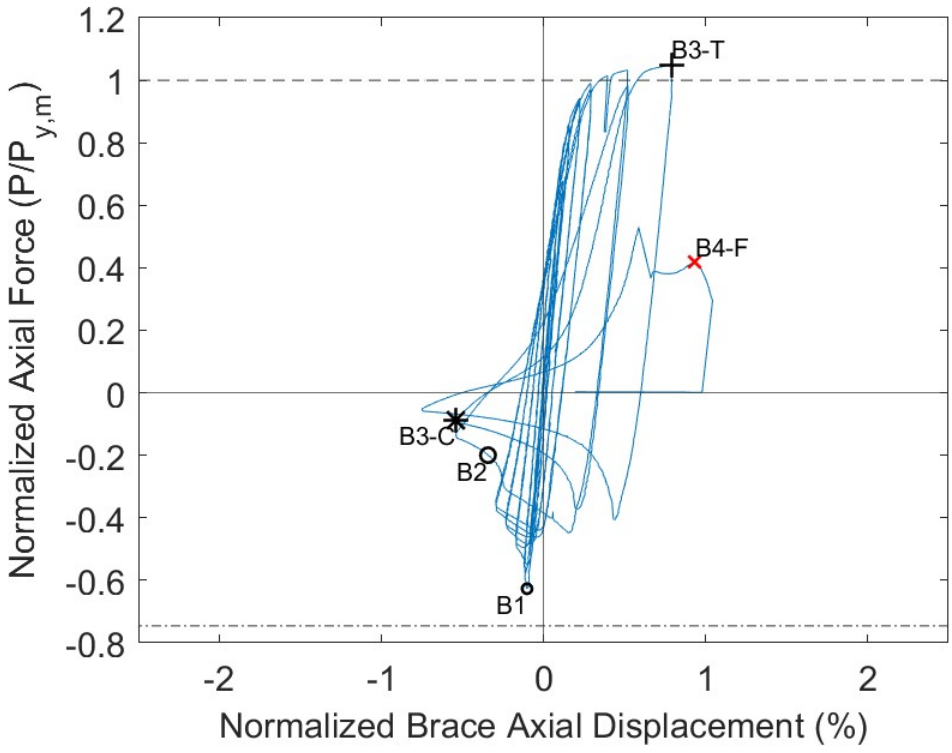

Figure 4.13 Normalized Force-Displacement Response: 8.625x3/16 Short

4.2.12 *8.625x1/4 A500 Short*

Initial Global Buckling occurred at a compressive load of 268 kips (0.83 of the expected critical buckling load) when the axial displacement was -0.34". Moderate Global Buckling appeared during the second 1.25" target displacement compressive cycle. Local cupping was first observed when the compressive axial deformation was 1.35". The cupping was estimated to be 1" deep when cupping first ensued and it progressed to about 1.8" deep the compression cycle before fracture. A peak tensile load of 426 kips occurred the tension cycle before fracture. The brace partially tore and eventually fractured when the axial brace deformation was equal to 1.73" and the axial load was 125 kips.

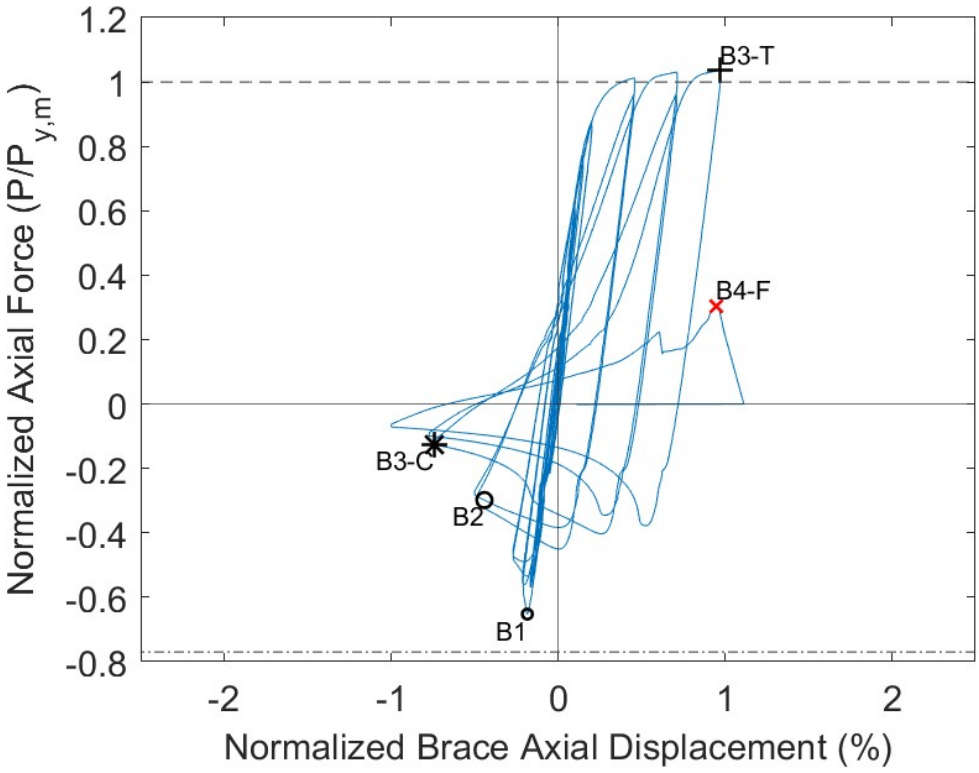

Figure 4.14 Normalized Force-Displacement Response: 8.625x1/4 Short

4.2.13 *8.625x3/8 A500 Short*

The 8.625x3/8 short specimen globally buckled at a compressive load of 341 kips (0.73 of the expected critical buckling load). Moderate global buckling took place at a brace axial displacement of -0.91” and a compressive load of 169 kips. The peak tensile load was 581 kips at a brace axial deformation of 1.21”. During the second 1.75” target displacement cycle, local cupping developed about 2” north of center. This initiated at a brace axial deformation of -1.57” and a compressive load of 73 kips. The magnitude of the depth of cupping increased in subsequent compression cycles. Striations were visible at the second tension peak of the 2.25” target displacement cycles. Brace fracture occurred at an axial brace displacement of 1.87” and a tensile load of 214 kips.

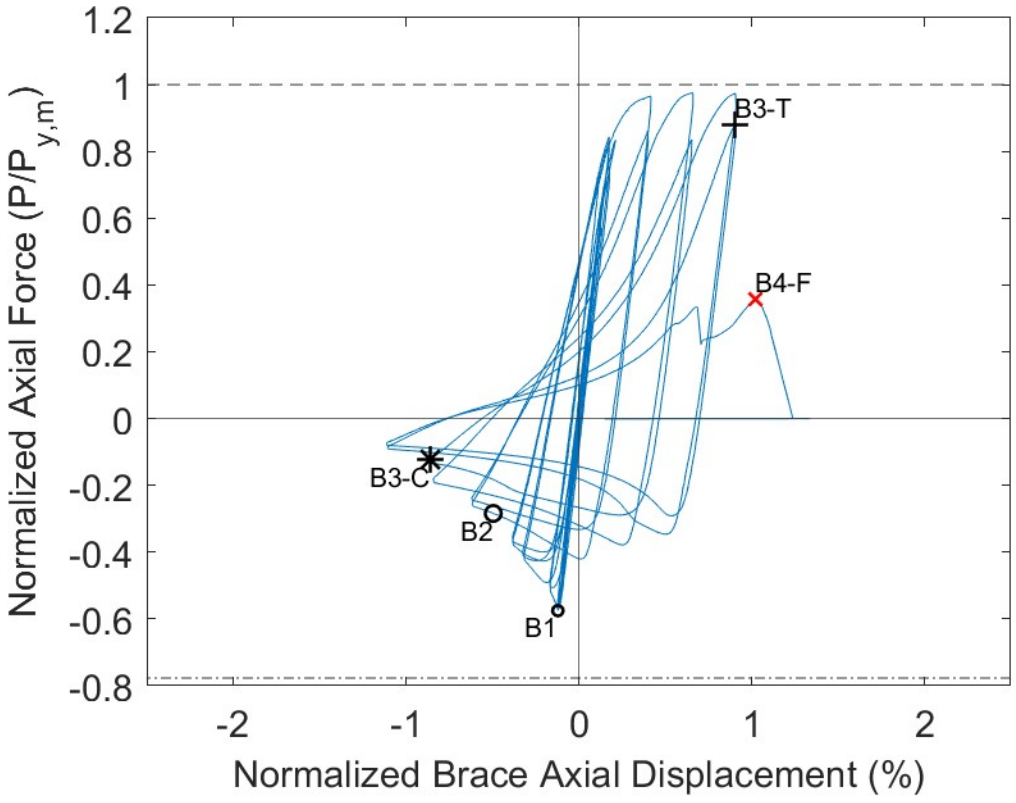

Figure 4.15 Normalized Force-Displacement Response: 8.625x3/8 Short

4.2.14 *10.75x1/4 A500 Short*

Global buckling of the 10.75x1/4 specimen occurred at a compressive axial deformation of 0.34” while the compressive force was 303 kips (0.69 the expected critical buckling load). Moderate Global Buckling occurred at a 83 kip compressive load when the axial brace deformation was 0.72”. Local cupping deformations became visible during the first compression cycle of the 1.25 target displacements. The local cupping region had multiple centers of cupping: a large main center of cupping present in other tests, and two smaller lobes. The magnitude of the depth of the main cupping started at 0.7” and progressed to 1.9” at the last compression cycle before fracture. Initial striations were observed at the peak tensile load of 475 kips. The brace fractured at a tensile load of 119 kips and a brace axial deformation of 2.0”.

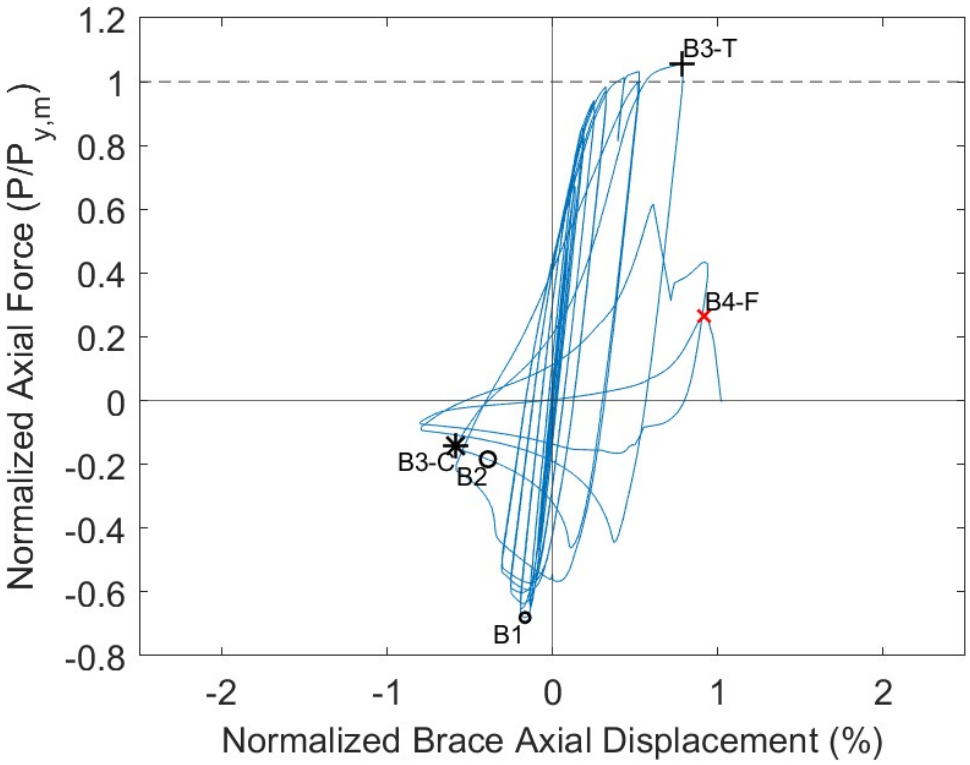

Figure 4.16 Normalized Force-Displacement Response: 10.75x1/4 Short

4.2.15 *10.75x0.365 A500 Short*

Initial Global Buckling occurred at a compressive load of 461 kips (0.75 of the expected critical buckling load) at a brace axial displacement of -0.29”. Moderate Global Buckling appeared during the first 1.75” target displacement compressive cycle. Local cupping was first observed when the brace axial displacement was equal to -1.52”. The cupping was estimated to be 1” deep when cupping first ensued and it progressed to about 2.3” deep the compression cycle before fracture. A peak tensile load of 686 kips occurred when the brace axial deformation was 1.32” during the 1.75 target displacement cycles. The brace partially tore during the tension cycle before fracture. The brace eventually fractured when the axial brace deformation was equal to 2.07” and the axial load was 159 kips.

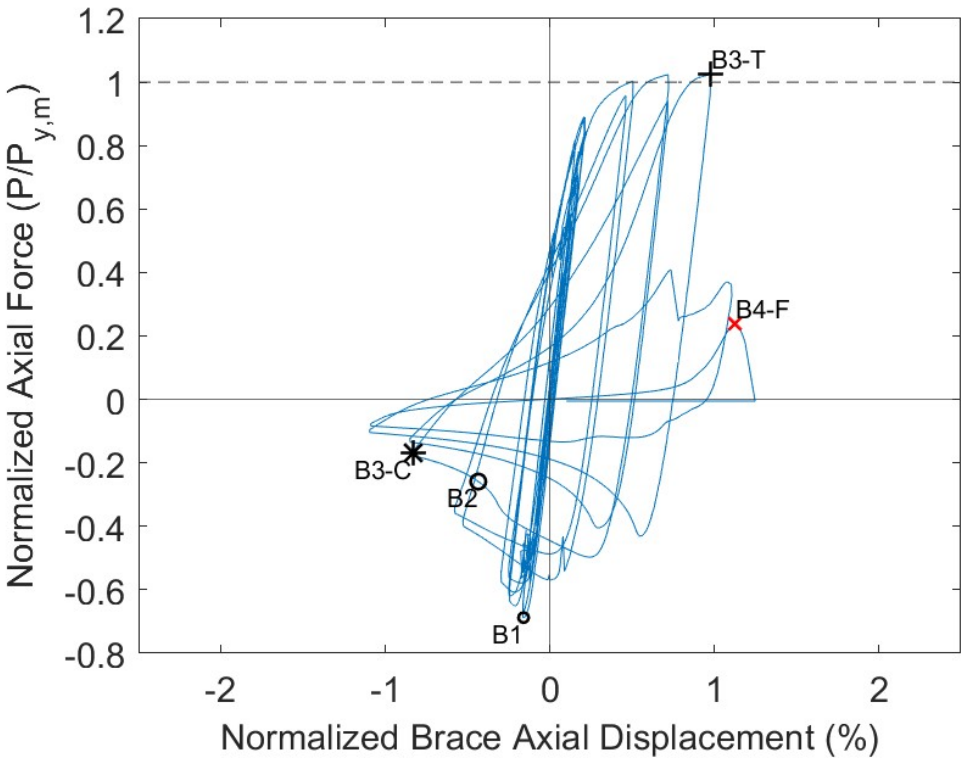

Figure 4.17 Normalized Force-Displacement Response: 10.75x0.365 Short

4.2.16 *6x6x3/16 A500 Long*

The 6x6x3/16 long specimen reached a maximum compressive force of 96 kips (0.75 the expected critical buckling load), at which point the specimen exhibited global buckling. Moderate Global Buckling appeared during the first 0.578" target displacement compressive cycle. Local cupping was first observed when the brace axial displacement was equal to -0.61". The cupping was centered 19" south of center. The cupping was estimated to be 0.5" deep when cupping first ensued and it progressed to about 1.1" deep the compression cycle before fracture. A peak tensile load of 257 kips occurred the tension cycle before fracture. The brace fractured when the axial brace deformation was equal to 0.87" and the axial load was 108 kips.

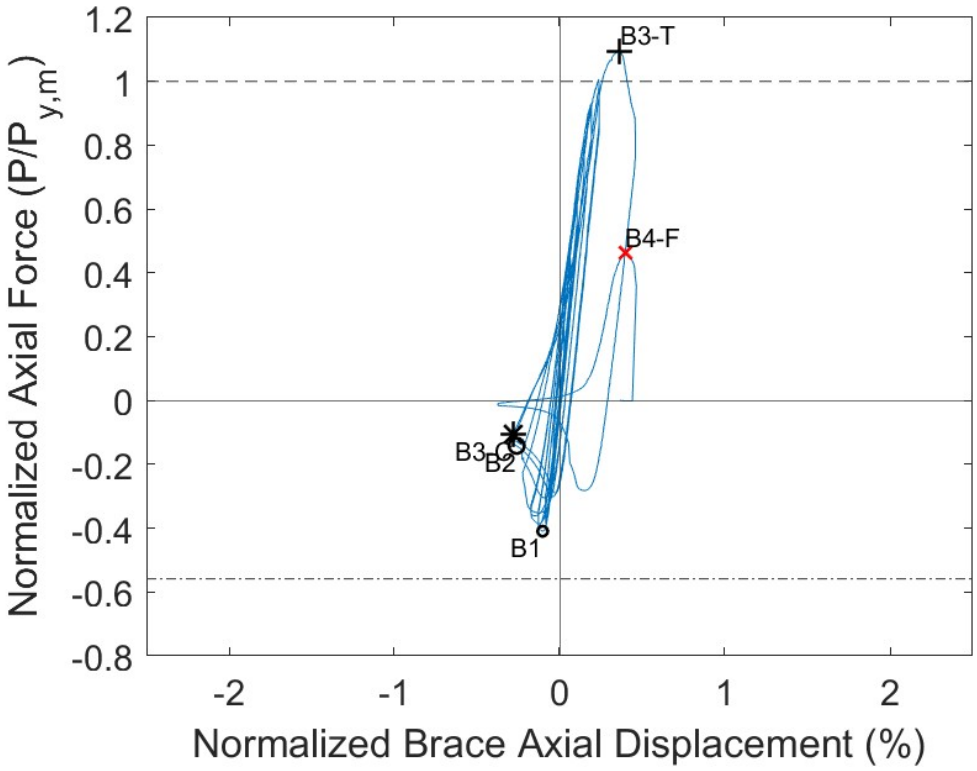

Figure 4.18 Normalized Force-Displacement Response: 6x6x3/16 Long

4.2.17 *6x6x1/4 A500 Long*

The 6x6x1/4 Long specimen globally buckled at a compressive load of 141 kips (0.83 of the expected critical buckling load). Moderate global buckling took place at a brace axial displacement of -0.61” and a compressive load of 108 kips. The peak tensile load was 376 kips at a brace axial deformation of 1.16”. During the second 1.16” target displacement cycle, local cupping developed about 0.5” north of center. This initiated at a brace axial deformation of -1.11” and a compressive load of 50 kips. The magnitude of the depth of cupping increased in subsequent compression cycles. Striations were visible the tension peak before fracture. Brace fracture occurred at an axial brace displacement of 1.25” and a tensile load of 104 kips.

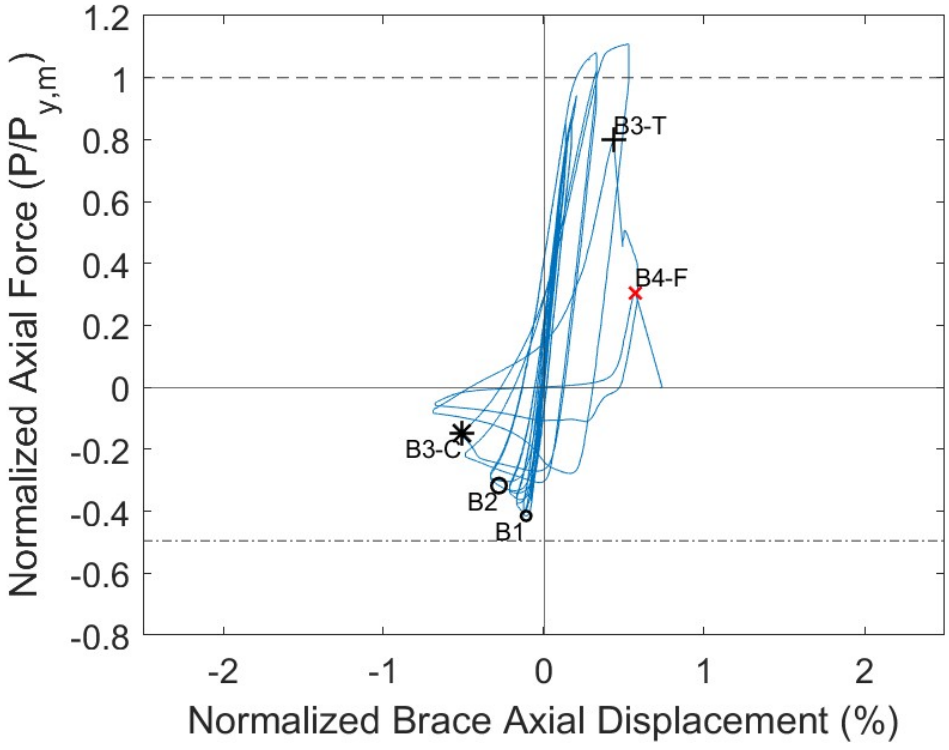

Figure 4.19 Normalized Force-Displacement Response: 6x6x1/4 Long

4.2.18 *7x7x1/4 A500 Long*

Initial Global Buckling occurred at a compressive load of 203 kips (0.82 of the expected critical buckling load) at a brace axial displacement of -0.26”. Moderate Global Buckling appeared during the first 1.16” target displacement compressive cycle. Local cupping was first observed 7.5” south of center when the brace axial displacement was equal to -0.49”. The cupping was estimated to be 0.4” deep when cupping first ensued and it progressed to about 1.6” deep the compression cycle before fracture. A peak tensile load of 415 kips was reached when the brace axial deformation was 0.85” during the 1.16 target displacement cycles. The brace partially tore during the tension cycle before fracture. The brace fractured when the axial brace deformation was equal to 0.90” and the axial load was 133 kips.

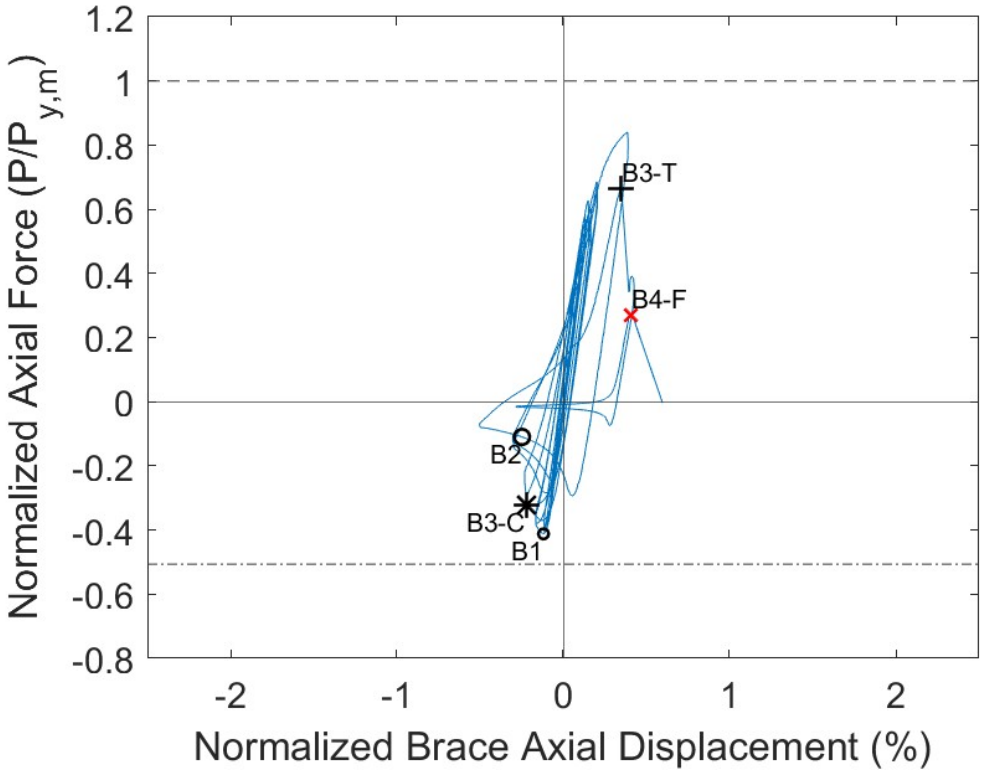

Figure 4.20 Normalized Force-Displacement Response: 7x7x1/4 Long

4.2.19 *8x8x5/16 A500 Long*

The 8x8x5/16 long specimen reached a maximum compressive force of 316 kips (0.78 the expected critical buckling load), at which point the specimen exhibited global buckling. Moderate Global Buckling appeared during the first 1.16” target displacement compressive cycle. Local cupping was first observed when the brace axial displacement was equal to -1.15”. The cupping was centered 6” north of center. The cupping was estimated to be 0.9” deep when cupping first ensued and it progressed to about 1.5” deep the compression cycle before fracture. A peak tensile load of 557 kips occurred the tension cycle before fracture. The brace partially tore and then fractured when the axial brace deformation was equal to 0.86” and the axial load was 278 kips.

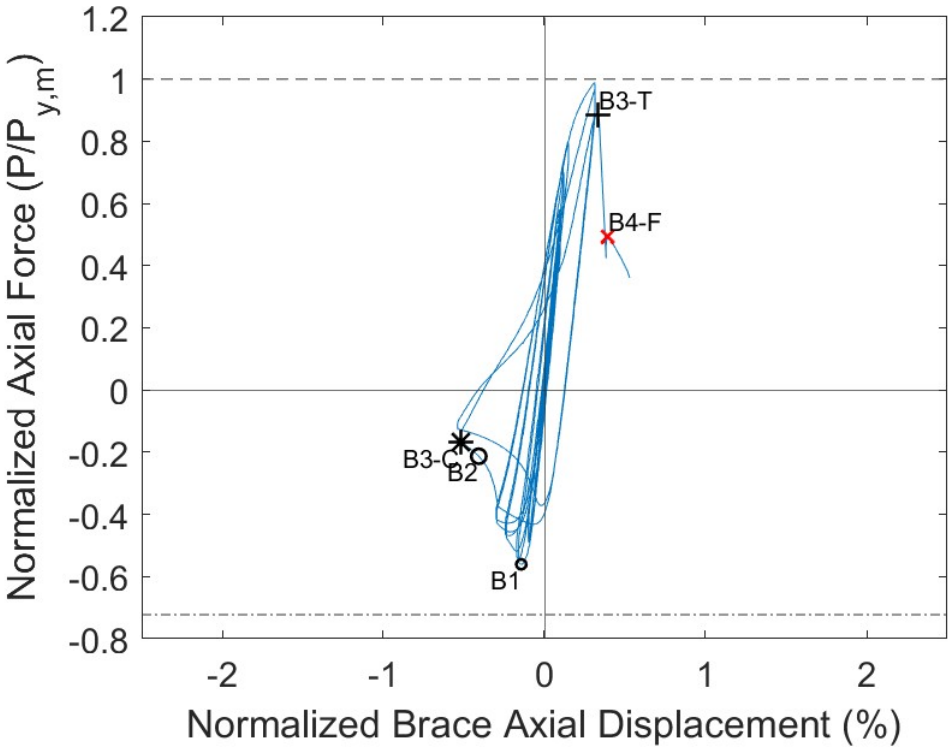

Figure 4.21 Normalized Force-Displacement Response: 8x8x5/16 Long

4.2.20 *6x3/16 A500 Long*

Global buckling of the 6x3/16 specimen occurred at a compressive axial deformation of 0.18” while the compressive force was 59 kips (0.74 the expected critical buckling load). Moderate Global Buckling occurred at a 44 kip compressive load when the axial brace deformation was 0.48”. Local cupping deformations became visible during the first compression cycle of the 2.54 target displacements. The magnitude of the depth of cupping started at 0.4” and progressed to 1.7” at the last compression cycle before fracture. Initial striations were observed the tension cycle after the peak tensile load of 184 kips. The brace fractured at a tensile load of 58 kips and a brace axial deformation of 2.86”.

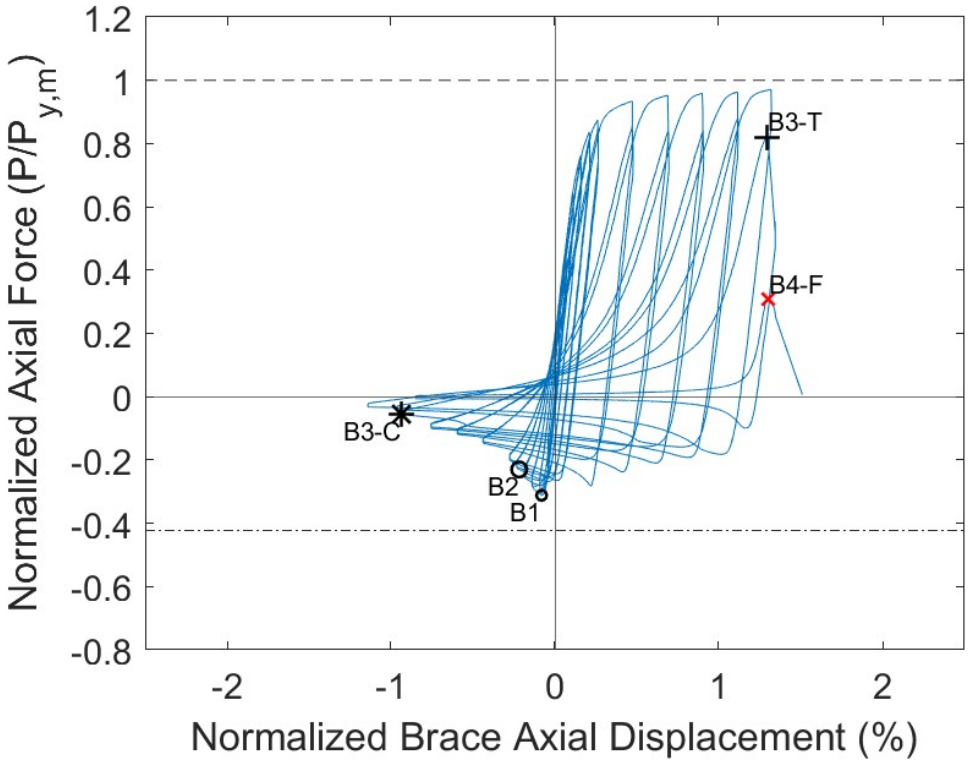

Figure 4.22 Normalized Force-Displacement Response: 6x3/16 Long

4.2.21 *6x1/4 A500 Long*

The 6x1/4 Long specimen globally buckled at a compressive load of 71 kips (0.68 of the expected critical buckling load). Moderate global buckling took place at a brace axial displacement of -0.50” and a compressive load of 52 kips. During the first compression cycle of 1.16” target displacements, the brace buckled switched buckling directions towards the east. During the second 3.47” target displacement cycle local cupping developed. This initiated at a brace axial deformation of -2.37” and a compressive load of 11 kips. The cupping was estimated to be 0.4” deep when cupping first ensued, and it progressed to about 1.2” deep the compression cycle before fracture. The peak tensile load was 238 kips at a brace axial deformation of 3.65”. The brace partially tore the tension cycle before fracture. Brace fracture occurred at an axial brace displacement of 3.57” and a tensile load of 65 kips.

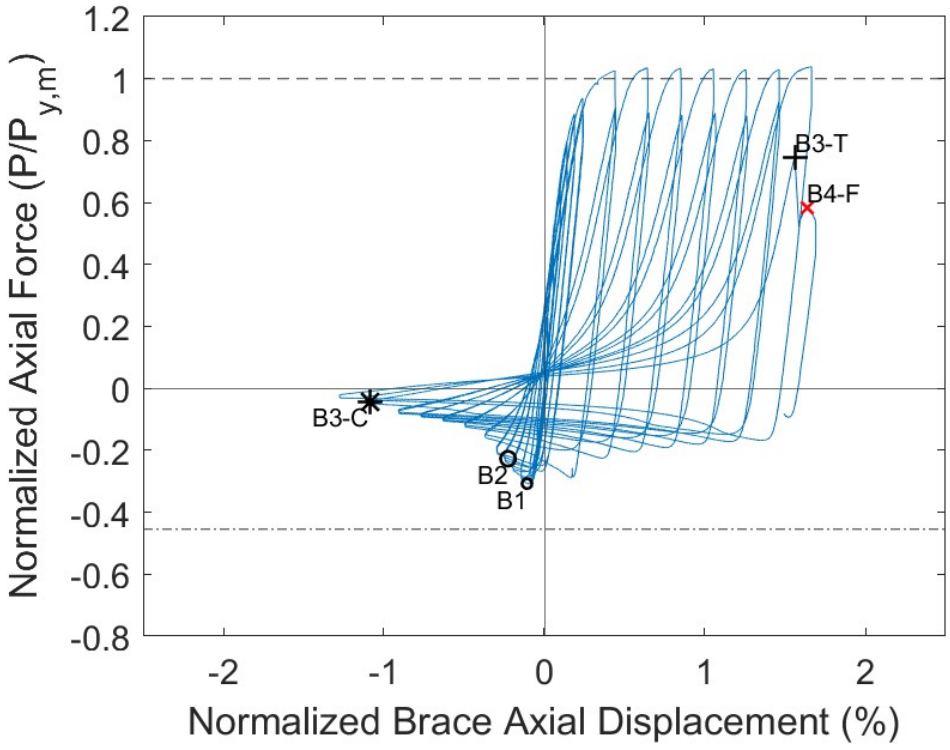

Figure 4.23 Normalized Force-Displacement Response: 6x1/4 Long

4.2.22 *6.625x3/16 A500 Long*

Initial Global Buckling occurred at a compressive load of 73 kips (0.69 of the expected critical buckling load) at a brace axial displacement of -0.26”. Moderate Global Buckling appeared during the first 0.69” target displacement compressive cycle. Local cupping was first observed when the brace axial displacement was equal to -1.82”. The cupping was estimated to be 0.3” deep when cupping first ensued, and it progressed to about 1.5” deep the compression cycle before fracture. A peak tensile load of 205 kips was reached when the brace axial deformation was 2.35” during the 2.54 target displacement cycles. The brace fractured when the axial brace deformation was equal to 2.34” and the axial load was 98 kips.

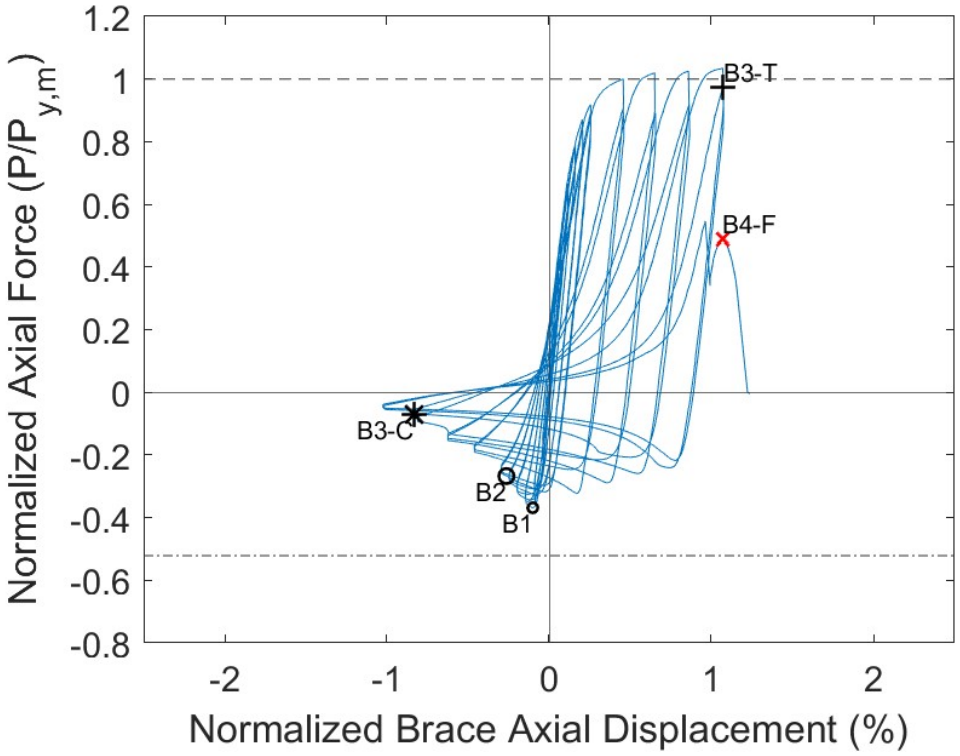

Figure 4.24 Normalized Force-Displacement Response: 6.625x3/16 Long

4.2.23 *6.625x1/4 A500 Long*

The 6.625x1/4 Long specimen globally buckled at a compressive load of 114 kips (0.81 of the expected critical buckling load). Moderate global buckling took place at a brace axial displacement of -0.62” and a compressive load of 73 kips. During the first compression cycle of 1.16” target displacements, the brace buckled switched buckling directions towards the east. During the second 2.54” target displacement cycle local cupping developed. This initiated at a brace axial deformation of -1.67” and a compressive load of 19 kips. The cupping was estimated to be 0.5” deep when cupping first ensued, and it progressed to about 1.8” deep the compression cycle before fracture. The peak tensile load was 283 kips at a brace axial deformation of 3.26”. Brace fracture occurred at an axial brace displacement of 3.14” and a tensile load of 104 kips.

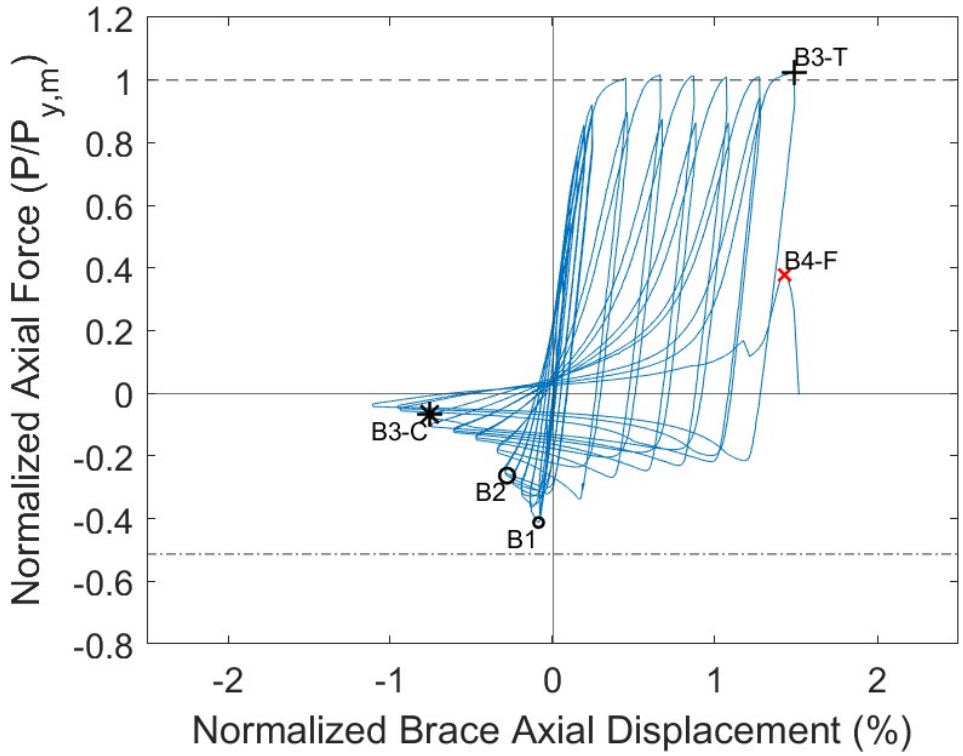

Figure 4.25 Normalized Force-Displacement Response: 6.625x1/4 Long

4.2.24 *6.625x3/8 A500 Long*

Global buckling of the 6.625x3/8 specimen occurred at a compressive axial deformation of 0.22” while the compressive force was 159 kips (0.80 the expected critical buckling load). Moderate Global Buckling occurred at a 114 kip compressive load when the axial brace deformation was 0.60”. The peak axial load of 420 kips was seen at peak of the first tension 1.62” target displacement cycle. Local cupping deformations became visible during the first compression cycle of the 3.00 target displacements. The magnitude of the depth of cupping started at 0.3” and progressed to 1.3” at the last compression cycle before fracture. Initial striations were observed the tension cycle before fracture. The brace fractured at a tensile load of 200 kips and a brace axial deformation of 3.31”.

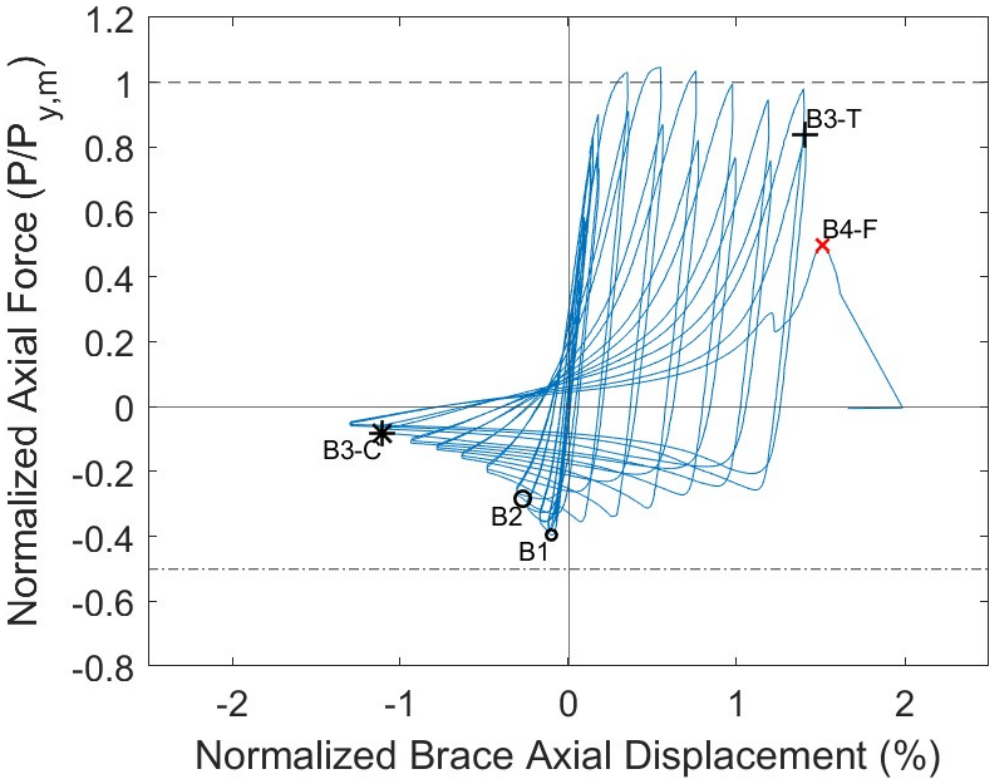

Figure 4.26 Normalized Force-Displacement Response: 6.625x3/8 Long

4.2.25 *6.625x1/2 A500 Long*

The 6.625x1/2 long specimen reached a maximum compressive force of 244 kips (0.96 the expected critical buckling load), at which point the specimen exhibited global buckling. Moderate Global Buckling appeared during the first 0.693" target displacement compressive cycle. A peak tensile load of 522 kips at the peak of the first large displacements step in the loading protocol – 1.16" T1. Local cupping was first observed when the brace axial displacement was equal to -3.53". The cupping was estimated to be 0.2" deep when cupping first ensued and it progressed to about 0.9" deep the compression cycle before fracture. The brace partially tore when the axial brace deformation was equal to 4.68" and the axial load was 224 kips. The brace cross-section fully separated when the brace went back into compression.

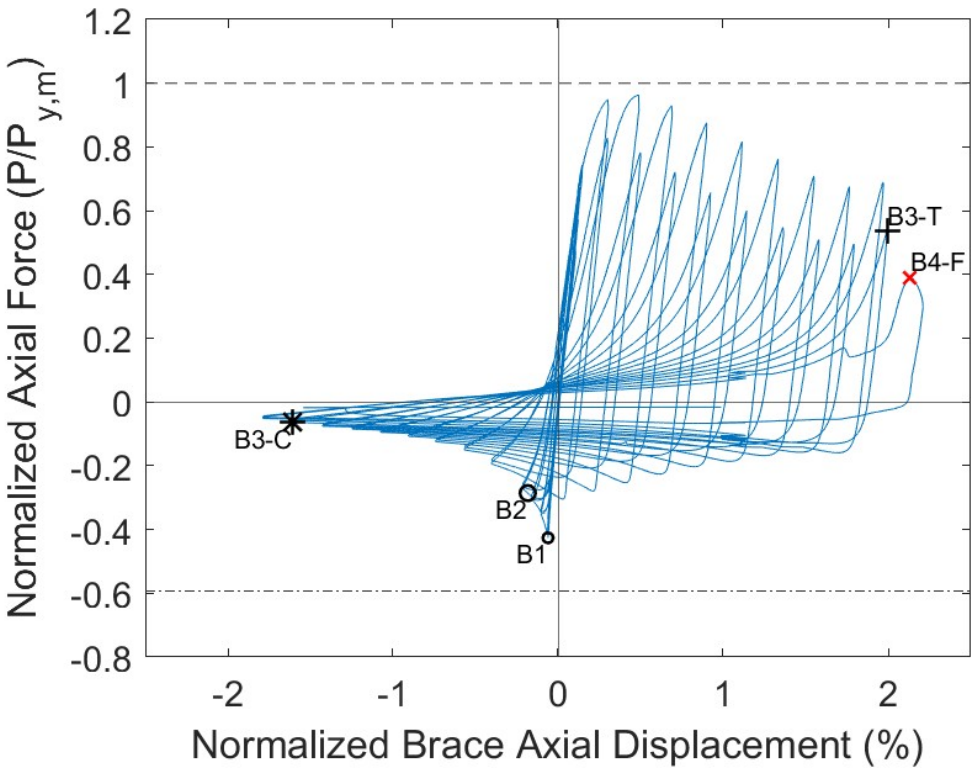

Figure 4.27 Normalized Force-Displacement Response: 6.625x1/2 Long

4.2.26 8.*625x3/16 A500 Long*

Initial Global Buckling occurred at a compressive load of 169 kips (0.80 of the expected critical buckling load) at a brace axial displacement of -0.23”. Moderate Global Buckling appeared during the first 0.63” target displacement compressive cycle. Local cupping was first observed when the brace axial displacement was equal to -1.01”. The cupping was estimated to be 0.4” deep when cupping first ensued, and it progressed to about 1.4” deep the compression cycle before fracture. A peak tensile load of 332 kips was reached when the brace axial deformation was 1.55” during the 1.75 target displacement cycles. The brace fractured when the axial brace deformation was equal to 1.37” and the axial load was 133 kips.

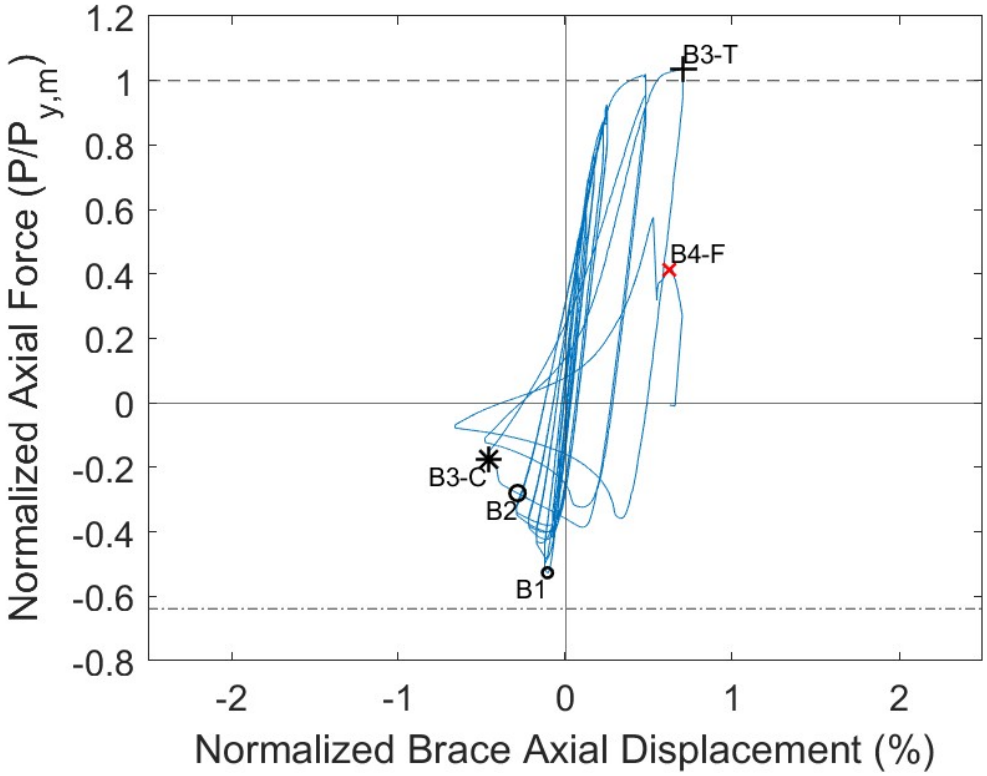

Figure 4.28 Normalized Force-Displacement Response: 8.625x3/16 Long

4.2.27 *8.625x1/4 A500 Long*

The 8.624x1/4 long specimen reached a maximum compressive force of 226 kips (0.82 the expected critical buckling load), at which point the specimen exhibited global buckling. Moderate buckling occurred during the first compression cycle of the 1.25 target displacements. Local cupping was first observed when the compressive axial deformation of the brace reached 1.58". Local cupping was approximately 1" deep when this damage state first appeared and progressed to about 1.4" the compression cycle before fracture. In the first tension cycle of 2.25 target displacements, the brace reached a peak tensile load of 419 kips at a brace axial displacement of 1.79". Striations and tearing appeared at a tensile force of 419 kips a tension cycle before fracture. The brace partially tore and in the same cycle fractured at an axial displacement of 1.65" and an axial load of 130 kips.

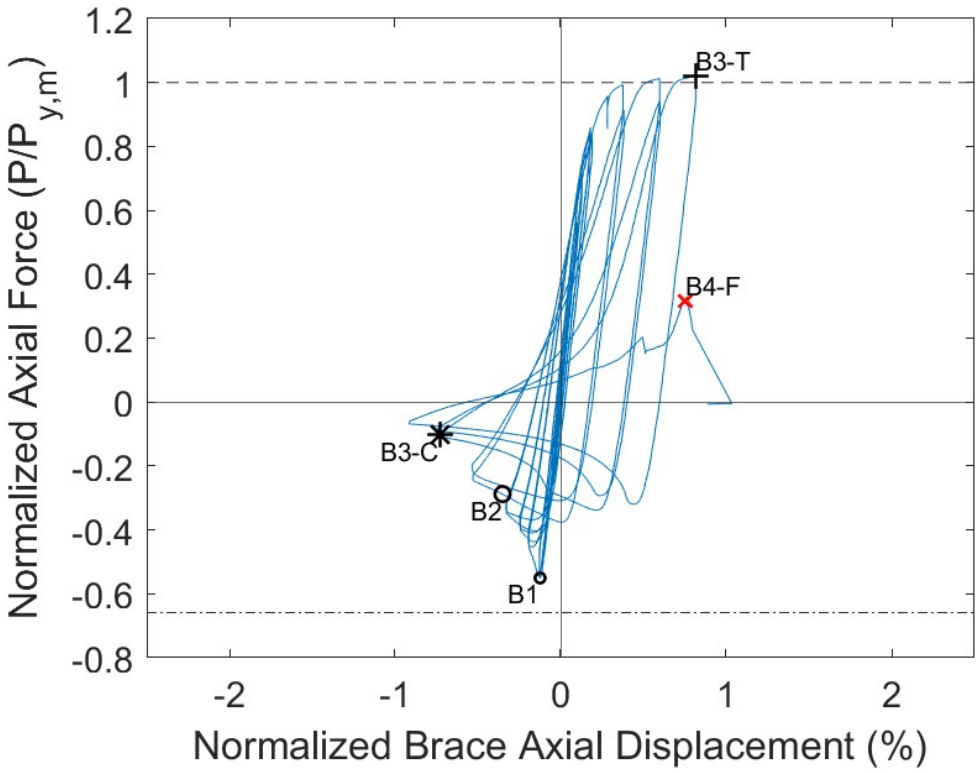

Figure 4.29 Normalized Force-Displacement Response: 8.625x1/4 Long

4.2.28 *8.625x3/8 A500 Long*

Global buckling of the 8.625x3/8 specimen occurred at a compressive axial deformation of 0.29” while the compressive force was 311 kips (0.79 the expected critical buckling load). Moderate Global Buckling occurred at a 165 kip compressive load when the axial brace deformation was 0.91”. Local cupping deformations became visible when the brace compressive axial deformation was 1.88”. The magnitude of the depth of cupping started at 0.1” and progressed to 1.6” at the last compression cycle before fracture. Initial striations and the peak tensile load of 579 kips were observed the tension cycle before fracture. The brace fractured at a tensile load of 212 kips and a brace axial deformation of 2.07”.

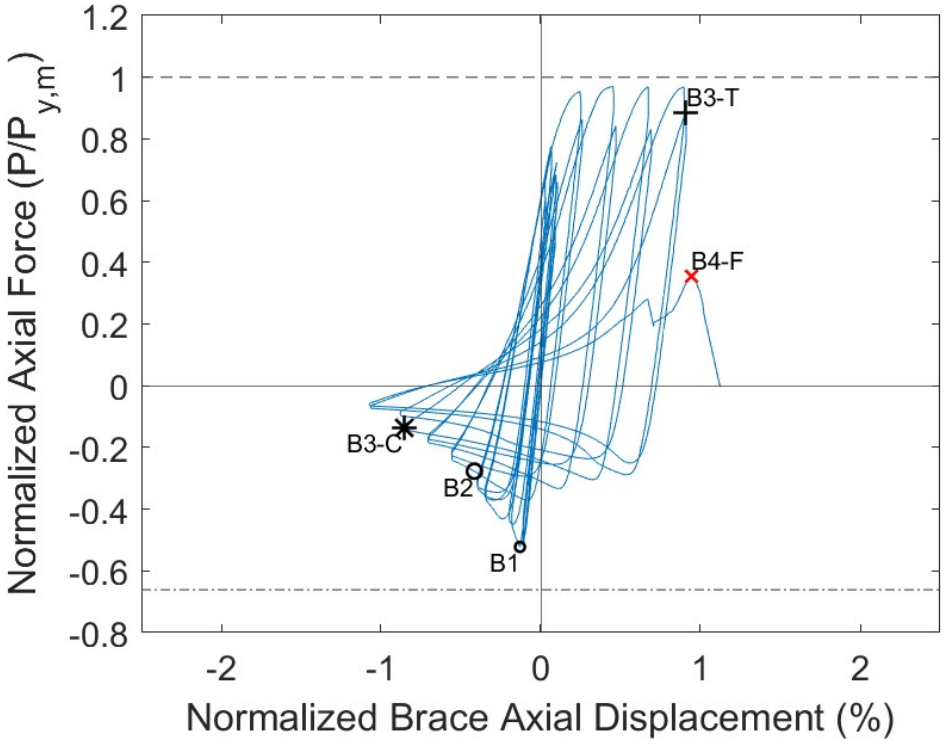

Figure 4.30 Normalized Force-Displacement Response: 8.625x3/8 Long

4.2.29 *10.75x1/4 A500 Long*

The 10.75x1/4 long specimen reached a maximum compressive force of 268 kips (0.67 the expected critical buckling load), at which point the specimen exhibited global buckling. Moderate Global Buckling appeared during the first 1.25” target displacement compressive cycle. Local cupping was first observed when the brace axial displacement was equal to -1.01”. The cupping was estimated to be 0.4” deep when cupping first ensued and it progressed to about 1.9” deep the compression cycle before fracture. A peak tensile load of 468 kips took place the tension cycle before the brace partially tore. The brace partially tore when the axial brace deformation was equal to 1.21” and the axial load was 336 kips. The brace went into another compression cycle before fracturing at a brace axial displacement of 1.54” and a load of 130 kips.

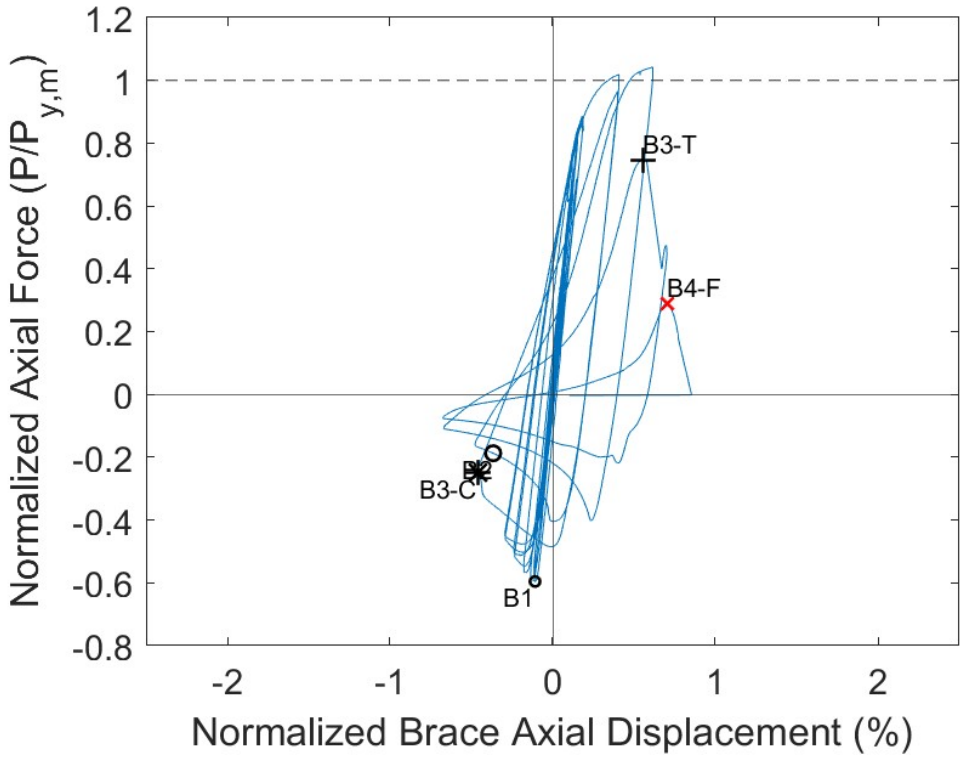

Figure 4.31 Normalized Force-Displacement Response: 10.75x1/4 Long

4.2.30 *10.75x0.365 A500 Long*

Initial Global Buckling occurred at a compressive load of 400 kips (0.72 of the expected critical buckling load) at a brace axial displacement of -0.39”. Moderate Global Buckling appeared during the first 0.63” target displacement compressive cycle. Local cupping was first observed when the brace axial displacement was equal to -1.43”. The cupping was estimated to be 0.7” deep when cupping first ensued, and it progressed to about 1.7” deep the compression cycle before fracture. A peak tensile load of 677 kips was reached when the brace axial deformation was 1.75” during the 2.08 target displacement cycles. The brace fractured when the axial brace deformation was equal to 2.08” and the axial load was 306 kips.

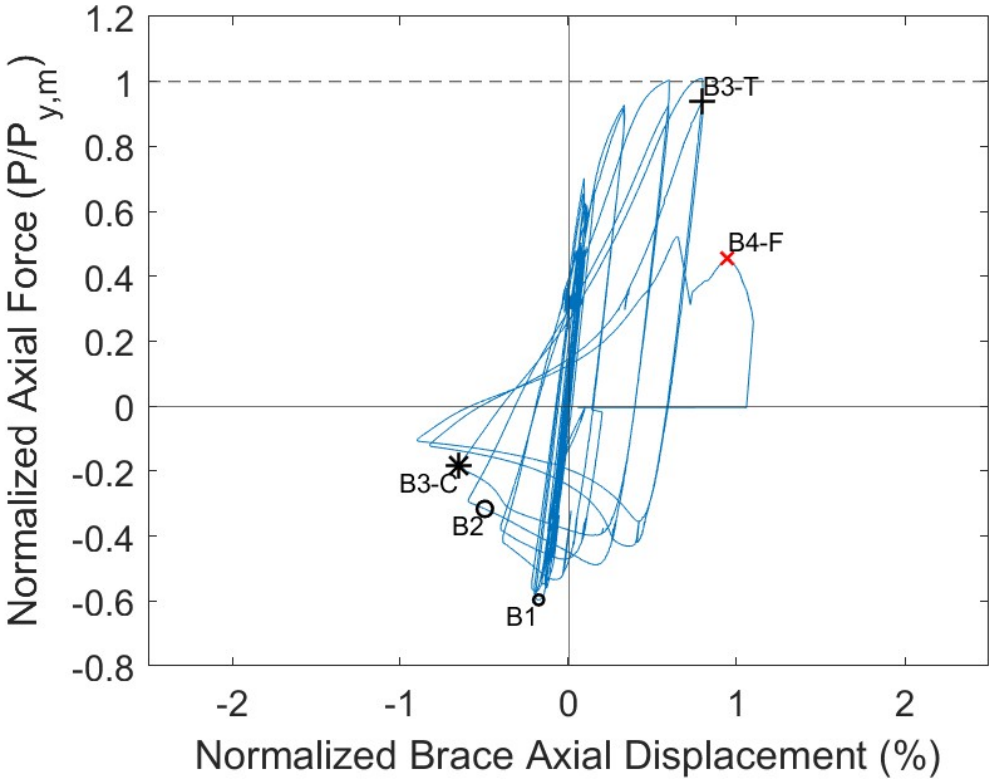

Figure 4.32 Normalized Force-Displacement Response: 10.75x0.365 Long

Table 4.4a Summary of Test Speciemen Damage States B1 and B2

Test Specimen	B1: Global Buckling			B2: Moderate Buckling		
	Target dis. (in.) *(Cycle)*	Deformation (in.) *(Approx. Drift (%))*	Force (k) *($P/P_{critical}$)*	Target dis. (in.) *(Cycle)*	Deformation (in.) *(Approx. Drift (%))*	Force (k) *($P/P_{critical}$)*
5x5x3/16 Short	0.25 (1)	-1.07 -(1.16)	243 (0.81)	0.625 (1)	-0.43 -(0.47)	-67 (0.63)
6x6x3/16 Short	0.25 (1)	-0.18 -(0.20)	-118 (0.74)	0.75 (1)	-0.66 -(0.72)	-33 (0.21)
6x6x3/16 Long	0.211 (1)	-0.22 -(0.20)	-96 (0.75)	0.578 (1)	-0.57 -(0.52)	-33 (0.26)
6x6x1/4 Short	0.375 (1)	-0.19 -(0.21)	-180 (0.83)	0.75 (1)	-0.59 -(0.64)	-115 (0.53)
6x6x1/4 Long	0.347 (1)	-0.24 -(0.22)	-141 (0.83)	0.693 (1)	-0.61 -(0.55)	-108 (0.64)
7x7x1/4 Short	0.375 (1)	-0.22 -(0.24)	-244 (0.82)	-[2] -[2]	-[2] -[2]	-[2] -[2]
7x7x1/4 Long	0.462 (1)	-0.26 -(0.24)	-203 (0.82)	1.16 (2)	-0.54 -(0.49)	-54 (0.22)
8x8x5/16 Short	0.5 (1)	-0.36 -(0.39)	-379 (0.82)	1.25 (1)	-0.86 -(0.93)	-92 (0.2)
8x8x5/16 Long	0.347 (1)	-0.31 -(0.28)	-316 (0.78)	1.16 (1)	-0.89 -(0.81)	-120 (0.3)
6x3/16 Short	0.25 (1)	-0.13 -(0.14)	-74 (0.71)	0.625 (1)	-0.48 -(0.52)	-47 (0.45)
6x3/16 Long	0.231 (1)	-0.18 -(0.16)	-59 (0.74)	0.578 (1)	-0.48 -(0.44)	-44 (0.54)
6x1/4 Short	0.25 (1)	-[1] -[1]	-92 (0.67)	0.625 (1)	-[1] -[1]	-60 (0.44)
6x1/4 Long	0.347 (1)	-0.22 -(0.20)	-71 (0.68)	0.693 (1)	-0.50 -(0.45)	-52 (0.5)
6.625x3/16 Long	0.347 (1)	-0.22 -(0.20)	-73 (0.69)	0.693 (1)	-0.58 -(0.53)	-53 (0.5)
6.625x1/4 Short	0.25 (1)	-0.13 -(0.14)	-131 (0.74)	0.75 (1)	-0.61 -(0.66)	-76 (0.43)
6.625x1/4 Long	0.347 (1)	-0.19 -(0.17)	-114 (0.81)	0.693 (1)	-0.62 -(0.56)	-73 (0.52)
6.625x3/8 Short	0.375 (1)	-0.18 -(0.20)	-197 (0.77)	0.75 (1)	-0.75 -(0.81)	-112 (0.44)
6.625x3/8 Long	0.347 (1)	-0.22 -(0.20)	-159 (0.8)	0.693 (1)	-0.60 -(0.55)	-114 (0.57)
6.625x1/2 Short	0.50 (1)	-0.21 -(0.23)	-296 (0.88)	0.75 (1)	-0.76 -(0.82)	-167 (0.49)
6.625x1/2 Long	0.462 (1)	-0.13 -(0.12)	-244 (0.96)	0.693 (1)	-0.40 -(0.36)	-164 (0.64)
8.625x3/16 Short	0.375 (1)	-0.19 -(0.21)	-201 (0.8)	1.25 (1)	-0.63 -(0.68)	-64 (0.26)
8.625x3/16 Long	0.375 (1)	-0.23 -(0.21)	-169 (0.8)	1.25 (1)	-0.63 -(0.57)	-90 (0.43)

Table 4.4a Summary of Test Speciemen Damage States B1 and B2 (continued).

	B1: Global Buckling			B2: Moderate Buckling		
Test Specimen	Target dis. (in.) *(Cycle)*	Deformation (in.) *(Approx. Drift (%))*	Force (k) *($P/P_{critical}$)*	Target dis. (in.) *(Cycle)*	Deformation (in.) *(Approx. Drift (%))*	Force (k) *($P/P_{critical}$)*
8.625x1/4 Short	0.625 (1)	-0.34 -(0.37)	-268 (0.83)	1.25 (1)	-0.81 -(0.88)	-123 (0.38)
8.625x1/4 Long	0.375 (1)	-0.27 -(0.25)	-226 (0.82)	1.25 (1)	-0.77 -(0.70)	-118 (0.43)
8.625x3/8 Short	0.5 (1)	-0.22 -(0.24)	-341 (0.73)	1.25 (1)	-0.91 -(0.99)	-169 (0.36)
8.625x3/8 Long	0.50 (1)	-0.29 -(0.26)	-311 (0.79)	1.25 (1)	-0.91 -(0.83)	-165 (0.42)
10.750x1/4 Short	0.50 (1)	-0.34 -(0.37)	-303 (0.69)	1.25 (1)	-0.72 -(0.78)	-83 (0.19)
10.750x1/4 Long	0.375 (1)	-0.24 -(0.22)	-268 (0.67)	1.25 (1)	-0.80 -(0.73)	-84 (0.21)
10.750x0.365 Short	0.5 (1)	-0.29 -(0.31)	-461 (0.75)	1.75 (1)	-0.8 -(0.87)	-174 (0.28)
10.750x0.365 Long	0.462 (1)	-0.39 -(0.35)	-400 (0.72)	1.62 (1)	-1.09 -(0.99)	-212 (0.38)

Table 4.4b Summary of Test Speciemen Damage States B3-C and B3-T

	B3-C: Local Cupping			B3-T: Striations/Tearing		
Test Specimen	Target dis. (in.) *(Cycle)*	Deformation (in.) *(Approx. Drift (%))*	Force (k) *($P/P_{critical}$)*	Target dis. (in.) *(Cycle)*	Deformation (in.) *(Approx. Drift (%))*	Force (k) *(P/P_{yield})*
5x5x3/16 Short	0.75 (1)	-0.69 -(0.75)	-46 (0.43)	1.25 (2)	0.75 (0.81)	132 (0.56)
6x6x3/16 Short	0.625 (1)	-0.59 -(0.64)	-53 (0.33)	1.25 (1)	0.37 (0.40)	133 (0.57)
6x6x3/16 Long	0.578 (2)	-0.61 -(0.55)	-25 (0.2)	1.16 (1)	0.8 (0.73)	256 (1.09)
6x6x1/4 Short	1.25 (1)	-1.19 -(1.29)	-47 (0.22)	1.25 (2)	0.98 (1.06)	348 (1.03)
6x6x1/4 Long	1.16 (2)	-1.11 -(1.01)	-50 (0.3)	1.62 (2)	0.95 (0.86)	271 (0.8)
7x7x1/4 Short	0.625 (1)	-0.6 -(0.65)	-97 (0.33)	1.25 (1)	0.37 (0.40)	271 (0.68)
7x7x1/4 Long	0.578 (2)	-0.49 -(0.45)	-159 (0.64)	1.16 (1)	0.77 (0.70)	328 (0.67)
8x8x5/16 Short	0.75 (1)	-0.60 -(0.65)	-291 (0.63)	1.25 (2)	0.40 (0.43)	287 (0.51)
8x8x5/16 Long	1.16 (1)	-1.15 -(1.05)	-95 (0.23)	1.61 (1)	0.73 (0.66)	498 (0.88)
6x3/16 Short	1.75 (2)	-1.53 -(1.66)	-13 (0.13)	2.75 (1)	2.23 (2.42)	148 (0.78)
6x3/16 Long	2.54 (1)	-2.05 -(1.86)	-11 (0.13)	3.00 (2)	2.84 (2.58)	155 (0.82)
6x1/4 Short	2.75 (2)	-[1] -[1]	-13 (0.09)	3.25 (2)	-[1] -[1]	227 (1.18)
6x1/4 Long	3.47 (1)	-2.37 -(2.16)	-11 (0.1)	3.93 (2)	3.60 (3.27)	133 (0.74)
6.625x3/16 Long	2.08 (1)	-1.82 -(1.66)	-14 (0.13)	2.54 (2)	2.35 (2.14)	194 (0.97)
6.625x1/4 Short	2.25 (1)	-2.09 -(2.27)	-23 (0.13)	2.75 (1)	2.54 (2.75)	284 (1.03)
6.625x1/4 Long	2.54 (2)	-1.67 -(1.52)	-19 (0.14)	3.47 (1)	3.26 (2.97)	283 (1.02)
6.625x3/8 Short	2.25 (2)	-2.23 -(2.42)	-36 (0.14)	3.25 (1)	2.93 (3.18)	403 (1.)
6.625x3/8 Long	3.00 (1)	-2.43 -(2.21)	-33 (0.17)	3.47 (2)	-3.09 -(2.81)	337 (0.84)
6.625x1/2 Short	3.25 (2)	-3.05 -(3.31)	-48 (0.14)	4.25 (1)	3.78 (4.10)	458 (0.8)
6.625x1/2 Long	4.39 (1)	-3.53 -(3.21)	-36 (0.14)	4.85 (2)	4.37 (3.98)	307 (0.53)
8.625x3/16 Short	1.25 (2)	-0.99 -(1.07)	-28 (0.11)	1.75 (1)	1.45 (1.57)	337 (1.05)
8.625x3/16 Long	1.25 (1)	-1.01 -(0.92)	-57 (0.27)	1.75 (1)	1.55 (1.41)	332 (1.03)

Table 4.4b Summary of Test Speciemen Damage States B3-C and B3-T (continued)

	B3-C: Local Cupping			B3-T: Striations/Tearing		
Test Specimen	Target dis. (in.) *(Cycle)*	Deformation (in.) *(Approx. Drift (%))*	Force (k) *($P/P_{critical}$)*	Target dis. (in.) *(Cycle)*	Deformation (in.) *(Approx. Drift (%))*	Force (k) *(P/P_{yield})*
8.625x1/4 Short	1.75 (2)	-1.35 -(1.46)	-52 (0.16)	2.25 (1)	1.78 (1.93)	426 (1.04)
8.625x1/4 Long	1.75 (1)	-1.58 -(1.44)	-42 (0.15)	2.25 (1)	1.79 (1.63)	419 (1.02)
8.625x3/8 Short	1.75 (2)	-1.57 -(1.70)	-73 (0.16)	2.25 (2)	1.66 (1.80)	524 (0.88)
8.625x3/8 Long	2.25 (1)	-1.88 -(1.71)	-80 (0.2)	2.75 (2)	1.99 (1.81)	527 (0.88)
10.750x1/4 Short	1.25 (1)	-1.07 -(1.16)	-62 (0.14)	1.75 (1)	1.45 (1.57)	475 (1.06)
10.750x1/4 Long	1.25 (1)	-1.01 -(0.92)	-112 (0.28)	1.75 (2)	1.21 (1.10)	336 (0.75)
10.750x0.365 Short	1.75 (1)	-1.52 -(1.65)	-114 (0.19)	2.25 (1)	1.8 (1.95)	686 (1.02)
10.750x0.365 Long	1.62 (2)	-1.43 -(1.30)	-123 (0.22)	2.08 (2)	1.75 (1.59)	629 (0.94)

Table 4.4c Summary of Test Speciemen Damage States B4-T and B4-F.

	B4-T: 50% Tearing			B4-F: Fracture		
Test Specimen	Target dis. (in.) *(Cycle)*	Deformation (in.) *(Approx. Drift (%))*	Force (k) *(P/P_{yield})*	Target dis. (in.) *(Cycle)*	Deformation (in.) *(Approx. Drift (%))*	Force (k) *(P/P_{yield})*
5x5x3/16 Short	1.25 (2)	1.04 (1.13)	207 (0.88)	-[4] -[4]	-[4] -[4]	-[4] -[4]
6x6x3/16 Short	1.25 (1)	0.76 (0.82)	227 (0.97)	-[4] -[4]	-[4] -[4]	-[4] -[4]
6x6x3/16 Long	-[3] -[3]	-[3] -[3]	-[3] -[3]	1.16 (1)	0.87 (0.79)	108 (0.46)
6x6x1/4 Short	1.75 (1)	1.25 (1.36)	280 (0.82)	-[4] -[4]	-[4] -[4]	-[4] -[4]
6x6x1/4 Long	-[3] -[3]	-[3] -[3]	-[3] -[3]	2.08 (1)	1.25 (1.14)	104 (0.3)
7x7x1/4 Short	1.25 (1)	0.94 (1.02)	147 (0.37)	-[4] -[4]	-[4] -[4]	-[4] -[4]
7x7x1/4 Long	-[3] -[3]	-[3] -[3]	-[3] -[3]	1.62 (1)	0.9 (0.82)	133 (0.27)
8x8x5/16 Short	1.25 (2)	0.65 (0.71)	446 (0.79)	-[4] -[4]	-[4] -[4]	-[4] -[4]
8x8x5/16 Long	-[3] -[3]	-[3] -[3]	-[3] -[3]	1.61 (1)	0.86 (0.78)	278 (0.49)
6x3/16 Short	2.75 (1)	2.48 (2.69)	100 (0.53)	-[4] -[4]	-[4] -[4]	-[4] -[4]
6x3/16 Long	-[3] -[3]	-[3] -[3]	-[3] -[3]	3.47 (1)	2.86 (2.60)	58 (0.31)
6x1/4 Short	3.75 (1)	-[1] -[1]	74 (0.39)	-[4] -[4]	-[4] -[4]	-[4] -[4]
6x1/4 Long	-[3] -[3]	-[3] -[3]	-[3] -[3]	4.39 (1)	3.57 (3.25)	65 (0.29)
6.625x3/16 Long	-[3] -[3]	-[3] -[3]	-[3] -[3]	3.00 (1)	2.34 (2.13)	98 (0.49)
6.625x1/4 Short	3.25 (1)	2.21 (2.40)	48 (0.17)	-[4] -[4]	-[4] -[4]	-[4] -[4]
6.625x1/4 Long	-[3] -[3]	-[3] -[3]	-[3] -[3]	3.47 (1)	3.14 (2.86)	104 (0.38)
6.625x3/8 Short	3.25 (1)	3.15 (3.42)	194 (0.48)	-[4] -[4]	-[4] -[4]	-[4] -[4]
6.625x3/8 Long	-[3] -[3]	-[3] -[3]	-[3] -[3]	3.93 (1)	3.31 (3.01)	200 (0.5)
6.625x1/2 Short	4.25 (1)	3.95 (4.28)	200 (0.34)	-[4] -[4]	-[4] -[4]	-[4] -[4]
6.625x1/2 Long	-[3] -[3]	-[3] -[3]	-[3] -[3]	5.31 (1)	4.68 (4.26)	224 (0.39)
8.625x3/16 Short	-[3] -[3]	-[3] -[3]	-[3] -[3]	1.75 (2)	1.72 (1.87)	134 (0.42)
8.625x3/16 Long	-[3] -[3]	-[3] -[3]	-[3] -[3]	1.75 (2)	1.37 (1.25)	133 (0.41)

Table 4.4c Summary of Test Speciemen Damage States B4-T and B4-F (continued)

Test Specimen	B4-T: 50% Tearing			B4-F: Fracture		
	Target dis. (in.) *(Cycle)*	Deformation (in.) *(Approx. Drift (%))*	Force (k) *(P/P_{yield})*	Target dis. (in.) *(Cycle)*	Deformation (in.) *(Approx. Drift (%))*	Force (k) *(P/P_{yield})*
8.625x1/4 Short	-[3]	-[3]	-[3]	2.25	1.73	125
	-[3]	-[3]	-[3]	(1)	(1.88)	(0.3)
8.625x1/4 Long	-[3]	-[3]	-[3]	2.25	1.65	130
	-[3]	-[3]	-[3]	(2)	(1.50)	(0.32)
8.625x3/8 Short	-[3]	-[3]	-[3]	2.75	1.87	214
	-[3]	-[3]	-[3]	(1)	(2.03)	(0.36)
8.625x3/8 Long	-[3]	-[3]	-[3]	3.25	2.07	212
	-[3]	-[3]	-[3]	(1)	(1.88)	(0.36)
10.750x1/4 Short	-[3]	-[3]	-[3]	2.25	2.00	119
	-[3]	-[3]	-[3]	(1)	(2.17)	(0.24)
10.750x1/4 Long	-[3]	-[3]	-[3]	2.25	1.54	130
	-[3]	-[3]	-[3]	(1)	(1.40)	(0.29)
10.750x0.365 Short	-[3]	-[3]	-[3]	2.75	2.07	159
	-[3]	-[3]	-[3]	(1)	(2.25)	(0.24)
10.750x0.365 Long	-[3]	-[3]	-[3]	2.54	2.08	306
	-[3]	-[3]	-[3]	(1)	(1.89)	(0.46)

Table 4.4d Summary of Test Speciemen Damage: Yielding and Peak Tensile Force

	Brace Yielding			Peak Tensile Force		
Test Specimen	Target dis. (in.) *(Cycle)*	Deformation (in.) *(Approx. Drift (%))*	Force (kips)	Target dis. (in.) *(Cycle)*	Deformation (in.) *(Approx. Drift (%))*	Force (kips) *(P/P_{yield})*
5x5x3/16 Short	1.25 (1)	0.77 (0.84)	235	1.25 (1)	1.07 (1.16)	243 (1.03)
6x6x3/16 Short	0.75 (1)	0.42 (0.46)	234	0.75 (1)	0.61 (0.66)	256 (1.09)
6x6x3/16 Long	1.16 (1)	0.52 (0.47)	234	1.16 (1)	0.79 (0.72)	257 (1.09)
6x6x1/4 Short	1.25 (1)	0.58 (0.63)	339	1.25 (1)	1.25 (1.36)	365 (1.07)
6x6x1/4 Long	1.16 (1)	0.45 (0.41)	339	1.62 (1)	1.16 (1.06)	376 (1.11)
7x7x1/4 Short	-[5] -[5]	-[5] -[5]	395	0.75 (1)	0.42 (0.46)	357 (0.9)
7x7x1/4 Long	-[5] -[5]	-[5] -[5]	395	1.16 (1)	0.85 (0.77)	415 (0.84)
8x8x5/16 Short	1.25 (1)	0.57 (0.62)	563	1.25 (1)	0.72 (0.78)	579 (1.03)
8x8x5/16 Long	-[5] -[5]	-[5] -[5]	563	1.16 (1)	0.68 (0.62)	557 (0.99)
6x3/16 Short	-[5] -[5]	-[5] -[5]	170	2.25 (1)	2.17 (2.35)	186 (0.98)
6x3/16 Long	-[5] -[5]	-[5] -[5]	170	3.00 (1)	2.89 (2.63)	184 (0.97)
6x1/4 Short	1.25 (1)	0.95 (1.03)	229	3.25 (1)	-[1] -[1]	241 (1.26)
6x1/4 Long	1.16 (1)	0.76 (0.69)	229	3.93 (1)	3.65 (3.32)	238 (1.04)
6.625x3/16 Long	1.62 (1)	1.26 (1.15)	199	2.54 (1)	2.35 (2.14)	206 (1.03)
6.625x1/4 Short	1.25 (1)	1.03 (1.12)	276	2.75 (1)	2.54 (2.75)	284 (1.03)
6.625x1/4 Long	1.16 (1)	0.93 (0.85)	276	3.47 (1)	3.26 (2.97)	283 (1.02)
6.625x3/8 Short	1.25 (1)	0.80 (0.87)	401	2.25 (1)	1.47 (1.59)	413 (1.03)
6.625x3/8 Long	1.16 (1)	0.64 (0.58)	401	1.62 (1)	1.20 (1.09)	420 (1.05)
6.625x1/2 Short	-[5] -[5]	-[5] -[5]	573	1.25 (1)	0.81 (0.88)	550 (0.96)
6.625x1/2 Long	-[5] -[5]	-[5] -[5]	573	1.16 (1)	1.07 (0.97)	522 (0.96)
8.625x3/16 Short	1.25 (1)	0.64 (0.69)	321	1.75 (1)	1.45 (1.57)	337 (1.05)
8.625x3/16 Long	1.16 (1)	0.86 (0.78)	321	1.75 (1)	1.55 (1.41)	332 (1.03)

Table 4.4d Summary of Test Speciemen Damage: Yielding and Peak Tensile Force (continued)

	Brace Yielding			Peak Tensile Force		
Test Specimen	Target dis. (in.) *(Cycle)*	Deformation (in.) *(Approx. Drift (%))*	Force (kips)	Target dis. (in.) *(Cycle)*	Deformation (in.) *(Approx. Drift (%))*	Force (kips) *(P/P_{yield})*
8.625x1/4 Short	1.25 (1)	0.71 (0.77)	411	2.25 (1)	1.78 (1.93)	426 (1.03)
8.625x1/4 Long	1.62 (1)	1.15 (1.05)	411	2.25 (1)	1.79 (1.63)	419 (1.02)
8.625x3/8 Short	-[5] -[5]	-[5] -[5]	596	1.75 (1)	1.21 (1.31)	581 (0.97)
8.625x3/8 Long	-[5] -[5]	-[5] -[5]	596	2.75 (1)	0.99 (0.90)	579 (0.97)
10.750x1/4 Short	-[5] -[5]	-[5] -[5]	448	1.75 (1)	1.45 (1.57)	475 (0.95)
10.750x1/4 Long	1.16 (1)	0.61 (0.55)	448	1.75 (1)	1.35 (1.23)	468 (1.04)
10.750x0.365 Short	1.25 (1)	0.90 (0.98)	670	1.75 (1)	1.32 (1.43)	686 (1.02)
10.750x0.365 Long	1.62 (1)	1.28 (1.16)	670	2.08 (1)	1.75 (1.59)	677 (1.01)

[1] Axial deformation data unavailable
[2] Damage state was not achieved
[3] Brace testing went past 50% tearing to full-fracture
[4] Brace testing stopped at 50% tearing and was not tested till full-fracture
[5] The specimen did not reach the calculated predicted yield force

Table 4.5 Summary of Maximum Axial Deformations and Drifts

Test Specimen	**Tension** Deformation (in) (*Approx. Drift (%)*)	**Compression** Deformation (in) (*Approx. Drift (%)*)	**Range** Deformation (in) (*Approx. Drift (%)*)
5x5x3/16 Short	1.03 (1.12)	1.14 (1.24)	2.18 (2.36)
6x6x3/16 Short	0.95 (1.03)	0.70 (0.76)	1.65 (1.79)
6x6x3/16 Long	0.91 (0.83)	0.81 (0.74)	1.73 (1.57)
6x6x1/4 Short	0.99 (1.07)	1.19 (1.29)	2.18 (2.36)
6x6x1/4 Long	1.23 (1.12)	1.50 (1.36)	2.73 (2.48)
7x7x1/4 Short	0.93 (1.01)	1.19 (1.29)	2.12 (2.30)
7x7x1/4 Long	0.86 (0.78)	1.09 (0.99)	1.95 (1.77)
8x8x5/16 Short	0.65 (0.71)	1.24 (1.35)	1.90 (2.06)
8x8x5/16 Long	0.86 (0.78)	1.18 (1.07)	2.03 (1.85)
6x3/16 Short	2.22 (2.41)	2.05 (2.22)	4.27 (4.63)
6x3/16 Long	2.84 (2.58)	2.48 (2.26)	5.32 (4.84)
6x1/4 Short	2.40 (2.60)	2.19 (2.38)	4.59 (4.98)
6x1/4 Long	3.54 (3.22)	3.15 (2.87)	6.69 (6.09)
6.625x3/16 Long	2.32 (2.11)	2.23 (2.03)	4.55 (4.14)
6.625x1/4 Short	2.53 (2.74)	2.55 (2.77)	5.08 (5.51)
6.625x1/4 Long	3.11 (2.83)	2.41 (2.19)	5.52 (5.02)
6.625x3/8 Short	3.13 (3.39)	3.16 (3.43)	6.29 (6.82)
6.625x3/8 Long	3.28 (2.98)	2.84 (2.58)	6.11 (5.56)
6.625x1/2 Short	3.94 (4.27)	4.05 (4.39)	7.98 (8.66)
6.625x1/2 Long	4.64 (4.22)	3.68 (3.35)	8.32 (7.57)
8.625x3/16 Short	1.71 (1.86)	1.36 (1.48)	3.08 (3.34)
8.625x3/16 Long	1.54 (1.40)	1.43 (1.30)	2.97 (2.70)

Table 4.5 Summary of Maximum Axial Deformations and Drifts (continued)

Test Specimen	**Tension** Deformation (in) (*Approx. Drift (%)*)	**Compression** Deformation (in) (*Approx. Drift (%)*)	**Range** Deformation (in) (*Approx. Drift (%)*)
8.625x1/4 Short	1.72 (1.87)	1.82 (1.97)	3.54 (3.84)
8.625x1/4 Long	1.79 (1.63)	1.95 (1.77)	3.74 (3.40)
8.625x3/8 Short	1.86 (2.02)	2.03 (2.20)	3.89 (4.22)
8.625x3/8 Long	2.33 (2.12)	2.41 (2.19)	4.74 (4.31)
10.750x1/4 Short	1.44 (1.56)	1.47 (1.59)	2.90 (3.15)
10.750x1/4 Long	1.53 (1.39)	1.46 (1.33)	2.99 (2.72)
10.750x0.365 Short	2.06 (2.23)	2.00 (2.17)	4.06 (4.40)
10.750x0.365 Long	2.09 (1.90)	1.96 (1.78)	4.05 (3.68)

Chapter 5. Data Analysis and Interpretation

5.1 Introduction

This chapter presents the analysis and interpretation of test data. Chapter 5 will provide the following information:

- Section 5.2 details the methods implemented in MATLAB scripts, used to process data from the experimental instrumentation described in Section 3.5. It was necessary to process raw data to produce clean, accurate, and useful data.
- Section 5.3 investigates the impact of local and global slenderness on brace axial deformation capacity. This section includes square HSS test data from Bergendahl (2021) and Kaldestad (2022)
- Section 5.4 reviews data from the optotrak coordinate measurement system with LED's located in the local cupping region to study how local and global slenderness affect concentration of strain at the hinge region. This section focuses on round HSS test data.

5.2 Data Processing

String Potentiometer, Duncan Potentiometer, and Strain Guage data was collected at a frequency of 5 Hz during testing using LabVIEW software by National Instruments. The acquisition of data was not stopped until brace fracture, but pauses were made in the loading protocol during data collection to make observations. The data files were processed with a MATLAB script that removed pauses from raw data that are shown in Figure 5.1(a), to create the continuous change in actuator displacement shown in Figure 5.1(b). The script also removed random spikes from electrical noise that occurred in various channels.

A separate acquisition system and software was used to record the 3-dimensional position data from the Optotrak sensors detailed in Section 3.6.4. NDI First Principles was the software used to collect this data at a frequency of 10 Hz, and an additional MATLAB script was used to process this data. MATLAB and NDI recording initiated at the same time so both timestamps started at time equal to zero. Linear interpolation and decimation was used to align the time series from the Optotrak to the data from LabView, which had different recording frequencies. Once aligned, the data were combined into a single data set. Pauses in the Optotrak data were removed using the same script used the process LabView data resulted in the processing of data from Figure 5.1(a) to Figure 5.1 (b). Lastly, the position of the sensors was transformed to a

coordinate system aligned with the sensor layout. This processed data was used to calculate average longitudinal strain utilized in Section 5.4 to investigate the concentration of strain at the hinge region.

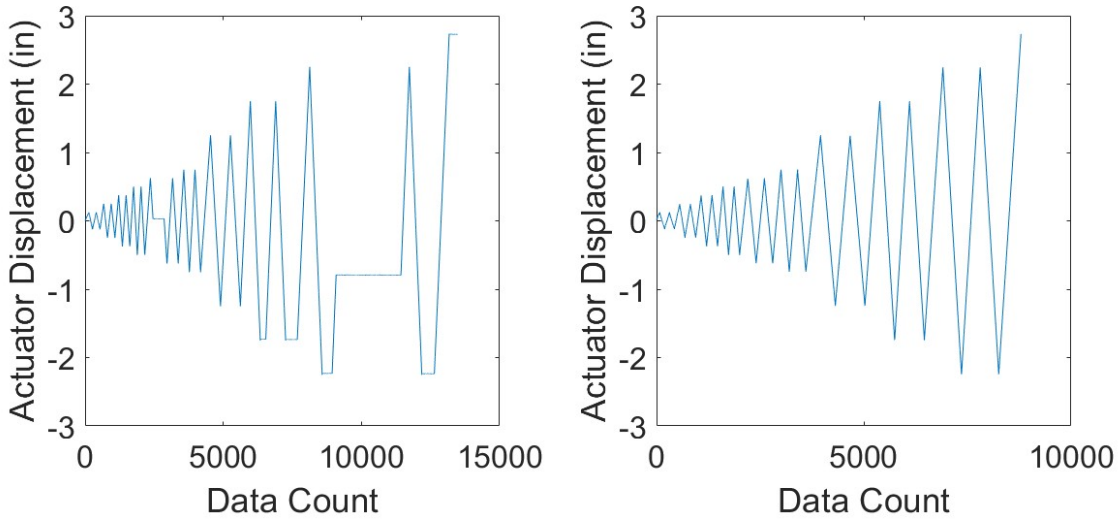

Figure 5.1 Raw (a) and Processed (b) LabVIEW Data

5.2.1 Brace Axial Deformation Correction

As the specimen buckled out-of-plane, the string potentiometer attached to the side of the brace rotated resulting in a larger measured axial compressive response than actual compressive deformation as illustrated schematically in Figure 5.2. A correction was applied to account for the discrepancy between measured and actual data. The angle of gusset plate rotation was estimated using deformation measurements in the out-of-plane direction from two string potentiometers along the gusset plate and the transverse distance between them. Once the gusset rotation was known, the measured location of the brace deformation string potentiometer (including its housing) could be used to determine the additional measured displacement due to gusset rotation. The equations used for this correction were calculated using MATLAB and the script can be found in Appendix D.2 in Kaldestad, 2022. The corrected brace axial displacement was utilized for all the short specimen force-displacement response analyses.

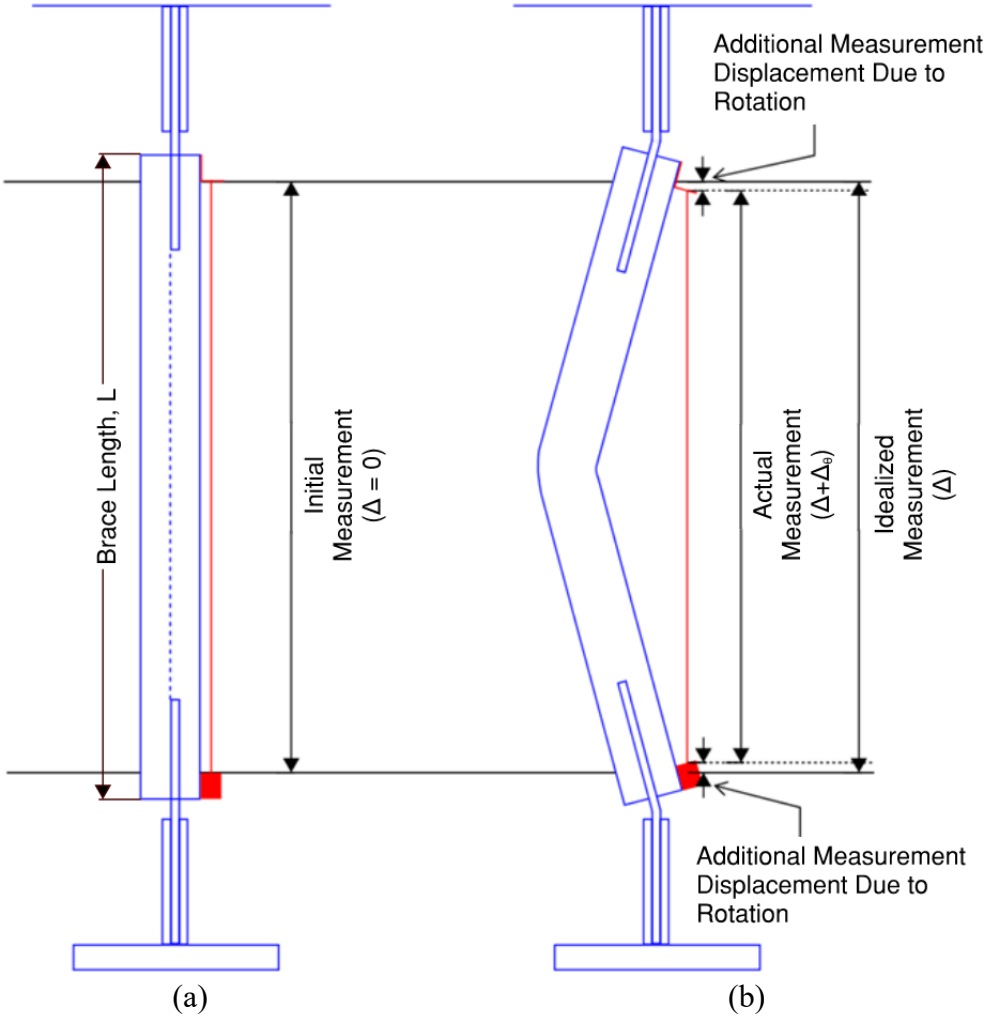

Figure 5.2 Brace Configuration in Original (a) and Rotated (b) position

Figure 5.3 was used to ensure accuracy of the corrections to brace axial deformation. Total axial displacement (defined next), original axial displacement (uncorrected from the potentiometer in Figure 5.2), and corrected axial displacement are compared. Total axial displacement used the string potentiometer that was attached between end connection plates to collect total axial displacement data, which included movement due to bolt bearing and bolt slip. The original data represents data that does not remove the compressive displacement component due to rotation of the gusset plate. The absolute value of corrected brace axial displacement data should never be greater than the absolute value of total axial displacement.

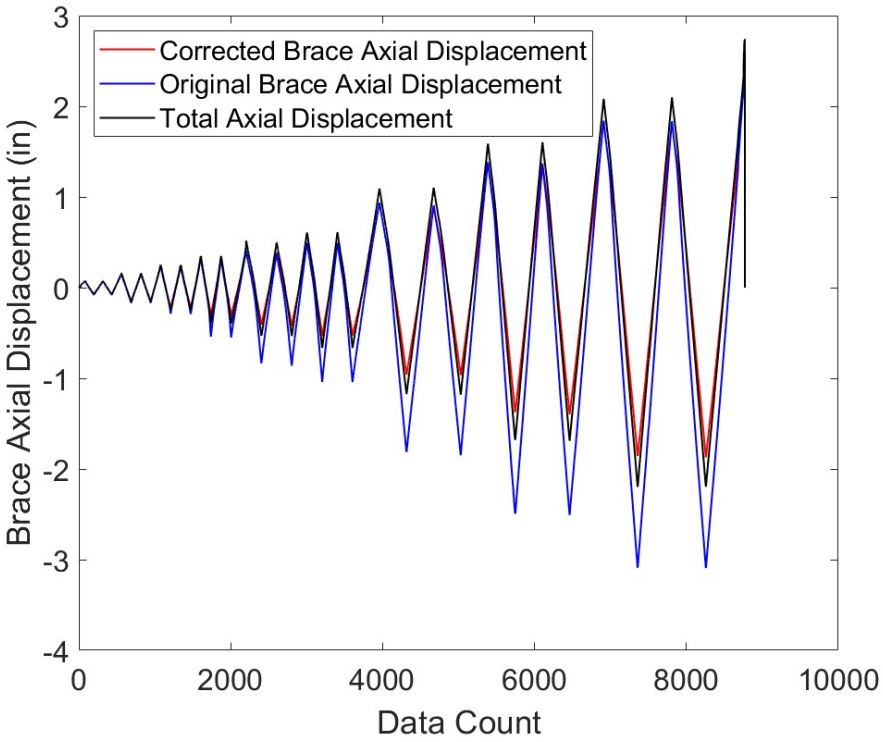

Figure 5.3 Original, Corrected, and Total Axial Displacement

For the long specimens, an additional string potentiometer, SP 22 - Figure 5.4, was attached to the brace as an additional measurement of brace axial deformation. SP 22 was connected between brace ends with an attachment that was free to move independently of gusset plate rotation. During out-of-plane rotation of the gusset plate, SP 22 would not rotate due tension of the string potentiometer line; the measured brace deformation data was equal to the actual response. The data collected by this updated string potentiometer configuration made it unnecessary to utilize the corrected brace axial deformation data. The axial displacement data from SP 22 was utilized for all the long specimen force-displacement response analyses.

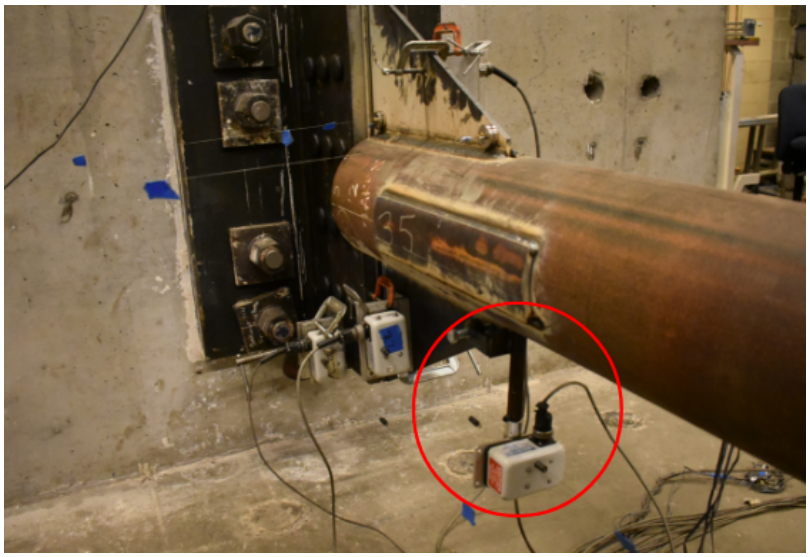

Figure 5.4 String Potentiometer 22

5.3 Impact of Brace Design Parameters

The following sections investigate the effect of brace parameters such as local and global slenderness on brace response. The brace parameters that were investigated are as follows:

- Section 5.3.1 - Brace local slenderness, *b/t* or *D/t*
- Section 5.3.2 - Brace global slenderness, L_c/r
- Section 5.3.3 - Combined parameter of local and global slenderness

Brace response was analyzed in terms of brace axial deformation capacity as normalized axial deformation range and equivalent story drift range. See Section 4.2 for the method used to convert measured brace axial deformation to approximate story drift. The story drift range is taken as the sum of the absolute values of maximum tensile and compressive deformation. All plots presented in this section are dual-Y-axes plots. The left Y-axis shows story drift range, while the right Y-axis represents normalized axial deformation range. The performance of the braces will be evaluated using two criteria. First, story drift range is compared to the current AISC 341-22 highly and moderately ductile limits. Second, as part of a coordinated research effort, Andrew Sen (2024) established minimum drift range capacities for brace fracture needed for ensuring good overall seismic performance, including meeting collapse criteria at the ASCE 7 MCE_R hazard level, for SCBFs and OCBFs using non-linear response history analysis of a series of brace frame archetypes. It was determined that the minimum story drift range needed is

3.5% for OCBFs and 5.0% for SCBFs. These drift range capacity targets are not dependent on HSS shape and are crucial for evaluating the current local slenderness limits.

5.3.1 Local Slenderness Ratio

Previous research has shown that brace local slenderness has a significant impact on brace response. The effect of this parameter on the ductile performance of Test Series 1, square HSS, and Test Series 2, round HSS, are investigated in this section. Figure 5.5 and Figure 5.6 show the relationship between the measured local slenderness and story drift range for the square and round HSS respectively. The target deformation capacity targets for SCBFs and OCBFs provided by Sen (2024) are plotted in terms of story drift range on both plots. The current AISC 341-22 highly and moderately ductile limits for square and round HSS are also plotted in both Figure 5.5 and Figure 5.6.

Figure 5.5 combines data from Test Series 1 and all previous test data (Bergendahl, 2021 and Kaldestad, 2022) on square HSS subjected to symmetric loading. As local slenderness decreases, story drift range capacity exponentially increases. This trend agrees with previous research. The power regression curve fitted to this data has an R^2 of 0.901 meaning that local slenderness accounts for a significant amount of variation in deformation range. All the square HSS braces in Figure 5.5 that meet the current AISC 341-22 moderately and highly ductile local slenderness limits also meet the target drift requirements for OCBFs and SCBFs, respectively. Some of the braces with local slenderness exceeding the current moderately ductile limit seem to meet the minimum drift range capacity for OCBFs. This observation will be used in subsequent sections to develop new recommended limits for OCBFs.

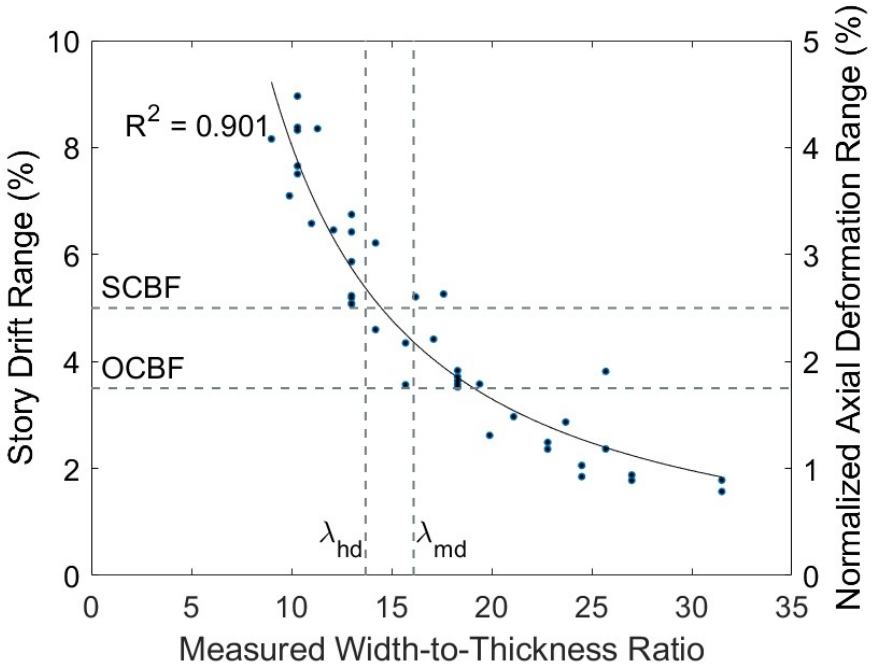

Figure 5.5 Story Drift Range and Normalized Axial Deformation Range vs Measured Local Slenderness – Square HSS

Figure 5.6 plots all data from Test Series 2, round HSS, as story drift range vs measured diameter-to-thickness. The trend is comparable to that of the square HSS whereas local slenderness decreases, brace axial deformation capacity exponentially increases. However, over the same range of local slenderness, the effect of this change on story drift range is more significant for square HSS than round HSS. The power regression curve fitted to this data has a R^2 of 0.853 indicating that local slenderness accounts for a significant amount of variation in deformation range. All the braces that meet the current AISC 341-22 moderately and highly ductile local slenderness limits also meet the target drift requirements for OCBFs and SCBFs respectively. Again, many of the sections outside of the current AISC moderately ductile limit meet the target drift requirement for OCBFs. In total, sixteen out of the twenty-one round HSS specimens meet the OCBF minimum drift range capacity requirement.

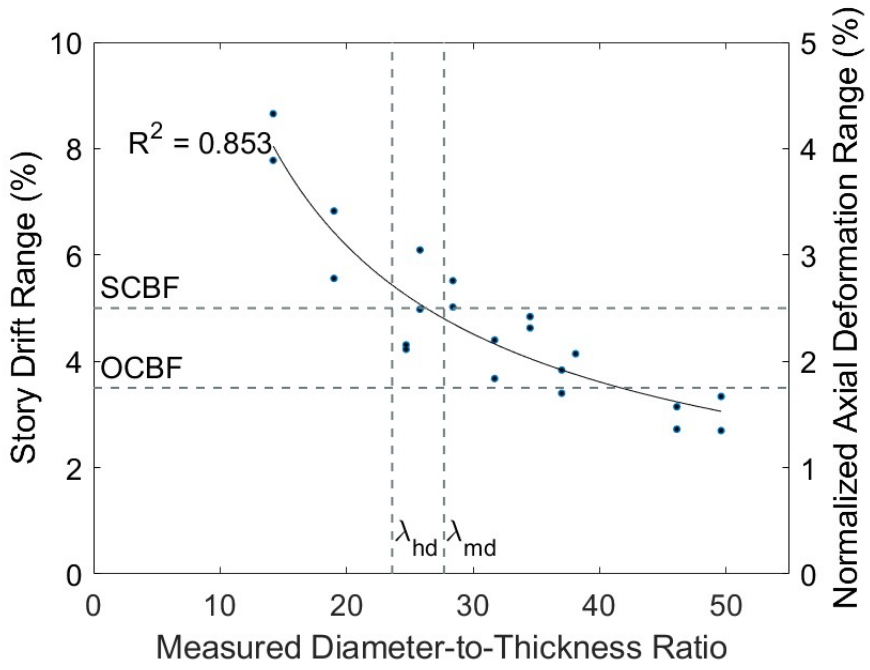

Figure 5.6 Story Drift Range and Normalized Axial Deformation Range vs Measured Local Slenderness – Round HSS

5.3.2 Global Slenderness Ratio

This section reviews the effect of global slenderness on brace response Previous research has shown that global slenderness is a primary factor that affects the ductile performance of braces. The plots included in this section include data from previous research, Test Series 1 and Test Series 2. Values of global slenderness for square and round HSS specimens range from 58 to 127 and 49 to 107, respectively.

Figure 5.7 shows the relationship between brace global slenderness and story drift range. There is a clear relationship that as brace global slenderness increases, story drift range also increases. The linear regression fit to this data has an R^2 of 0.621. Global slenderness accounts for much of the variation in this regression, but other factors such as local slenderness also affect drift range capacity. Braces with similar global slenderness can have drastically different local slenderness. For example, in Figure 5.7, braces with a global slenderness of approximately 80, have local slenderness ranging from 13 to 27. The difference in story drift range capacity between braces with similar global slenderness can be attributed to this factor. Braces with global slenderness less than 100 had a larger range of local slenderness than braces with global slenderness greater than 100. In part, this explains the tighter band of data around the trendline for global slenderness values above 100. While increasing global slenderness does help

specimens attain a larger story drift range there is considerably more variability than for local slenderness.

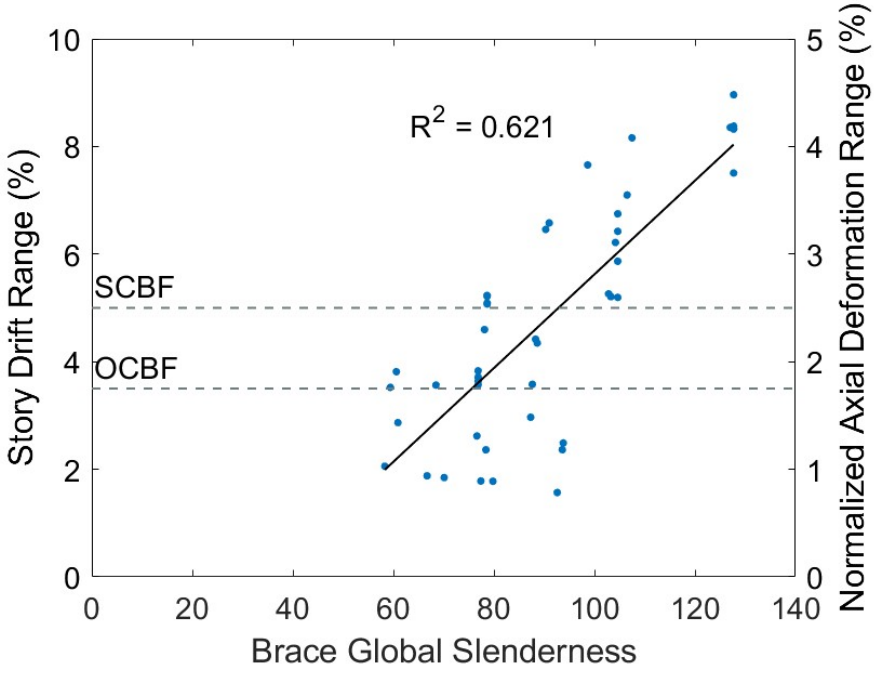

Figure 5.7 Story Drift Range and Normalized Axial Deformation Range vs Brace Global Slenderness – Square HSS

Figure 5.8 plots the relationship between global slenderness and story drift range for the round HSS specimens. The relationship between brace global slenderness and story drift range for the round HSS specimens is analogous to the square HSS specimens; as brace global slenderness increases, story drift range capacity increases. The R^2 for the linear fit trend line is 0.336. The data indicates that global slenderness does not have as large of an impact on drift range capacity for round HSS as square HSS based on the lower R^2 and the lower slope of the trend line. For round HSS, as brace global slenderness increases, story drift range does increase, but not as significantly as square HSS specimens. Much of the scatter in the data can again be attributed to the range of local slenderness values associated with various global slenderness values. This is apparent for six round specimens with global slenderness between 73 and 84. The smallest *D/t* of these specimens was 14.2 and achieved a story drift range of 8.7% and the largest *D/t* of these specimens was 49.6 and reached a story drift range of 2.7%.

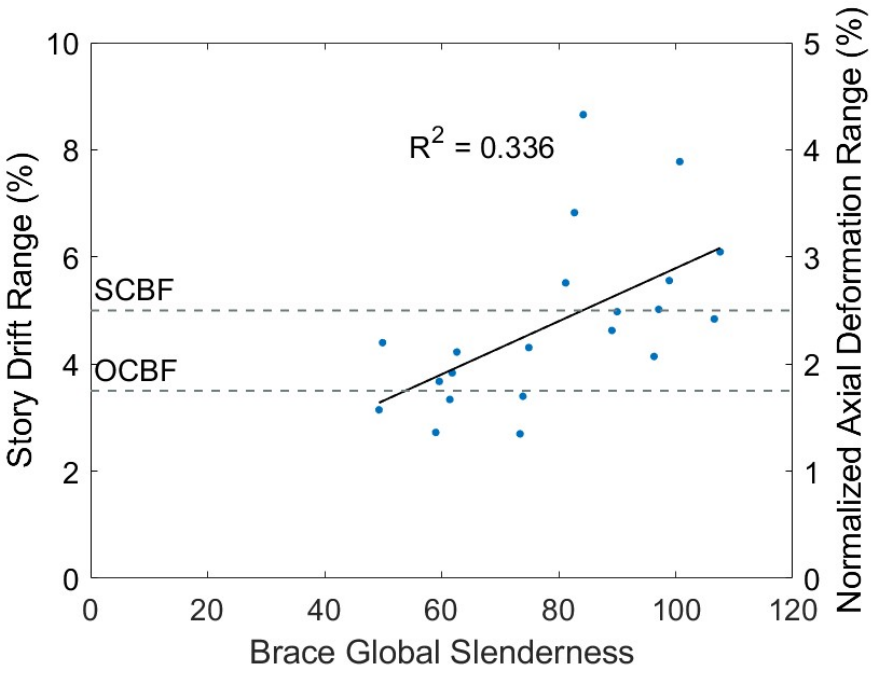

Figure 5.8 Story Drift Range and Normalized Axial Deformation Range vs Brace Global Slenderness – Round HSS

5.3.3 Combined Local and Global Slenderness Ratio

Data from Sections 5.3.1 and 5.3.2 have shown that brace deformation capacity is dependent on both local and global slenderness. The effect of these parameters on brace deformability is consistent with prior research. As local slenderness decreases and global slenderness increases, brace deformation capacity increases. The current AISC local slenderness limits have no minimum requirement for global slenderness. Low global slenderness can hinder a braces ability to behave in a ductile manner. This section will explore the use of a combined parameter that considers both local and global slenderness. Chapter 6 will present recommendations for an update to AISC 341 that has the limiting local slenderness ratio depending on the brace's global slenderness.

In order to study the dependence of brace axial deformation capacity on both local and global slenderness at the same time, a combined parameter was reviewed consisting of the following variables: D/t or b/t, local slenderness, L_c/r, global slenderness, E, modulus of elasticity, and R_yF_y, nominal yield strength including overstrength or $F_{y,m}$, measured yield strength. The formulation of the combined parameter was created to reflect the same general format as the current AISC limits.

Figure 5.9 plots story drift range and normalized axial deformation range versus the combined parameter for square HSS using nominal values for local slenderness, global slenderness and material yield. The power regression curve that was fitted to the data had a corresponding R^2 of 0.936. The correlation of the combined parameter provides a more suitable fit for story drift range than the individual variables of local or global slenderness. As local slenderness decreases, and global slenderness increases, brace deformation capacity exponentially increases. The target drift range capacities for OCBFs and SCBFs are plotted in terms of story drift range and normalized axial deformation range. All but twelve specimens met the deformation capacity requirement for OCBFs which is the same amount as Figure 5.5 – Story Drift Range and Normalized Axial Deformation Range vs Measured Local Slenderness. The same can be said for the highly ductile deformation capacity target. Figure 5.10 plots drift range versus combined parameter for square HSS using measured local slenderness and measured yield stress. A power regression fit to this data increased the R^2 from 0.936 on the nominal plot to 0.949. Using measured values for local slenderness and yield strength did not increase the number of specimens that meet the target drift requirement for OCBFs, but it did shift much of the data to the left.

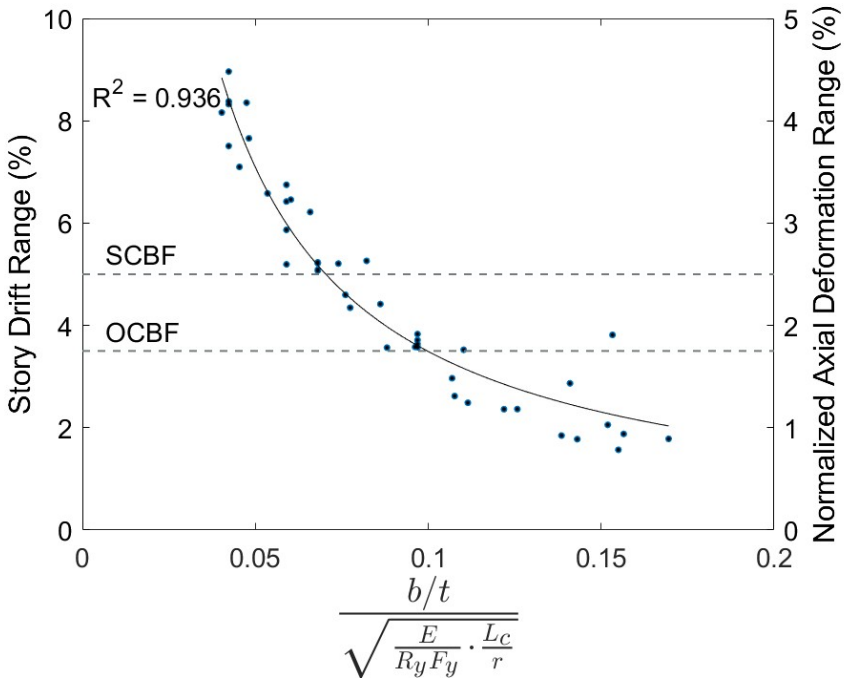

Figure 5.9 Story Drift Range and Normalized Axial Deformation Range vs Nominal Combined Parameter – Square HSS

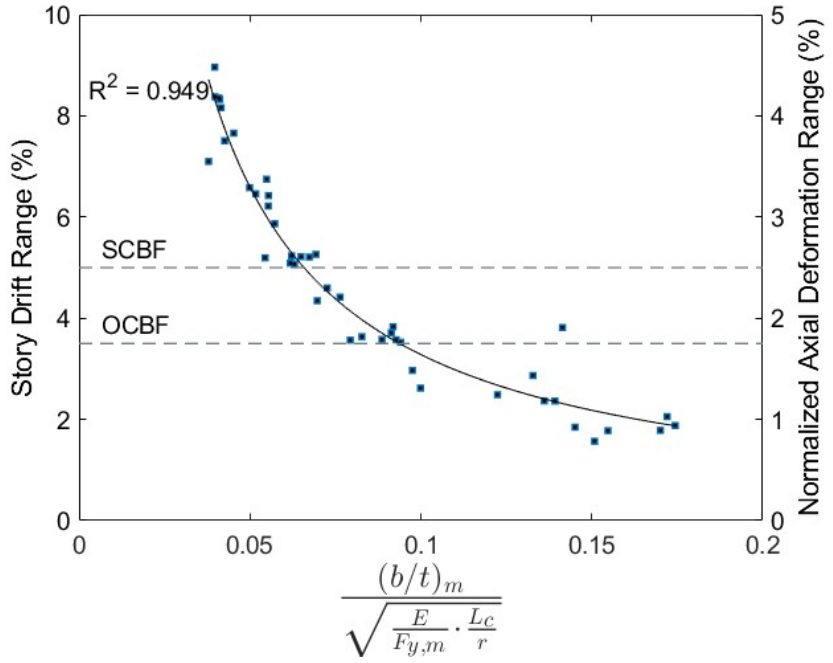

Figure 5.10 Story Drift Range and Normalized Axial Deformation Range vs Measured Combined Parameter – Square HSS

Figure 5.11 plots story drift range versus the combined parameter for round HSS using nominal values for local slenderness and material yield. The power regression curve that was fitted to the data had an R^2 of 0.880. The correlation of the combined parameter provides a more suitable fit for story drift range than the individual variables of local or global slenderness. The same relationship between the combined parameter and deformation capacity for the square specimens can be seen for the round specimens. As local slenderness decreases, and global slenderness increases brace deformation capacity exponentially increases. Figure 5.12 plots drift range versus combined parameter for round HSS using measured values for local slenderness and material yield. Using the measured parameters causes most of the data to shift slightly to the left. It does not affect the number of specimens that do or do not meet the target deformation capacities for OCBFs or SCBFs.

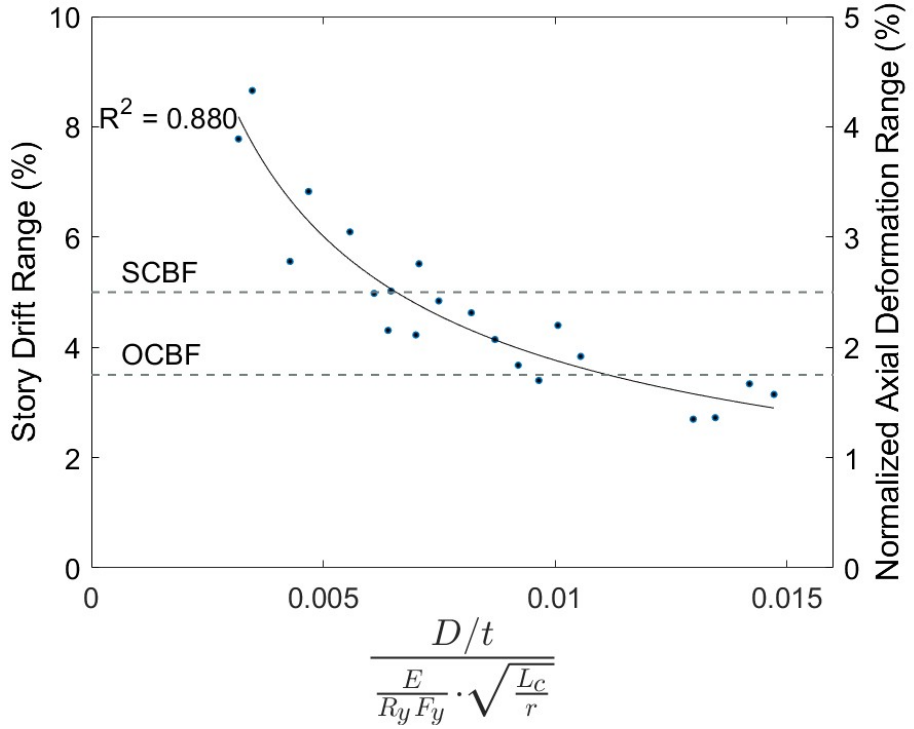

Figure 5.11 Story Drift Range vs Nominal Combined Parameter – Round HSS

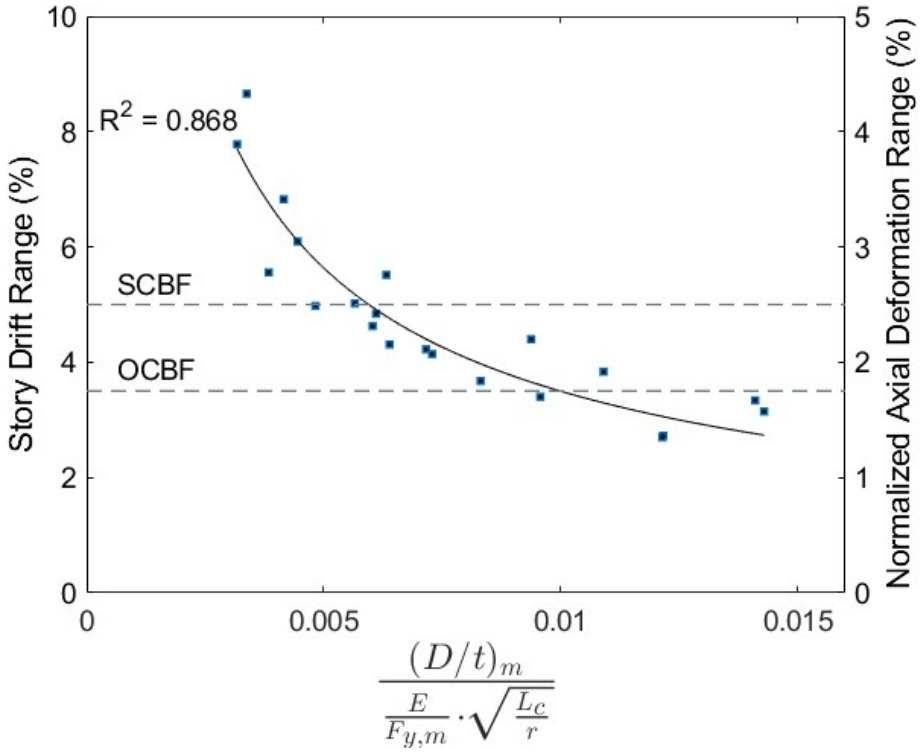

Figure 5.12 Story Drift Range vs Measured Combined Parameter - Round HSS

5.4 Distribution of Local Cupping

Observations from testing and data analysis have shown that the initiation of cupping leads to subsequent tearing and fracture at the plastic hinge. Braces with larger deformation capacity generally have cupping develop later in the load history and that cupping appears by eye to be distributed over a longer region. The onset, severity and distribution of cupping deformations are investigated in this section to document their influence on brace inelastic deformation capacity and their dependence on brace local and global slenderness. This section will only use data related to the round HSS specimens – Test Series 2 as only those specimens had instrumentation configured to provide useful data for measuring cupping region deformations.

Thirty optotrak sensors, which were used to measure 3D displacement with accuracy better than 1mm, were spaced approximately 1-inch apart centered along the brace length at brace midspan (see Section 3.6.4) for the round HSS specimens. They were attached to the center of the top face of the brace as shown in Figure 5.13. The X location starts at 0 inches (sensor 1, south end) and ends at 29 inches (sensor 30, north end). The average longitudinal strain along the length of sensors was calculated using a developed MATLAB script that is summarized as follows:

1. The center of cupping was manually identified and input from photos and varied a few inches away from brace midpoint in some cases.
2. After the location of cupping was identified, marker sets with increasing gauge lengths centered on the previously identified center of cupping point were utilized to calculate an average strain over their gauge lengths. For example, if the cupping was centered 3 inches south of center, the sensor at the center of cupping is sensor 13. Sensors 12 and 14 were then used to calculate the average longitudinal strain between them and had a gauge length of 2 in. Sensors 11 and 15 were then used to compute an average longitudinal strain between them and had a gauge length of 4 in. See Figure 5.14 for a layout of this example.
3. This pattern continues for the complete sets of sensors.

This method was used to calculate an approximate strain because it provides the most consistent and clean data and can be easily interpreted while also accounting for the variable location of the center of cupping.

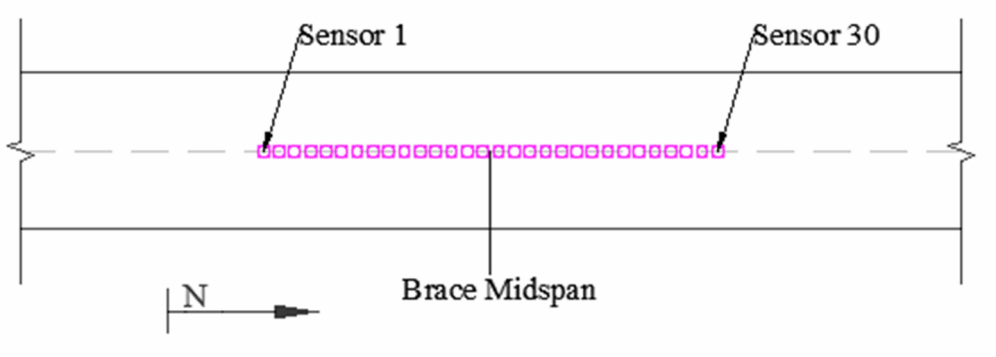

Figure 5.13 Optotrak Sensor Layout

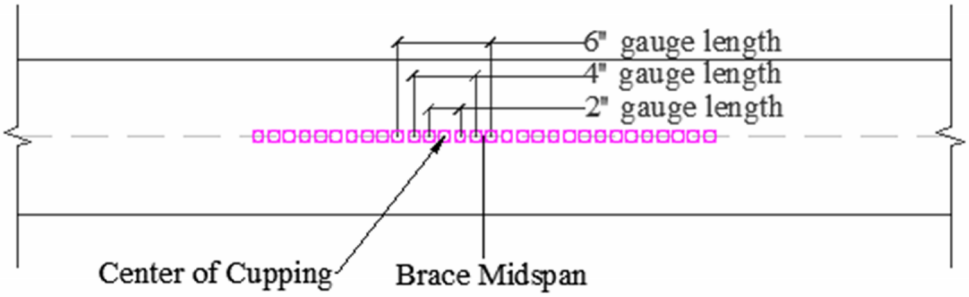

Figure 5.14 Example of Gauge Layout for Center of Cupping - 3" South of Center

Table 5.1 compares six of the twenty-one round specimens: 8.625x3/16 Short, 8.625x3/16 Long, 8.625x1/4 Short, 8.625x1/4 Long, 8.625x3/8 Short, 8.625x3/8 Long. The local and global slenderness characteristics of the six specimens represents a large range of local slenderness values tested in Test Series 2. The effect of global slenderness on the concentration of strain will be reflected by the difference between the short and long specimens with the same local slenderness. The graphs on the left side of the table plot the average longitudinal strain vs gauge length for the three compression cycles before brace fracture. During testing it was common for sensors to go out of range of the Optotrak camera at the peak of compression cycles due to the large deformations of the cupping region. As such, there may be missing points for the smallest gauge lengths. In addition, because of the variation in location of local cupping, not all specimens have the same total number of gauge lengths. The points plotted in the figures on the left of Table 5.1, correspond to the cycles noted in the common legend in Figure 5.15. The blue circles represent the average longitudinal strain for each gauge length at the peak of the compression cycle when cupping initiated. The initiation of cupping is defined as the cycle in which visible local cupping deformations form near or at the midpoint of the brace. The orange plus signs represent the average longitudinal strain for a compression cycle after initiation of

cupping which also occurred two compression cycles before fracture. The yellow stars represent the average longitudinal strain for each gauge length for the compression cycle before fracture. The picture of local cupping provided in the right column was taken at the peak of the compression cycle before fracture. After the initiation of cupping, the compressive strain increases and concentrates at smaller gauge lengths (i.e., around the middle of the cupping region) in subsequent cycles until fracture. It is also visible from the plots that braces with higher local slenderness show less evidence of cupping and have higher strain concentration in the smaller gauge lengths for compression cycles before fracture.

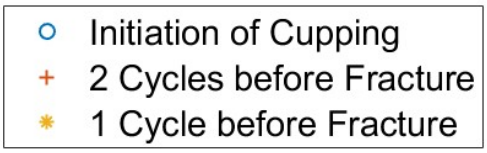

Figure 5.15 Common Legend for Average Longitudinal Strain Plots

Table 5.1 Summary of Concentration of Strain at the Local Cupping Region

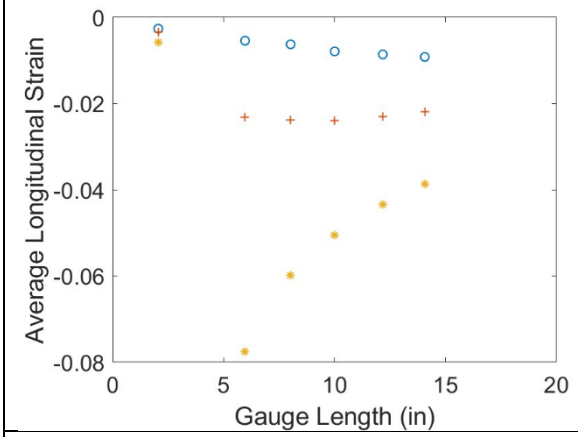	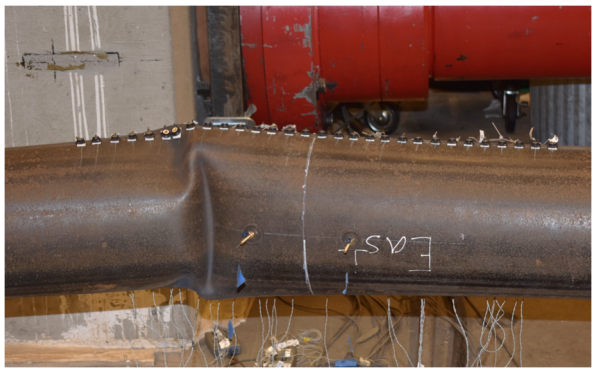
8.625x3/16 Short: D/t = 49.6, L_c/r = 61.4	
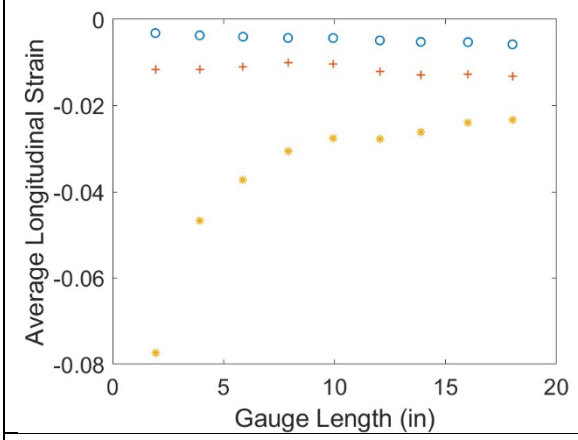	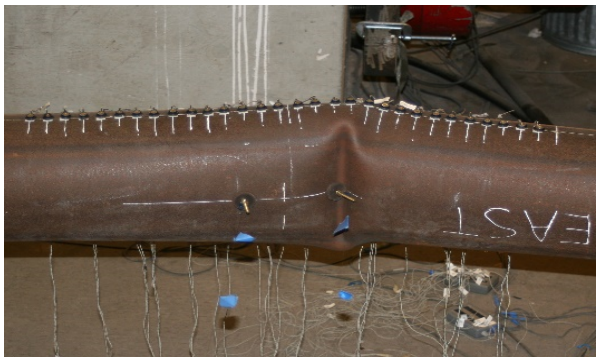
8.625x3/16 Long: D/t = 49.6, L_c/r = 73.4	
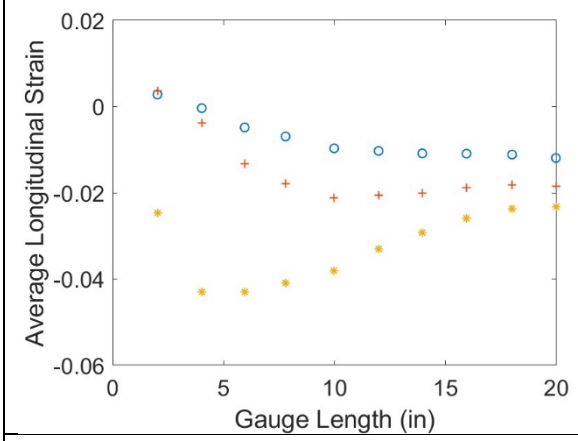	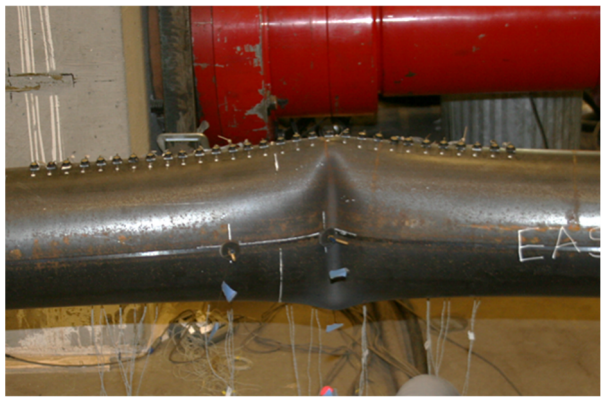
8.625x1/4 Short: D/t = 37.0, L_c/r = 61.8	

Table 5.1 Summary of Concentration of Strain at the Local Cupping Region (continued)

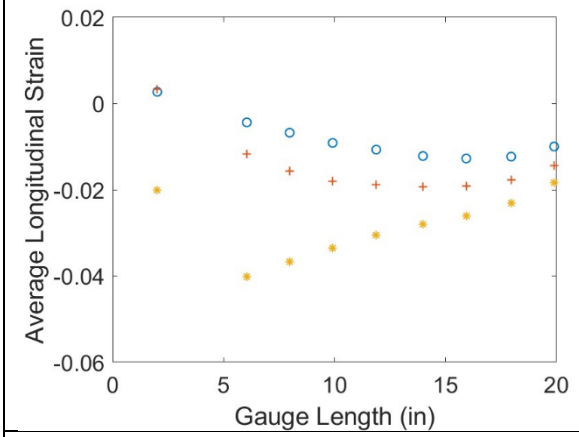

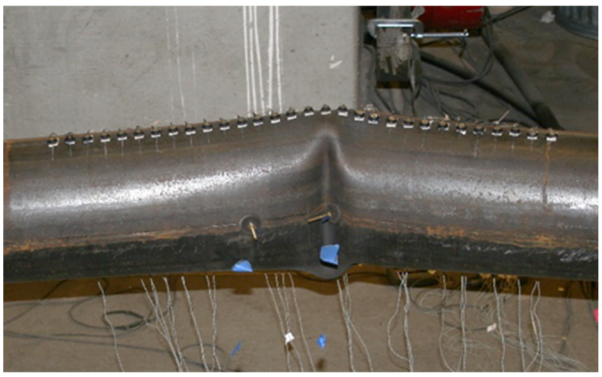

8.625x1/4 Long: D/t = 37.0, L_c/r = 73.9

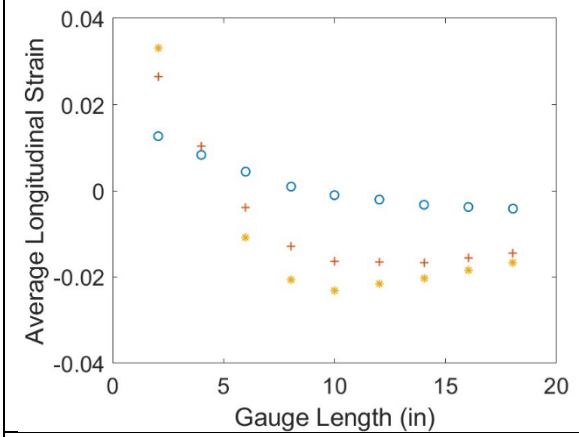

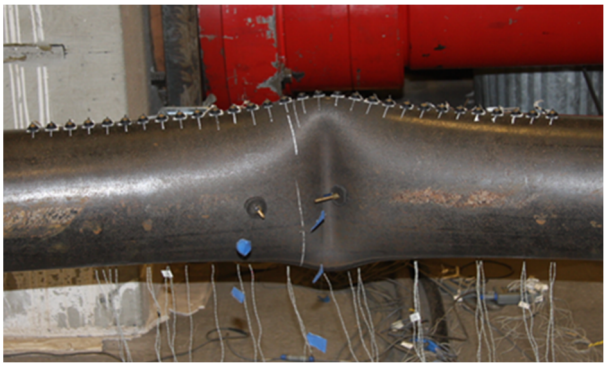

8.625x3/8 Short: D/t = 24.7, L_c/r = 62.6

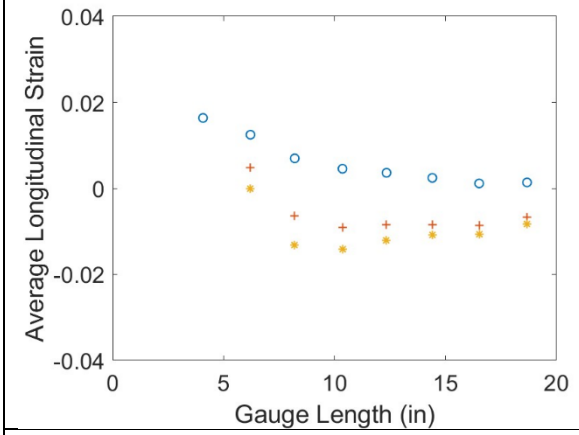

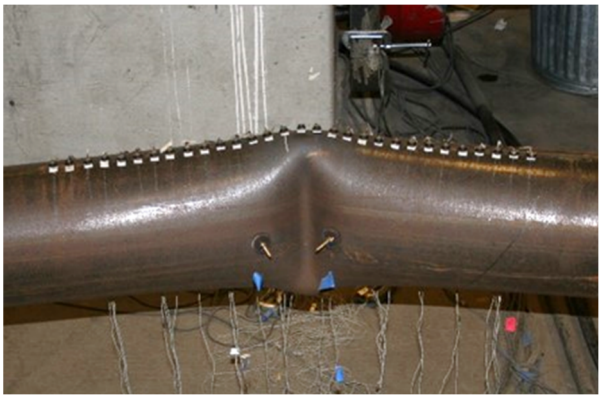

8.625x3/8 Long: D/t = 24.7, L_c/r = 74.9

Figure 5.16 combines the average longitudinal strain lines at the compression cycle before fracture from all six 8.625” diameter specimens. The color of the lines correspond to the thickness of the wall: red for 3/16”, yellow for 1/4", and green for 3/8”. The shape of the points on the line plot represents the length of the specimens. Triangles correlate to the short brace length specimens, and squares correlate to the long brace length specimens. The short specimens experienced larger compressive longitudinal strains compared to the long specimens. As global slenderness decreases, the magnitude of strain increases. As local slenderness increases, so does the concentration of strain over the cupping region. In other words, braces experience larger longitudinal strains over a smaller area as local slenderness increases. The 3/8” specimens exhibited about 0.02 of compressive strain over approximately 8” while the 3/16” specimens exhibited almost 0.08 of compressive strain over approximately 4”. The 1/4” specimens showed behavior between these two extremes: 0.04 of compressive strain over approximately 6”. This behavior of strain concentration coincides with the relationship between local and global slenderness and inelastic deformation capacity.

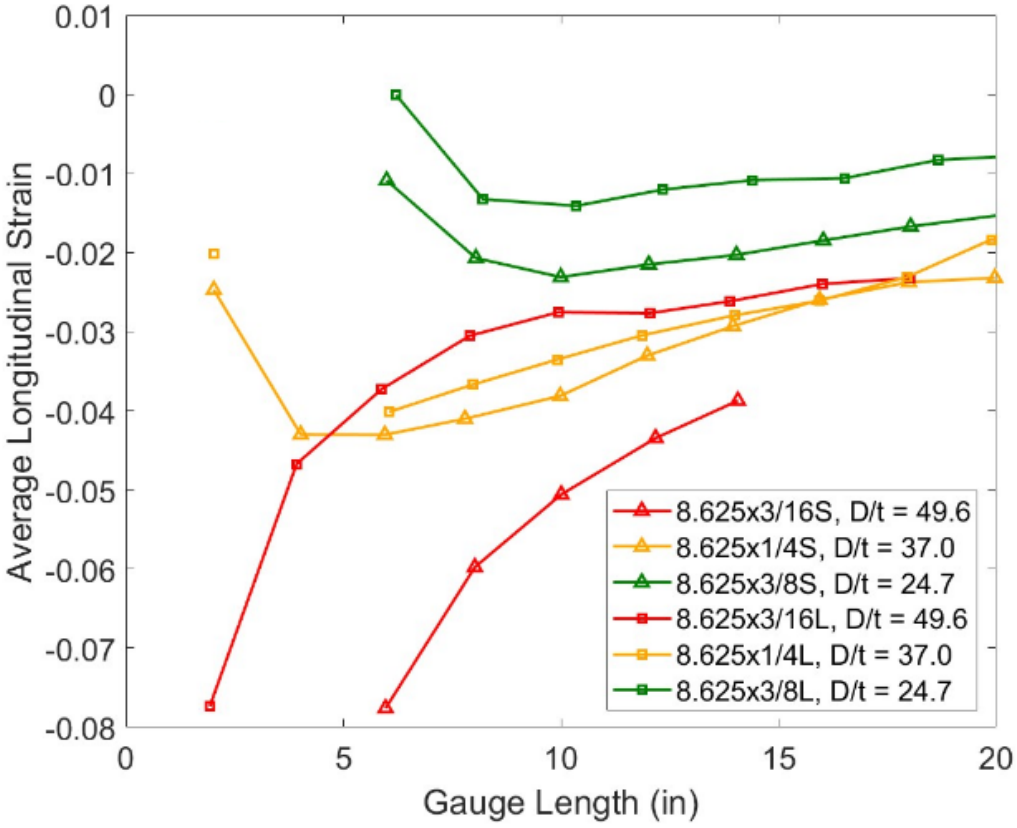

Figure 5.16 Average Longitudinal Strain at the Compression Cycle Before Fracture vs Gauge Length (in): 8.625 Dia. Specimens

Chapter 6. Assessment of Performance-Based Engineering Tools and Design Standards

6.1 Introduction

This chapter uses experimental results to assess the current engineering tools in AISC 342-22 and design standards in AISC 341-22. The sections detailed in this chapter are as follows.

- Section 6.2 evaluates the current AISC 341-22 local slenderness limits, and presents new equations derived from database of experimental results on hollow HSS braces. This database includes the hollow HSS braces that were tested as part of this research program as well as the prior research at the UW SRL.
- Section 6.3 compares non-linear modeling methods for hollow round HSS braces, as recommended by AISC 342-22, against experimental force-displacement results. This analysis seeks to determine the accuracy of current modeling parameters. Note that only the round HSS tests were used since prior work has evaluated these methods for hollow square HSS braces.

6.2 Evaluation and Recommendations to AISC 341-22 Seismic Provisions

The current AISC 341-22 limiting local slenderness ratios for braces were established from limited experimental and computational data. The experimental data in this research project (including the earlier phase) created a comprehensive data set to evaluate the limiting width-/diameter-to-thickness ratios for OCBFs and SCBFs. This section will discuss this evaluation and describe the background to establish performance-based requirements for the highly and moderately ductile limit.

A study at Marquette University by Andrew Sen (2024) was undertaken to understand the performance requirements of HSS brace members in OCBFs and SCBFs. The current local slenderness limits were created with a focus on component behavior when inherently these braces are one component that exist as a part of a larger seismic-force-resisting system. The research objectives by Sen (2024) were to evaluate the seismic performance of current SCBF and OCBF systems and to establish performance requirements in terms of minimum target story drift range for the occurrence of brace fracture in SCBF and OCBF systems. Based on the nonlinear response-history analysis of SCBF and OCBF systems, the recommended target story drift capacity for braces is 5% and 3.5% respectively.

Analysis of data in Chapter 5 strongly suggests the re-evaluation of the current highly and moderately ductile limits. Data also shows that brace inelastic deformation capacity is not only dependent on local slenderness, but also global slenderness; Plots from Chapter 5 showed that a combined parameter of local and global slenderness is the best fit for the relationship between brace parameters and story drift range capacity. Based on the target story drift ranges and for SCBFs and OCBFs and the experimental data in terms of combined local and global slenderness, below are the proposed equations to replace the current AISC 341-22 local slenderness limits.

For square HSS braces:

$$\lambda_{hd} \leq 0.075 \sqrt{\frac{E}{R_y F_y}} \sqrt{\frac{L_c}{r}} \leq 20 \tag{6.7}$$

$$\lambda_{md} \leq 0.1 \sqrt{\frac{E}{R_y F_y}} \sqrt{\frac{L_c}{r}} \leq 25 \tag{6.8}$$

For round HSS braces:

$$\lambda_{hd} \leq 0.0063 \frac{E}{R_y F_y} \sqrt{\frac{L_c}{r}} \leq 40 \tag{6.9}$$

$$\lambda_{md} \leq 0.011 \frac{E}{R_y F_y} \sqrt{\frac{L_c}{r}} \leq 45 \tag{6.10}$$

The form of the proposed equations reflects the interaction between brace local and global slenderness on drift capacity. It also captures that local deformation of square HSS is closely related to bending and buckling of a flat plate and local deformation of round HSS is consistent with plate buckling for curved plates. An upper bound was placed on all proposed equations because the data shows that braces with very large *b/t* or *D/t* do not perform well regardless of the L_c/r.

Figure 6.1 and Figure 6.2 plot story drift range and normalized axial deformation range versus the combined parameter for square HSS using nominal values and measured values respectively. Figure 6.3 and Figure 6.4 plot story drift range and normalized axial deformation range versus the combined parameter for round HSS using nominal values and measured values respectively. On all four plots, the target story drift range of 5.0% for SCBFs and 3.5% for

OCBFs are noted. Vertical Green dashed lines represent the proposed limits based on combined local and global slenderness for square and round HSS.

Section 3.4.2 details the measured yield stress for each cross-section. For the square specimens, the average measured yield stress is 64.7 ksi with the lowest yield stress of 58.9 ksi and the highest yield stress of 71.6 ksi. For the round specimens, the average measured yield stress is 61.0 ksi which includes the lowest yield stress of 53.6 ksi and the highest yield stress of 69.5 ksi. For the square and round specimens, the average yield stress is less than the expected stress, R_yF_y, which equals 65 ksi for A500 Gr. C steel. In addition to the variation in yield stress, measured local slenderness, *b/t* or *D/t*, was almost always lower than nominal values. The measured local slenderness for square specimens from previous research (Kaldestad, 2022) and square and round specimens from the current phase of research are detailed in Section 2.5 of the literature review and Section 3.4.1 respectively. The lower-than-expected yield stress and lower-than-nominal local slenderness, shifts most points slightly, or in some cases, significantly to the left in Figure 6.1 to Figure 6.2 and Figure 6.3 to Figure 6.4. Points on the plots with measured values (Figure 6.2 and Figure 6.4) are marked in red if their measured values place them to the left of the moderately or highly ductile limit and they did not meet the limit using nominal values and if they fail to achieve the target story drift range. The limits proposed above were selected based on nominal cross-section and material values as those values are what the designer of an CBF would be using in calculations and specifications.

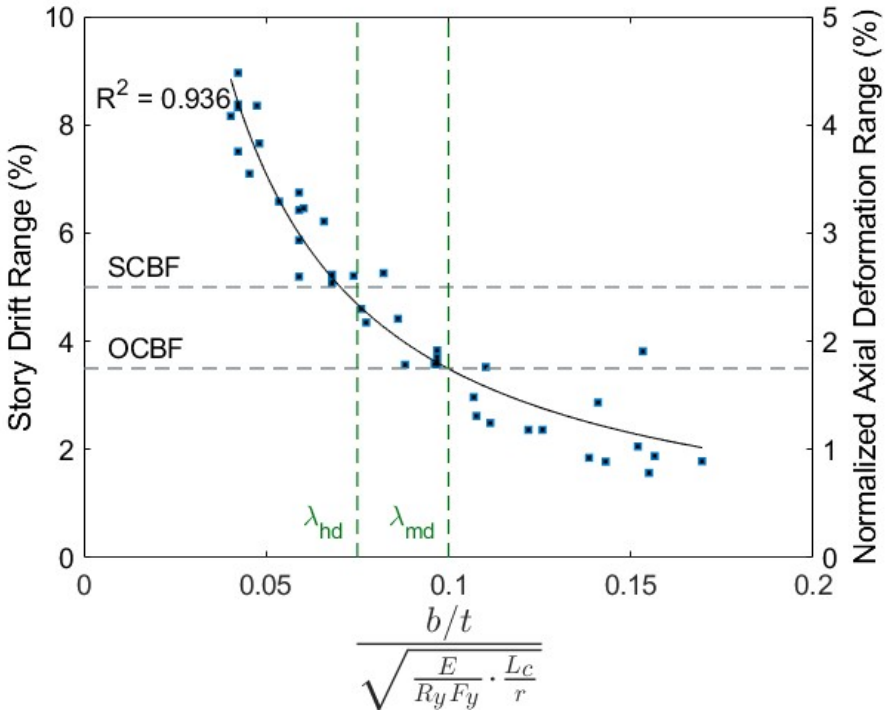

Figure 6.1 Proposed Limiting Width-to-Thickness Ratios – Square HSS, Nominal Material and Cross-Sectional Properties

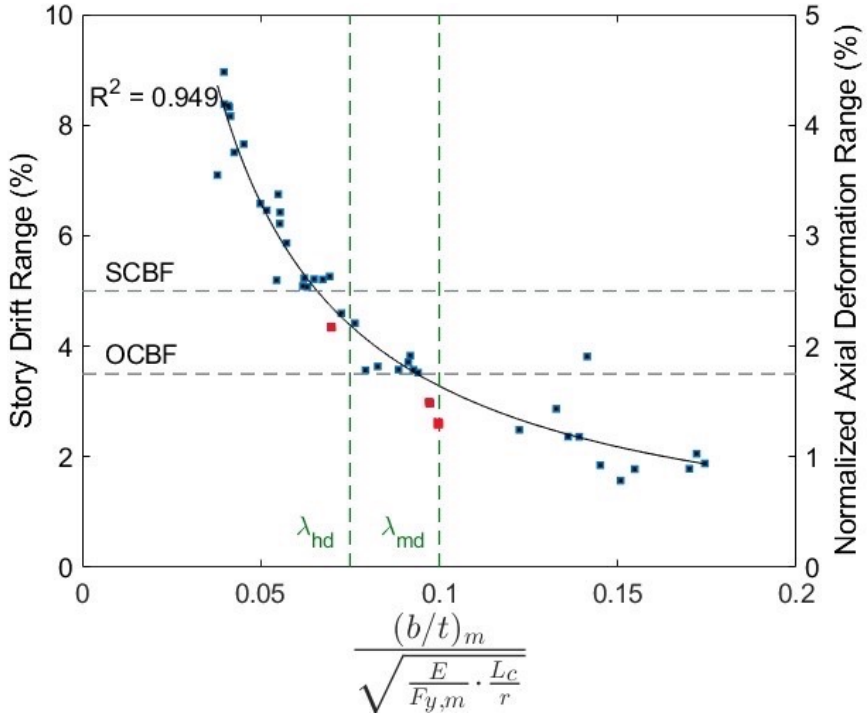

Figure 6.2 Proposed Limiting Width-to-Thickness Ratios – Square HSS, Measured Material and Cross-Sectional Properties

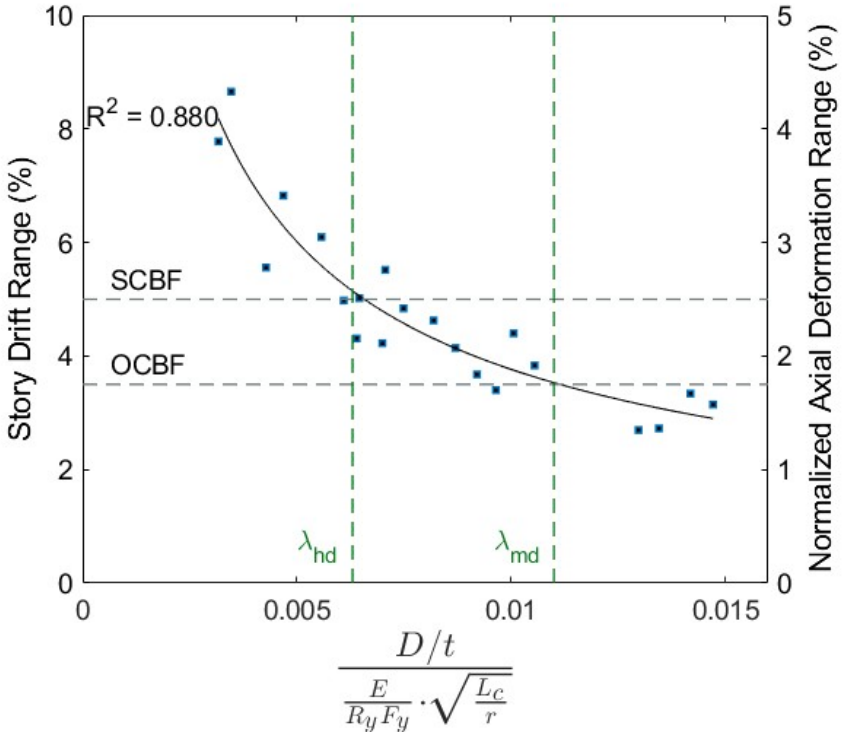

Figure 6.3 Proposed Limiting Diameter-to-Thickness Ratios – Round HSS, Nominal Material and Cross-Sectional Properties

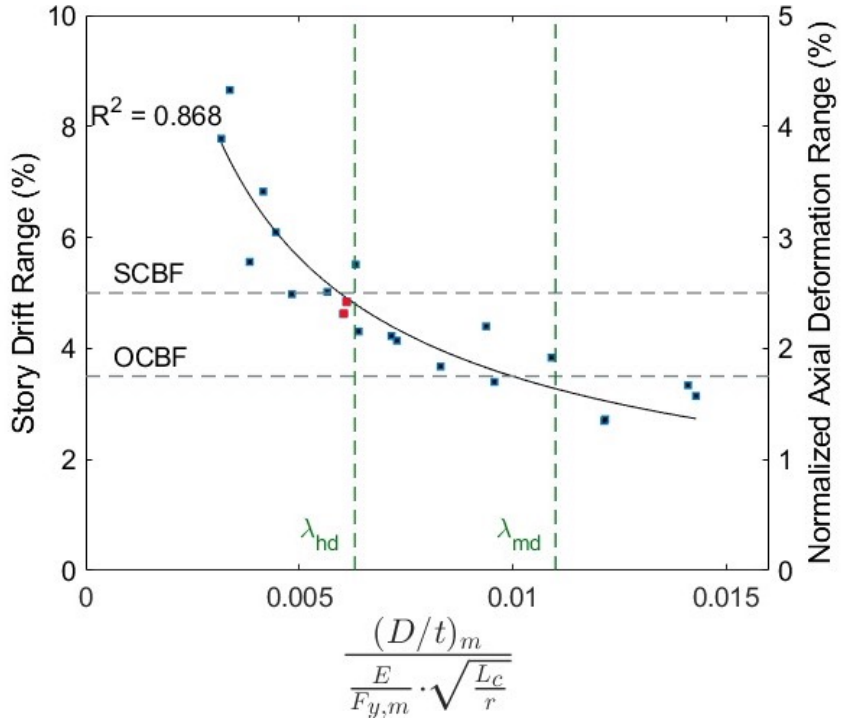

Figure 6.4 Proposed Limiting Diameter-to-Thickness Ratios – Round HSS, Measured Material and Cross-Sectional Properties

Table 6.1 and Table 6.2 provide an example of how the proposed limits change with global slenderness and summarize the percent change from the AISC 341-22 Provisions. The orange boxes indicate a decrease in allowable local slenderness and the blue boxes indicate an increase in allowable local slenderness. Only at a global slenderness of 60, do the proposed limits reduce the highly ductile local slenderness limits for square and round HSS. With global slenderness above 80, the proposed limits increase the allowable highly and moderately ductile local slenderness limits. The proposed limits create considerably more design options for HSS braces in CBF frames, with a particularly larger increase in allowable local slenderness for round HSS compared to square HSS.

Table 6.1 Percent Change for Proposed AISC 341-27 Limits to AISC 341-22 Width-to-Thickness Limits– Square HSS

ASTM	F_y (ksi)	L_c/r	λ_{hd}	λ_{md}
			$\lambda_{hd} \le 0.075 \sqrt{\frac{E}{R_y F_y}} \sqrt{\frac{L_c}{r}} \le 20$	$\lambda_{md} \le 0.1 \sqrt{\frac{E}{R_y F_y}} \sqrt{\frac{L_c}{r}} \le 25$
A500 C	50	60	12.27	16.36
% Diff from 341-22			**-10.6%**	**1.9%**
A500 C	50	80	14.17	18.89
% Diff from 341-22			**3.2%**	**17.7%**
A500 C	50	100	15.84	21.12
% Diff from 341-22			**15.4%**	**31.6%**
A500 C	50	120	17.35	23.14
% Diff from 341-22			**26.4%**	**44.2%**

Table 6.2 Percent Change for Proposed AISC 341-27 Limits to 341-22 Diameter-to-Thickness Limits – Round HSS

ASTM	F_y (ksi)	L_c/r	λ_{hd}	λ_{md}
			$\lambda_{hd} \le 0.0063 \frac{E}{R_y F_y} \sqrt{\frac{L_c}{r}} \le 40$	$\lambda_{md} \le 0.011 \frac{E}{R_y F_y} \sqrt{\frac{L_c}{r}} \le 45$
A500 C	50	60	21.77	38.01
% Diff from 341-22			**-7.9%**	**37.4%**
A500 C	50	80	25.14	43.90
% Diff from 341-22			**6.3%**	**58.7%**
A500 C	50	100	28.11	45.00
% Diff from 341-22			**18.8%**	**62.7%**
A500 C	50	120	30.79	45.00
% Diff from 341-22			**30.2%**	**62.7%**

6.3 Assessment of AISC 342 Backbone Curves for Round HSS Braces

AISC 342-22 (AISC, 2022) entitled *Seismic Provisions for Evaluation and Retrofit of Existing Structural Steel Buildings*, replaces the provisions for structural steel systems previously provided by Chapter 9 of ASCE/SEI 41 (ASCE, 2016). AISC 342-22 provides guidelines and engineering tools including nonlinear modeling procedures for members in existing steel structures. This section will evaluate these performance-based engineering tools for modeling the nonlinear behavior of hollow HSS braces in steel frames. Previous research focused on modeling parameters of hollow square HSS (Kaldestad, 2022). That work provided the basis of the methods in AISC 341-22 but only included square sections. This section uses a similar approach to evaluate the accuracy of the nonlinear modeling parameters developed for square HSS braces but applied to round HSS braces. AISC 342-22 provides parameters based on brace material and geometric properties to construct generalized force-deformation curves, as illustrated in Figure 6.5. Here, the experimental force-displacement response of each round HSS specimen is compared to the behavior prescribed in AISC 342-22 to assess the accuracy of the modeling parameters. Note that the generalized deformation curves provided in AISC 342-22 will be referred to as backbone curves.

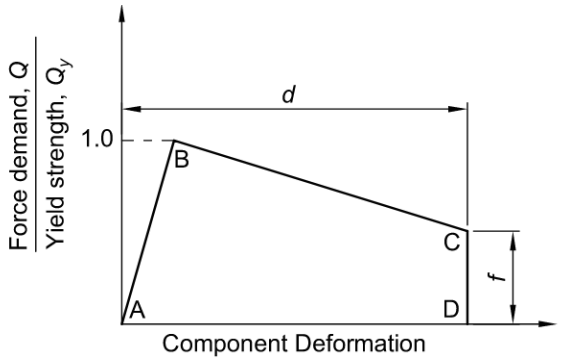

Figure 6.5 Generalized Force-Deformation Relation for Buckling Braces (AISC 342-22, Fig. C3.1)

The methodology and equations to construct the backbone curves for non-linear modeling are provided in AISC 342-22, Chapter C3, and summarized below. Separate backbone curves are created for the tensile and compressive force-displacement response of an HSS brace defined by the total axial deformation capacity, d, and the residual strength ratio, f. These are the steps to developing the backbone curve for hollow HSS braces.

1. The tensile axial deformation capacity is calculated using Equation 6.1. Equation 6.1 uses the predicted displacement at tensile yield, Δ_T (Equation. 6.3).

2. The compressive axial deformation capacity (negative) is calculated using Equation 6.4 for compression. Equation 6.4 used the predicted displacement at global buckling, Δ_C (Equation 6.6).
3. Equation 6.1 and 6.4 use n to predict the maximum axial deformation in tension, Equation 6.2, and compression, Equation 6.5. The variable n depends on the following parameters:
    a. The local slenderness ratio, λ, of the HSS brace.
    b. The AISC 341-22 highly ductile limit, λ_{hd} (Table D1.1a). The measured value of $F_{y,m}$ is used here.
    c. The global slenderness ratio, L_c/r
    d. The modulus of elasticity, E
    e. The measured material yield strength, $F_{y,m}$. According to AISC 342-22, $F_{y,m}$, is to be used in place of, R_yF_y, expected material yield strength, when experimental testing values are available. The measured value of $F_{y,m}$ is used here.
    f. The expected tensile strength, T_{CE} and expected compressive strength, P_{CE}. The measured value of $F_{y,m}$ is used here.
    g. The strength ratio, f, is 1.0 for tension (i.e., the residual strength is equal to P_y) and 0.2 for compression (20% of P_{CE}). The compressive strength ratio is much less than 1.0 to represent the post-buckling strength degradation.

The equations referenced in the procedure to develop the tension and compression backbone curves for a hollow round HSS brace are provided below.

The AISC 342-22 backbone parameters for a round HSS brace in tension are:

$$f = 1.0$$

$$d = n\Delta_T \tag{6.1}$$

Where:

$$n = 2.8\left(\frac{\lambda}{\lambda_{hd}}\right)^{-1.7}\left(\frac{L_c/r}{\sqrt{E/F_{y,m}}}\right)^{0.45} \tag{6.2}$$

$$\Delta_T = \frac{T_{CE}L_c}{EA_g} \tag{6.3}$$

The AISC 342-22 backbone parameters for a round HSS brace in compression are:

$$f = 0.2$$

$$d = n\Delta_C \tag{6.4}$$

Where:

$$n = 4.7\left(\frac{\lambda}{\lambda_{hd}}\right)^{-1.7}\left(\frac{L_c/r}{\sqrt{E/F_{y,m}}}\right)^{0.45} \tag{6.5}$$

$$\Delta_C = \frac{P_{CE}L_c}{EA_g} \tag{6.6}$$

A summary of the calculated modeling parameters for each round HSS test specimen is shown below in Table 6.3. The first column provides the yield and global buckling deformation. Next, the *n* factor and the total axial deformation, *d*, is provided for both tension and compression. The last column summarizes the residual strength, *f*P,* where *P* is the expected tensile yield load and the expected compressive buckling load for tension and compression, respectively.

Table 6.3 AISC 432-22 Backbone Modeling Parameters for the Round HSS Specimen

Test Specimen	Δ_T (in.)	Δ_C (in.)	n factor		d (in.)		f*P (kips)	
			Tens.	Comp.	Tens.	Comp.	Tens.	Comp.
6x3/16 Short	0.34	0.19	3.74	6.28	1.27	1.17	189	21
6x3/16 Long	0.41	0.17	4.06	6.81	1.65	1.17	189	16
6x1/4 Short	0.34	0.21	6.06	10.2	2.08	2.09	229	27
6x1/4 Long	0.41	0.19	6.57	11.0	2.69	2.06	229	21
6.625x3/16 Long	0.43	0.23	3.03	5.08	1.30	1.16	199	21
6.625x1/4 Short	0.37	0.19	4.34	7.28	1.62	1.34	276	27
6.625x1/4 Long	0.45	0.23	4.70	7.89	2.10	1.78	276	28
6.625x3/8 Short	0.37	0.23	8.81	14.8	3.25	3.47	401	51
6.625x3/8 Long	0.44	0.22	9.55	16.0	4.21	3.51	401	40
6.625x1/2 Short	0.40	0.24	12.8	21.5	5.16	5.10	573	68
6.625x1/2 Long	0.48	0.21	13.9	23.3	6.68	4.97	573	51
8.625x3/16 Short	0.44	0.34	1.16	1.95	0.51	0.67	321	50
8.625x3/16 Long	0.53	0.35	1.26	2.12	0.66	0.73	321	42
8.625x1/4 Short	0.42	0.33	2.03	3.40	0.86	1.13	411	65
8.625x1/4 Long	0.51	0.34	2.20	3.69	1.11	1.25	411	55
8.625x3/8 Short	0.42	0.33	4.17	7.00	1.73	2.28	596	93
8.625x3/8 Long	0.50	0.33	4.52	7.59	2.50	2.51	596	79
10.750x1/4 Short	0.40	0.39	1.39	2.33	0.55	0.91	450	88
10.750x1/4 Long	0.47	0.42	1.51	2.53	0.72	1.07	450	80
10.750x0.365 Short	0.38	0.35	2.79	4.69	1.07	1.64	670	123
10.750x0.365 Long	0.46	0.38	3.02	5.07	1.38	1.93	670	112

6.2.1 Nonlinear Modeling of Round HSS Bracing Members

The following section compares the AISC 342-22 backbone curves for round HSS braces to the experimental force-displacement response of the twenty-one round HSS specimens in Test Series 2: Figure 6.6 - Figure 6.26. The modeling parameters from Table 6.3 correspond to the values of the black backbone curve line. The plots suggest the following:

- The tensile and compressive axial deformation capacities are significantly underestimated for specimens with local slenderness above the moderately ductile limit in Table D1.1a in AISC 341-22.
- The tensile and compressive axial deformation capacities are overestimated for specimens with very low local slenderness, such as the 6.625x1/2 specimens with a D/t of 14.2.
- Variations in measured yield stress impacts the accuracy of the predicted deformation capacity. Using the measured yield stresses (provided in Section 3.4.2), the average measured yield stress for the round HSS brace specimens is 61.0 ksi. Because the average yield stress is low compared to RyFy, 65 ksi, the first term after the coefficient in Equations 6.2 and 6.5 increases, while the second term decreases. Each exponent scales the impact of its associated terms on the predicted tensile and compressive deformation.
- The axial displacement at tensile yield and compressive global buckling is generally accurate.
- The predicted maximum compressive force is not accurate, which is likely due to the moment induced by the slot eccentricity that was necessary in the testing to ensure the braces buckled in the desired direction.
- The predicted maximum tensile force is very accurate for all specimens because the measured yield strength was used to calculate T_{CE}. If measured yield stress was not available, there would be a lot of variation due to the difference between R_yF_y and the actual yield stress.
- The compressive strength degradation magnitude and rate seems to not accurately predicted, but it is hard to assess the accuracy when the maximum compressive deformation is not accurately predicted.

- The predicted tensile residual strength ratio, *f*, shows no strength degradation. There are two cases where the tensile force decreases after yield, axial deformations increase: 6.625x1/2 Short and 6.625x1/2 Long.

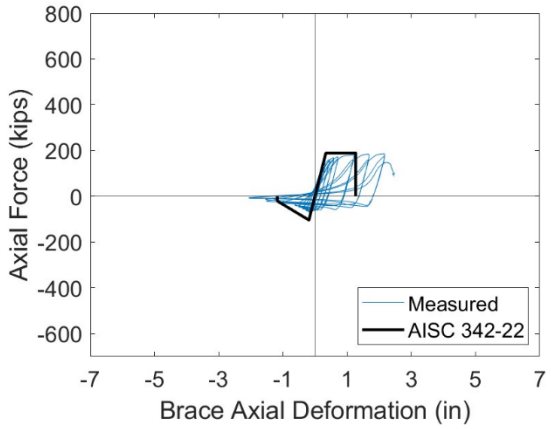

Figure 6.6 6x3/16 Short (L_c/r = 89.1, D/t = 34.5)

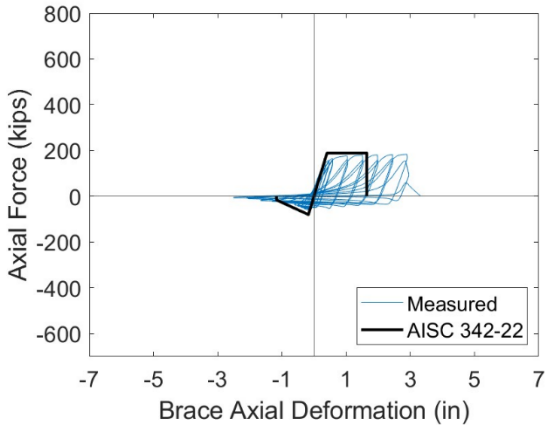

Figure 6.7 6x3/16 Long (L_c/r = 106.6, D/t = 34.5)

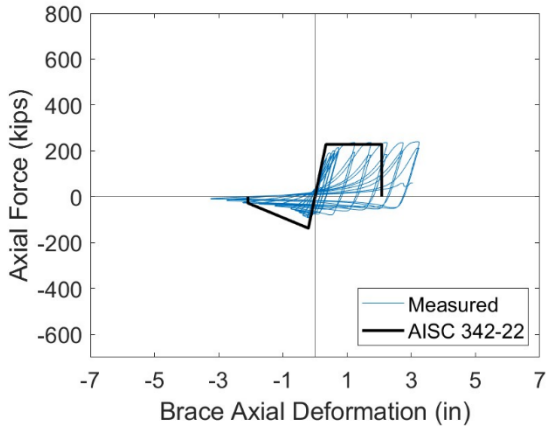

Figure 6.8 6x1/4 Short (L_c/r = 90.0, D/t = 25.8)

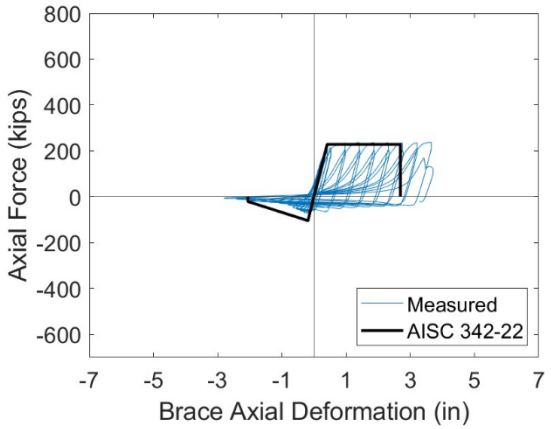

Figure 6.9 6x1/4 Long (L_c/r = 107.6, D/t = 25.8)

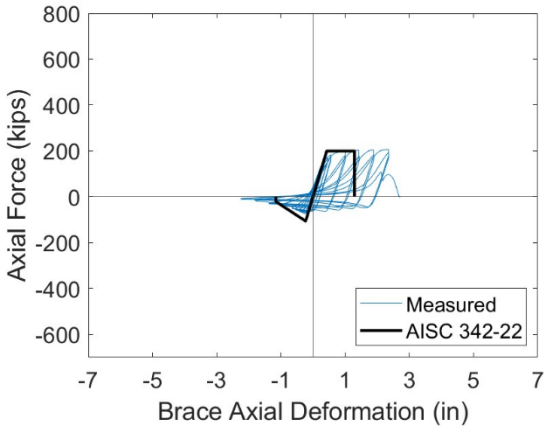

Figure 6.10 6.625x3/16 Long (L_c/r = 90.0, D/t = 25.8)

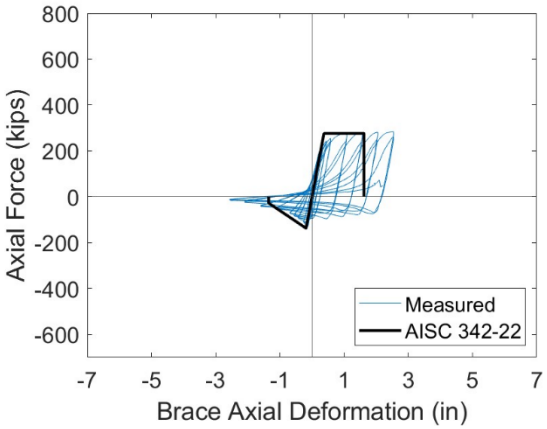

Figure 6.11 6.625x1/4 Short (L_c/r = 81.2, D/t = 28.4)

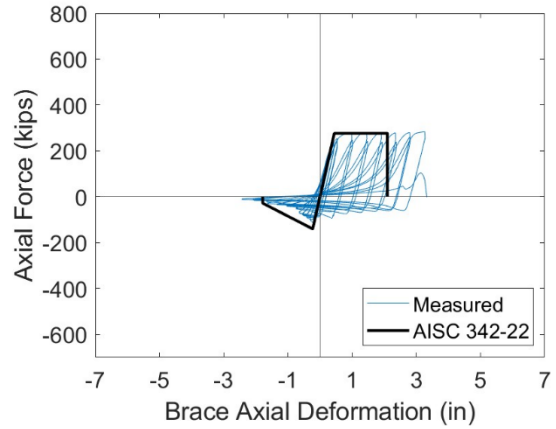

Figure 6.12 6.625x1/4 Long (L_c/r = 97.1, D/t = 28.4)

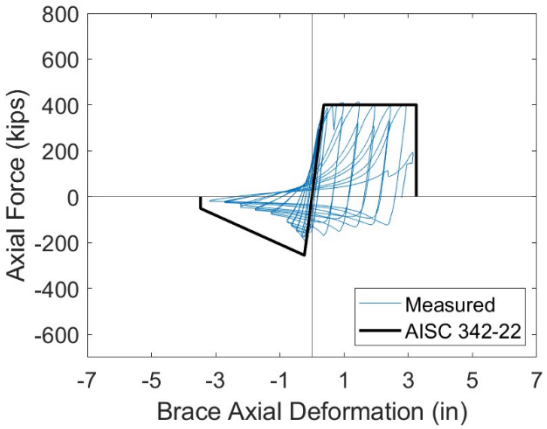

Figure 6.13 6.625x3/8 Short (L_c/r = 82.7, D/t = 19.0)

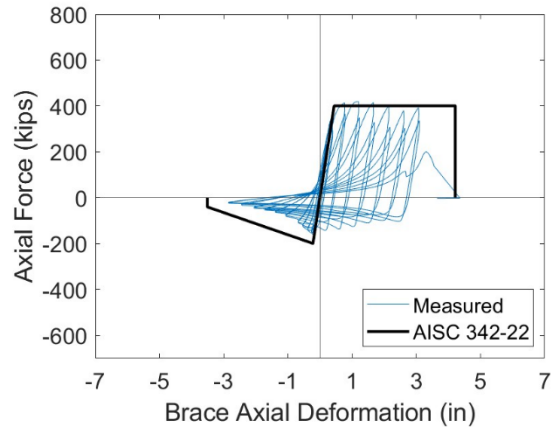

Figure 6.14 6.625x3/8 Long (L_c/r = 98.9, D/t = 19.0)

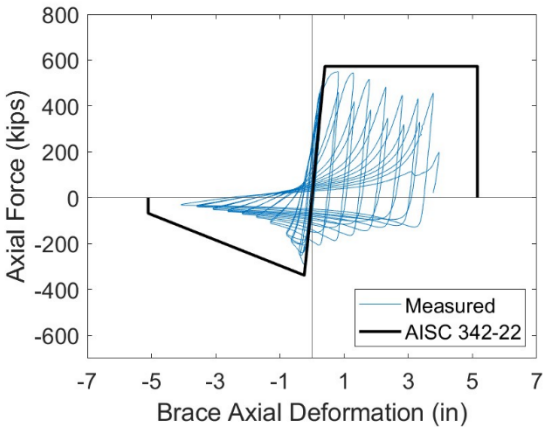

Figure 6.15 6.625x1/2 Short (L_c/r = 84.2, D/t = 14.2)

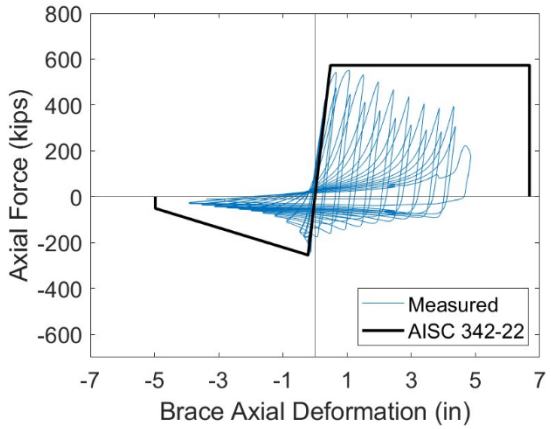

Figure 6.16 6.625x1/2 Long (L_c/r = 100.7, D/t = 14.2)

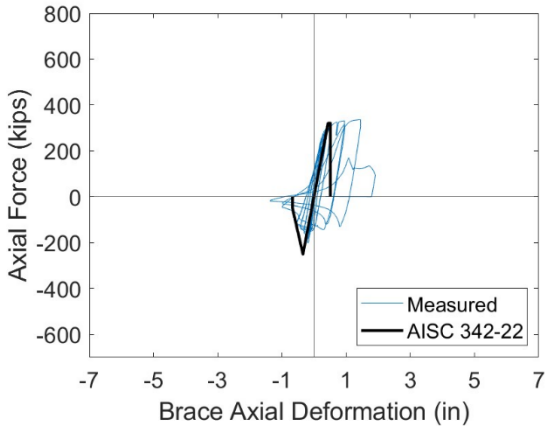

Figure 6.17 8.625x3/16 Short (L_c/r = 61.4, D/t = 49.6)

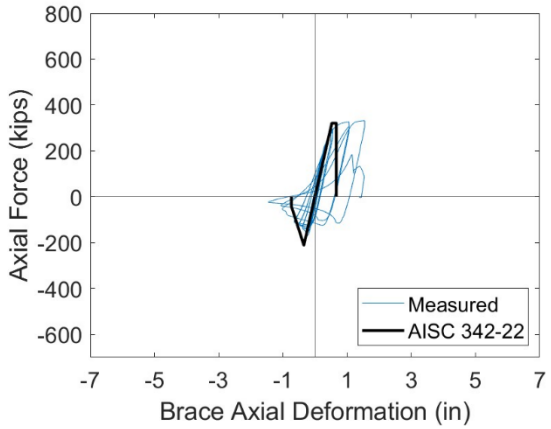

Figure 6.18 8.625x3/16 Long (L_c/r = 73.4, D/t = 49.6)

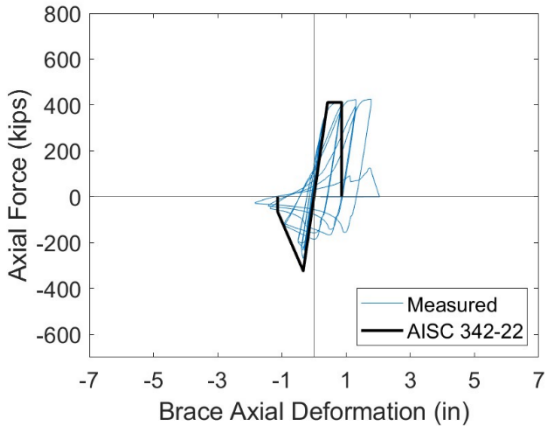

Figure 6.19 8.625x1/4 Short (L_c/r = 61.8, D/t = 37.0)

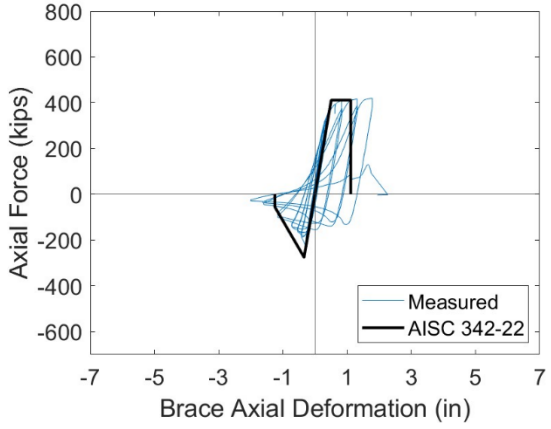

Figure 6.20 8.625x1/4 Long (L_c/r = 73.9, D/t = 37.0)

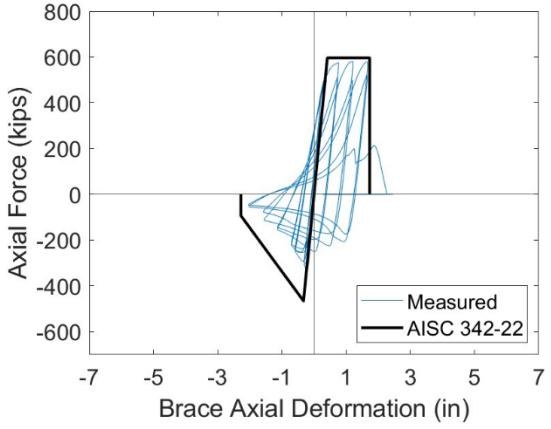

Figure 6.21 8.625x3/8 Short (L_c/r = 62.6, D/t = 24.7)

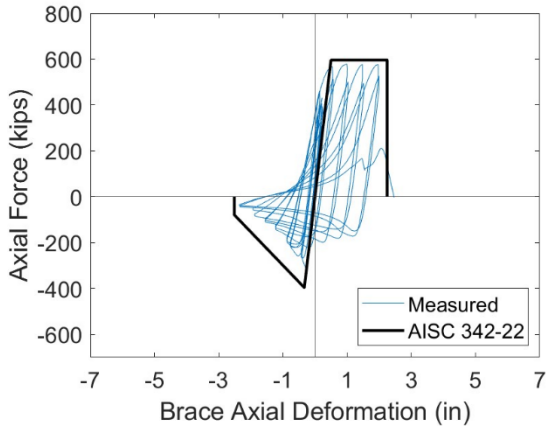

Figure 6.22 8.625x3/8 Long (L_c/r = 74.9, D/t = 24.7)

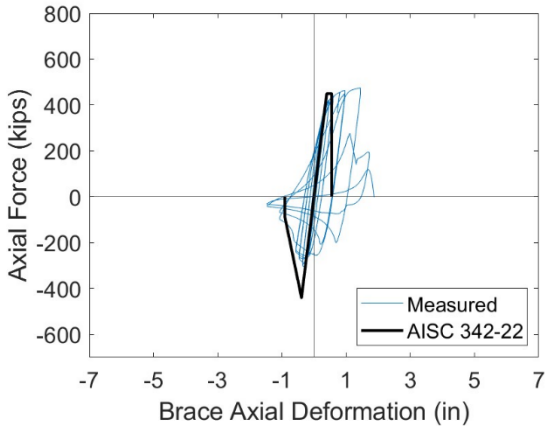

Figure 6.23 10.75x1/4 Short (L_c/r = 49.3, D/t = 46.1)

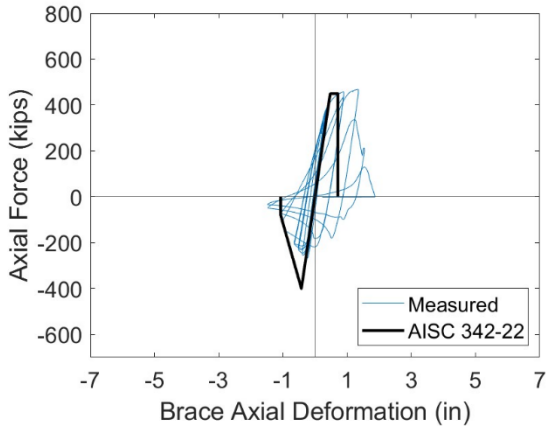

Figure 6.24 10.75x1/4 Long (L_c/r = 59.0, D/t = 46.1)

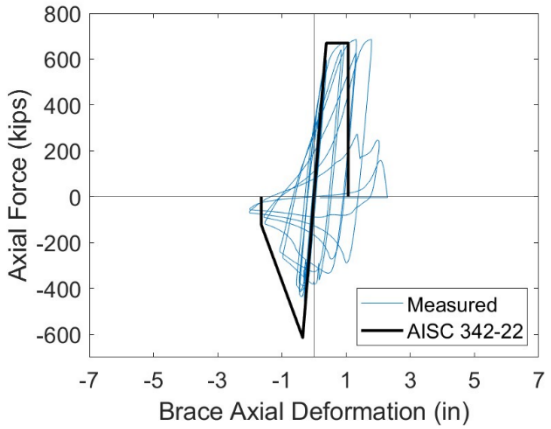

Figure 6.25 10.75x0.365 Short (L_c/r = 49.9, D/t = 31.7)

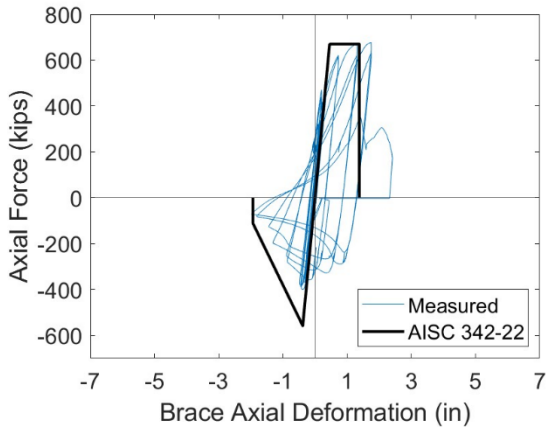

Figure 6.26 10.75x0.365 Long (L_c/r = 49.9, D/t = 31.7)

6.2.2 Comparison of AISC 342-22 and Measured Axial Deformation Capacities for Round HSS Braces

The previous section compared the predicted force-displacement response from AISC 342-22 to measured experimental data for round HSS braces. This section will present more tables and figures to further investigate the accuracy of modeling parameters. Table 6.4 shows a summary of total axial displacement from modeling parameters and experimental data for tension and compression. The last column shows the ratio between experimental and predicted values. There is a trend that as local slenderness, *D/t,* increases, so does the difference between experimental and predicted values.

Table 6.4 Comparison of AISC 342-22 and Measured Brace Axial Deformation

Test Specimen	D/t	$d_{342\text{-}22}$ (in)		$d_{measured}$ (in)		$d_{meas.} / d_{342.}$	
		Tens.	Comp.	Tens.	Comp.	Tens.	Comp.
6x3/16 Short	34.5	1.27	1.17	2.22	2.05	1.75	1.75
6x3/16 Long	34.5	1.65	1.17	2.84	2.48	1.72	2.12
6x1/4 Short	25.8	2.08	2.09	2.40	2.19	1.15	1.05
6x1/4 Long	25.8	2.69	2.06	3.54	3.15	1.32	1.53
6.625x3/16 Long	38.1	1.30	1.16	2.32	2.23	1.78	1.92
6.625x1/4 Short	28.4	1.62	1.34	2.53	2.55	1.56	1.91
6.625x1/4 Long	28.4	2.10	1.78	3.11	2.41	1.48	1.35
6.625x3/8 Short	19.0	3.25	3.47	3.13	3.16	0.96	0.91
6.625x3/8 Long	19.0	4.21	3.51	3.28	2.84	0.78	0.81
6.625x1/2 Short	14.2	5.16	5.10	3.94	4.05	0.76	0.79
6.625x1/2 Long	14.2	6.68	4.97	4.64	3.68	0.69	0.74
8.625x3/16 Short	49.6	0.51	0.67	1.71	1.36	3.36	2.04
8.625x3/16 Long	49.6	0.66	0.73	1.54	1.43	2.33	1.96
8.625x1/4 Short	37.0	0.86	1.13	1.72	1.82	2.00	1.61
8.625x1/4 Long	37.0	1.11	1.25	1.79	1.95	1.61	1.56
8.625x3/8 Short	24.7	1.73	2.28	1.86	2.03	1.08	0.89
8.625x3/8 Long	24.7	2.50	2.51	2.33	2.41	0.93	0.96
10.750x1/4 Short	46.1	0.55	0.91	1.44	1.47	2.62	1.61
10.750x1/4 Long	46.1	0.72	1.07	1.53	1.46	2.12	1.37
10.750x0.365 Short	31.7	1.07	1.64	2.06	2.00	1.92	1.22
10.750x0.365 Long	31.7	1.38	1.93	2.09	1.96	1.51	1.01

Figure 6.27 and Figure 6.28 plot measured over ASIC 342-22 predicted values for tensile and compressive deformation respectively versus *D/*t. For braces with local slenderness from 19-25, the predicted brace axial deformation is in good agreement with the experimental brace

behavior. As local slenderness increases, the accuracy of predicted brace deformation decreases. The ratio between experimental and predicted data is closer to 1.00 for most long specimens compared to the short specimen of the same cross-section. As global slenderness increases, it slightly increases the accuracy for most braces. The predicted brace deformation significantly underestimates real brace deformation capacity at moderate and high local slenderness. The experimental brace deformation capacity was up to 3 times larger than the predicted values for tension and compression for large *D*/*t*.

Figure 6.29 and Figure 6.30 plot measured over ASIC 342-22 predicted values for tensile and compressive deformation respectively versus L_c/r. The R^2 value for tensile deformation capacity is 0.275 and is 0 for compressive deformation capacity. The AISC 342-22 equations for tensile and compressive deformation capacity and the measured response are individually a function of L_c/r. The low R^2 values indicate that the difference between measured and AISC 342 deformation capacity is not a function of L_c/r. Tensile deformation response has a small correlation that at an L_c/r greater than 100, the modeling parameters provide a slightly more accurate prediction for tensile deformation capacity.

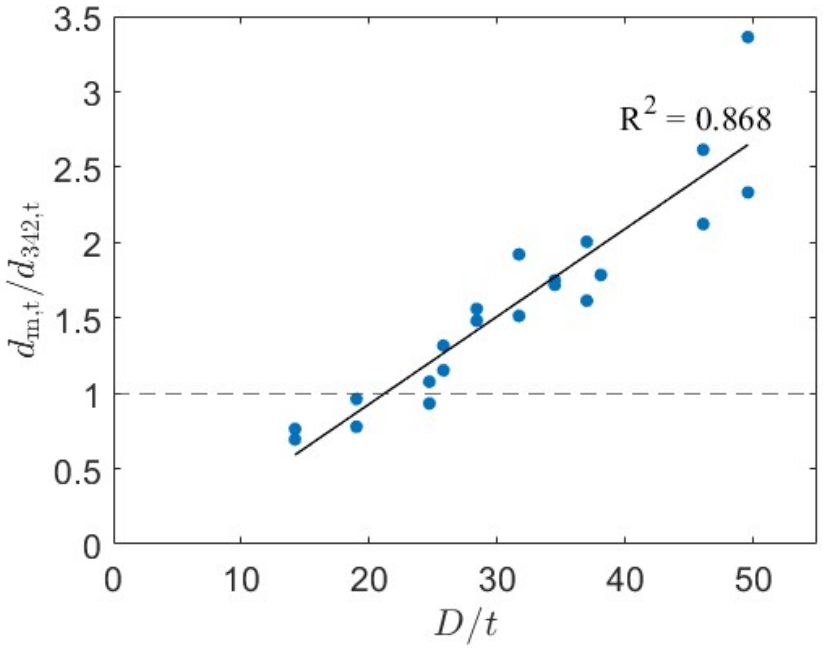

Figure 6.27 Ratio of AISC 342-22 and Measured Tensile Deformation Capacity vs D/t

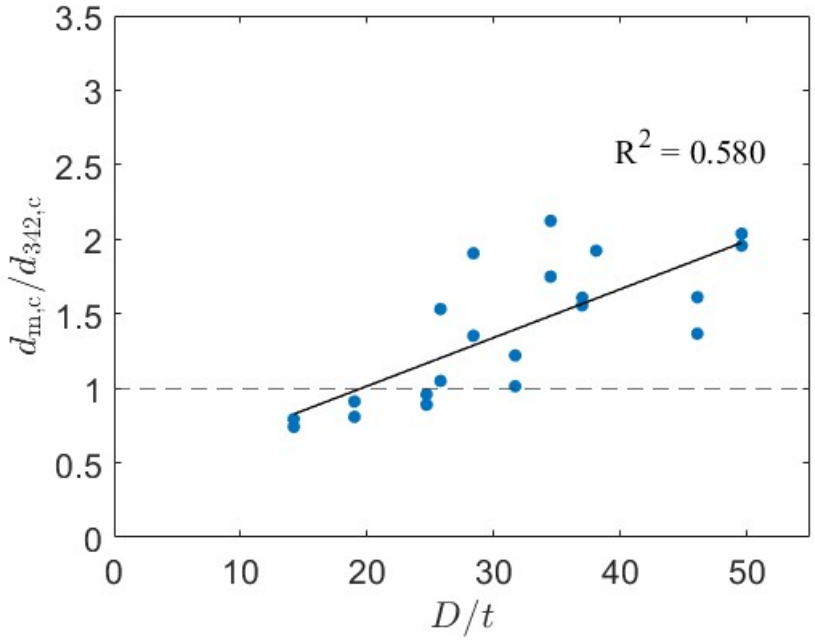

Figure 6.28 Ratio of AISC 342-22 and Measured Compressive Deformation Capacity vs D/t

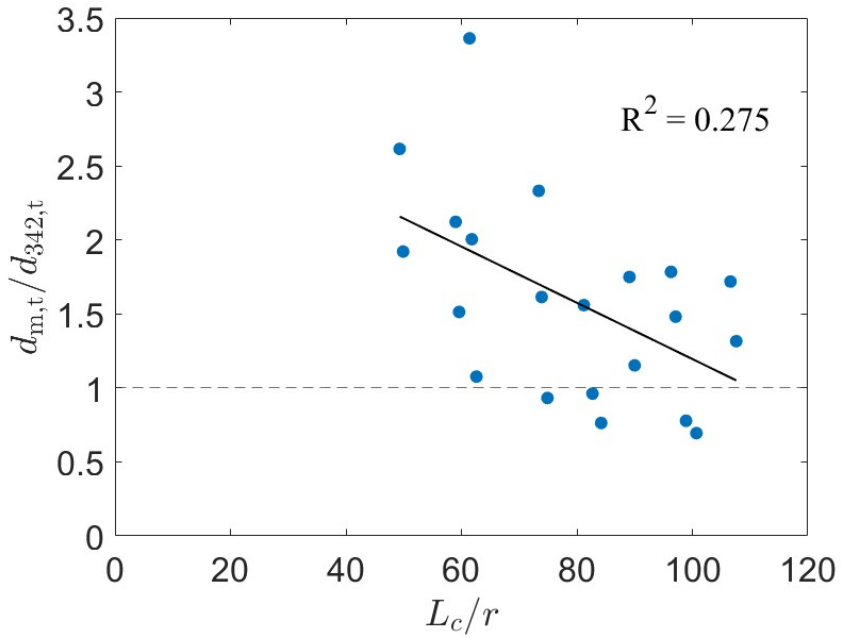

Figure 6.29 Ratio of AISC 342-22 and Measured Tensile Deformation Capacity vs L_c/r

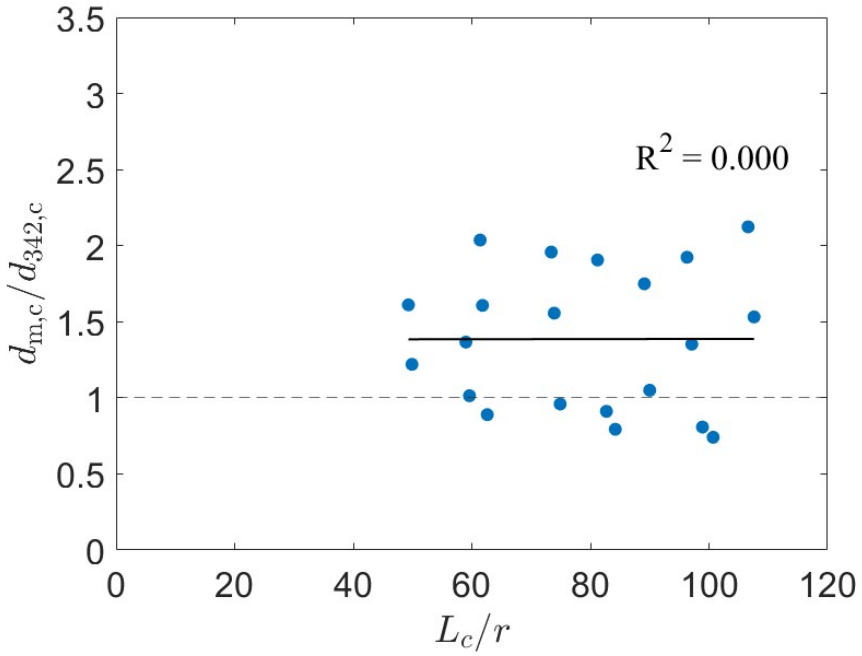

Figure 6.30 Ratio of AISC 342-22 and Measured Compressive Deformation Capacity vs L_c/r

Figure 6.31, Figure 6.32, and Figure 6.33 plot predicted versus measured properties for tension, compression, and deformation range, respectively. A 1-to-1 line is plotted in black to represent the target for predicted values. In all three plots, the experimental deformation capacity is noticeably larger than the AISC 342-22 modeling parameters predict for the majority of braces tested. As mentioned, the braces with local slenderness from 19-25 are generally well predicted, but for all the specimens with local slenderness larger than 25 AISC 342-22 underestimates the experimental deformation (below the black line). In Figure 6.31 and Figure 6.32, the six points that are above 1-to-1 line (where AISC 342-22 predicts larger deformation capacity that was obtained in the experiments) correspond to specimens with a low local slenderness.

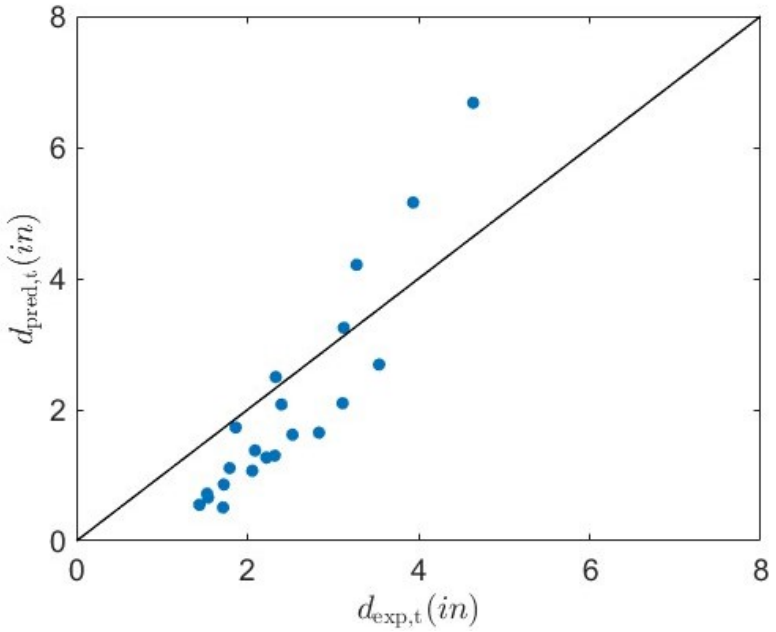

Figure 6.31 AISC 342-22 versus Measured Tensile Deformation Capacity

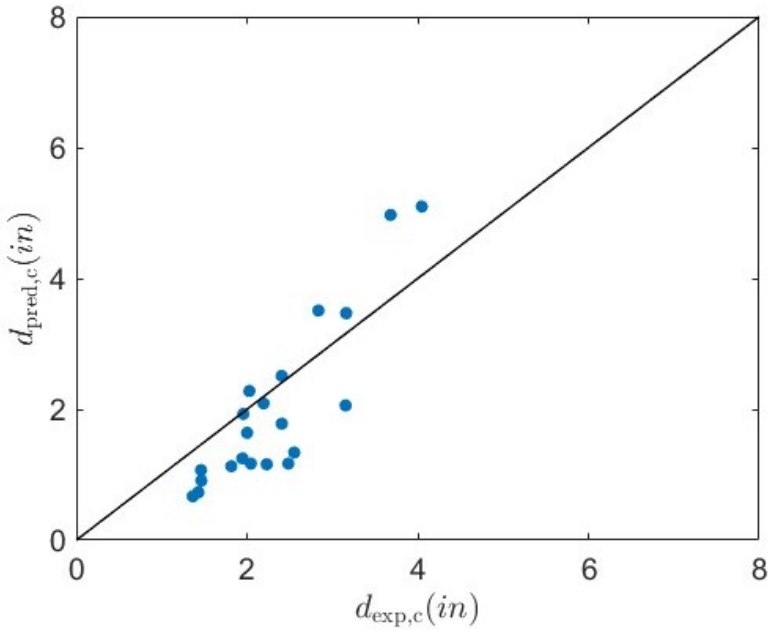

Figure 6.32 AISC 342-22 versus Measured Compressive Deformation Capacity

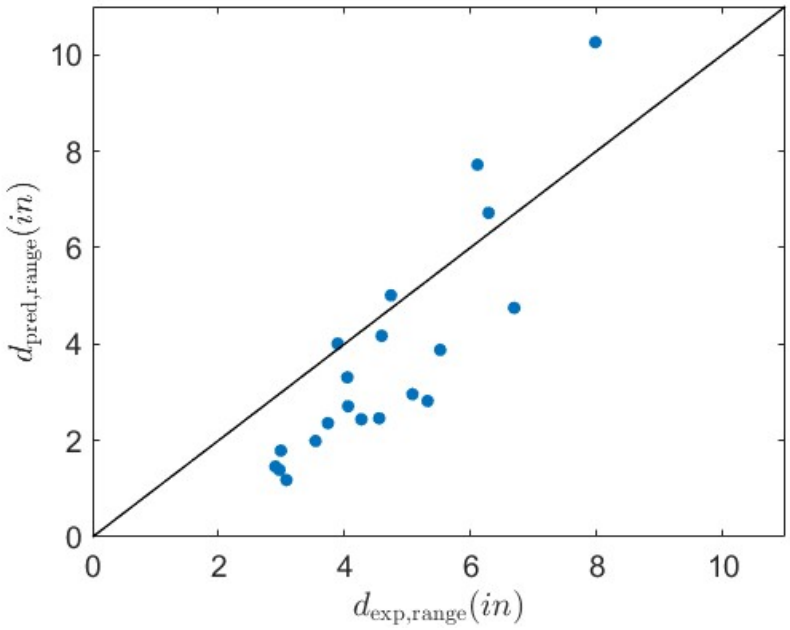

Figure 6.33 AISC 342-22 versus Measured Deformation Capacity Range

The analysis in this section establishes the need revise the current AISC 342-22 modeling parameters for round HSS braces using the new experimental data documented in this thesis. A regression analysis should be performed to recalibrate the exponents and coefficients of the modeling equations. Consideration should also be taken to adjust the form of the equation to accurately represent plate buckling of curved plates (i.e., E/F_y should be under a radical). Many other equations in the AISC specifications address the buckling of round HSS using the ratio of material parameters E and R_yF_y or $F_{y,m}$ directly, without taking the square root.

Chapter 7. Conclusions and Future Work

HSS braces in OCBF and SCBF systems act as the primary fuse elements that yield in tension and buckle in compression to dissipate energy. The braces remain elastic until axial deformations cause yielding in tension and global buckling in compression. Subsequent deformation caused by story drift induces the formation of a plastic hinge at brace midspan in compression. After the development of the plastic hinge, or in some cases at the same time as local cupping, strains rapidly accumulate at the hinge location. Brace fracture results from local cupping and additional axial deformation. Previous research has shown that a brace's ability to withstand local cupping is directly impacted by brace local slenderness, b/t or D/t, and global slenderness, L_c/r. A more locally compact and globally slender brace will exhibit larger inelastic axial deformation before brace fracture than a brace with large local slenderness and small global slenderness which is prone to early brace fracture at the location of cupping.

Previous research on square A500 and A1085 HSS braces performed in the UW SRL by Bergendahl (Bergendahl, 2021) and Kaldestad (Kaldestad, 2022) tested a large number of square HSS braces with b/t ratios near the AISC 341-16 high and moderate ductility limits. This research was performed to evaluate the variation in brace response with steel producer, material grade, and loading protocol. Results showed that these variables did not have a large impact on inelastic brace deformation capacity, and that the current local slenderness limits for square HSS braces are conservative and should be re-evaluated to accurately represent brace behavior.

There remained a need to test additional square sections with b/t ratios between 20 and 30 and there was general lack of data on the cyclic response of round HSS braces using modern steel. As such, a comprehensive experimental program on the inelastic deformation capacity of square and round HSS was conducted to evaluate the current local slenderness limits in AISC 341. This chapter will provide a summary and the conclusions of this thesis along with recommendations for future work on braces in CBFs.

7.1 Summary

This experimental research study consisted of thirty HSS brace specimens subjected to a symmetrical displacement-controlled loading protocol till brace fracture. Test Series 1 included nine square HSS with local slenderness larger than the current ASIC 341-22 moderately ductile local slenderness limit. Test Series 2 included twenty-one round HSS with D/t ratios near and

outside of the AISC 341-22 high and moderate ductility limits. The square and round specimens encompassed a large range of global slenderness. The focus of the study was to investigate the combined effect of local and global slenderness on brace inelastic deformation capacity.

The cyclic response of HSS brace specimens was evaluated based on axial deformation range in terms of approximate story drift range. The story drift range targets for OCBFs and SCBFs were established from non-linear response history analysis studies by Sen (2024). The target story drift range was set at 3.5% for OCBFs and 5.0% for SCBFs. The proposed limits for AISC 341-27 detailed in this thesis were based on the evaluation of experimental drift capacity using these target story drift requirements. Detailed test reports containing the experimental summary and results of each specimen can be found in Appendix E.

The concentration of strain at brace midspan during local cupping deformations was documented to analyze the effect of brace local and global slenderness on local deformations. Specifically, the onset, severity and distribution of cupping deformations are investigated to identify their influence on brace inelastic deformation capacity.

The accuracy of the current AISC 342-22 modeling parameters for round HSS braces were evaluated using the experimental brace force-displacement response. The backbone curves' ability to capture strength and degradation behavior was evaluated by examining how variations in local and global slenderness affected agreement with the experimental response.

7.2 Conclusions

The conclusions made based on experimental results and data analysis are summarized here.

- Ductility and inelastic deformation capacity of HSS bracing members is most significantly impacted by the brace local and global slenderness. As brace local slenderness decreases and global slenderness increases, deformation capacity increases. This relationship is consistent with prior research.
- Braces with the same local slenderness have a larger inelastic deformation capacity with longer length and larger global slenderness than shorter length with smaller global slenderness.
- Brace local slenderness has a greater impact on brace deformation capacity than global slenderness. Braces with very large b/t or D/t do not perform well regardless of the L_c/r.

- As local slenderness increases and global slenderness decreases, the concentration of strain in the cupping region at brace midspan increases. Furthermore, with increasing local slenderness, the number of cycles in which the concentration of cupping occurs decreases, while the magnitude of strain increases. The accumulation of strain at the center of cupping is less severe in braces with low local slenderness.
- The AISC 342-22 non-linear models for round HSS braces significantly underestimate the deformation capacity range of braces with moderate and low ductility. The models slightly overestimate the deformation capacity of braces with high ductility.
- This study proposes new limits for brace local slenderness that consider the influence of global slenderness, including an upper bound that constrains local slenderness when global slenderness becomes significantly large.

7.3 Recommendations for Future Research

This research project provided a comprehensive report on the cyclic response of square and round HSS. To better understand the behavior of braces in CBFs and to improve their performance, the following research is recommended:

- Research has shown that the onset of cupping and local deformations at brace midspan is the primary damage state that leads to brace fracture. To increase the inelastic deformation capacity of HSS, solutions should be investigated to further delay the onset of cupping. A research study by Ammons et al (2021) investigated the effect of foam fill on the cyclic response of round HSS. The foam fill successfully improved the ductile response of HSS braces with moderate ductility. Concrete-filled HSS braces where the fill is unbonded could similarly show an increase the inelastic deformation response of HSS by delaying the onset of cupping and increasing the compressive deformation capacity.
- The non-linear models for OCBF systems used to establish the target story drift range only modeled brace fracture and did not model other failure modes. The model was unable to achieve brace fracture if other failure modes were modeled. An investigation should be undertaken to review the intended system performance of OCBFs in accordance with ASCE and AISC.

- A study is needed to re-calibrate the AISC 342-22 backbone curves for round HSS using new experimental data collected in this thesis.
- There is a lack of data for AISC 342-22 modeling parameters of other cross-section shapes. While the design of new CBFs with angles and channels is uncommon, they are present in existing buildings and should have experimental data to validate modeling parameters.
- The average R_y value for round HSS obtained from the material testing in this thesis was 1.23. However, the implications of this finding are difficult to assess due to the limited dataset. During the fabrication process, round HSS have less cold working than square or rectangular HSS. Cold working strain hardens the steel and increases R_y. Additional material testing focused on round HSS would be beneficial to better evaluate the appropriate Ry factor for round HSS.

Bibliography

AISC (2010). "Specification for Structural Steel Buildings." ANSI/AISC 360-10, American Institute of Steel Construction, Chicago, IL.

AISC (2021). "Seismic Provisions for Structural Steel Buildings." ANSI/AISC 341-21, American Institute of Steel Construction, Chicago, IL.

AISC (2022). Seismic Provisions for Evaluation and Retrofit of Existing Steel Structural Buildings." AISC 342-22, American Institute of Steel Construction, Chicago, IL.

Ammons, M., Shimada, H., McCormick, J., and Kurata, M. (2021). “Experimental Investigation of Foam-Filled CHS Braces under Cyclic Loading.” Journal of Structural Engineering, 147(5).

ASCE (2023). "Seismic Evaluation and Retrofit of Existing Buildings." ASCE/SEI 41-23, American Society of Civil Engineers, Reston, VA.

ASTM (2024). "Standard Test Methods and Definitions for Mechanical Testing of Steel Products." ASTM A370-24, ASTM International, West Conshohocken, PA.

ATC (1992). "Guidelines for Cyclic Seismic Testing of Components of Steel Structures for Buildings." Report ATC-24, Applied Technology Council, Redwood City, CA.

Bergendahl, W, (2021). “Experimental Investigation to Compare the Cyclic Response of A500 and A1085 HSS Braces.” MS Thesis, University of Washington, Seattle.

Bradley, C. R., Fahnestock, L. A., Hines, E. M., and Sizemore, J. G. (2017). "Full-Scale Cyclic Testing of Low-Ductility Concentrically Braced Frames." Journal of Structural Engineering, 143(6), 04017029.

Elchalakani, M., Zhao, X.-L., & Grzebieta, R. (2003). Tests of Cold-Formed Circular Tubular Braces under Cyclic Axial Loading. Journal of Structural Engineering, 129(4), 507–514.

Fell, B. V., Kanvinde, A. M., Deierlein, G. G., and Myers, A. T. (2009). "Experimental Investigation of Inelastic Cyclic Buckling and Fracture of Steel Braces." Journal of Structural Engineering, 135(1), 19-32.

Gugerli, H. and Goel, S. C. (1982). "Inelastic Cyclic Behavior of Steel Bracing Members." Report UMCE 82R1, University of Michigan, Ann Arbor.

Hsiao, P.-C. (2012). "Seismic Performance Evaluation of Concentrically Braced Frames." Phd Dissertation, University of Washington, Seattle.

ICBO (1988.) Uniform Building Code. International Conference of Building Officials, Whittier,

CA.

Kaldestad, J, (2022). “Experimental Investigation into the Cyclic Response of A1085 HSS Braces” MS Thesis, University of Washington, Seattle.

Krawinkler, H. (2009). Loading Histories for Cyclic Tests in Support of Performance Assessment of Structural Components.

Lee, S. (1988.) "Seismic Behavior of Hollow and Concrete-Filled Square Tubular Bracing Members, Report UMCE 87-11, University of Michigan, Ann Arbor.

Liu, Z. and Goel, S. C. (1987). "Investigation of Concrete-Filled Steel Tubes under Cyclic Bending and Buckling." PhD Dissertation, University of Michigan, Ann Arbor.

Roeder, C., W., Sen, A. D., Asada, H., Ibarra, S. M., Lehman, D. E., Berman, J. W., Tsai, K. C., Tsai, C. Y., Wu, A. C., Wang, K. J., and Liu, R. (2020). "Inelastic Behavior and Seismic Design of Multistory Chevron-Braced Frames with Yielding Beams." Journal of Constructional Steel Research, v. 167, p. 105817.

Sabelli, R., Roeder, C. W., and Hajjar, J. R. (2013). "Seismic Design of Steel Concentrically Braced Frame Systems." NEHRP Seismic Design Technical Brief No. 8, National Institute of Standards and Technology Engineering Laboratory, Gaithersburg, MD.

Sen, A. D (2024). “Task Group Report on Seismic Local Buckling Limits – Braces Working Group, Seismic Deformation Capacity Criteria for Buckling Braces” Task Group report, AISC, 42-53.

Swatosh, M. A. (2016), "Seismic Evaluation and Retrofit of Concentrically Braced Frames." MS Thesis, University of Washington, Seattle.

Takeuchi, T., & Matsui, R. (2011). Cumulative Cyclic Deformation Capacity of Circular Tubular Braces under Local Buckling. Journal of Structural Engineering, 137(11), 1311–1318.

Terpstra, C. (2017). "Impact of Beam Strength on Seismic Performance of Chevron Concentrically Braced Frames." MS Thesis, University of Washington, Seattle.

Tremblay, R. (2002). "Inelastic Seismic Response of Steel Bracing Members." Journal of Constructional Steel Research, v. 58, p. 665-701.

Tremblay, R. (2008). "Inelastic Cyclic Testing of Large Size Steel Bracing Members." The 14th World Conference on Earthquake Engineering, Beijing, China.

Appendix A – Connection Details

A.1 Gusset Plate Details

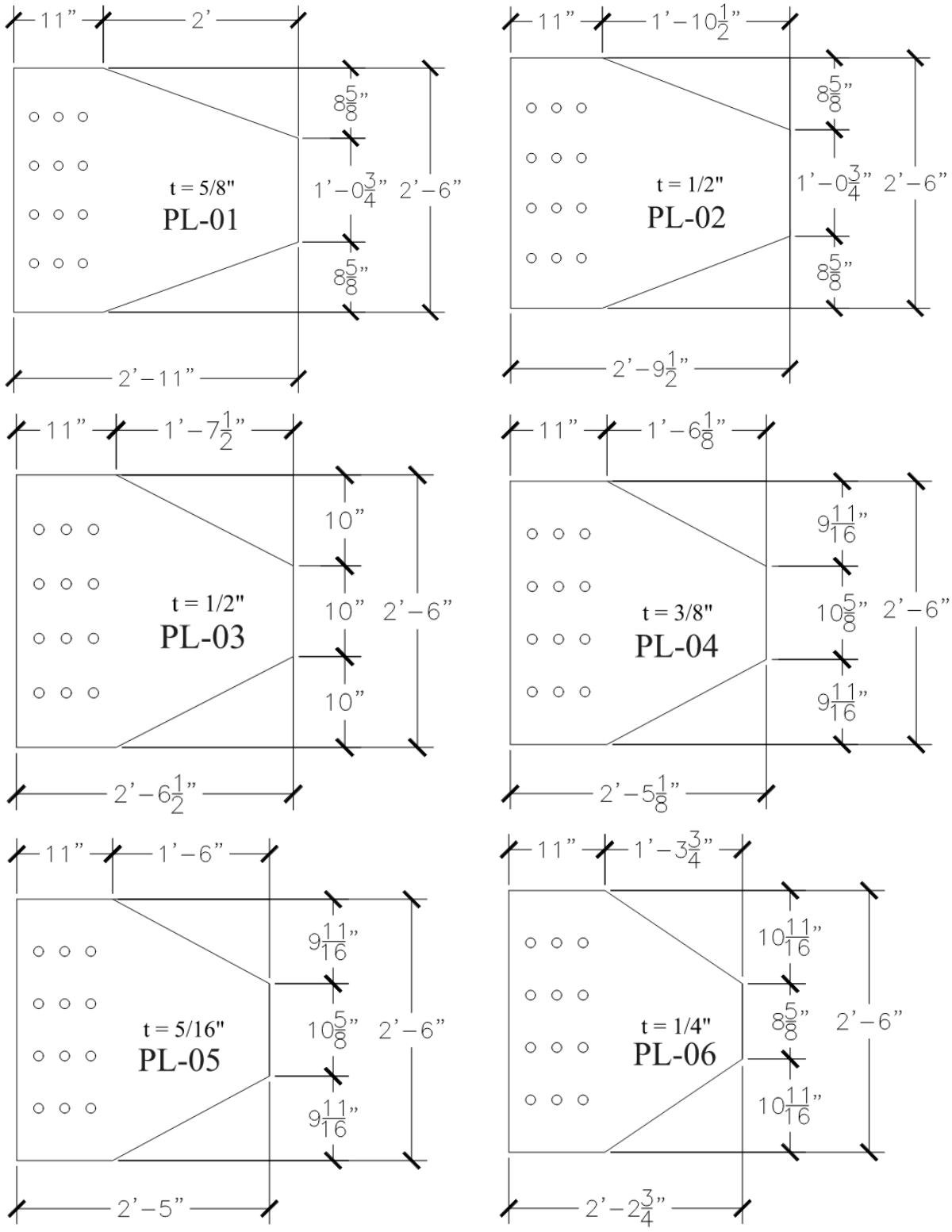

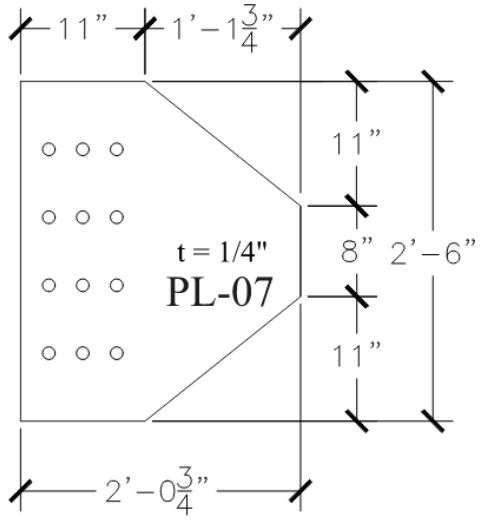

A.2 Gusset Plate Schedule

Section	Gusset Plate				Slot			Weld
	Plate Type	Length - Sloped	Thickness	Length	Width	Eccentricity	Length	Size
		(in)	(in)	(in)	(in)	(in)	(in)	(in)
HSS 5x5x3/16	PL-06	16.750	0.250	15.0	0.375	0.1875	16.0	3/8
HSS 6x6x3/16	PL-06	16.750	0.250	15.0	0.375	0.1875	16.0	3/8
HSS 6x6x1/4	PL-04	19.125	0.375	17.0	0.500	0.1875	18.0	3/8
HSS 7x7x1/4	PL-04	19.125	0.375	17.0	0.500	0.1875	18.0	3/8
HSS 8x8x5/16	PL-03	20.500	0.500	18.0	0.625	0.1875	19.0	3/8
HSS 6.000x0.188	PL-07	14.750	0.250	13.0	0.375	0.1875	14.0	3/8
HSS 6.000x0.250	PL-07	14.750	0.250	13.0	0.375	0.1875	14.0	3/8
HSS 6.625x0.188	PL-07	14.750	0.250	13.0	0.375	0.1875	14.0	3/8
HSS 6.625x0.250	PL-07	14.750	0.250	13.0	0.375	0.1875	14.0	3/8
HSS 6.625x0.375	PL-04	19.125	0.375	17.0	0.500	0.1875	18.0	3/8
HSS 6.625x0.500	PL-03	20.500	0.500	18.0	0.625	0.1875	19.0	3/8
HSS 8.625x0.188	PL-05	19.000	0.313	17.1	0.438	0.1875	18.1	3/8
HSS 8.625x0.250	PL-04	19.125	0.375	17.0	0.500	0.1875	18.0	3/8
HSS 8.625x0.375	PL-02	23.500	0.500	21.0	0.625	0.1875	22.0	3/8
HSS 10.750x0.250	PL-02	23.500	0.500	21.0	0.625	0.1875	22.0	3/8
HSS 10.750x0.365	PL-01	24.875	0.625	22.0	0.750	0.1875	23.0	3/8

A.3 Connection Design

Expected Forces– SEE EXAMPLE IN APPENDIX B OF KALDESTAD, 2022
Weld Design– SEE EXAMPLE IN APPENDIX B OF KALDESTAD, 2022

Bolt Design – SEE EXAMPLE IN APPENDIX B OF KALDESTAD, 2022

Gusset Plate Design– SEE EXAMPLE IN APPENDIX B OF KALDESTAD, 2022

A.4 Net Section Reinforcement Design

Sample Net Section Reinforcement calculation:

(SEE APPENDIX B OF KALDESTAD, 2022 FOR SQUARE HSS EXAMPLE)

6.625x3/8 Short A500:

Section Properties

Yield stress	F_y	50	ksi
Tensile strength	F_u	62	ksi
Yield Strength Factor	R_y	1.3	
Ultimate Strength Factor	R_t	1.2	
Elastic modulus	E	29000	ksi
Gross area	A_g	6.88	in^2
Brace Diameter	D	6	in.
Wall thickness	t_{des}	0.349	in.
Gusset Plate Width	w_{GP}	0.375	in.
Radius of Brace	R	3.31	in.

$w_s = w_{GP} + 0.125" = 0.375" + 0.125" = 0.50"$ [Slot Width]

$A_{nb} = A_g - 2 \cdot t_{des} \cdot w_s$ [Net Area at Slot]

$= 6.88\ in^2 - 2 \cdot 0.349" \cdot 0.50" = 6.53\ in^2$

$b_{cp} = 3.00"$ [Design Cover Plate Width]

$t_{cp} = 0.375"$ [Design Cover Plate Thickness]

$A_{cp} = b_{cp} \cdot t_{cp} = 1.125\ in^2$ [Cover Plate Area]

$L_{cp} = 14"$ [Design Cover Plate Length]

$$\theta = \left(90 - \sin^{-1}\frac{w_{GP}}{R}\right)\left(\frac{\pi}{180}\right) = \left(90 - \sin^{-1}\frac{0.375"}{3.31"}\right)\left(\frac{\pi}{180}\right) = 1.5569\ rad \quad \text{[Theta]}$$

$$\underline{x} = \frac{R\sin\theta}{\theta} - \frac{1}{2}t_p = \frac{3.31"\sin(1.569)}{(1.569)} - \frac{1}{2}(0.375") = 1.924" \quad \text{[Connection Eccentricity]}$$

$$U = \left[1 + \left(\frac{\underline{x}}{L_{cp}}\right)^{3.2}\right]^{-10} = \left[1 + \left(\frac{1.924"}{14"}\right)^{3.2}\right]^{-10} = 0.991 \quad \text{[Shear Lag Factor]}$$

Net Section Rupture Limit State

$$A_e = U\left(A_{nb} + 2 \cdot A_{cp}\right) \quad \text{[Section Effective Net Area]}$$

$$= 0.991(6.53\ in^2 + 2 \cdot 1.125\ in^2) = 8.69\ in^2$$

$$\frac{A_g}{A_e} = \frac{6.88\ in^2}{8.69\ in^2} = 0.79 \text{ [OK: } A_e > A_g\text{]}$$

Longitudinal Weld Design– SEE EXAMPLE IN APPENDIX B OF KALDESTAD, 2022

A.5 Net Section Reinforcement Schedule

Section	Thickness	Width	Length	Weld Size
	(in)	(in)	(in)	(in)
HSS 5x5x3/16	3/8	2.5	12	1/4
HSS 6x6x3/16	3/8	3.5	16	1/4
HSS 6x6x1/4	3/8	3.5	16	1/4
HSS 7x7x1/4	3/8	4.0	17	1/4
HSS 8x8x5/16	3/8	4.0	17	1/4
HSS 6.000x0.188	3/8	3.0	14	1/4
HSS 6.000x0.250	3/8	3.0	14	1/4
HSS 6.625x0.188	3/8	3.0	14	1/4
HSS 6.625x0.250	3/8	3.0	14	1/4
HSS 6.625x0.375	3/8	3.0	14	1/4
HSS 6.625x0.500	3/8	3.0	14	1/4
HSS 8.625x0.188	3/8	3.5	16	1/4
HSS 8.625x0.250	3/8	3.5	16	1/4
HSS 8.625x0.375	3/8	3.5	18	1/4
HSS 10.750x0.250	3/8	4.0	18	1/4
HSS 10.750x0.365	3/8	4.0	18	1/4

Appendix B – AISC 342 Non-Linear Modeling Parameters – 6.625x3/8 A500 Short

Material and Geometric Properties

$$E = 29000\ ksi$$

$$A_g = 6.88\ in^2$$

$$F_{ye} = R_y F_y = 1.3 \cdot 50\ ksi = 65\ ksi$$

$$F_{ym} = 58.3\ ksi$$

$$L_c = K \cdot L_b = 1.0 \cdot 183.5\ in = 183.5\ in.$$

$$r = 2.22\ in.$$

$$F_e = \frac{\pi^2 E}{\left(\frac{L_c}{r}\right)^2} = 41.9\ ksi$$

$$F_{crm} = \left(0.658^{\left(\frac{F_{ym}}{F_e}\right)}\right) \cdot F_{ym} = 32.6\ ksi$$

$$\lambda = \frac{D}{t} = 19.0$$

$$\lambda_{hd,m} = 0.053 \cdot \frac{E}{F_{ym}} = 0.053 \cdot \frac{29000\ ksi}{58.3\ ksi} = 26.4$$

Expected strengths and yield deformations

$$P_{ye} = F_{ym} \cdot A_g = 58.3\ ksi \cdot 6.88\ in^2 = 401\ k$$

$$P_{ce} = F_{crm} \cdot A_g = 30.3\ ksi \cdot 6.88\ in^2 = 255\ k$$

$$\Delta_T = \frac{(P_{ye} \cdot L_c)}{A_g \cdot E} = \frac{(447\ k \cdot 183.5\ in.)}{6.88\ in^2 \cdot 29000\ ksi} = 0.37\ in.$$

$$\Delta_C = \frac{(P_{ce} \cdot L_c)}{A_g \cdot E} = \frac{(266\ k \cdot 183.5\ in.)}{6.88\ in^2 \cdot 29000\ ksi} = 0.23\ in$$

Nonlinear Analysis

For tension of a rectangular HSS brace:

$$n = 2.8 \cdot \left(\frac{\lambda}{\lambda_{hd,m}}\right)^{-1.7} \cdot \left(\frac{\left(\frac{L_c}{r}\right)}{\sqrt{\frac{E}{F_{ym}}}}\right)^{0.45} = 2.8 \cdot \left(\frac{19.0}{26.4}\right)^{-1.7} \left(\frac{\left(\frac{183.5\ in.}{2.22\ in.}\right)}{\sqrt{\frac{29000\ ksi}{58.3\ ksi}}}\right)^{0.45} = 8.81$$

For compression of a rectangular HSS brace:

$$n = 4.7 \cdot \left(\frac{\lambda}{\lambda_{hd,m}}\right)^{-1.7} \cdot \left(\frac{\left(\frac{L_c}{r}\right)}{\sqrt{\frac{E}{F_{ym}}}}\right)^{0.45} = 3.0 \cdot \left(\frac{19.0}{26.4}\right)^{-1.7} \cdot \left(\frac{\left(\frac{183.5\ in.}{2.22\ in.}\right)}{\sqrt{\frac{29000\ ksi}{58.3\ ksi}}}\right)^{0.45} = 14.8$$

For tension of a rectangular HSS brace:

$$d = n \cdot \Delta_T = 8.81 \cdot 0.37\ in. = 3.25\ in.$$

$$f = 1.0$$

$$f \cdot P_{ye} = 1.0 \cdot P_{ye} = 1.0 \cdot 401\ k = 401\ k$$

For compression of a rectangular HSS brace:

$$d = n \cdot \Delta_C = 14.8 \cdot 0.23\ in. = 3.47\ in.$$

$$f = 0.2$$

$$f \cdot P_{ce} = 0.2 \cdot P_{ce} = 0.2 \cdot 255\ k = 51\ k$$

Appendix C – Material Testing

Producer	Section Size	Section Area (sq. in.)	Thickness (in.)	Grade	Chemical Composition																	Carbon Equivalent (%)
					C	Mn	Si	Al	B	Ca	Cb	Cr	Cu	Mo	N	Nb	Ni	P	S	Sb	Ti	V	
					(%) x 100	(%) x 100	(%) x 100	(%) x 1000	(%) x 1000	(%) x 1000	(%) x 1000	(%) x 1000	(%) x 1000	(%) x 1000	(%) x 1000	(%) x 1000	(%) x 1000	(%) x 1000	(%) x 1000	(%) x 1000	(%) x 1000	(%) x 1000	
Blue	5x5x3/16	3.28	0.168	A500	19	39	3.2	29	0.1	1.8	6	50	110	10	5.9	6	30	7	3	-	2	2	47.77
Blue	6x6x3/16	3.98	0.172	A500	22	76	16.9	28	0.4	1.4	1	50	110	10	6.1	1	30	10	3	-	1	5	59.82
Blue	6x6x1/4	5.24	0.224	A500	20	39	2.6	34	0.1	1.2	7	50	120	10	6.3	7	30	6	3	-	1	2	49.33
Blue	7x7x1/4	6.17	0.226	A500	20	38	2.7	34	0.1	1.8	6	50	160	10	6.8	6	40	7	3	-	2	2	52.52
Blue	8x8x5/16	8.76	0.280	A500	19	37	2	26	0	2.1	5	40	110	10	7.3	5	30	4	4	-	1	2	45.23
Blue	8.625x0.188	4.62	0.177	A500	20	42	3.4	26	0.4	1.8	6	60	130	10	6.6	6	40	7	2	-	1	4	53.70
Blue	8.625xSCH20	6.14	0.228	A500	20	40	2.9	30	0.1	1.6	6	40	120	10	7.3	6	40	7	2	-	1	1	48.02
Blue	8.625x0.375	9.07	0.337	A500	20	40	1.8	32	0.3	1.4	6	50	120	10	5.1	6	30	10	1	-	0	3	49.57
Blue	10.750xSCH40	11.91	0.331	A500	20	42	2.6	37	-	-	-	40	100	10	-	6	30	8	4	-	-	2	46.50
Blue	10.750xSCH20	7.70	0.227	A500	19	39	2.4	26	0.1	0.8	5	50	150	10	5.3	5	40	7	3	-	0	2	50.97
Red	6.625x0.188	3.53	0.172	A500	22	81	14	-	-	-	-	3	2	0	-	-	1	9	3	-	-	1	38.83
Red	6x0.188	3.18	0.175	A500	22	85	16	-	-	-	-	4	3	0	-	-	2	19	5	-	-	1	40.17
Red	6x0.250	4.22	0.231	A500	22	85	14	-	-	-	-	3	1	0	-	-	1	13	4	-	-	1	39.43
Red	6.625x0.250	4.68	0.231	A500	21	81	15	-	-	-	-	3	3	0	-	-	1	9	5	-	-	1	38.07
Red	6.625x0.375	6.88	0.361	A500	6	119	30	-	-	-	-	4	3	0	-	-	1	8	2	-	-	7	33.30
Red	6.625x0.500	9.00	0.456	A500	5	124	30	-	-	-	-	5	2	1	-	-	1	8	1	-	-	9	33.87

Producer	Section Size	Mill Certification Properties				Experimental Tensile Test				Comparison (Measured/MC)			Comparison (Measured/Nom.)	
		Yield Stre	Tensile Strength	Fu/Fy	Elongation	Yield Strength	Tensile Strength	Fu/Fy	Elongation	Yield Strength	Tensile Strength	Elongation	Yield Strength	Tensile Strength
		(psi)	(psi)		(%)	(psi)	(psi)		(%)	(-)	(-)	(-)	(-)	(-)
Blue	5x5x3/16	58700	77400	1.3	35.0	71550	83170	1.16	31.62	1.22	1.07	0.90	1.4	1.3
Blue	6x6x3/16	64500	85200	1.3	32.0	58900	80520	1.37	30.22	0.91	0.95	0.94	1.2	1.3
Blue	6x6x1/4	60600	76800	1.3	34.0	64710	78590	1.21	31.25	1.07	1.02	0.92	1.3	1.3
Blue	7x7x1/4	62700	78400	1.3	33.0	64100	78750	1.23	30.33	1.02	1.00	0.92	1.3	1.3
Blue	8x8x5/16	61500	78900	1.3	33.0	64330	75810	1.18	34.19	1.05	0.96	1.04	1.3	1.2
Blue	8.625x0.188	63200	77300	1.2	34.0	69530	81570	1.17	29.45	1.10	1.06	0.87	1.4	1.3
Blue	8.625xSCH20	64300	76600	1.2	31.0	67020	79490	1.19	30.32	1.04	1.04	0.98	1.3	1.3
Blue	8.625x0.375	61500	72300	1.2	37.5	65740	75170	1.14	36.01	1.07	1.04	0.96	1.3	1.2
Blue	10.750xSCH40	61000	76300	1.3	36.0	62720	74800	1.19	34.23	1.03	0.98	0.95	1.3	1.2
Blue	10.750xSCH20	53800	72400	1.3	35.0	60400	76960	1.27	35.6	1.12	1.06	1.02	1.2	1.2
Red	6.625x0.188	58060	74450	1.3	23.8	56490	76750	1.36	34.75	0.97	1.03	1.46	1.1	1.2
Red	6x0.188	56100	74130	1.3	26.8	53600	73470	1.37	33.21	0.96	0.99	1.24	1.1	1.2
Red	6x0.250	54660	69740	1.3	29.9	54190	71590	1.32	40.45	0.99	1.03	1.35	1.1	1.2
Red	6.625x0.250	58310	75420	1.3	28.7	59030	74560	1.26	36.24	1.01	0.99	1.26	1.2	1.2
Red	6.625x0.375	62630	74410	1.2	28.2	58340	63690	1.09		0.93	0.86		1.2	1.0
Red	6.625x0.500	62850	66060	1.1	33.6	63690	65950	1.04	36.71	1.01	1.00	1.09	1.3	1.1

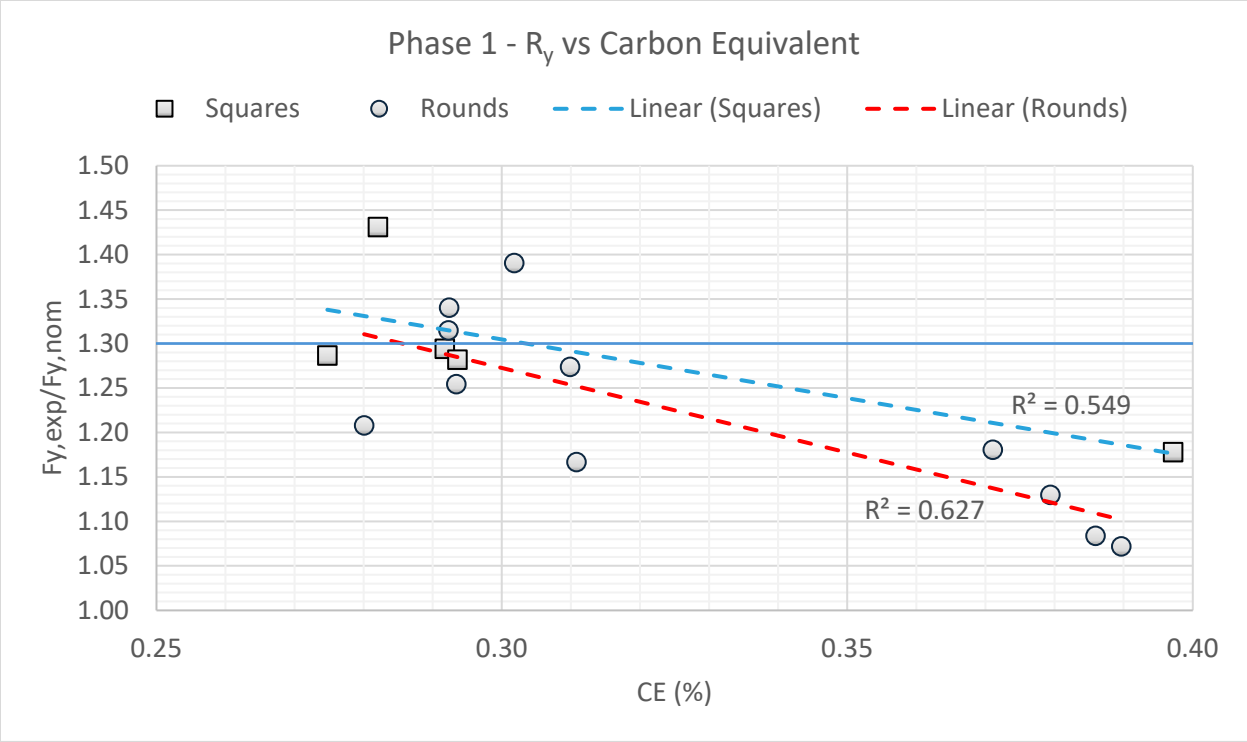

Figure 34: Ratio of Experimental Yield Strength to Nominal Yield Strength versus Carbon Equivalent

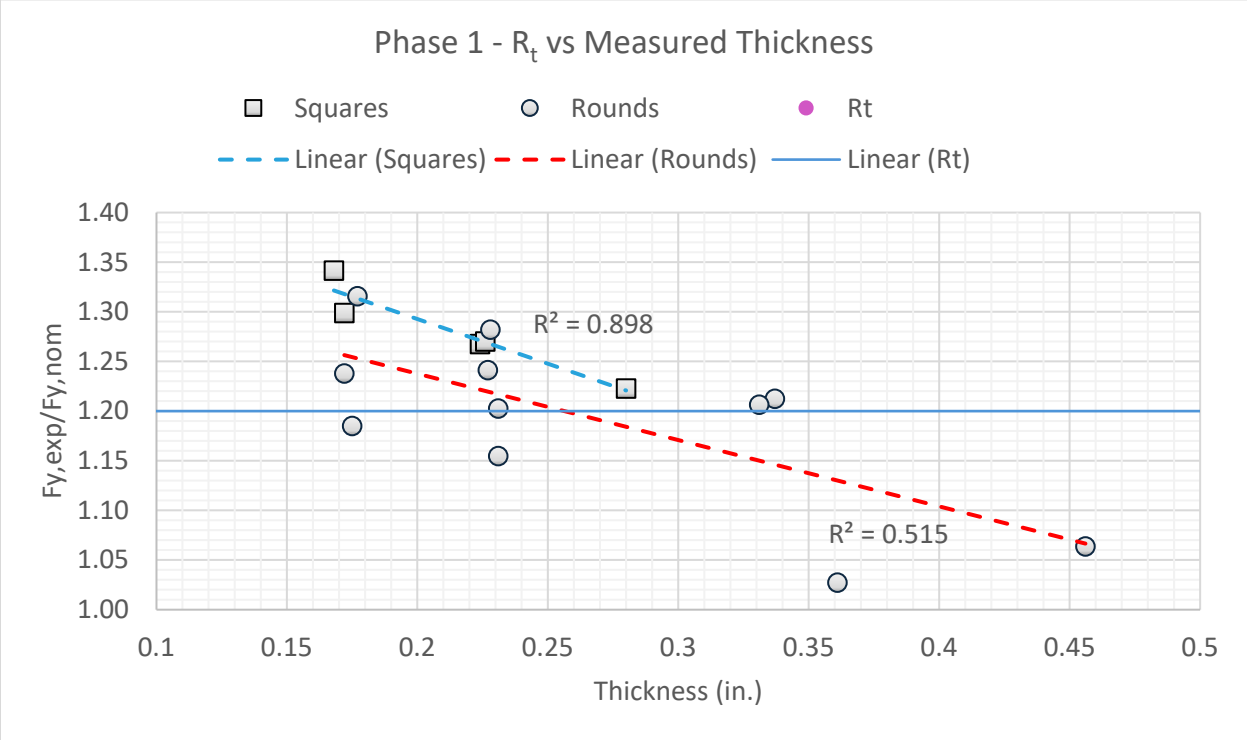

Figure 35: Ratio of Experimental Ultimate Strength to Nominal Ultimate Strength versus Measured Thickness

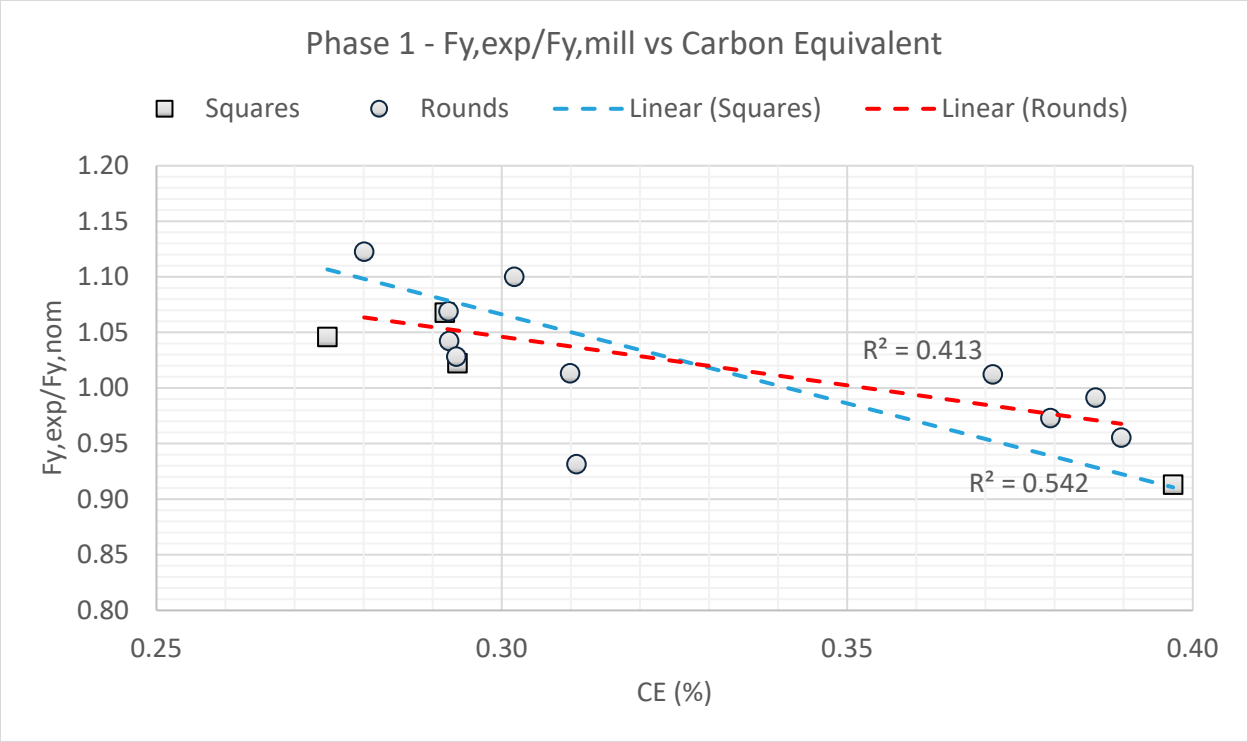

Figure 36: Ratio of Experimental Yield Strength to Mill Certification Yield Strength versus Carbon Equivalent

Carbon Equivalent Equation from AWS: CE = C + Mn/6 + (Cr+Mo+V)/5 + (Ni+Cu)/15 [1]

Appendix D – MATLAB

SEE EXAMPLE IN APPENDIX D OF KALDESTAD, 2022 FOR CLEANING AND CORRECTION SCRIPTS

OPTOTRAK DATA SCRIPT

```
% Inputs
lab_view_data = 'Output Data 8_625x3_16 A500 Long';
optotrak_data = 'op_data_8_625x3_16_long.txt';
initiation_cupping = 13; %cycle of initiation of cupping
mid_cupping = 14;
fracture = 15; %compression cycle before fracture

center_east = 20;  % Choose center of cupping

specimen = '8_625x3_16L';
folderPath = 'C:\Users\Lily Swanson\OneDrive - UW\Research\Thesis\Figures\Optotrak';
folderPath_2 = 'C:\Users\Lily Swanson\OneDrive - UW\Research\MATLAB optotrak';

%-- Load Labview data and extract data
lv_data = readmatrix(lab_view_data);
data2 = lv_data;

% Iterate through the data to adjust for laps in time
% Initialize the adjusted time column
time = lv_data(:,3);
adjusted_time = lv_data(:,3);

% Iterate through the time data to adjust for laps
for i = 2:length(time)
    if time(i) < time(i-1) % A lap has occurred
        adjusted_time(i:end) = adjusted_time(i:end) + 60;
    end
end

% Normalize to start at 0
lv_time = adjusted_time - adjusted_time(1);

%-- Load optotrack data
ot_data = importdata(optotrak_data);
[m,n] = size(ot_data);

%-- create time vector for optotrack data
Fs_ot = 10; % assume 10 Hz sampling frequency
ot_time = (0:(1/Fs_ot):(1/Fs_ot)*(length(ot_data)-1));

%-- create load vector for optotrack (linear interpolation)
ot_data_int = interp1(ot_time,ot_data,lv_time);
ot_data_int = ot_data_int * 0.0393701;  %Convert from mm to in

data = [lv_data, ot_data_int(:,2:91)];

%% Find Peaks
n = size(data,1);            %number of rows
m = size(data,2);            %number of columns
```

```
small_Act_Disp = -1*data(:,9);
point = data(:,6);

[pks,loc] =
findpeaks(small_Act_Disp,point,'MinPeakProminence',.1,'MinPeakDistance',200);
peaks = [pks, loc];

t = size(peaks,1);            %number of rows

for i = 1:t
    count(i) = [i]';
end
idx = count.';

for i = 1:t
    target(i) = ceil(idx(i)/2);
end
target = target.';
peaks = [idx, pks, loc, target];

%% Add column for target displacement to data matrix
for i = 1:n-1
    for j = 1:t-1
        if data(i,6) > loc(j)
           data(i,40) = target(j);
        end
    end
end

for i = 1:n-1
    if data(i,6) < loc(1)
       data(i,40) = 1;
    end
end

%% Remove unwanted data during holds
delete = zeros(n,1);
j = 1;
%Trimming Tolerances
tol1 = 0.00075;     %For targets 1-3
tol2 = 0.00045;     %For targets 4-9
tol3 = 0.0015;      %For targets >9

for e = 1:n-1
    if  data(e,40) <= 3
        diff = abs(data(e+2,18) - data(e,18));
        if diff < tol1
            delete(j,1) = e;
            j = j+1;
        end

    elseif (4 <= data(e,40)) && (data(e,40) <= 9)
        diff = abs(data(e+1,18) - data(e,18));
        if diff < tol2
            delete(j,1) = e;
```

```
            j = j+1;
        end
    else
        diff = abs(data(e-1,18) - data(e-3,18));
        if diff < tol3
            delete(j,1) = e;
            j = j+1;
        end
    end
end
delete = delete(1:j-1,1);
data([delete],:)= [];

small_Act_Disp = data(:,9);
point = data(:,6);
[pks,loc] =
findpeaks(small_Act_Disp,point,'MinPeakProminence',.1,'MinPeakDistance',200);
peaks_com = [pks, loc];

%-- extracts initial position of targets
position = data(:,41:130);
X = position(:,1:3:size(position,2)); X = X(:,1:30).';   % X coordinate position
vector
Y = position(:,2:3:size(position,2)); Y = Y(:,1:30).';   % Y coordinate position
vector
Z = position(:,3:3:size(position,2)); Z = Z(:,1:30).';   % Z coordinate position
vector
pos1 = [X(:,1),Y(:,1),Z(:,1)];                           % position vector rearranged
[t x 3]

% position at 0.75" peak
value = peaks_com(11,2);
rowNum = find(data(:, 6) == value);

pos2 = [X(:,rowNum),Y(:,rowNum),Z(:,rowNum)];

%-- cleans up code (target numbers)
opt = 1; % origin point
xpt = 30; % point on the x-axis
ypt = 15; % point on the y-axis

%-- calculate transformed coordinate vectors
n = cross(pos1(xpt,:)-pos1(opt,:),pos2(ypt,:)-pos1(opt,:));
n = n/vecnorm(n); % normal to the plane (1 x 3)
t = pos1(xpt,:)-pos1(opt,:);
t = t/vecnorm(t); % along the x-axis (1 x 3)
s = cross(n,t); % along the new y-axis (1 x 3) close to ypt target but 90 deg

%-- Transformation matrix
T = [t;s;n]; % newx, newy, newz

%-- Transformed postitions
Xt = zeros(size(X));
Yt = zeros(size(Y));
Zt = zeros(size(Z));
```

```
%-- loops through points
for ii = 1:size(X,2)
    pos = [X(:,ii),Y(:,ii),Z(:,ii)];
    sft = pos - ones(size(pos))*diag(pos1(opt,:)); %shifted coordinates
    rot = (T*sft.').'; % rotated coordinates (need to transpose for multiplication)
    Xt(:,ii) =  rot(:,1).';
    Yt(:,ii) =  rot(:,2).';
    Zt(:,ii) =  rot(:,3).';
end

% reorder rows for order of sensors
[~, sortIdx] = sort(Xt(:, 1));
Xt = Xt(sortIdx,:);
Yt = Yt(sortIdx,:);
Zt = Zt(sortIdx,:);

Xt = Xt.';
Yt = Yt.';
Zt = Zt.';

% % X AXIS DATA
% compute distances and strains between sensors
% dis_btw_sens = Xt(:, 2:end) - Xt(:, 1:end-1);
dis_btw_sens = Xt(:,1:end-2) - Xt(:,3:end);
strain_Xt_sens = (dis_btw_sens-dis_btw_sens(1,:))./dis_btw_sens(1,:);

% compute distances between x coordinates with varying guage length
dis_Xt = Xt(:,30:-1:16) - Xt(:,1:15);
strain_Xt = (dis_Xt-dis_Xt(1,:))./dis_Xt(1,:);


% Computing relative strain plots maually choosing center of cupping
center = 30 - center_east;
num_pairs = min(center - 1, size(Xt,2) - center);  % How many pairs you can form
symmetrically

% Create indices for symmetric pairs around the center
left_indices = center - (1:num_pairs);
right_indices = center + (1:num_pairs);

% Calculate distances between symmetric pairs
dis_Xt_real = Xt(:, right_indices) - Xt(:, left_indices);

% Compute strain relative to the initial frame (e.g., first row of Xt, or Xt(1,:))
strain_Xt_real = (dis_Xt_real - dis_Xt_real(1,:)) ./ dis_Xt_real(1,:);
```

AISC Brace Test Summary

Test Name: 5x5x3/16 A500 short
Test Date: 1/9/24

Brace Properties

Measured Yield Stress (ksi)	71.6
Measured Ultimate Stress (ksi)	83.1
Measured Yield Load (kips)	235
Critical Buckling Load (kips)	107
Percent Elongation – 2" (%)	31.6
Brace Length (in.)	183.5
Global Slenderness Ratio (L_c/r)	93.6

Area (in^2)	3.28
Moment of Inertia (in^4)	12.6
Thickness – Nominal (in.)	0.174
Thickness – Measured (in.)	0.190
Brace Compactness Ratio (b/t) – Nominal	25.7
Brace Compactness Ratio (b/t) – Measured	26.5

Specimen Damage State

Test Event	Axial Brace Deformation (in.)	Target Displacement Cycle (in.)	Force (kips)	$P / P_{(y/c)}$
Peak Tension Load	1.07	1.25 (T1)	243	1.03 (Y)
B1: Initial Global Buckling	-0.18	0.25 (C1)	-87	0.81 (C)
B2: Moderate Global Buckling	-0.43	0.625 (C1)	-67	0.63 (C)
B3-C: Local Cupping	-0.69	0.75 (C1)	-46	0.43 (C)
B3-T: Striations & Tearing	0.75	1.25 (T2)	132	0.56 (Y)
B4-T: 50% Tearing	1.04	1.25 (T2)	207	0.88 (Y)

Key Observations

Cycle #	Target Displacement (in.)	Observations
7-8	0.5	Bolt slip T1 cycle – North gusset plate
11-12	0.75	Bolt slip T1 cycle – North gusset plate Minor local cupping (~0.2") at C1 peak ~3" south of center After first full cycle, T_C1 moved 2.5inches south of center Moderate local cupping (~0.8") at C2 peak
13-14	1.25	Bolt slip T1 cycle – North gusset plate Major local cupping (~1.1") at C1, OOP disp. = 10.4" Brace tear >50% T2

Test Results

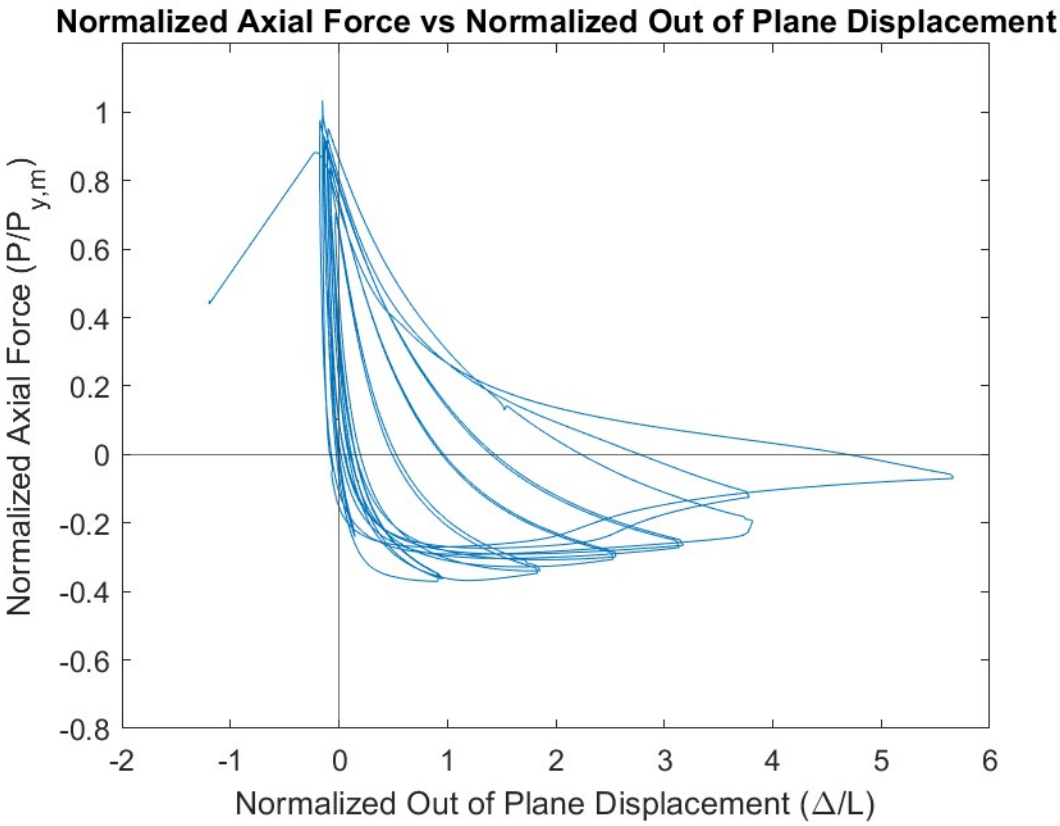

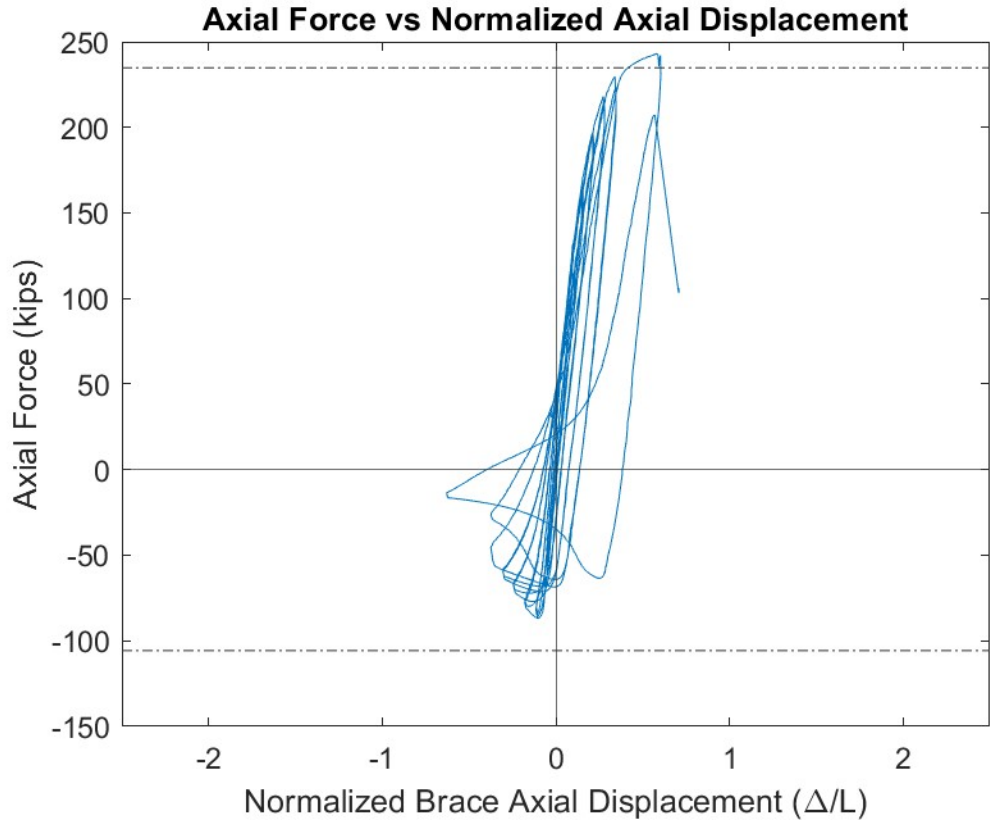

Photos

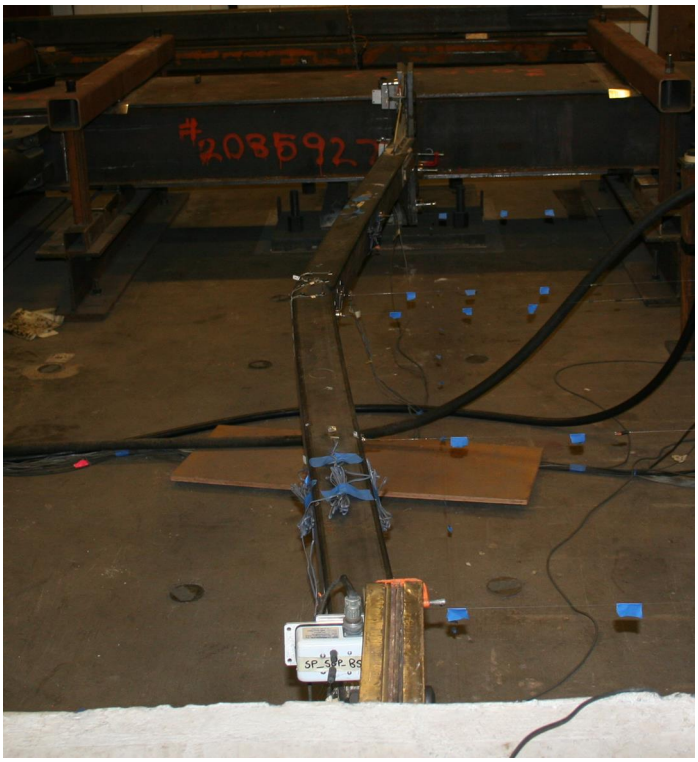

Peak Out of Plane Displacement: 1.25” Cycles

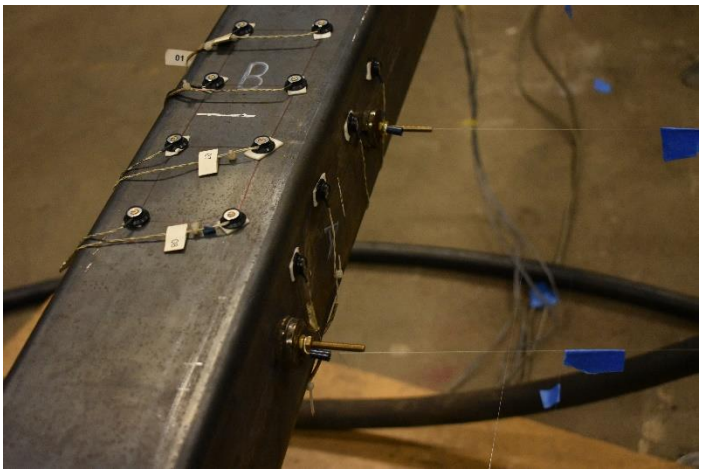

Minor Cupping ~3” south of center: 0.75” C1

Major Cupping ~3” south of center: 1.25” C1

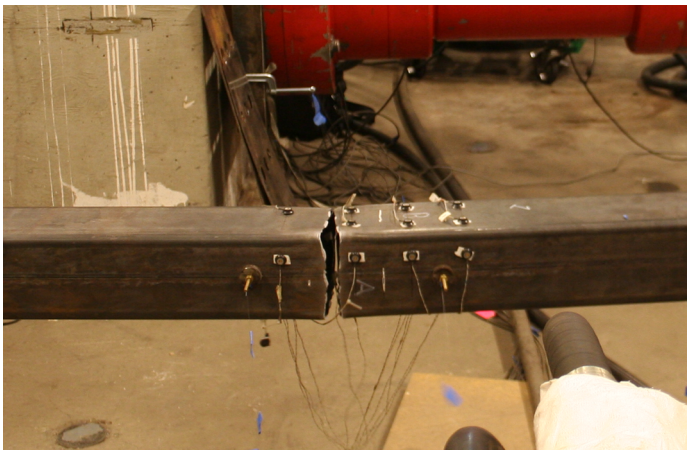

Brace tear >50%: 1.25” T2

AISC Brace Test Summary

Test Name: 6x6x3/16 A500 short
Test Date: 2/16/24

Brace Properties

Measured Yield Stress (ksi)	58.9
Measured Ultimate Stress (ksi)	80.5
Measured Yield Load (kips)	234
Critical Buckling Load (kips)	160
Percent Elongation – 2" (%)	30.2
Brace Length (in.)	183.5
Global Slenderness Ratio (L_c/r)	77.4

Area (in^2)	3.98
Moment of Inertia (in^4)	22.3
Thickness – Nominal (in.)	0.174
Thickness – Measured (in.)	0.181
Brace Compactness Ratio (b/t) – Nominal	31.5
Brace Compactness Ratio (b/t) – Measured	33.2

Specimen Damage State

Test Event	Axial Brace Deformation (in.)	Target Displacement Cycle (in.)	Force (kips)	$P / P_{(y/c)}$
Peak Tension Load	0.61	0.75 (T1)	256	1.09 (Y)
B1: Initial Global Buckling	-0.18	0.25 (C1)	-118	0.74 (C)
B2: Moderate Global Buckling	-0.66	0.75 (C1)	-33	0.21 (C)
B3-C: Local Cupping	-0.59	0.625 (C1)	-53	0.33 (C)
B3-T: Striations & Tearing	0.37	1.25 (T1)	133	0.57 (Y)
B4-T: 50% Tearing	0.76	1.25 (T1)	227	0.97 (Y)

Key Observations

Cycle #	Target Displacement (in.)	Observations
9-10	0.625	Minor local cupping (~0.5") at C1 peak 6.75" north of center Moderate local cupping (~0.9") at C2 peak
11-12	0.75	Major local cupping (~1.1") at C1 peak Striations forming at top and bottom corners of brace – T2 Major local cupping (~1.3") at C2 peak, OOP disp. = 5.4"
13-14	1.25	Brace tear >50% T1

Test Results

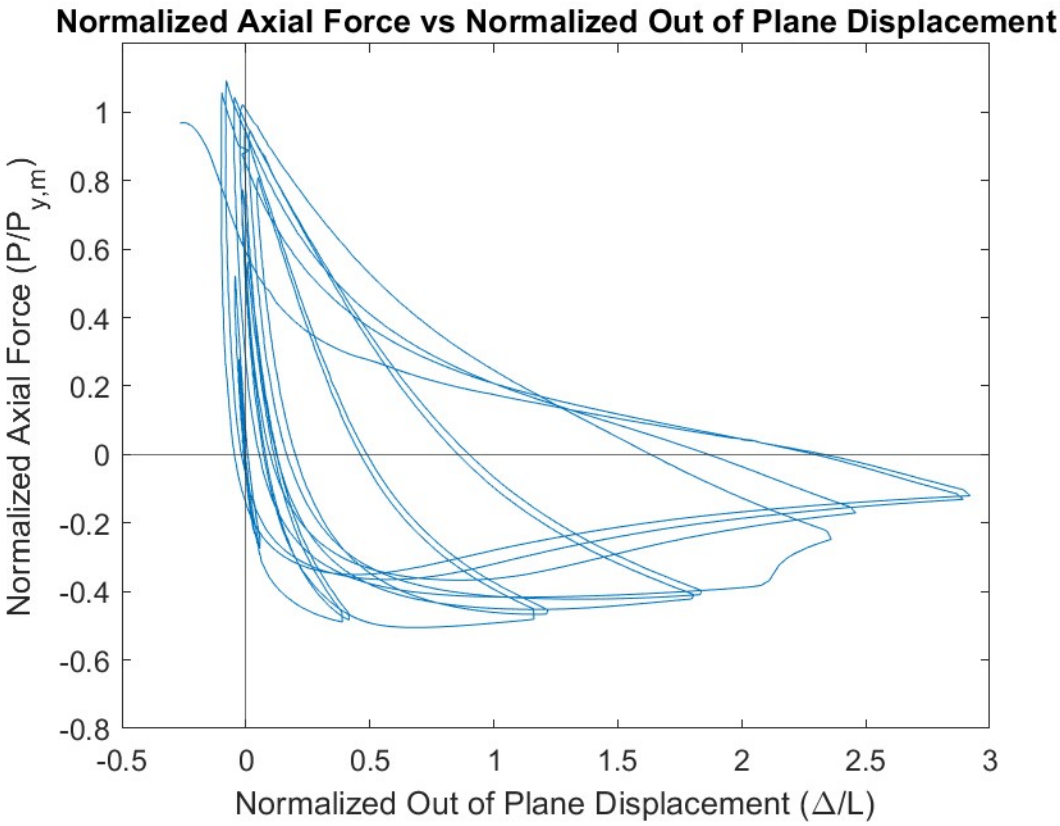

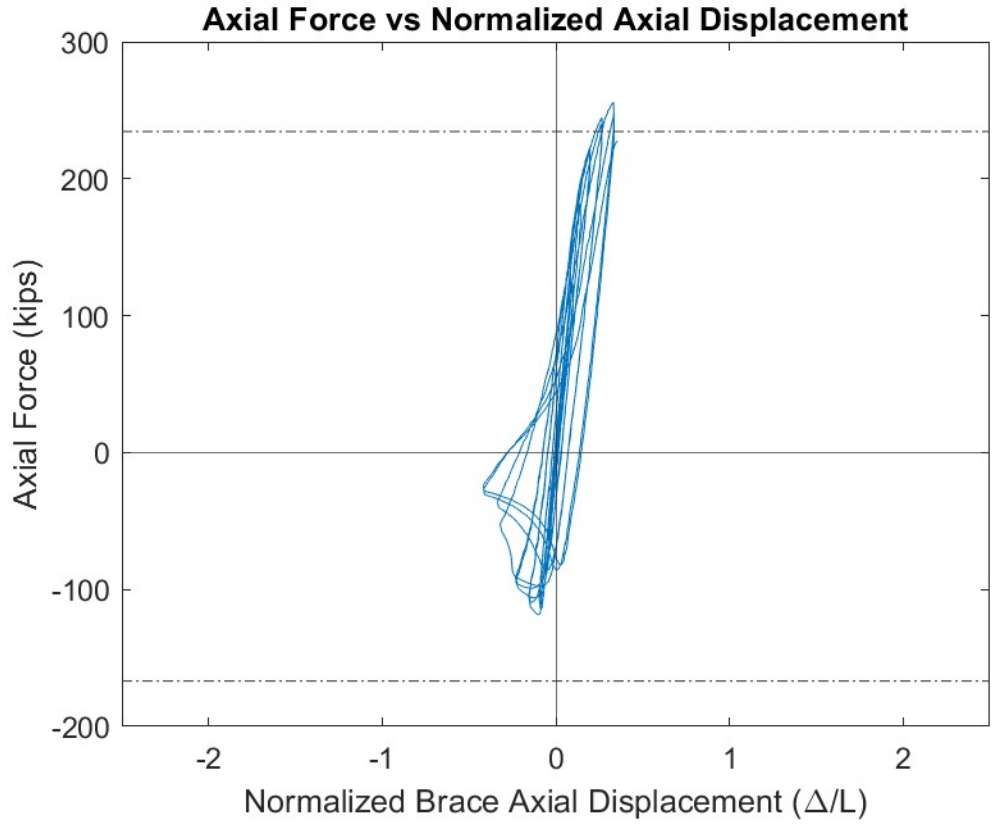

Photos

<table>
<tr><td> 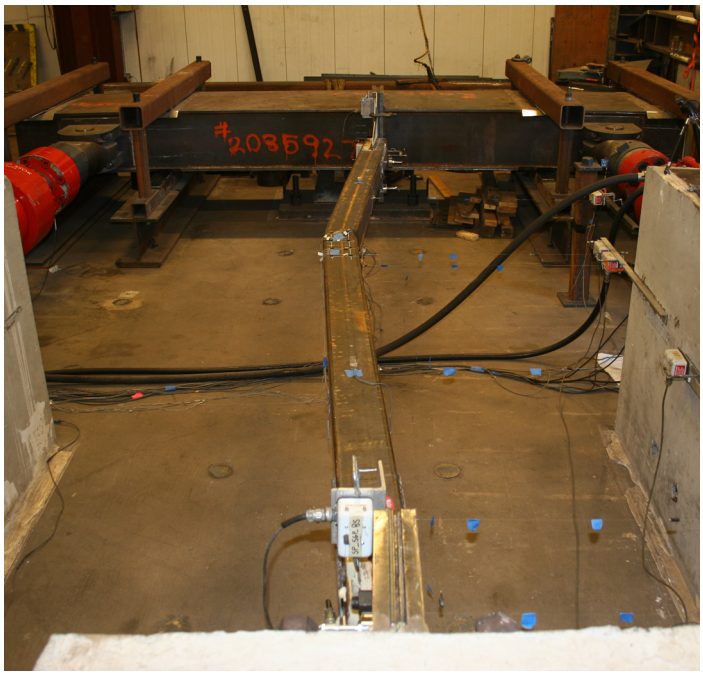 </td><td> 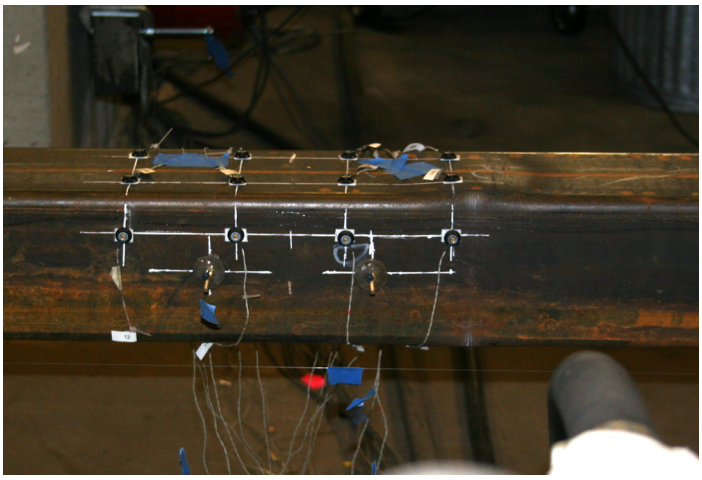 </td></tr>
<tr><td>Peak Out of Plane Displacement: 0.75” Cycles</td><td>Striations ~6.25” north of center: 0.75” T2</td></tr>
<tr><td> 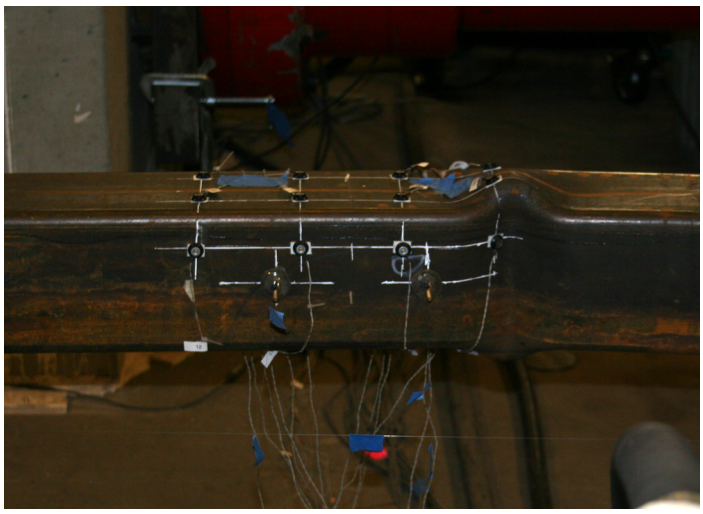 </td><td> 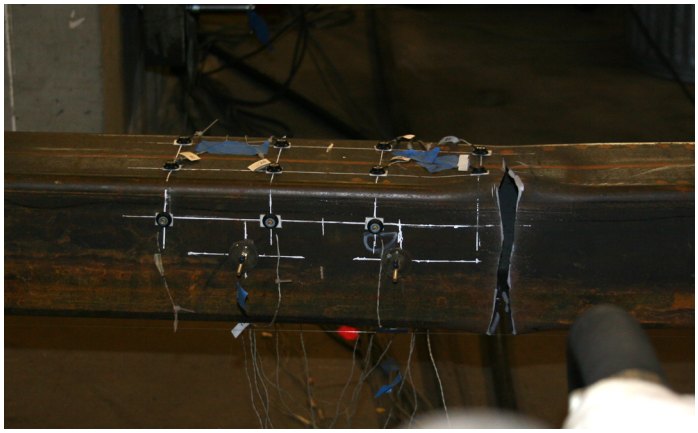 </td></tr>
<tr><td>Major Cupping ~6.25” north of center: 0.75” C2</td><td>Brace tear >50%: 1.25” T1</td></tr>
</table>

AISC Brace Test Summary

Test Name: 6x6x1/4 A500 short
Test Date: 2/13/24

Brace Properties

Measured Yield Stress (ksi)	64.7
Measured Ultimate Stress (ksi)	78.6
Measured Yield Load (kips)	339
Critical Buckling Load (kips)	216
Percent Elongation – 2" (%)	31.3
Brace Length (in.)	183.5
Global Slenderness Ratio (L_c/r)	78.4

Area (in^2)	5.24
Moment of Inertia (in^4)	28.6
Thickness – Nominal (in.)	0.233
Thickness – Measured (in.)	0.231
Brace Compactness Ratio (b/t) – Nominal	22.8
Brace Compactness Ratio (b/t) – Measured	26.1

Specimen Damage State

Test Event	Axial Brace Deformation (in.)	Target Displacement Cycle (in.)	Force (kips)	$P / P_{(y/c)}$
Peak Tension Load	1.25	1.25 (T1)	364	1.07 (Y)
B1: Initial Global Buckling	-0.19	0.375 (C1)	-180	0.83 (C)
B2: Moderate Global Buckling	-0.59	0.75 (C1)	-115	0.53 (C)
B3-C: Local Cupping	-1.19	1.25 (C1)	-47	0.22 (C)
B3-T: Striations & Tearing	0.98	1.25 (T2)	348	1.03 (Y)
B4-T: 50% Tearing	1.25	1.75 (T1)	280	0.82 (Y)

Key Observations

Cycle #	Target Displacement (in.)	Observations
7-8	0.5	Large bolt slip T1 cycle – North gusset plate
9-10	0.625	Small bolt slip T1 cycle – South gusset plate
11-12	0.75	Small bolt slip T1 cycle – South gusset plate
13-14	1.25	Small bolt slip T1 cycle – South gusset plate Moderate local cupping (~0.8") at C1 peak 7.75" north of center Major local cupping (~1.1") at C2 peak, OOP disp. = 9.8"
15	1.75	Brace tear >50% T1

Test Results

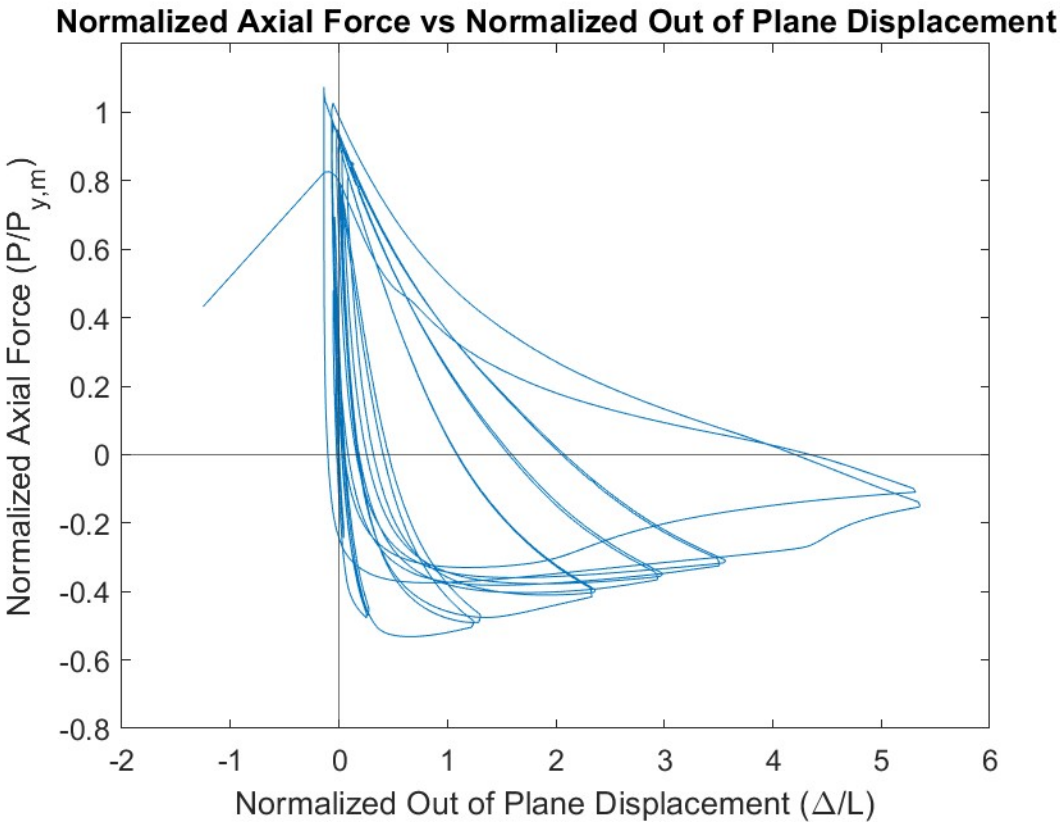

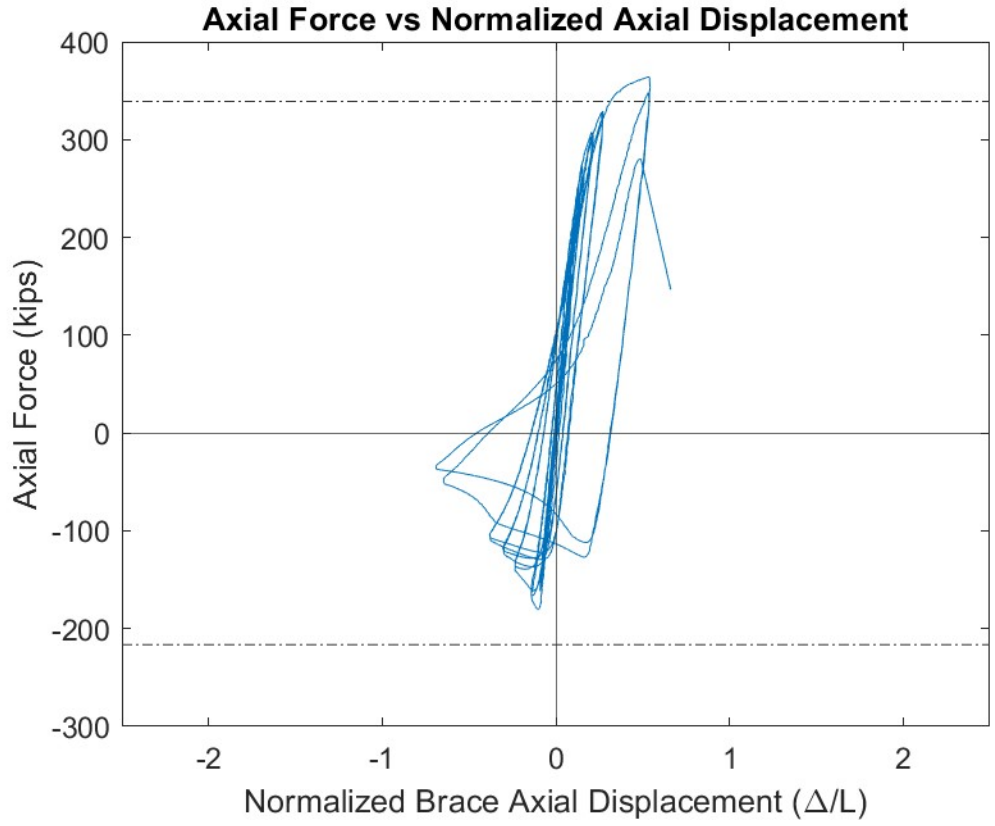

Photos

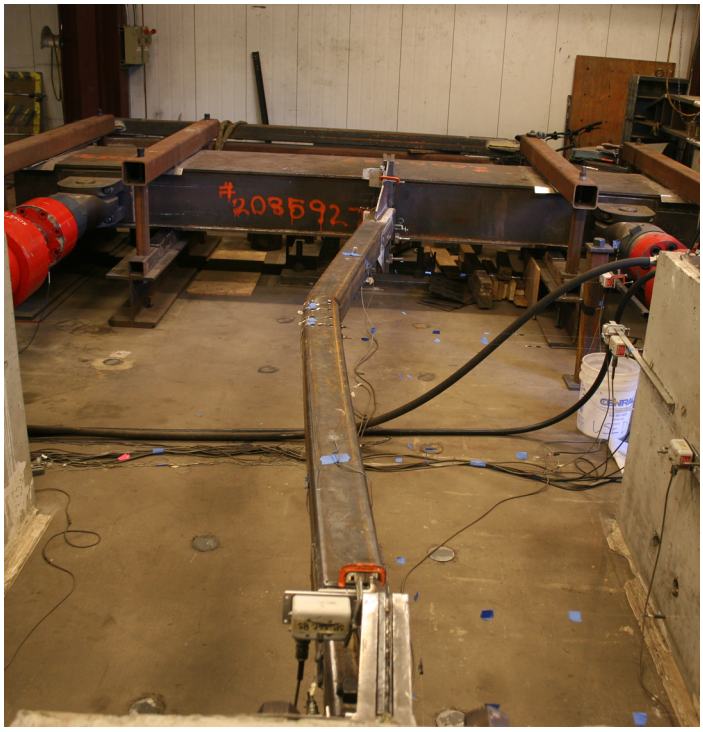

Peak Out of Plane Displacement: 1.25” Cycles

Cupping ~7.75” north of center: 1.25” C1

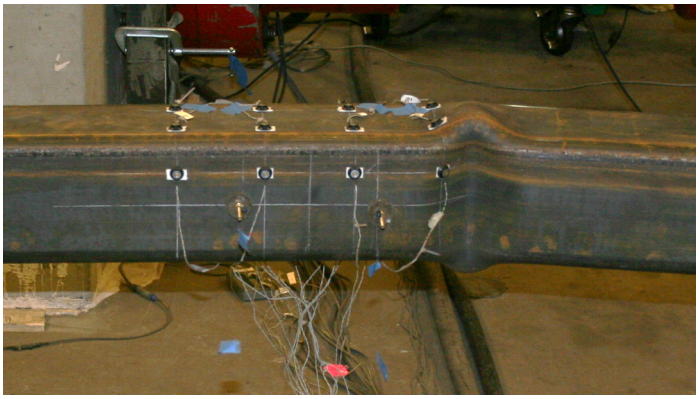

Major Cupping ~7.75” north of center: 1.25” C2

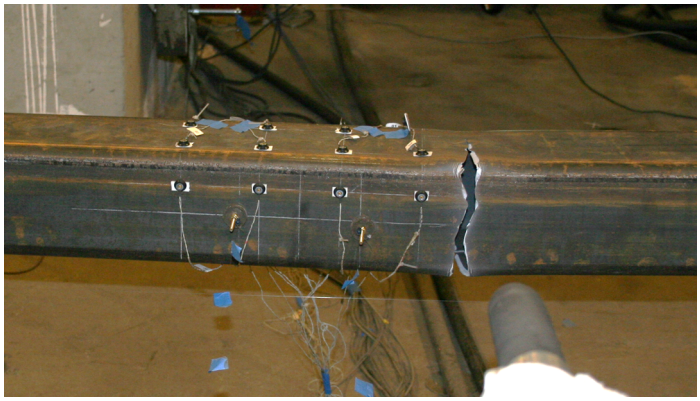

Brace tear >50%: 1.75” T1

AISC Brace Test Summary

Test Name: 7x7x1/4 A500 short
Test Date: 2/8/24

Brace Properties

Measured Yield Stress (ksi)	64.1
Measured Ultimate Stress (ksi)	78.8
Measured Yield Load (kips)	395
Critical Buckling Load (kips)	297
Percent Elongation – 2" (%)	30.3
Brace Length (in.)	183.5
Global Slenderness Ratio (L_c/r)	66.7

Area (in^2)	6.17
Moment of Inertia (in^4)	46.5
Thickness – Nominal (in.)	0.233
Thickness – Measured (in.)	0.232
Brace Compactness Ratio (b/t) – Nominal	27.0
Brace Compactness Ratio (b/t) – Measured	30.3

Specimen Damage State

Test Event	Axial Brace Deformation (in.)	Target Displacement Cycle (in.)	Force (kips)	$P / P_{(y/c)}$
Peak Tension Load	0.42	0.75 (T1)	357	0.90 (Y)
B1: Initial Global Buckling	-0.22	0.375 (C1)	-244	0.82 (C)
B3-C: Local Cupping	-0.60	0.625 (C1)	-97	0.33 (C)
B3-T: Striations & Tearing	0.37	1.25 (T1)	271	0.68 (Y)
B4-T: 50% Tearing	0.94	1.25 (T1)	147	0.37 (Y)

* Moderate Global Buckling did not occur during this test

Key Observations

Cycle #	Target Displacement (in.)	Observations
5-6	0.375	Bolt slip T1 and T2 cycle – North gusset plate
7-8	0.5	Large Bolt slip T1 and T2 cycle – North gusset plate
9-10	0.625	Minor local cupping (~0.6") at C1 peak ~3" north of center After first full cycle, T_C2 moved 3 inches north of center Moderate local cupping (~0.9") at C2 peak
11-12	0.75	Moderate local cupping (~1") at C1 peak Major local cupping (~1.25") at C2 peak, OOP disp. = 6.2"
13-14	1.25	Brace tear >50% T1

Test Results

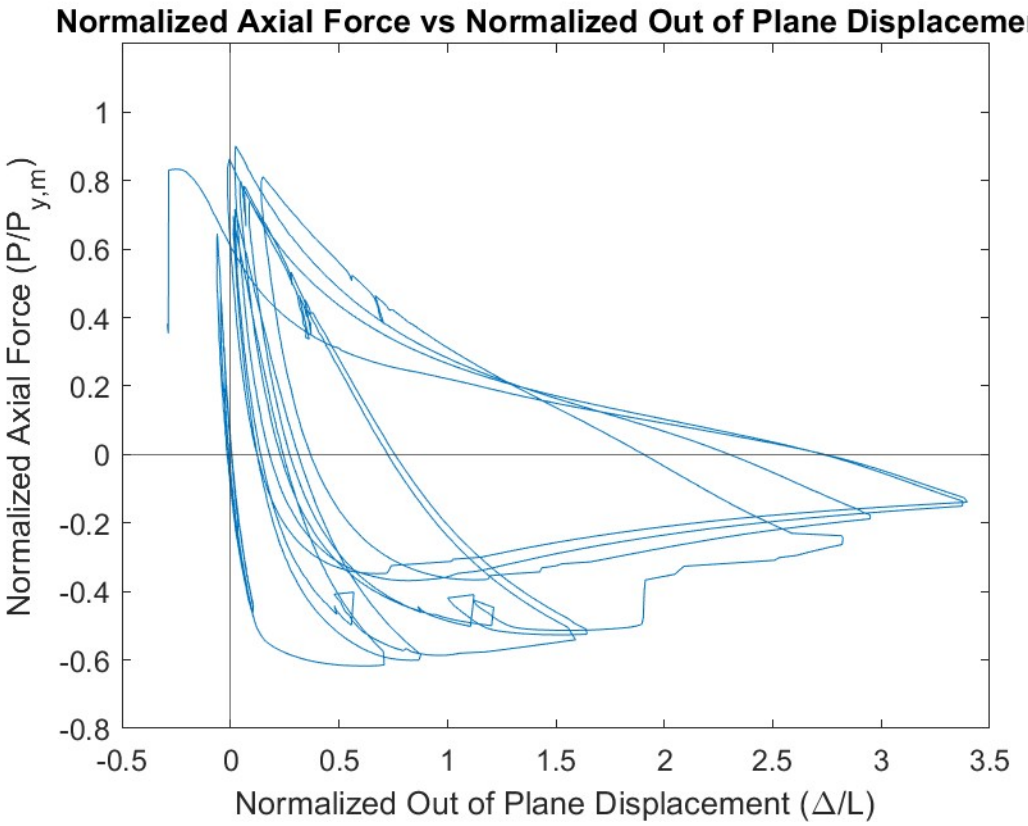

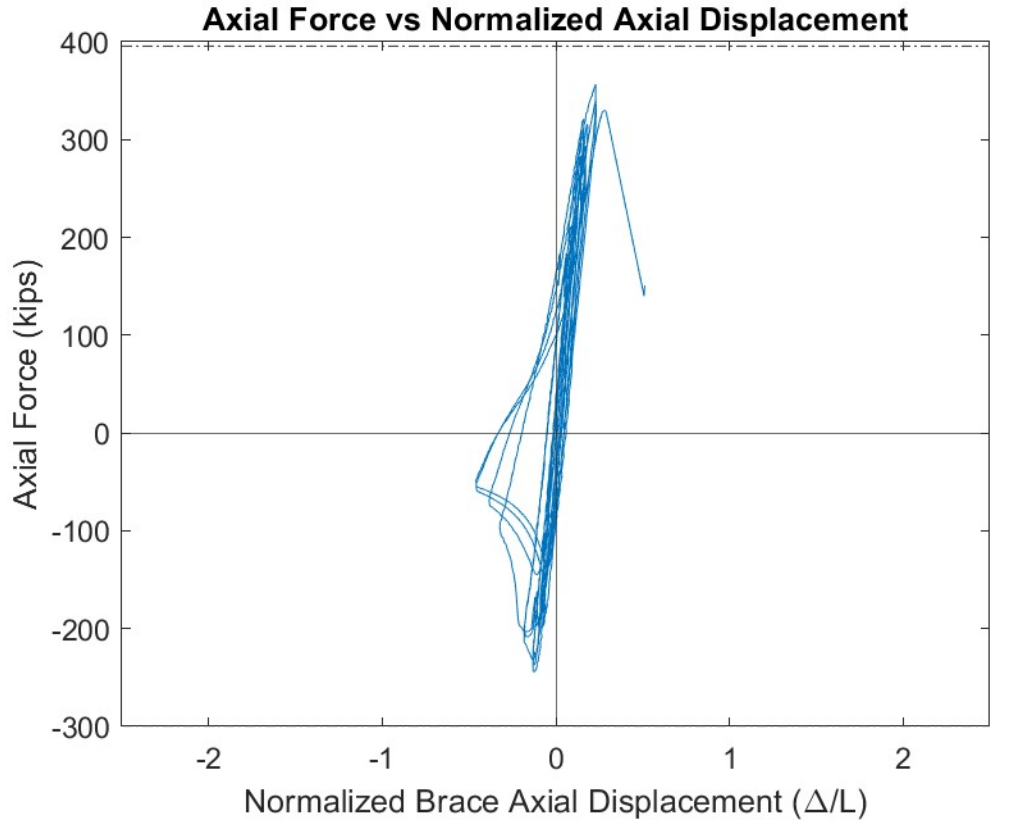

Photos

Peak Out of Plane Displacement: 0.75” Cycles

Minor Cupping ~3.5” north of center: 0.625” C1

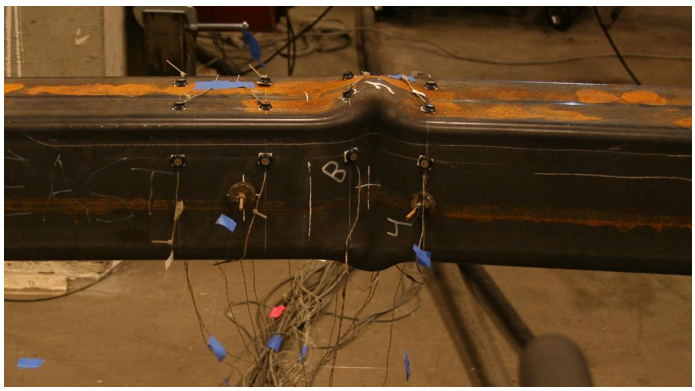

Major Cupping ~3.5” north of center: 0.75” C2

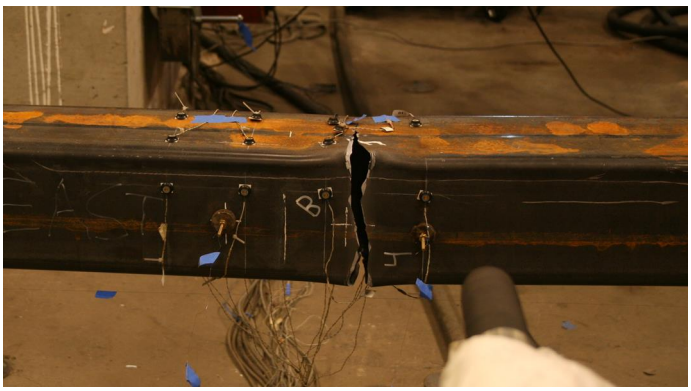

Brace tear >50%: 1.25” T1

AISC Brace Test Summary

Test Name: 8x8x5/16 A500 short
Test Date: 2/2/24

Brace Properties

Measured Yield Stress (ksi)	64.3
Measured Ultimate Stress (ksi)	75.8
Measured Yield Load (kips)	563
Critical Buckling Load (kips)	465
Percent Elongation – 2" (%)	34.2
Brace Length (in.)	183.5
Global Slenderness Ratio (L_c/r)	58.6

Area (in^2)	8.76
Moment of Inertia (in^4)	85.6
Thickness – Nominal (in.)	0.291
Thickness – Measured (in.)	0.287
Brace Compactness Ratio (b/t) – Nominal	24.5
Brace Compactness Ratio (b/t) – Measured	27.9

Specimen Damage State

Test Event	Axial Brace Deformation (in.)	Target Displacement Cycle (in.)	Force (kips)	$P / P_{(y/c)}$
Peak Tension Load	0.72	1.25 (T1)	579	1.03 (Y)
B1: Initial Global Buckling	-0.36	0.50 (C1)	-379	0.82 (C)
B2: Moderate Global Buckling	-0.86	1.25 (C1)	-92	0.20 (C)
B3-C: Local Cupping	-0.60	0.75 (C1)	-291	0.63 (C)
B3-T: Striations & Tearing	0.40	1.25 (T2)	287	0.51 (Y)
B4-T: 50% Tearing	0.65	1.25 (T2)	446	0.79 (Y)

Key Observations

Cycle #	Target Displacement (in.)	Observations
7-8	0.5	Large Bolt slip T1 and T2 cycle – North gusset plate
9-10	0.625	Bolt slip T1 and T2 cycle – North and South gusset plate
11-12	0.75	Large Bolt slip T1 cycle – North gusset plate Minor local cupping (~0.4") at C1 peak ~4" north of center Moderate local cupping (~1") at C2 peak
13-14	1.25	Bolt slip T1 cycle – North gusset plate Major local cupping (~1.5") at C1, OOP disp. = 8.8" Brace tear >50% T2

Test Results

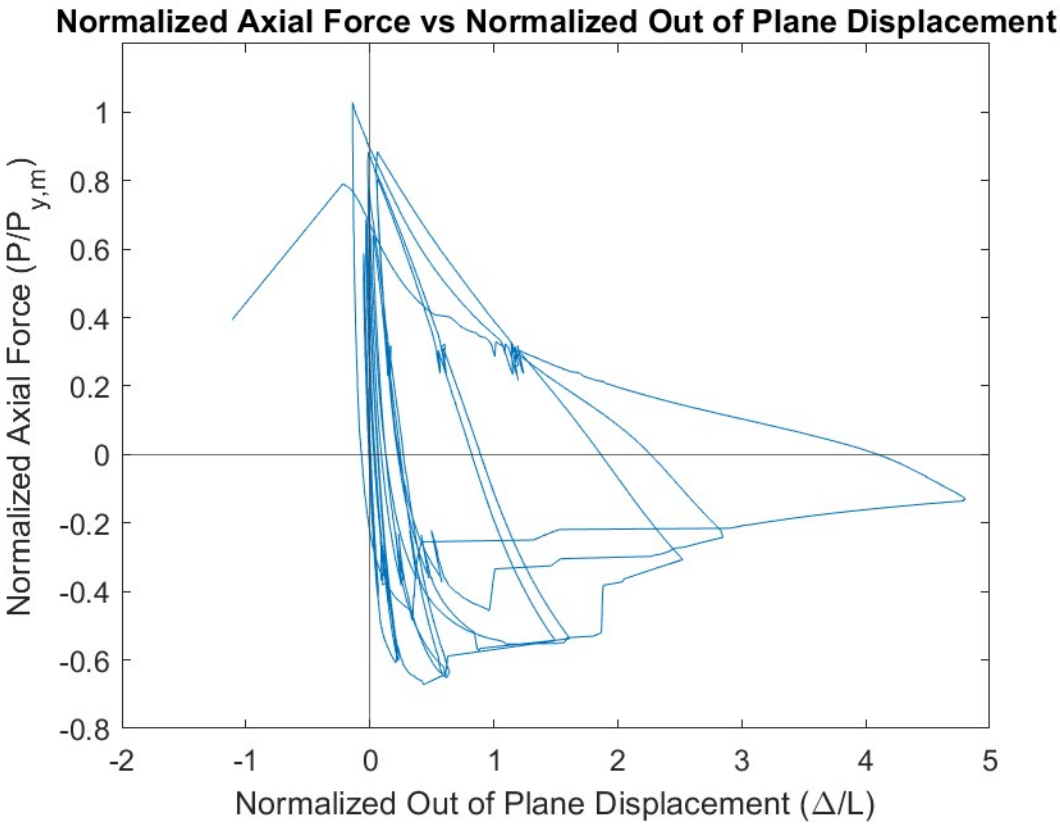

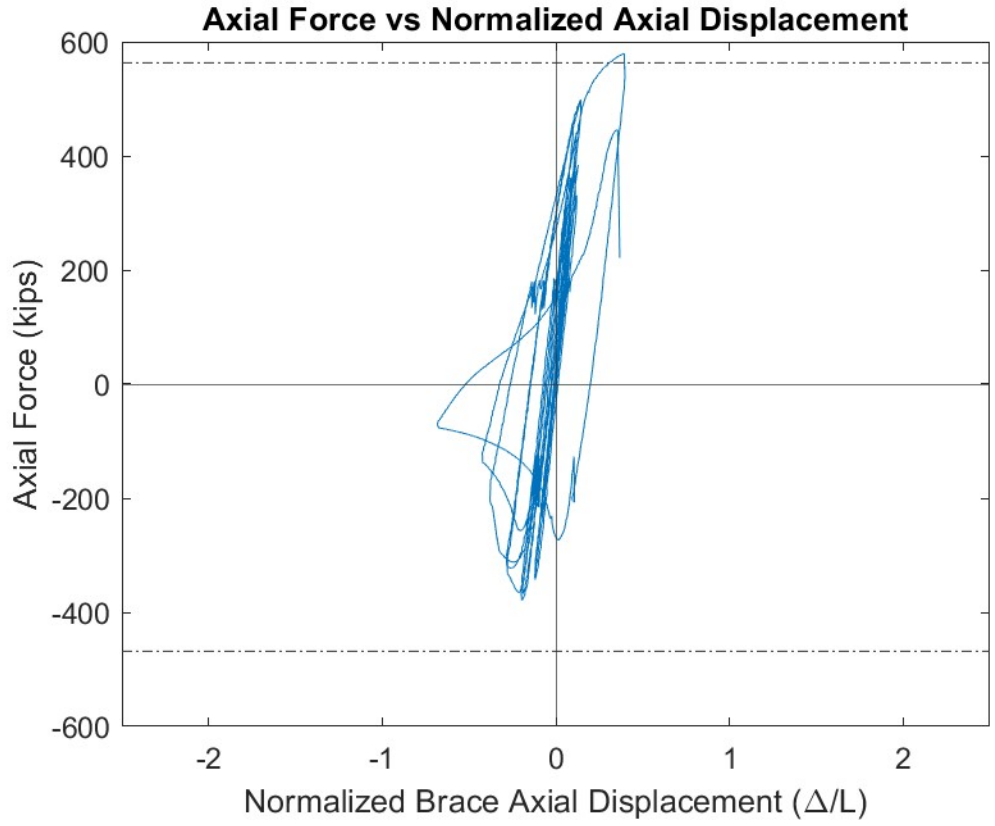

Photos

Peak Out of Plane Displacement: 1.25” Cycles

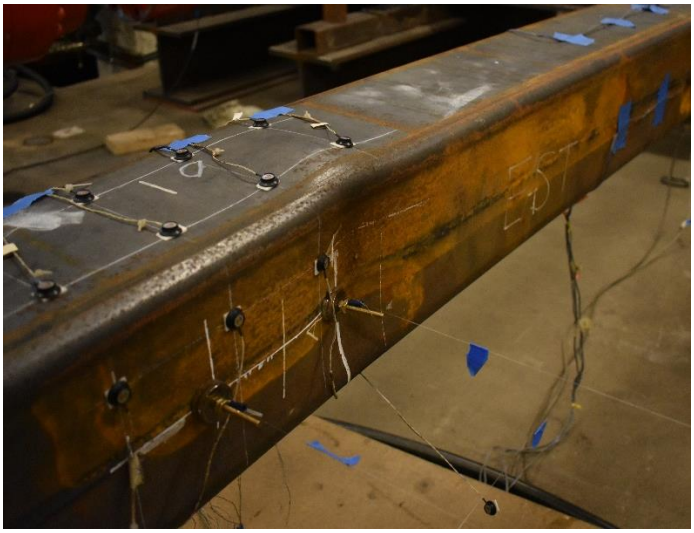

Minor Cupping ~4” north of center: 0.75” C1

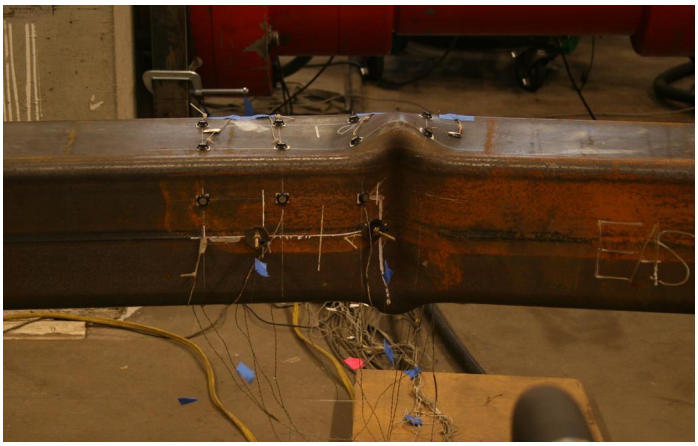

Major Cupping ~4” north of center: 1.25” C1

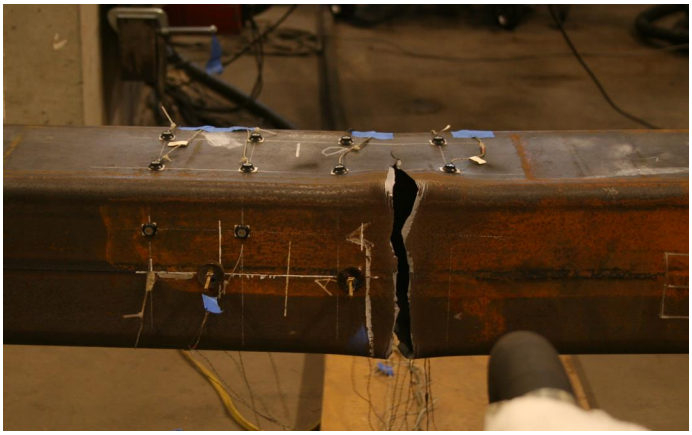

Brace tear >50%: 1.25” T2

AISC Brace Test Summary

Test Name: 6x3/16 A500 short
Test Date: 3/27/24

Brace Properties

Measured Yield Stress (ksi)	53.6
Measured Ultimate Stress (ksi)	73.4
Measured Yield Load (kips)	189
Critical Buckling Load (kips)	104
Percent Elongation – 2" (%)	33.2
Brace Length (in.)	183.5
Global Slenderness Ratio (L_c/r)	89.1

Area (in^2)	3.18
Moment of Inertia (in^4)	13.5
Thickness – Nominal (in.)	0.174
Thickness – Measured (in.)	0.195
Brace Compactness Ratio (b/t) – Nominal	34.5
Brace Compactness Ratio (b/t) – Measured	30.8

Specimen Damage State

Test Event	Axial Brace Deformation (in.)	Target Displacement Cycle (in.)	Force (kips)	$P / P_{(y/c)}$
Peak Tension Load	2.17	2.25 (T1)	186	0.98 (Y)
B1: Initial Global Buckling	-0.13	0.25 (C1)	-74	0.71 (C)
B2: Moderate Global Buckling	-0.48	0.625 (C1)	-47	0.45 (C)
B3-C: Local Cupping	-1.53	1.75 (C2)	-13	0.13 (C)
B3-T: Striations & Tearing	2.23	2.75 (T1)	148	0.78 (Y)
B4-T: 50% Tearing	2.48	2.75 (T1)	100	0.53 (Y)

Key Observations

Cycle #	Target Displacement (in.)	Observations
15-16	1.75	Minor local cupping (~0.5") at C2 peak
17-18	2.25	Major local cupping (~1.3") at C1 peak Major local cupping (~1.4") at C2 peak. OOP disp. = 18.0"
19	2.75	Brace tear >50% T1

Test Results

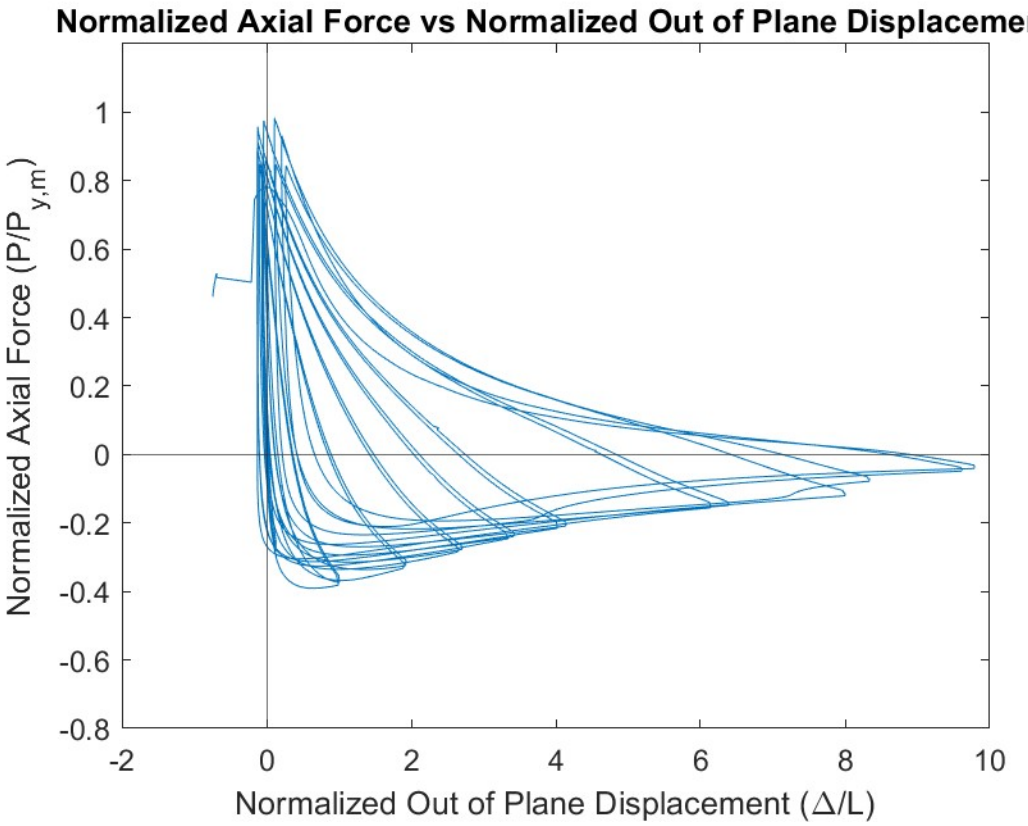

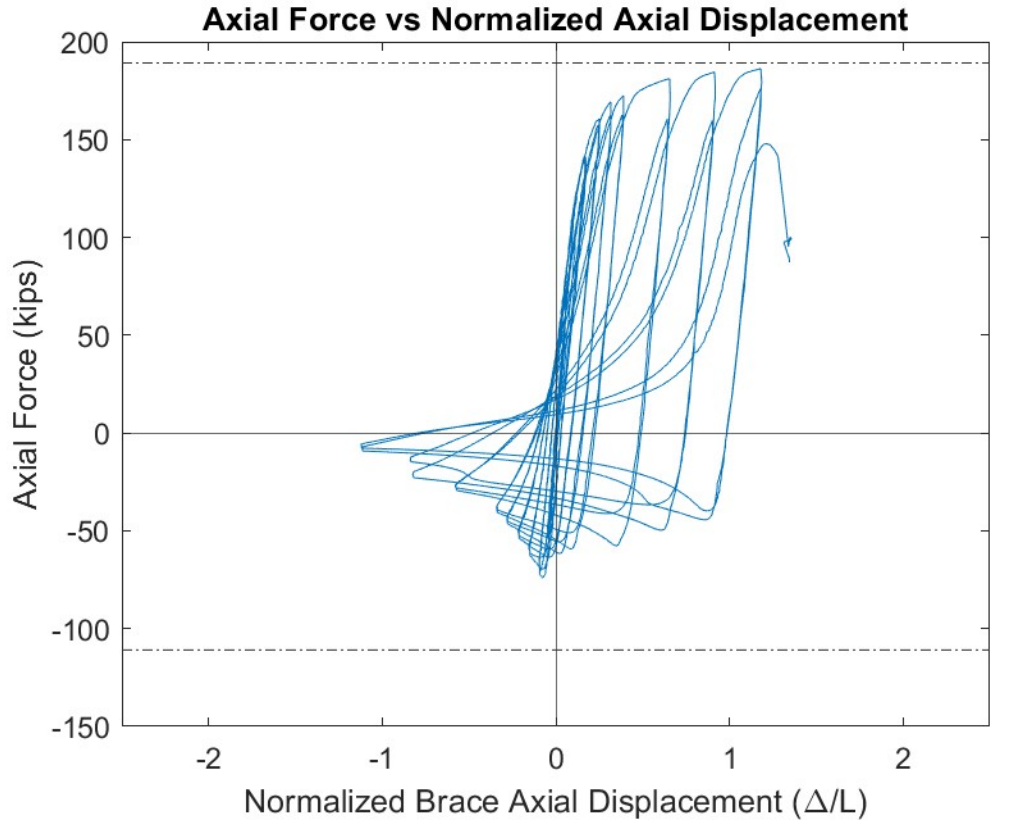

Photos

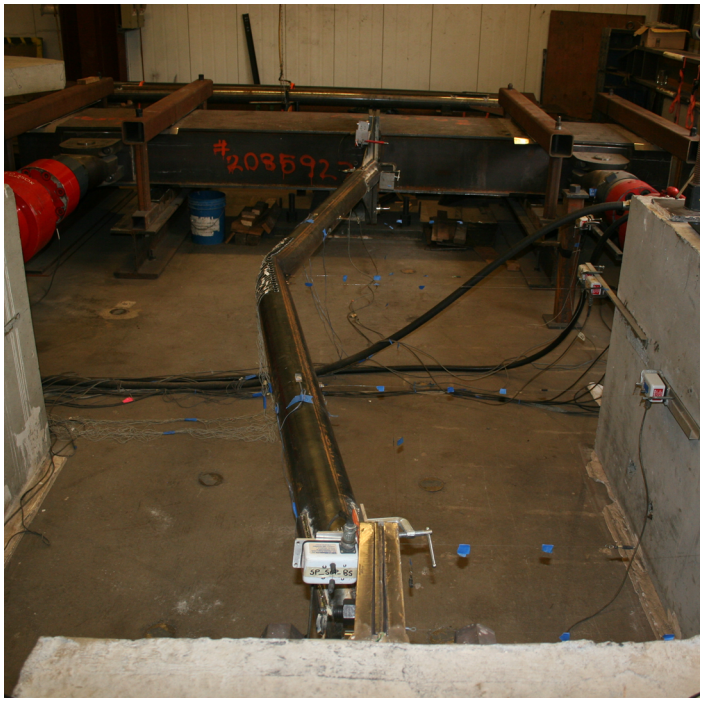

Peak Out of Plane Displacement: 2.25” Cycles

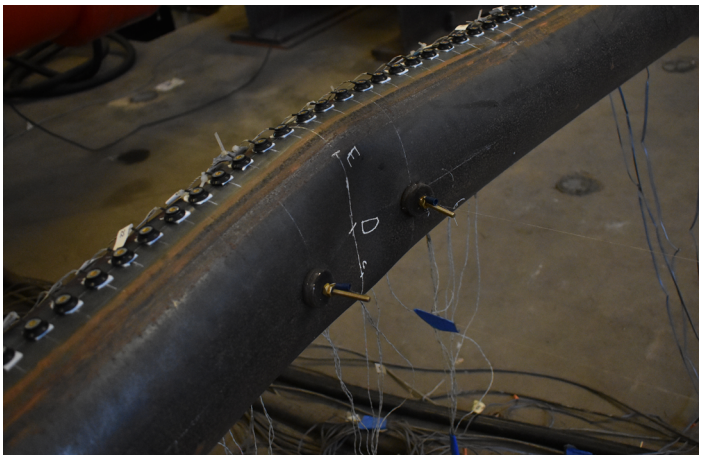

Minor cupping: 1.75” C2 cycle

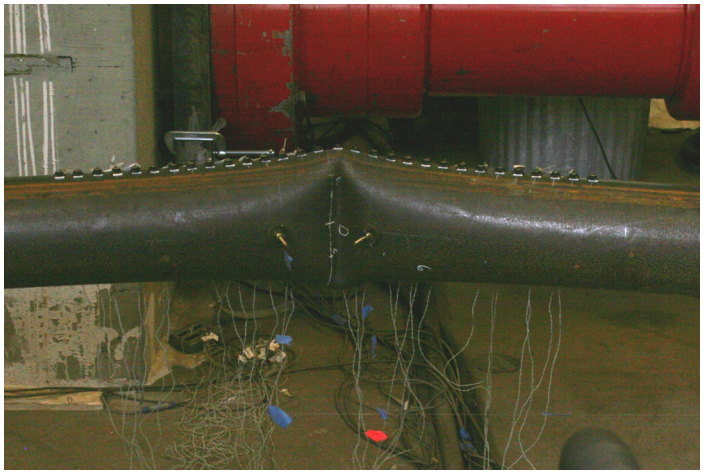

Major Cupping: 2.25” C2 cycle

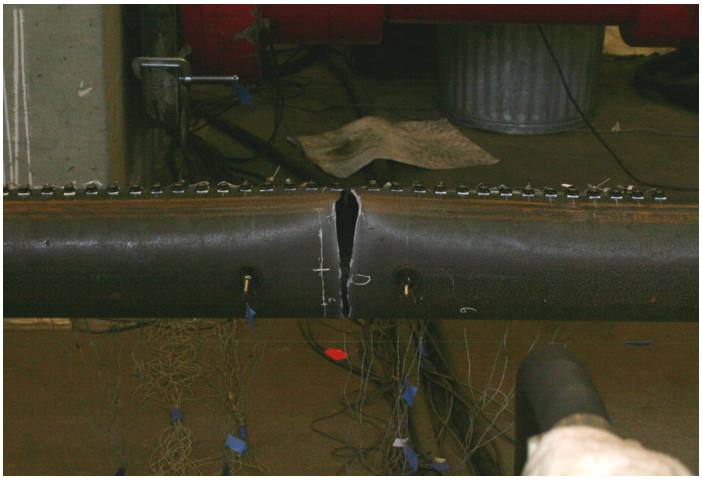

Brace tear >50%: 2.75” T1 cycle

AISC Brace Test Summary

Test Name: 6x1/4 A500 short
Test Date: 3/29/24

Brace Properties

Measured Yield Stress (ksi)	54.2
Measured Ultimate Stress (ksi)	71.6
Measured Yield Load (kips)	229
Critical Buckling Load (kips)	137
Percent Elongation – 2" (%)	40.5
Brace Length (in.)	183.5
Global Slenderness Ratio (L_c/r)	90.0

Area (in^2)	4.22
Moment of Inertia (in^4)	17.6
Thickness – Nominal (in.)	0.233
Thickness – Measured (in.)	0.245
Brace Compactness Ratio (b/t) – Nominal	25.8
Brace Compactness Ratio (b/t) – Measured	24.5

Specimen Damage State

Test Event	Axial Brace Deformation (in.)	Target Displacement Cycle (in.)	Force (kips)	$P / P_{(y/c)}$
Peak Tension Load	-	3.25 (T1)	241	1.06 (Y)
B1: Initial Global Buckling	-	0.25 (C1)	-92	0.67 (C)
B2: Moderate Global Buckling	-	0.625 (C1)	-60	0.44 (C)
B3-C: Local Cupping	-	2.75 (C2)	-13	0.09 (C)
B3-T: Striations & Tearing	-	3.25 (T2)	227	0.99 (Y)
B4-T: 50% Tearing	-	3.75 (T1)	74	0.32 (Y)

Key Observations

Cycle #	Target Displacement (in.)	Observations
7-8	0.5	Bolt slip T1 cycle – North gusset plate Small bolt slip T2 cycle – South gusset plate
9-10	0.625	Bolt slip T1 cycle – South gusset plate
11-12	0.75	Small bolt slip – T1
13-14	1.25	Direction of buckling switched to East during C1 cycle. Instrumentation adjusted.
19-20	2.75	Minor local cupping at C1 peak Moderate local cupping (~0.8") at C2 peak
21-22	3.25	Major local cupping (~1.3") at C1 peak Striations along west face of brace – T2 Major local cupping (~1.5") at C2 peak, OOP disp. = 20.2"
23	3.75	Brace tear >50% T1

Test Results

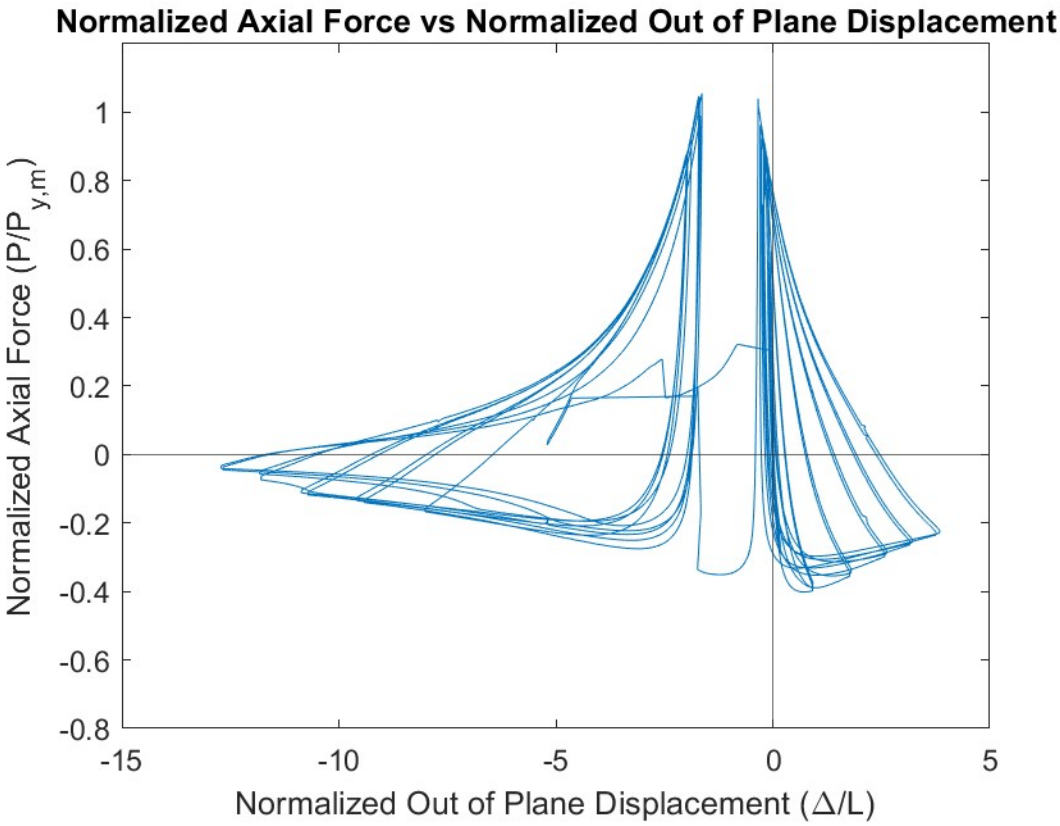

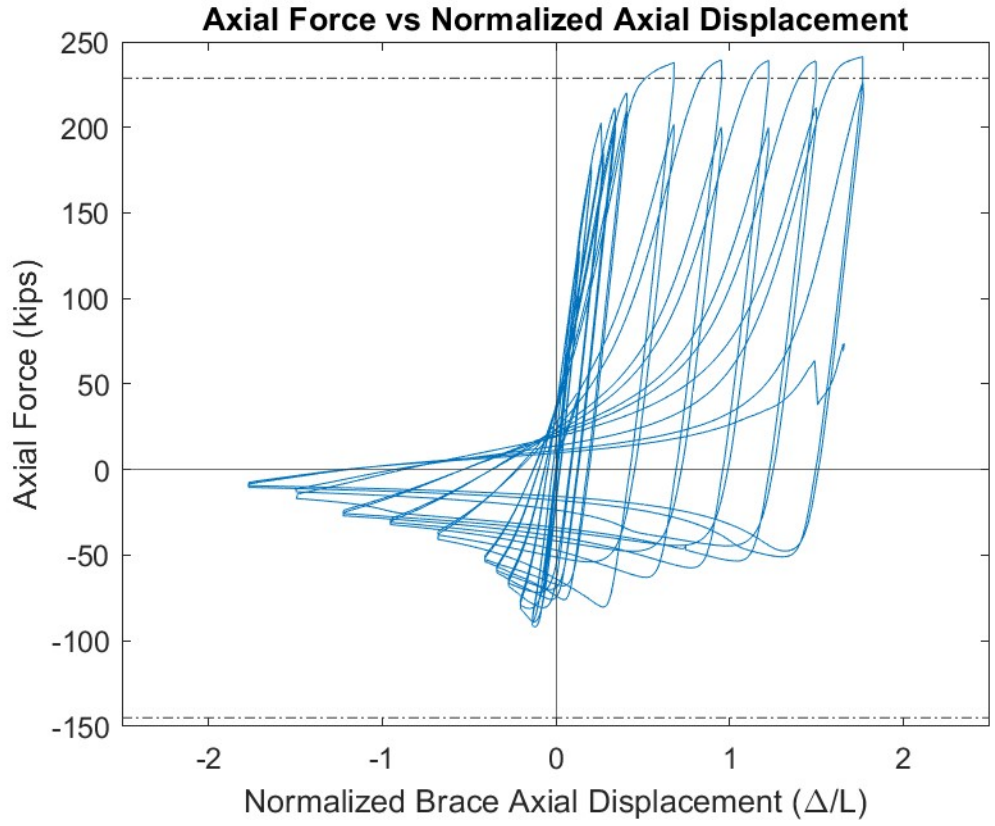

Photos

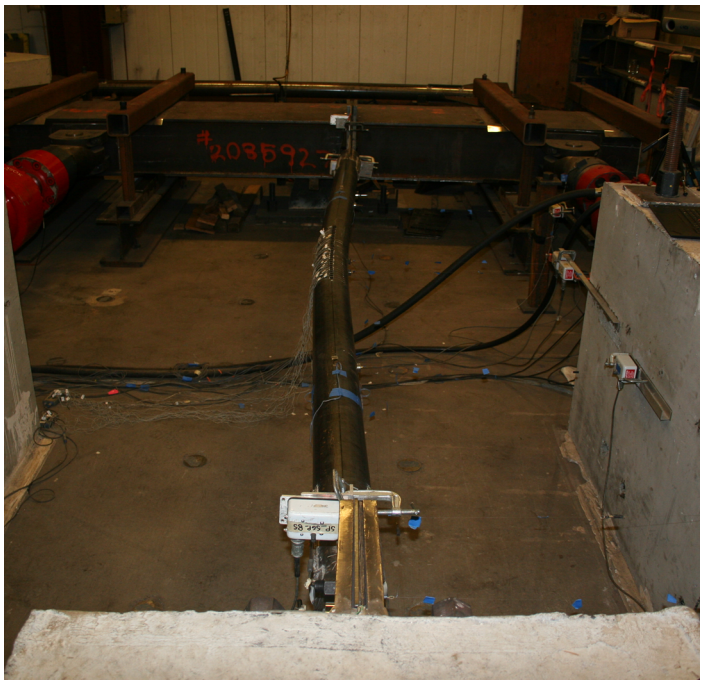

Out of Plane Displacement towards the West before direction of buckling switched: 0.75” Cycles

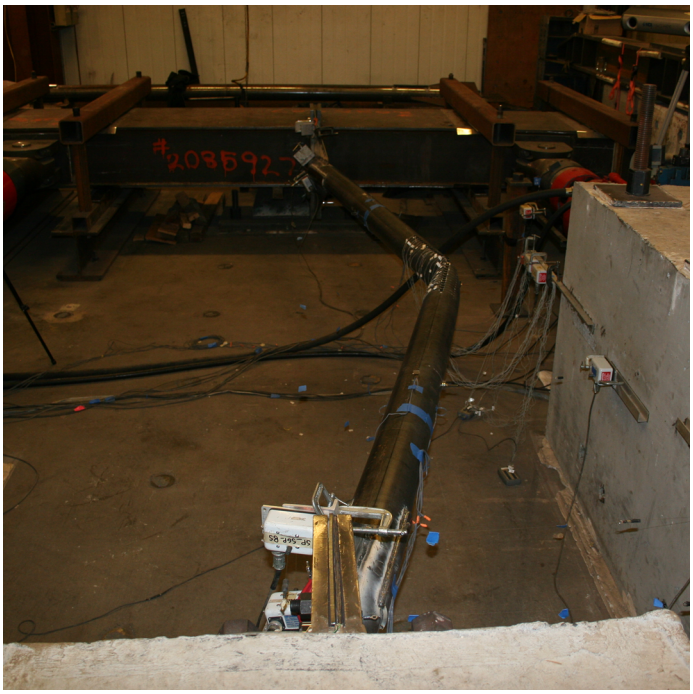

Peak Out of Plane Displacement towards the East: 3.25” Cycles

Major Cupping: 3.25” C2 cycle

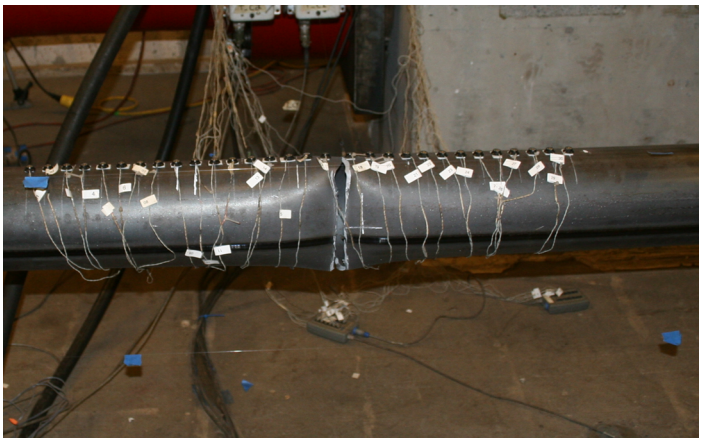

Brace tear >50%: 3.75” T1 cycle

AISC Brace Test Summary

Test Name: 6.625x1/2 A500 short
Test Date: 4/11/24

Brace Properties

Measured Yield Stress (ksi)	63.7
Measured Ultimate Stress (ksi)	66.0
Measured Yield Load (kips)	573
Critical Buckling Load (kips)	338
Percent Elongation – 2" (%)	36.7
Brace Length (in.)	183.5
Global Slenderness Ratio (L_c/r)	84.2

Area (in^2)	9.00
Moment of Inertia (in^4)	42.9
Thickness – Nominal (in.)	0.465
Thickness – Measured (in.)	0.473
Brace Compactness Ratio (b/t) – Nominal	14.2
Brace Compactness Ratio (b/t) – Measured	14.1

Specimen Damage State

Test Event	Axial Brace Deformation (in.)	Target Displacement Cycle (in.)	Force (kips)	$P / P_{(y/c)}$
Peak Tension Load	0.81	1.25 (T1)	550	0.96 (Y)
B1: Initial Global Buckling	-0.21	0.50 (C1)	-296	0.88 (C)
B2: Moderate Global Buckling	-0.76	0.75 (C1)	-167	0.49 (C)
B3-C: Local Cupping	-3.05	3.25 (C2)	-48	0.14 (C)
B3-T: Striations & Tearing	3.78	4.25 (T1)	458	0.80 (Y)
B4-T: 50% Tearing	3.95	4.25 (T2)	200	0.34 (Y)

Key Observations

Cycle #	Target Displacement (in.)	Observations
3-4	0.25	Bolt slip T1 cycle – North gusset plate Clicking/slipping sounds C1 and C2 cycle – North gusset plate
5-6	0.375	Large bolt slip from T1 to C1 – North gusset plate
7-8	0.5	Bolt slip T1 cycle – South gusset plate Bolt slip T2 cycle – North and South gusset plate
9-10	0.625	Clicking/slipping sounds T1 cycle – North and South gusset plate
21-22	3.25	Minor local cupping (~0.2") at C1 peak Minor local cupping (~0.4") at C2 peak
23-24	3.75	Moderate local cupping (~0.8") at C1 peak Moderate local cupping (~1.1") at C2 peak
25-26	4.25	Striations along east face of brace – T1 Major local cupping (~1.6") at C1 peak, OOP disp. = 25.8" Brace tear >50% T2

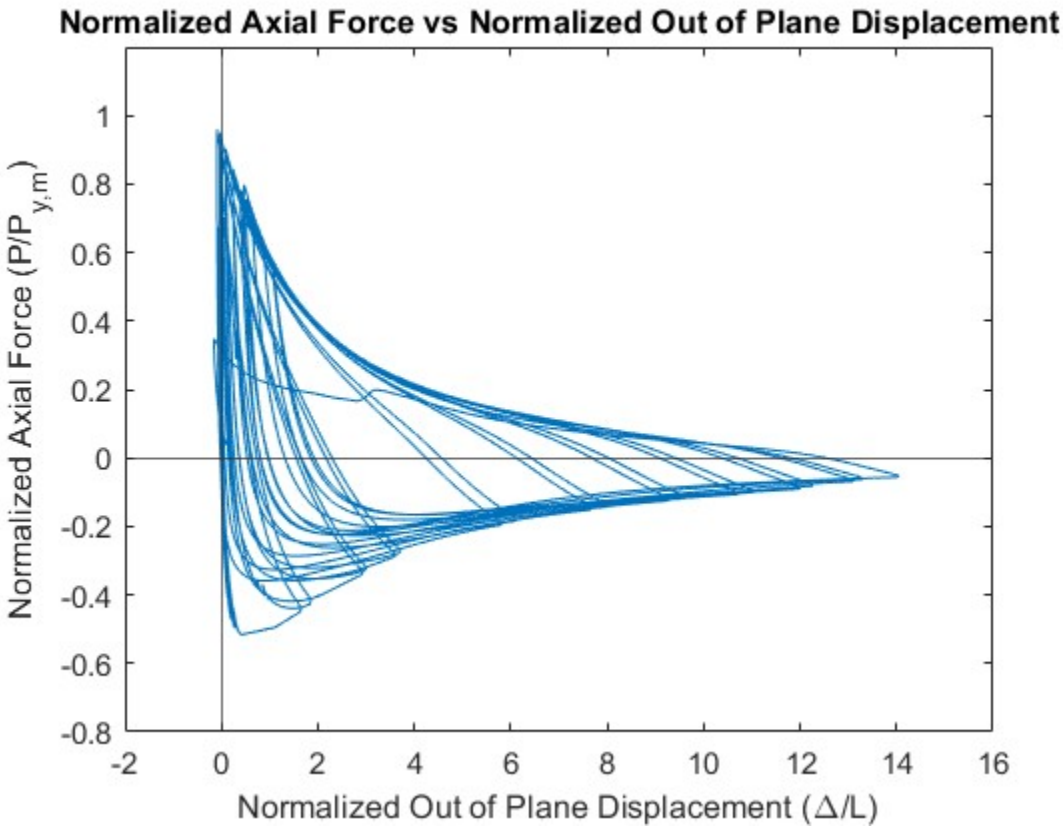
Normalized Axial Force vs Normalized Out of Plane Displacement
Normalized Axial Force (P/P$_{y,m}$)
1
0.8
0.6
0.4
0.2
0
-0.2
-0.4
-0.6
-0.8
-2
0
2
4
6
8
10
12
14
16
Normalized Out of Plane Displacement (Δ/L)

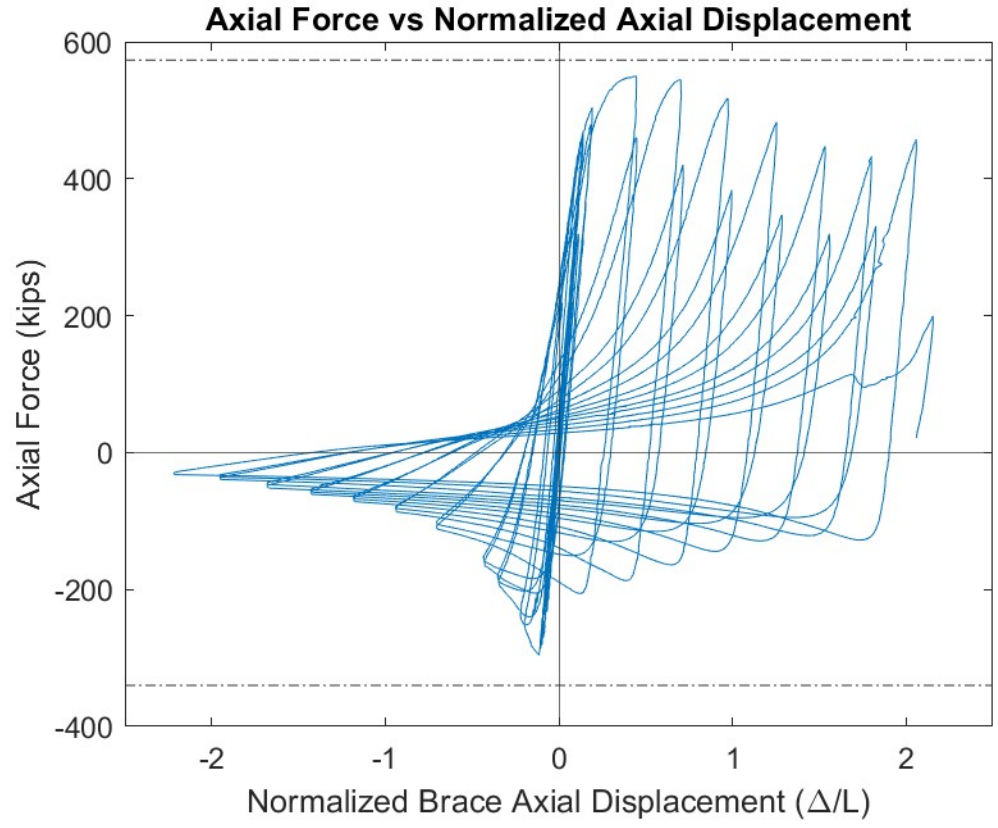
Axial Force vs Normalized Axial Displacement
Axial Force (kips)
600
400
200
0
-200
-400
-2
-1
0
1
2
Normalized Brace Axial Displacement (Δ/L)

Photos

Peak Out of Plane Displacement: 4.25” Cycles

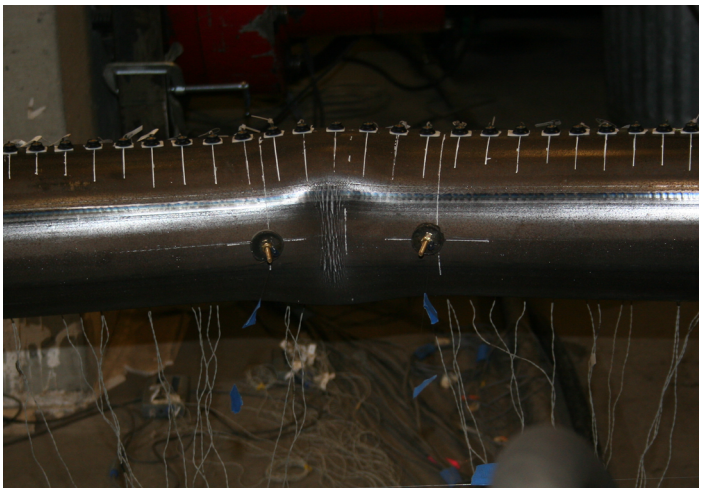

Striations along east face of brace: T1 4.25” cycle

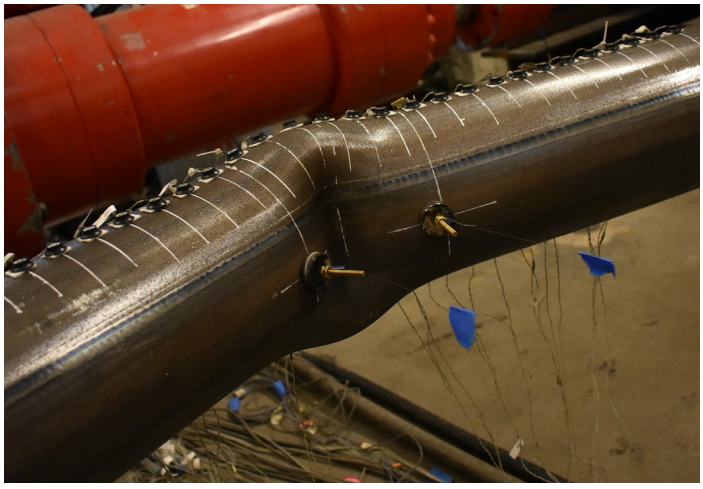

Major Cupping: 4.25” C1 cycle

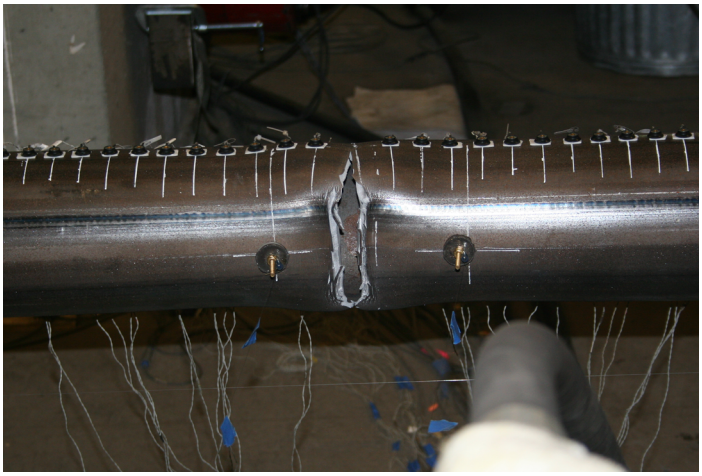

Brace tear >50%: 4.25” T2 cycle

AISC Brace Test Summary

Test Name: 6.625x1/4 A500 short
Test Date: 4/3/24

Brace Properties

Measured Yield Stress (ksi)	59.0
Measured Ultimate Stress (ksi)	74.6
Measured Yield Load (kips)	276
Critical Buckling Load (kips)	178
Percent Elongation – 2" (%)	36.2
Brace Length (in.)	183.5
Global Slenderness Ratio (L_c/r)	90.0

Area (in^2)	4.22
Moment of Inertia (in^4)	17.6
Thickness – Nominal (in.)	0.233
Thickness – Measured (in.)	0.243
Brace Compactness Ratio (b/t) – Nominal	25.8
Brace Compactness Ratio (b/t) – Measured	24.7

Specimen Damage State

Test Event	Axial Brace Deformation (in.)	Target Displacement Cycle (in.)	Force (kips)	$P / P_{(y/c)}$
Peak Tension Load	2.54	2.75 (T1)	284	1.03 (Y)
B1: Initial Global Buckling	-0.13	0.25 (C1)	-131	0.74 (C)
B2: Moderate Global Buckling	-0.61	0.75 (C1)	-76	0.43 (C)
B3-C: Local Cupping	-2.09	2.25 (C1)	-23	0.13 (C)
B3-T: Striations & Tearing	2.54	2.75 (T1)	284	1.03 (Y)
B4-T: 50% Tearing	2.21	3.25 (T1)	48	0.17 (Y)

Key Observations

Cycle #	Target Displacement (in.)	Observations
5-6	0.375	Small bolt slip T1 cycle – South gusset plate
7-8	0.5	Large bolt slip T1 cycle – North gusset plate Bolt slip T1 cycle – South gusset plate
9-10	0.625	Bolt slip T1 cycle – South gusset plate
11-12	0.75	Small bolt slip T1 cycle – South gusset plate
13-14	1.25	Clicking T1 – South gusset plate
17-18	2.25	Moderate local cupping (~0.6") at C1 peak Major local cupping (~1.2") at C2 peak
19-20	2.75	Major local cupping (~1.6") at C1 peak Striations along east face of brace - T2 Major local cupping (~1.7") at C2 peak, OOP disp. = 20.0"
21	3.25	Brace tear >50% T1

Test Results

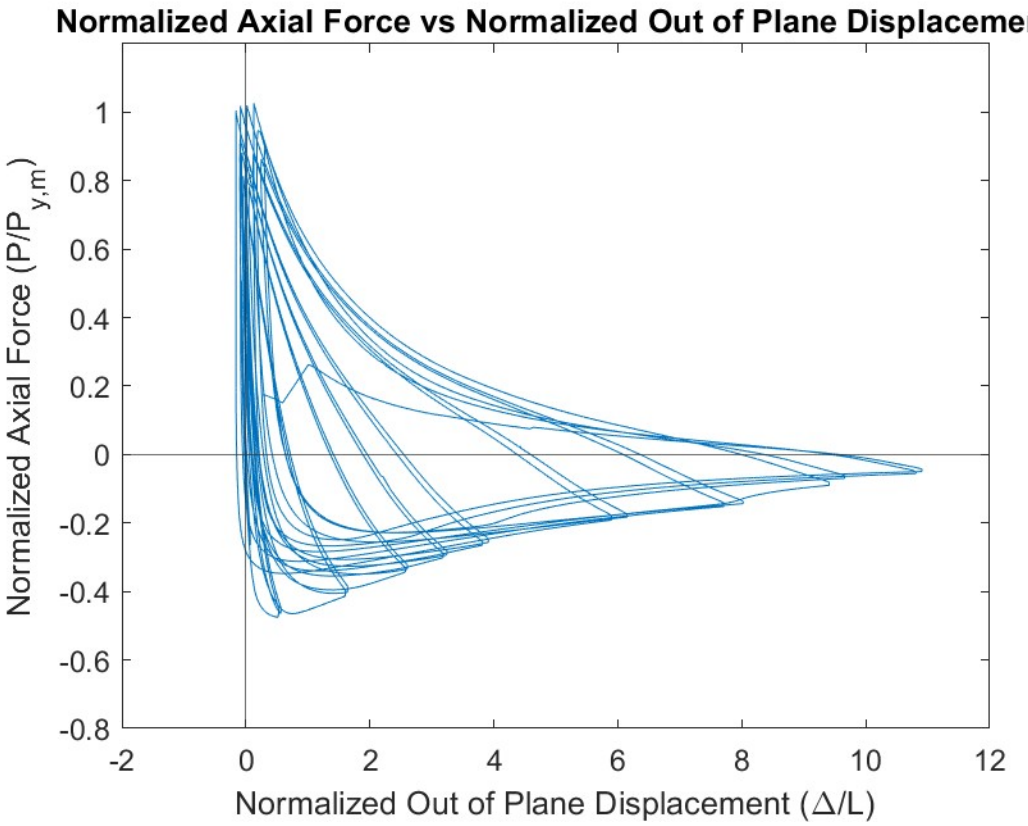

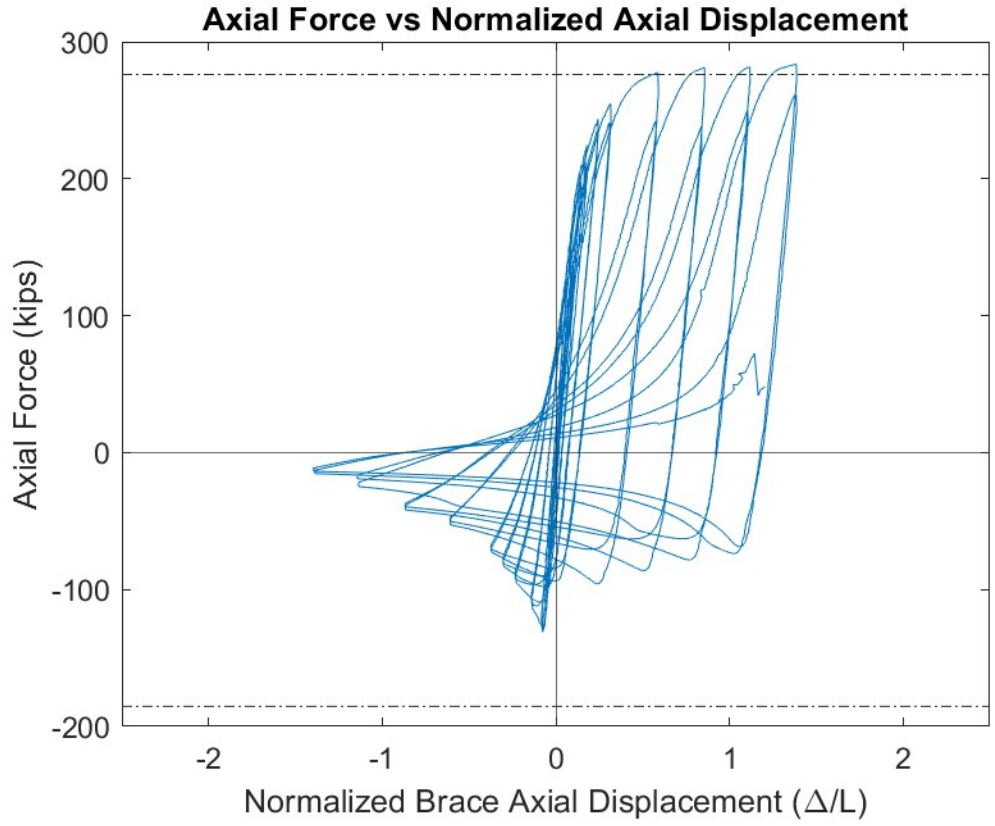

Photos

Peak Out of Plane Displacement: 2.75” Cycles

Striations along east face of brace: T2 2.75” cycle

Major Cupping: 2.75” C2 cycle

Brace tear >50%: 3.25” T1 cycle

AISC Brace Test Summary

Test Name: 6.625x3/8 A500 short
Test Date: 4/8/24

Brace Properties

Measured Yield Stress (ksi)	58.3
Measured Ultimate Stress (ksi)	63.7
Measured Yield Load (kips)	401
Critical Buckling Load (kips)	255
Percent Elongation – 2" (%)	-
Brace Length (in.)	183.5
Global Slenderness Ratio (L_c/r)	82.7

Area (in^2)	6.88
Moment of Inertia (in^4)	34.0
Thickness – Nominal (in.)	0.349
Thickness – Measured (in.)	0.353
Brace Compactness Ratio (b/t) – Nominal	19.0
Brace Compactness Ratio (b/t) – Measured	18.8

Specimen Damage State

Test Event	Axial Brace Deformation (in.)	Target Displacement Cycle (in.)	Force (kips)	$P / P_{(y/c)}$
Peak Tension Load	1.47	2.25 (T1)	413	1.03 (Y)
B1: Initial Global Buckling	-0.18	0.375 (C1)	-197	0.77 (C)
B2: Moderate Global Buckling	-0.75	0.75 (C1)	-112	0.44 (C)
B3-C: Local Cupping	-2.23	2.25 (C2)	-36	0.14 (C)
B3-T: Striations & Tearing	2.93	3.25 (T1)	403	1.00 (Y)
B4-T: 50% Tearing	3.15	3.25 (T2)	194	0.48 (Y)

Key Observations

Cycle #	Target Displacement (in.)	Observations
5-6	0.375	Bolt slip T2 cycle – South gusset plate
7-8	0.5	Bolt slip T1 cycle – South gusset plate
9-10	0.625	3 small clicks during T2 cycle – South gusset plate
11-12	0.75	Small bolt slip T1 cycle – South gusset plate
13-14	1.25	Very large bolt slip T1 – South gusset plate. Multiple optotrak sensors came off but were put back on after the cycle went back down to 0 actuator displacement.
15-16	1.75	Small bolt slip T1 cycle – North gusset plate
17-18	2.25	Minor local cupping (~0.5") at C2 peak
19-20	2.75	Major local cupping (~1.1") at C1 peak Major local cupping (~1.5") at C2 peak
21	3.25	Striations along east face of brace – T1 Major local cupping (~1.7") at C1 peak, OOP disp. = 21.8" Brace tear >50% T2

Test Results

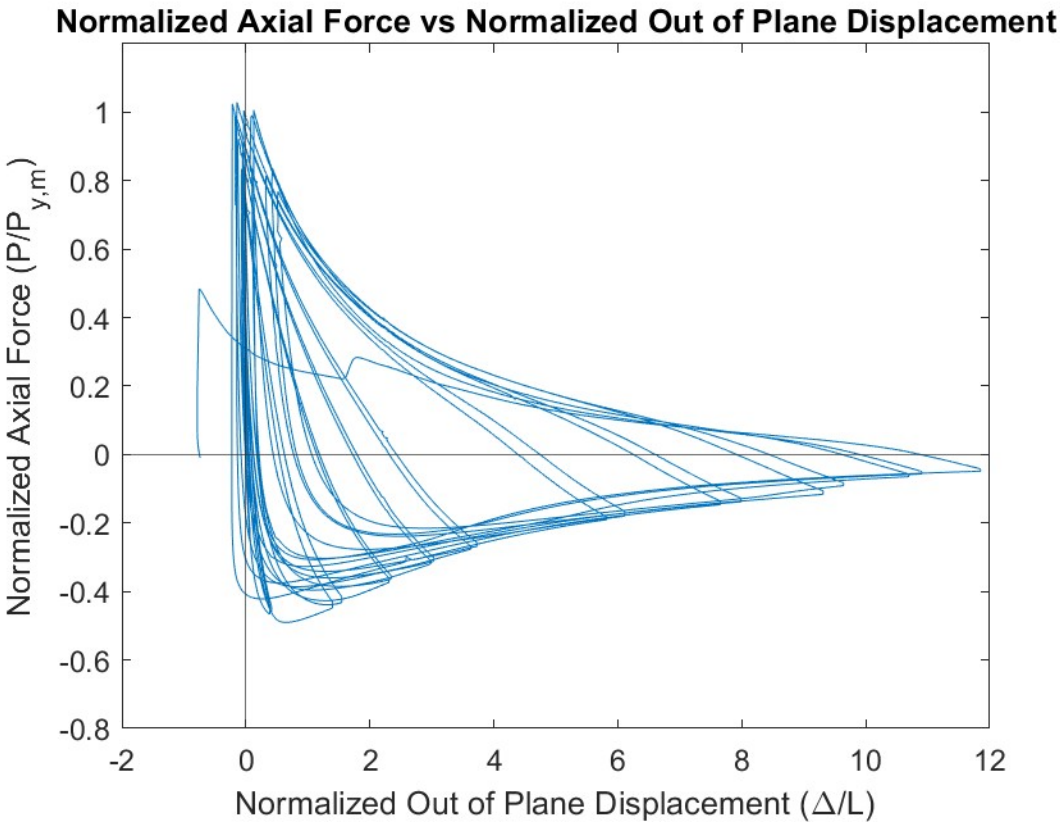

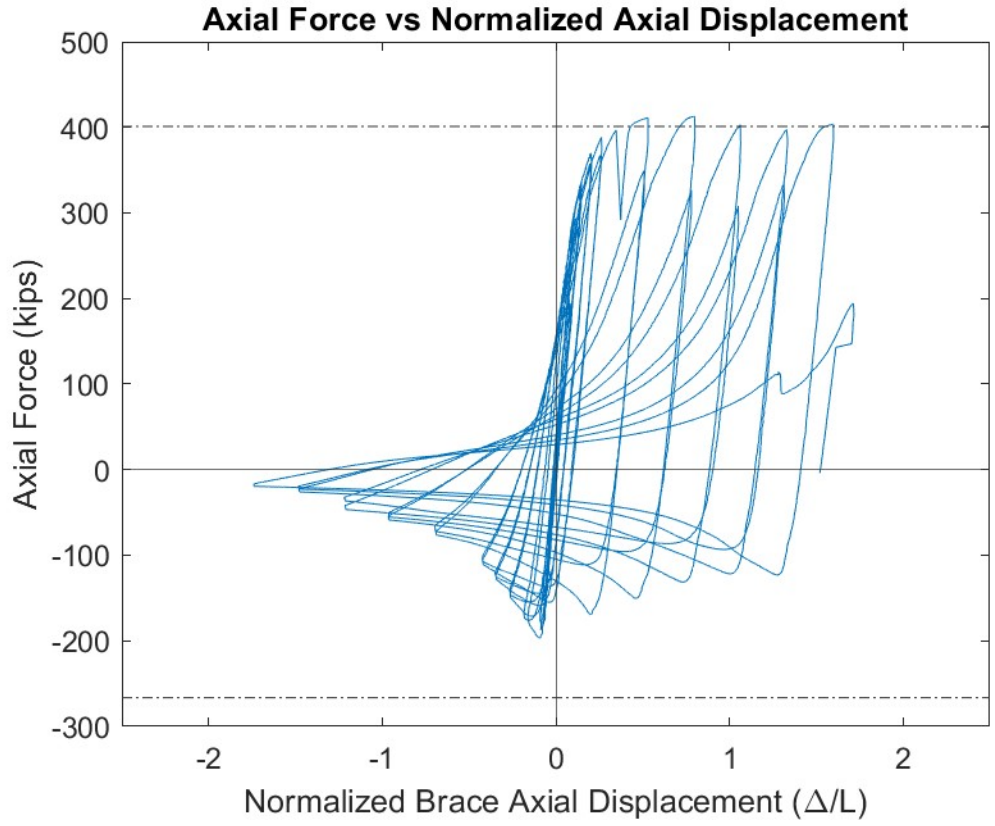

Photos

Peak Out of Plane Displacement: 3.25” Cycles

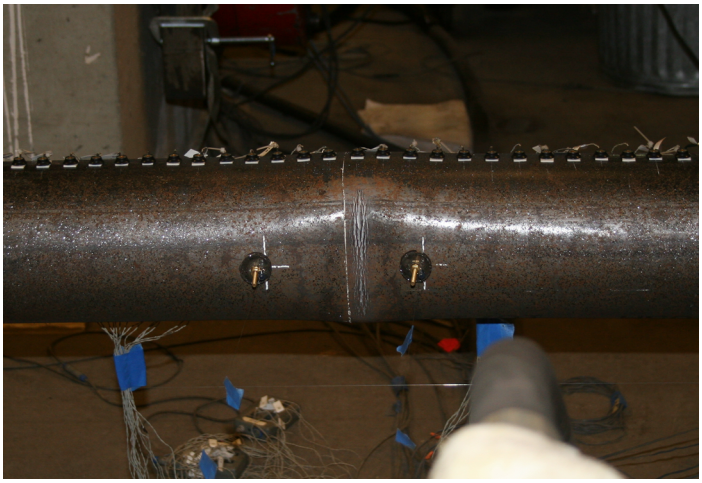

Striations along east face of brace: T1 3.25” cycle

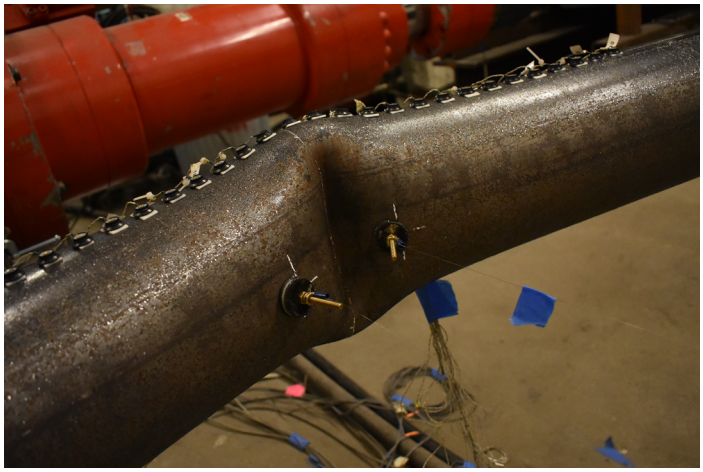

Major Cupping: 3.25” C1 cycle

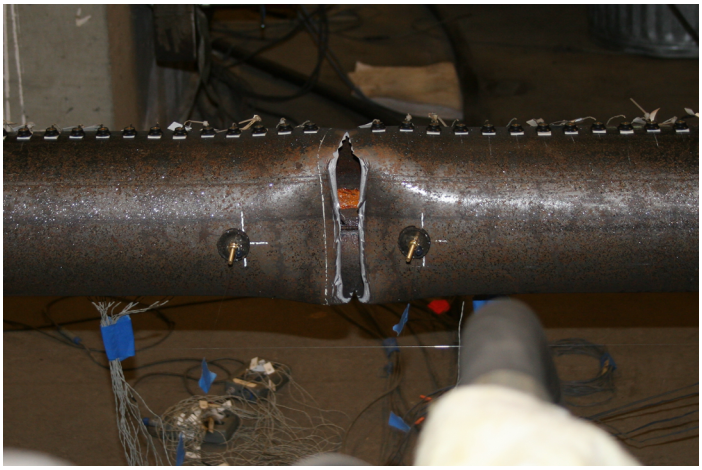

Brace tear >50%: 3.25” T2 cycle

AISC Brace Test Summary

Test Name: 8.625x1/4 A500 short
Test Date: 5/13/24

Brace Properties

Measured Yield Stress (ksi)	67.0
Measured Ultimate Stress (ksi)	79.5
Measured Yield Load (kips)	411
Critical Buckling Load (kips)	323
Percent Elongation – 2" (%)	30.3
Brace Length (in.)	183.5
Global Slenderness Ratio (L_c/r)	61.8

Area (in^2)	6.14
Moment of Inertia (in^4)	54.1
Thickness – Nominal (in.)	0.233
Thickness – Measured (in.)	0.243
Brace Compactness Ratio (b/t) – Nominal	37.0
Brace Compactness Ratio (b/t) – Measured	37.1

Specimen Damage State

Test Event	Axial Brace Deformation (in.)	Target Displacement Cycle (in.)	Force (kips)	P / P_y
Peak Tension Load	1.78	2.25 (T1)	426	1.03 (Y)
B1: Initial Global Buckling	-0.34	0.625 (C1)	-268	0.83 (C)
B2: Moderate Global Buckling	-0.81	1.25 (C2)	-123	0.38 (C)
B3-C: Local Cupping	-1.35	1.75 (C1)	-52	0.16 (C)
B3-T: Striations & Tearing	1.78	2.25 (T1)	426	1.03 (Y)
B4-F: Fracture	1.73	2.25 (T2)	125	0.30 (Y)

Key Observations

Cycle #	Target Displacement (in.)	Observations
3-4	0.25	Small bolt slip NGP and SGP T1
5-6	0.375	Clicking T1 – North gusset plate
7-8	0.5	Small creaking and clicking between tension and compression – North Gusset plate
9-10	0.625	Small creaking and clicking between tension and compression – North Gusset plate
11-12	0.75	Small creaking and clicking between tension and compression – North Gusset plate
13-14	1.25	Small creaking and clicking between tension and compression – North Gusset plate
15-16	1.75	Lots of clicking throughout cycles – North gusset plate Major local cupping (~1") 3.25" north of center at C1 peak Major local cupping (~1.5") at C2 peak
17-18	2.25	Striations along east face of brace – T1 Major local cupping (~1.8") at C1 peak, OOP disp. = 15.9" Brace Fracture T2

Test Results

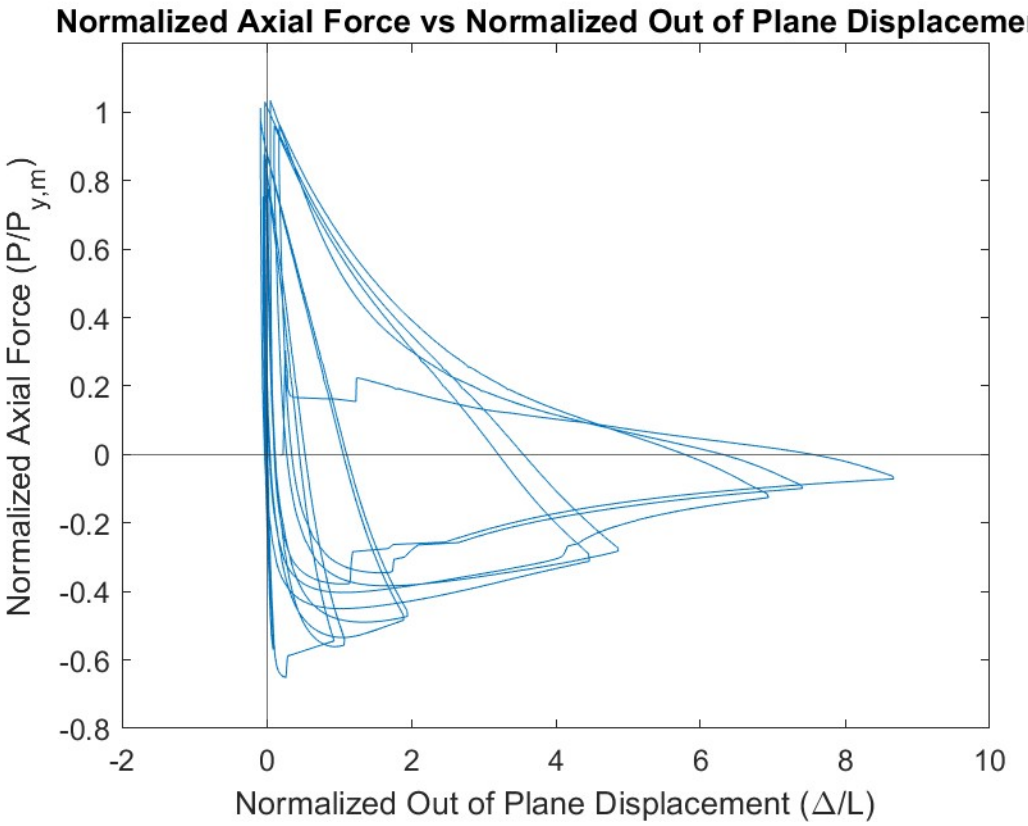

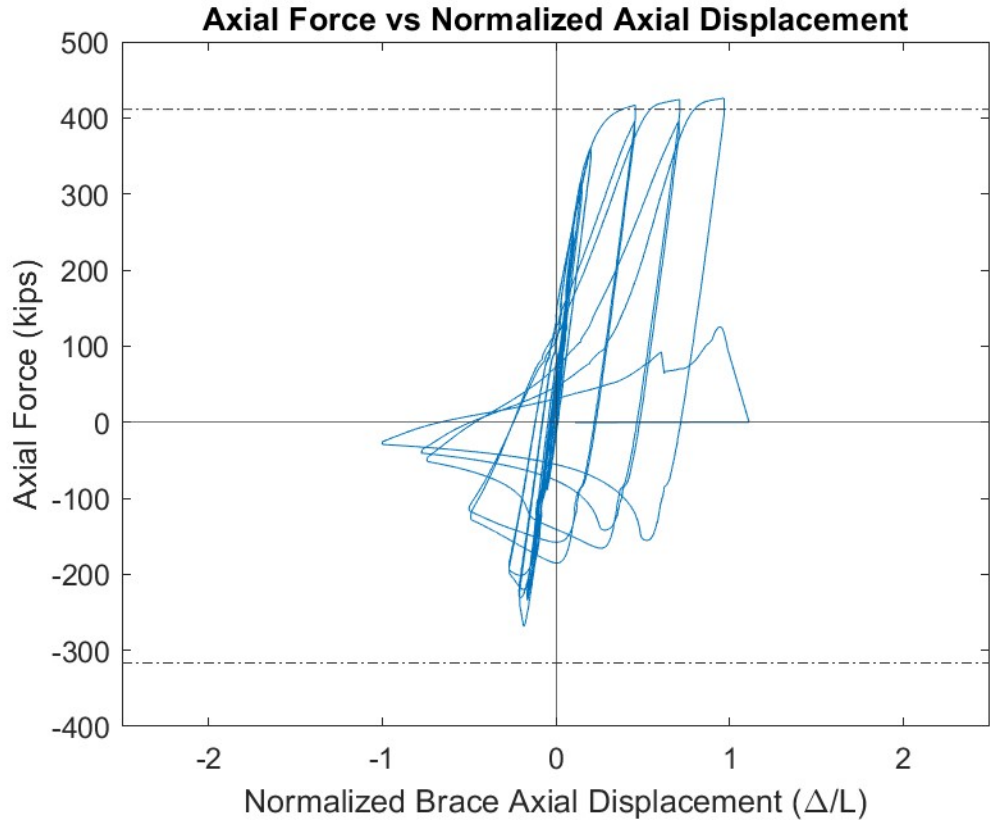

Photos

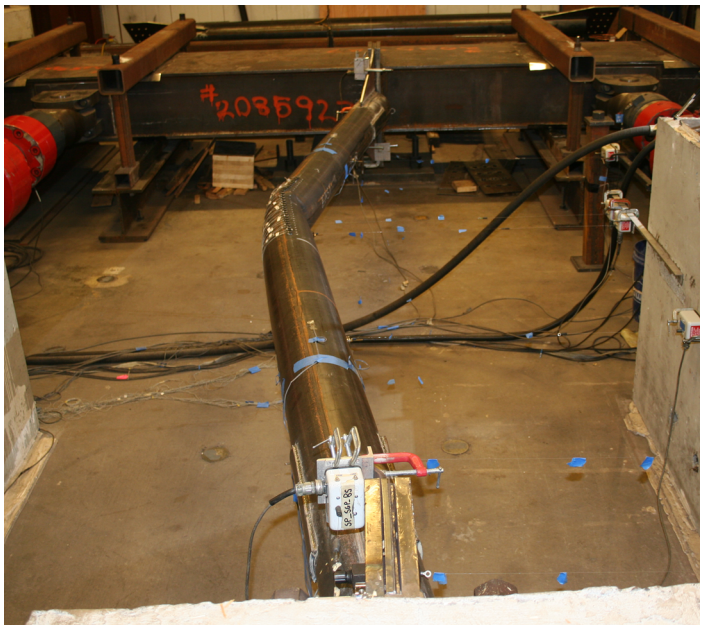

Peak Out of Plane Displacement: 2.25” Cycles

Striations along east face of brace: T1 2.25” cycle

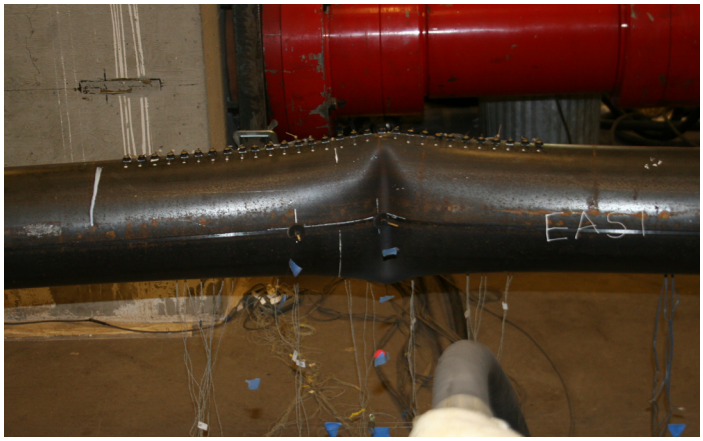

Major Cupping: 2.25” C1 cycle

Brace Fracture: 2.25” T2 cycle

AISC Brace Test Summary

Test Name: 8.625x3/8 A500 short
Test Date: 5/15/24

Brace Properties

Measured Yield Stress (ksi)	65.7
Measured Ultimate Stress (ksi)	75.2
Measured Yield Load (kips)	596
Critical Buckling Load (kips)	466
Percent Elongation – 2" (%)	36.0
Brace Length (in.)	183.5
Global Slenderness Ratio (L_c/r)	62.6

Area (in^2)	9.07
Moment of Inertia (in^4)	77.8
Thickness – Nominal (in.)	0.349
Thickness – Measured (in.)	0.345
Brace Compactness Ratio (b/t) – Nominal	24.7
Brace Compactness Ratio (b/t) – Measured	25.0

Specimen Damage State

Test Event	Axial Brace Deformation (in.)	Target Displacement Cycle (in.)	Force (kips)	$P / P_{(y/c)}$
Peak Tension Load	1.21	1.75 (T1)	581	0.97 (Y)
B1: Initial Global Buckling	-0.22	0.5 (C1)	-341	0.73 (C)
B2: Moderate Global Buckling	-0.91	1.25 (C1)	-169	0.36 (C)
B3-C: Local Cupping	-1.57	1.75 (C2)	-73	0.16 (C)
B3-T: Striations & Tearing	1.66	2.25 (T2)	524	0.88 (Y)
B4-F: Brace Fracture	1.87	2.75 (T1)	214	0.36 (Y)

Key Observations

Cycle #	Target Displacement (in.)	Observations
9-10	0.625	Large bolt slip T1 – North gusset plate Bolt slip T1 – South gusset plate: SP_SGP_E slipped but was fixed when actuators reached 0" displacement Clicking sounds into C1 cycle – North gusset plate Clicking sounds T2 – North gusset plate
11-12	0.75	Clicking throughout all cycles – North gusset plate
13-14	1.25	Clicking through T1 and T2 cycles – North gusset plate Bolt slip T1 – South gusset plate
15-16	1.75	Clicking through T1 and T2 cycles – North gusset plate Small bolt slip T1 – South gusset plate Moderate local cupping (~0.8") 2" north of center at C2 peak
17-18	2.25	Major local cupping (~1.4") at C1 peak Striations along east face of brace – T2 Major local cupping (~1.6") at C2 peak, OOP disp. = 17.6"
19	2.75	Brace Fracture T1

Test Results

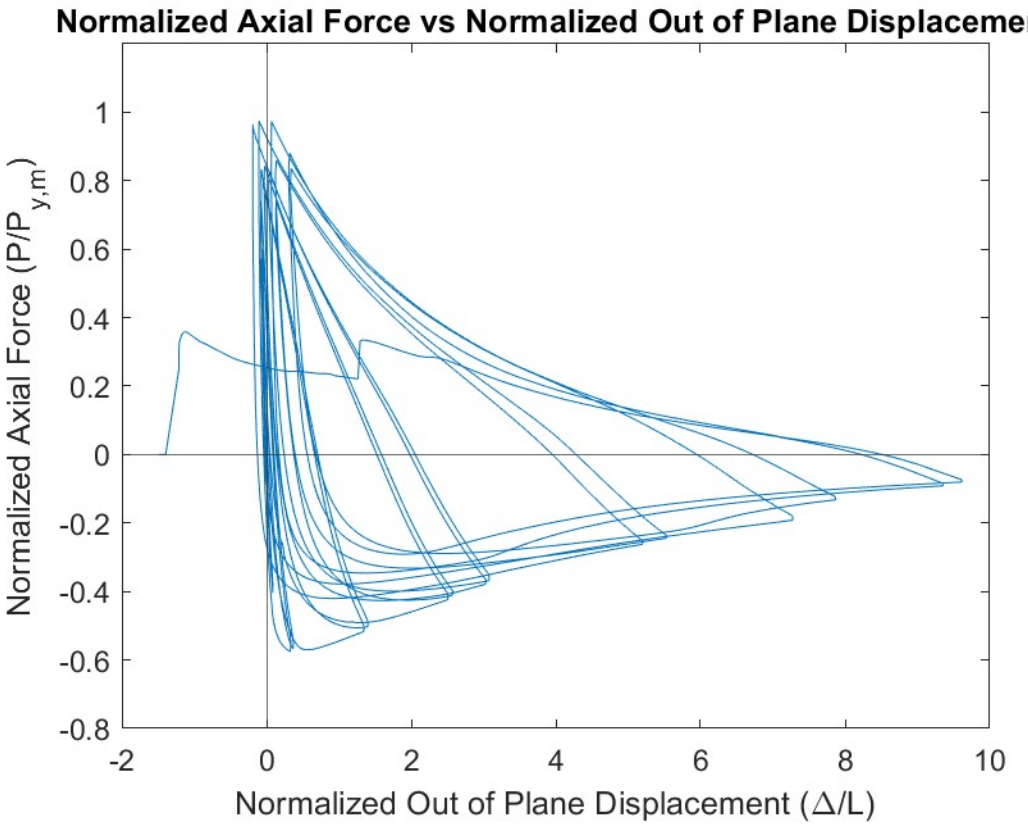

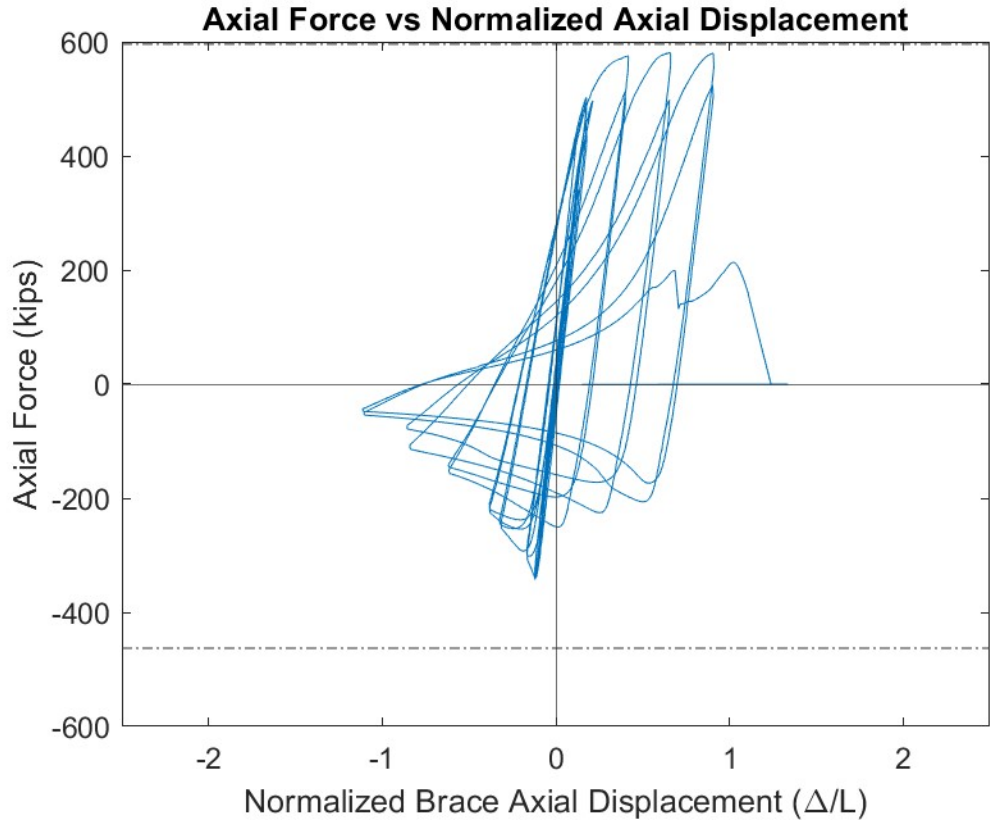

Photos

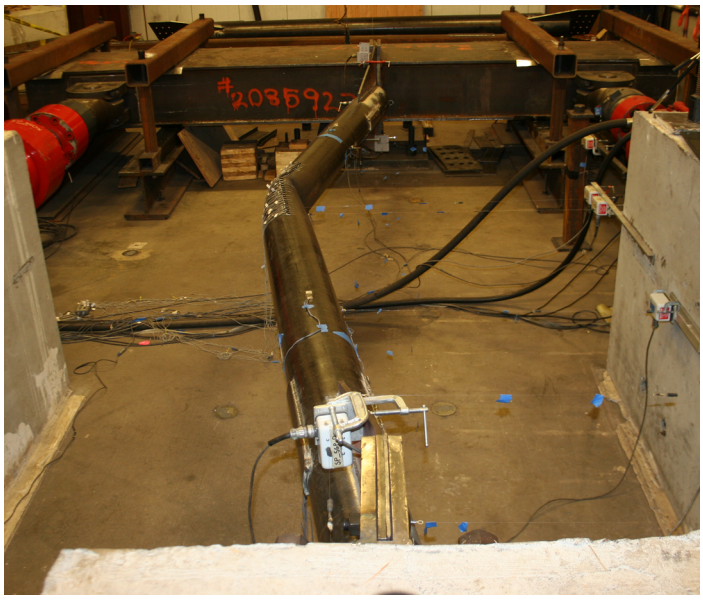

Peak Out of Plane Displacement: 2.25” Cycles

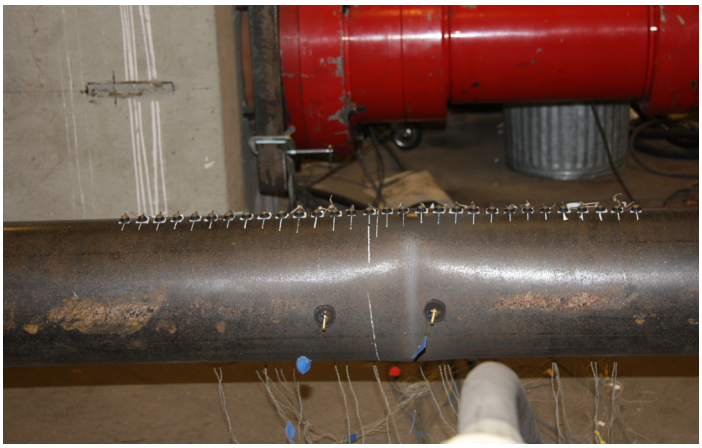

Striations along east face of brace: T2 2.25” cycle

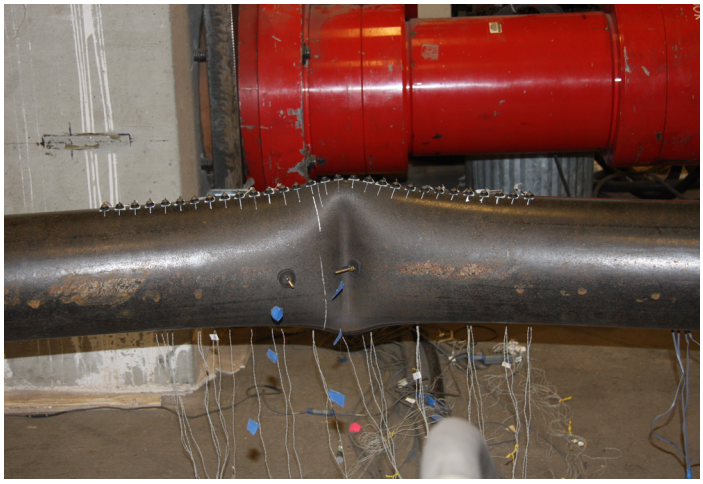

Major Cupping: 2.25” C2 cycle

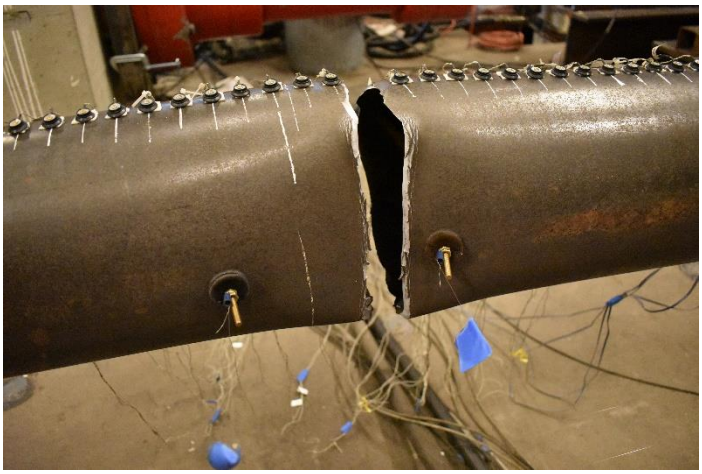

Brace Fracture: 2.75” T1 cycle

AISC Brace Test Summary

Test Name: 8.625x3/16 A500 short
Test Date: 4/30/24

Brace Properties

Measured Yield Stress (ksi)	69.5
Measured Ultimate Stress (ksi)	81.6
Measured Yield Load (kips)	321
Critical Buckling Load (kips)	250
Percent Elongation – 2" (%)	29.5
Brace Length (in.)	183.5
Global Slenderness Ratio (L_c/r)	61.4

Area (in^2)	4.62
Moment of Inertia (in^4)	41.3
Thickness – Nominal (in.)	0.174
Thickness – Measured (in.)	0.187
Brace Compactness Ratio (b/t) – Nominal	49.6
Brace Compactness Ratio (b/t) – Measured	46.1

Specimen Damage State

Test Event	Axial Brace Deformation (in.)	Target Displacement Cycle (in.)	Force (kips)	P / P_y
Peak Tension Load	1.45	1.75 (T1)	337	1.05 (Y)
B1: Initial Global Buckling	-0.19	0.375 (C1)	-201	0.80 (C)
B2: Moderate Global Buckling	-0.63	1.25 (C1)	-64	0.26 (C)
B3-C: Local Cupping	-0.99	1.25 (C2)	-28	0.11 (C)
B3-T: Striations & Tearing	1.45	1.75 (T1)	337	1.05 (Y)
B4-F: Fracture	1.72	1.75 (T2)	134	0.42 (Y)

Key Observations

Cycle #	Target Displacement (in.)	Observations
13-14	1.25	Very large bolt slip T1 – South gusset plate. A few optotrak sensors popped off, but were replaced when actuators returned to 0 displacement. Local cupping initiated approximately 6" south of center at C1 peak Small clicking T2 – North gusset plate Major local cupping (~1.4") at C2 peak
15-16	1.75	Striations along east face of brace – T1 Major local cupping (~1.7") at C1 peak, OOP disp. = 13.1" Brace Fracture T2

Test Results

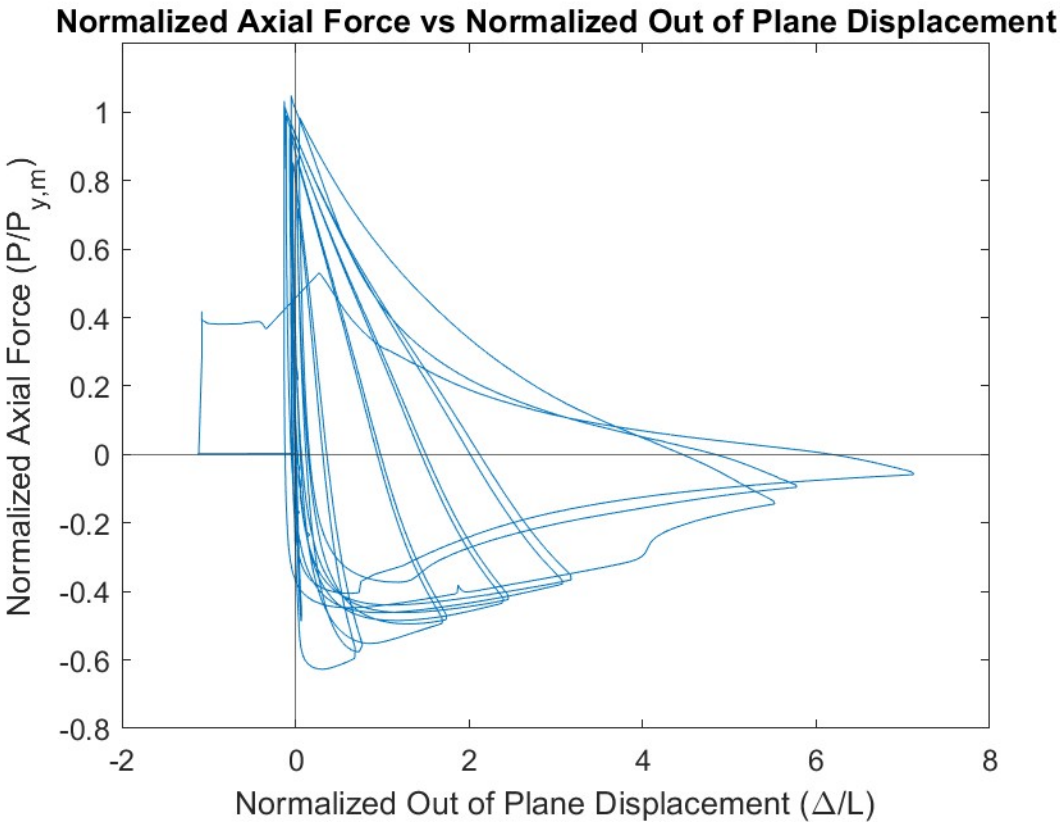

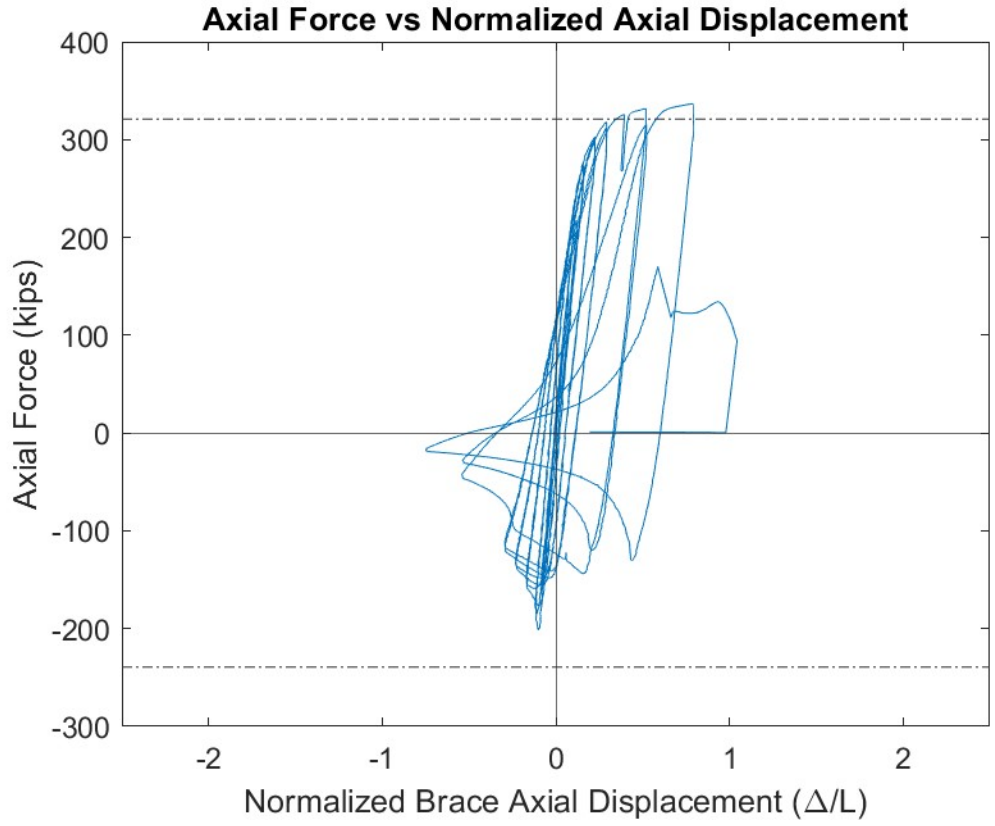

Photos

Peak Out of Plane Displacement: 1.75” Cycles

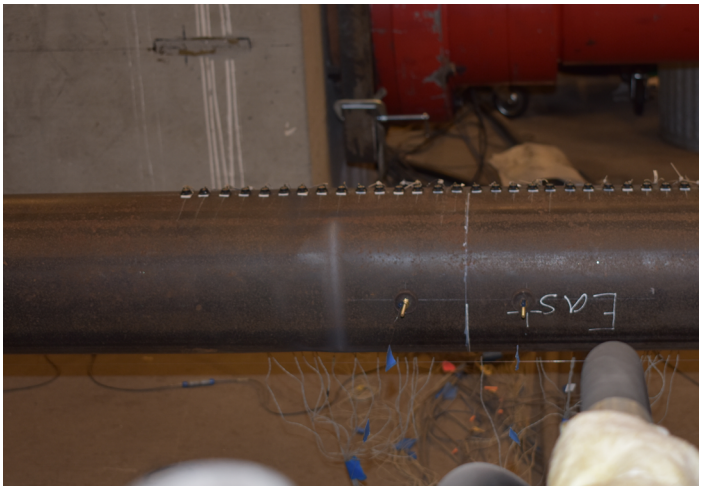

Striations along east face of brace: T1 1.75” cycle

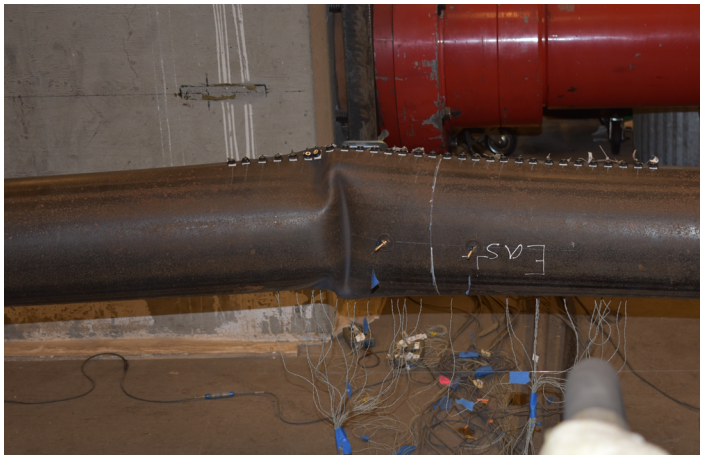

Major Cupping: 1.75” C1 cycle

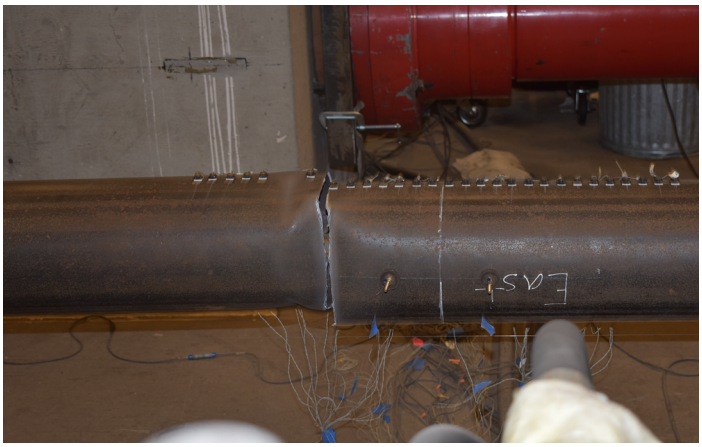

Brace Fracture: 1.75” T2 cycle

AISC Brace Test Summary

Test Name: 10.75x0.365 A500 short
Test Date: 5/8/24

Brace Properties

Measured Yield Stress (ksi)	60.4
Measured Ultimate Stress (ksi)	77.0
Measured Yield Load (kips)	670
Critical Buckling Load (kips)	614
Percent Elongation – 2" (%)	35.6
Brace Length (in.)	183.5
Global Slenderness Ratio (L_c/r)	49.9

Area (in^2)	11.1
Moment of Inertia (in^4)	150
Thickness – Nominal (in.)	0.339
Thickness – Measured (in.)	0.339
Brace Compactness Ratio (b/t) – Nominal	31.7
Brace Compactness Ratio (b/t) – Measured	31.9

Specimen Damage State

Test Event	Axial Brace Deformation (in.)	Target Displacement Cycle (in.)	Force (kips)	$P / P_{(y/c)}$
Peak Tension Load	1.32	1.75 (T1)	686	1.02 (Y)
B1: Initial Global Buckling	-0.29	0.5 (C1)	-461	0.75 (C)
B2: Moderate Global Buckling	-0.80	1.75 (C1)	-174	0.28 (C)
B3-C: Local Cupping	-1.52	1.75 (C1)	-114	0.19 (C)
B3-T: Striations & Tearing	1.80	2.25 (T1)	686	1.02 (Y)
B4-F: Brace Fracture	2.07	2.75 (T1)	159	0.24 (Y)

Key Observations

Cycle #	Target Displacement (in.)	Observations
5-6	0.375	Small bolt slip T1 – South gusset plate
7-8	0.5	Bolt slip T1 – South gusset plate
9-10	0.625	Large bolt slip T1 and T2 – North gusset plate Clicking sounds T2 – North gusset plate Large bolt slip C2 – North gusset plate
11-12	0.75	Lots of clicking throughout cycles – North gusset plate Large bolt slip T1 and T2 – North gusset plate
13-14	1.25	Lots of clicking throughout cycles – North gusset plate Bolt slip into C1 – North gusset plate 2 bolt slips T2 – North gusset plate
15-16	1.75	Lots of clicking throughout cycles – North gusset plate Small bolt slip T1 – South gusset plate Major local cupping (~1") 1.5" north of center at C1 peak Major local cupping (~1.6") at C2 peak
17-18	2.25	Striations along east face of brace – T1 Major local cupping (~2.1") at C1 peak Major local cupping (~2.3") at C2 peak, OOP disp. = 17.9"
19	2.75	Brace Fracture T1

Test Results

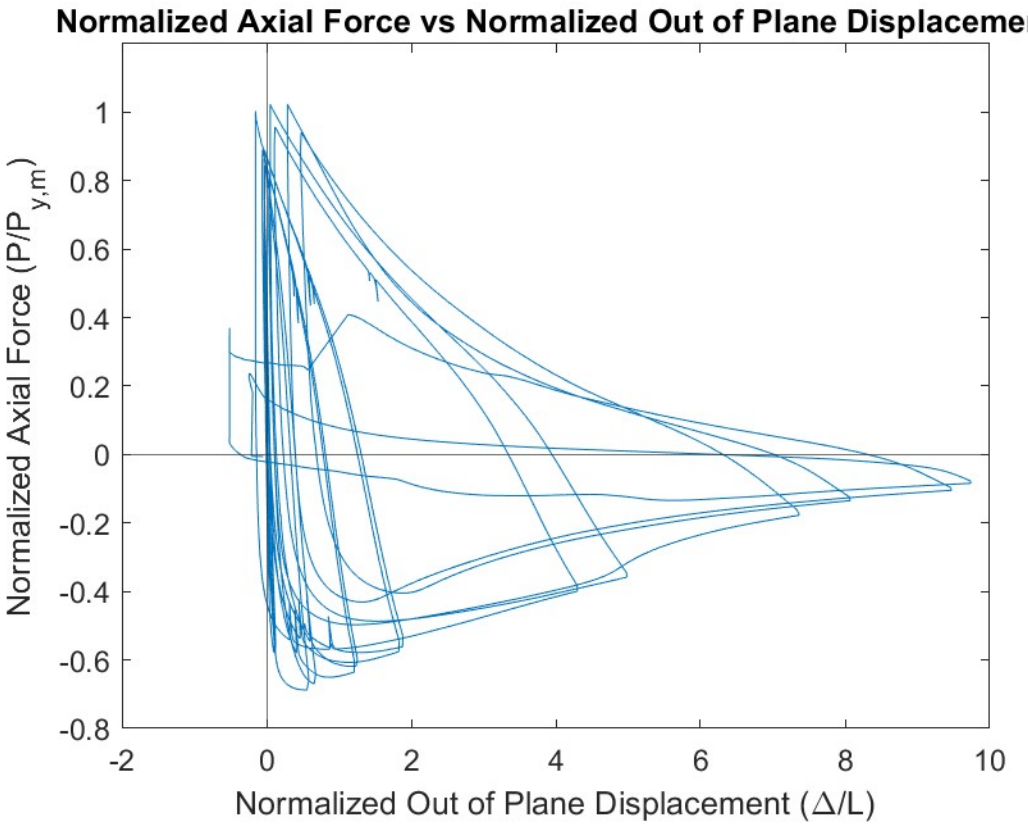

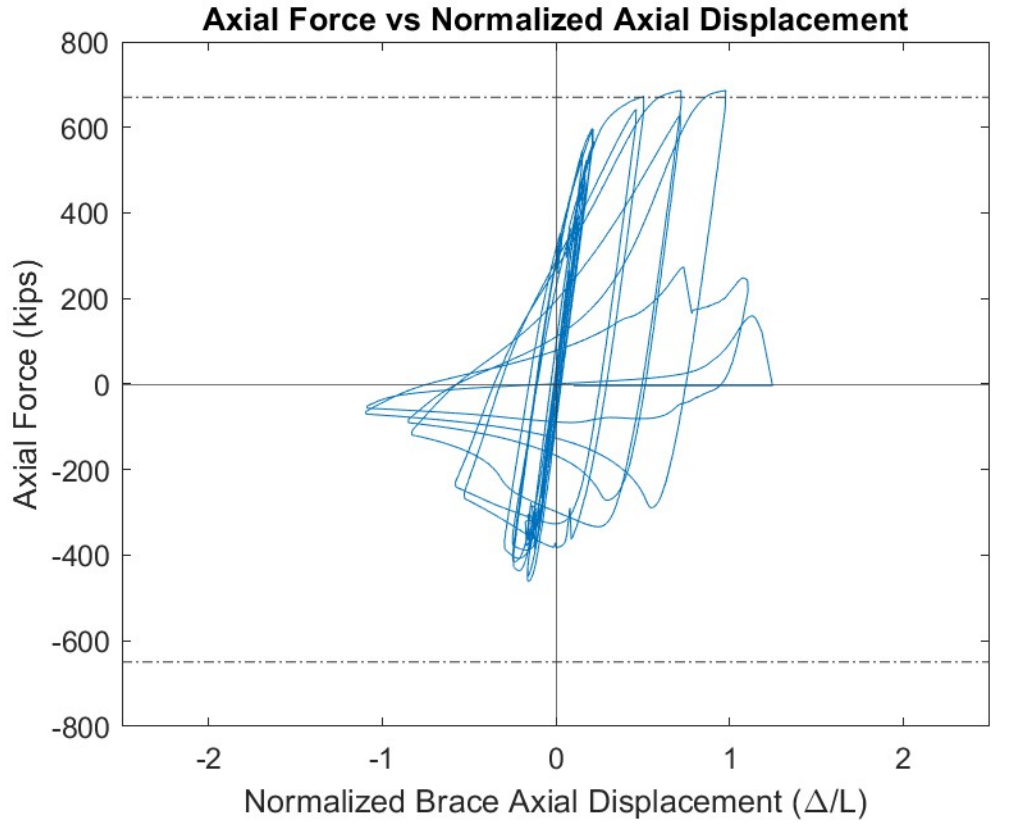

Photos

Peak Out of Plane Displacement: 2.25” Cycles

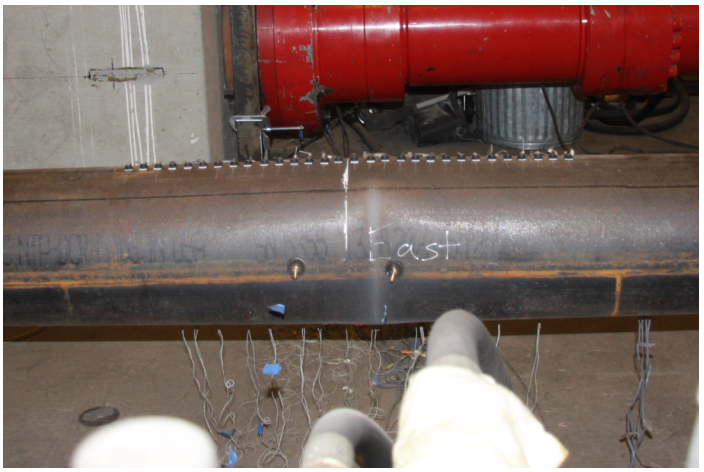

Striations along east face of brace: T1 2.25” cycle

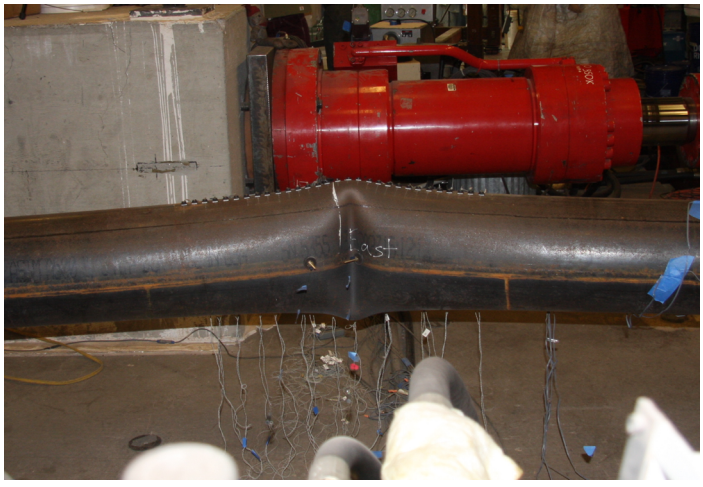

Major Cupping: 2.25” C1 cycle

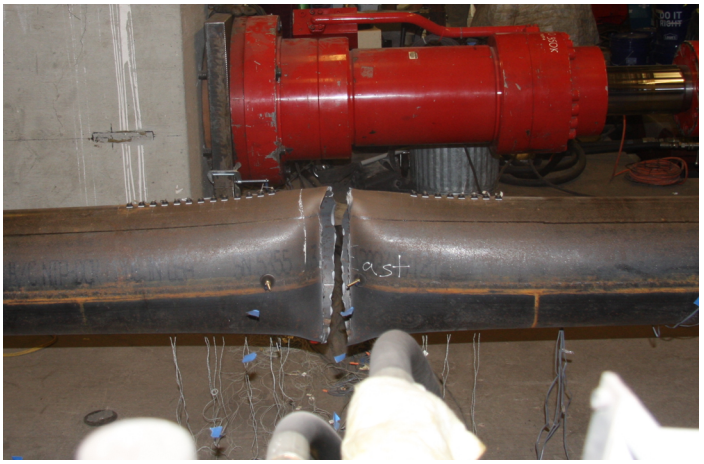

Brace Fracture: 2.75” T1 cycle

AISC Brace Test Summary

Test Name: 10.75x0.250 A500 short
Test Date: 5/21/24

Brace Properties

Measured Yield Stress (ksi)	62.7
Measured Ultimate Stress (ksi)	74.8
Measured Yield Load (kips)	501
Critical Buckling Load (kips)	440
Percent Elongation – 2" (%)	34.2
Brace Length (in.)	183.5
Global Slenderness Ratio (L_c/r)	49.3

Area (in^2)	7.15
Moment of Inertia (in^4)	85.3
Thickness – Nominal (in.)	0.233
Thickness – Measured (in.)	0.232
Brace Compactness Ratio (b/t) – Nominal	46.1
Brace Compactness Ratio (b/t) – Measured	46.4

Specimen Damage State

Test Event	Axial Brace Deformation (in.)	Target Displacement Cycle (in.)	Force (kips)	$P / P_{(y/c)}$
Peak Tension Load	1.45	1.75 (T1)	475	0.95 (Y)
B1: Initial Global Buckling	-0.34	0.5 (C1)	-303	0.69 (C)
B2: Moderate Global Buckling	-0.72	1.25 (C1)	-83	0.19 (C)
B3-C: Local Cupping	-1.07	1.25 (C1)	-62	0.14 (C)
B3-T: Striations & Tearing	1.45	1.75 (T1)	475	0.95 (Y)
B4-F: Brace Fracture	2.00	2.25 (T1)	119	0.24 (Y)

Key Observations

Cycle #	Target Displacement (in.)	Observations
7-8	0.5	Small bolt slip T1 – North gusset plate
9-10	0.625	Small bolt slip T1 – North gusset plate
13-14	1.25	Very large bolt slip T1 – North gusset plate Moderate local cupping (~0.7") 3.5" north of center at C1 peak Clicking sounds T2 – North gusset plate Major local cupping (~1.4") at C2 peak
15-16	1.75	Clicking sounds T1 – North gusset plate Major local cupping (~1.9") at C1 peak, OOP disp. = 14.3" Partial brace tear T2
17-18	2.25	Brace fracture – T1

Test Results

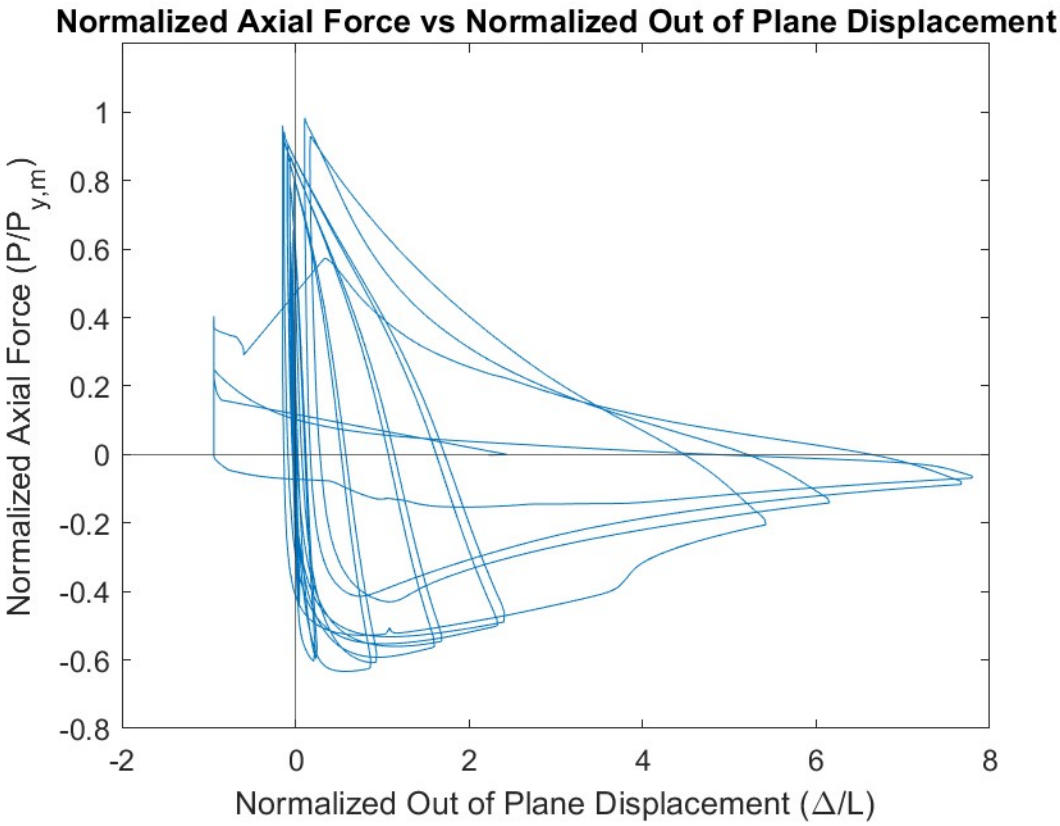

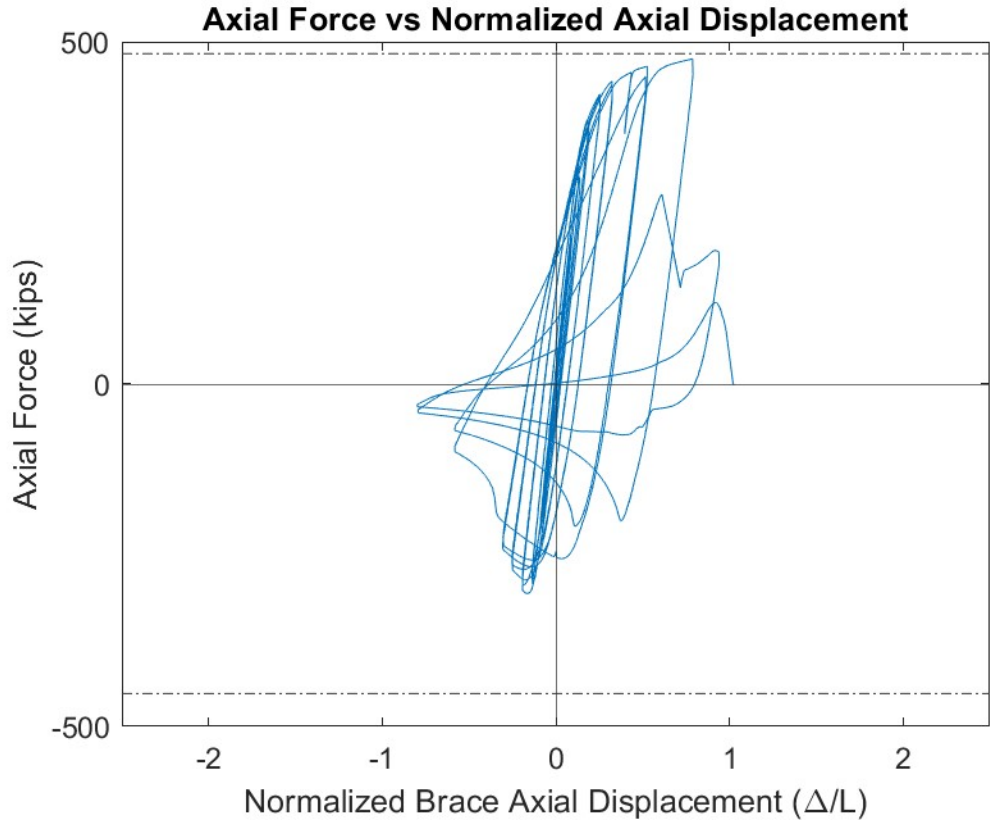

Photos

Peak Out of Plane Displacement: 1.75” Cycles

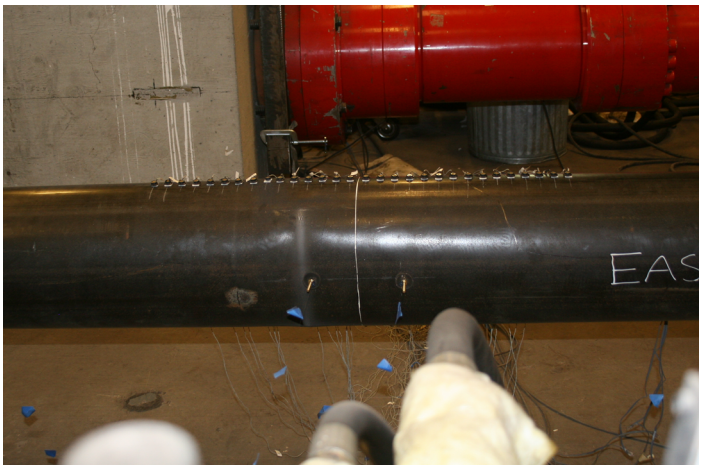

Striations along east face of brace: T1 1.75” cycle

Major Cupping: 1.75” C1 cycle

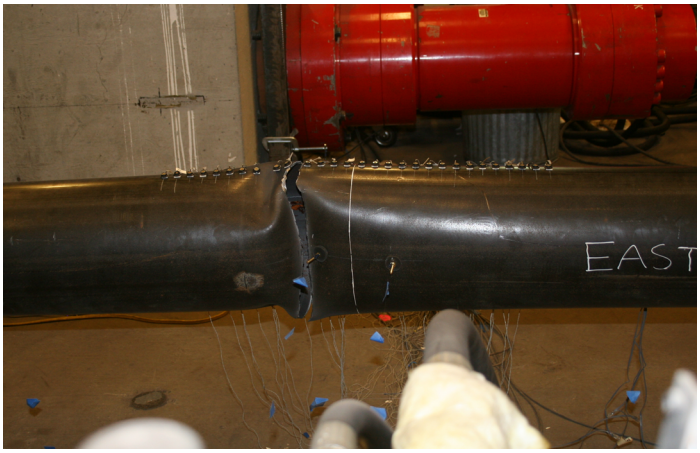

Brace Fracture: 2.25” T1 cycle

AISC Brace Test Summary

Test Name: 6x6x3/16 A500 Long
Test Date: 8/27/24

Brace Properties

Measured Yield Stress (ksi)	58.9
Measured Ultimate Stress (ksi)	80.5
Measured Yield Load (kips)	234
Critical Buckling Load (kips)	128
Percent Elongation – 2" (%)	30.2
Brace Length (in.)	219.5
Global Slenderness Ratio (L_c/r)	92.6

Area (in^2)	3.98
Moment of Inertia (in^4)	22.3
Thickness – Nominal (in.)	0.174
Thickness – Measured (in.)	0.187
Brace Compactness Ratio (D/t) – Nominal	31.5
Brace Compactness Ratio (D/t) – Measured	32.2

Specimen Damage State

Test Event	Axial Brace Deformation (in)	Target Displacement Cycle (in)	Force (kips)	$P / P_{(y/c)}$
Peak Tension Load	0.79	1.16 (T1)	257	1.09 (Y)
B1: Initial Global Buckling	-0.22	0.211 (C1)	-96	0.75 (C)
B2: Moderate Global Buckling	-0.57	0.578 (C1)	-33	0.26 (C)
B3-C: Local Cupping	-0.61	0.578 (C2)	-25	0.20 (C)
B3-T: Striations & Tearing	0.80	1.16 (T1)	256	1.09 (Y)
B4-F: Brace Fracture	0.87	1.16 (T2)	108	0.46 (Y)

Key Observations

Cycle #	Target Displacement (in.)	Observations
7-8	0.462	Clicking sounds T1 – North and South gusset plate
9-10	0.578	Minor local cupping initiated (~0.5") at C2 peak, ~19" south of center
11-12	0.693	Major local cupping (~1") at C1 peak Striations on east face T2 Major local cupping (~1.1") at C2 peak, OOP disp. = 6.0"
13-14	1.16	Partial brace tear – T1 Brace buckled towards the East after partial tear Brace Fracture T2

Test Results

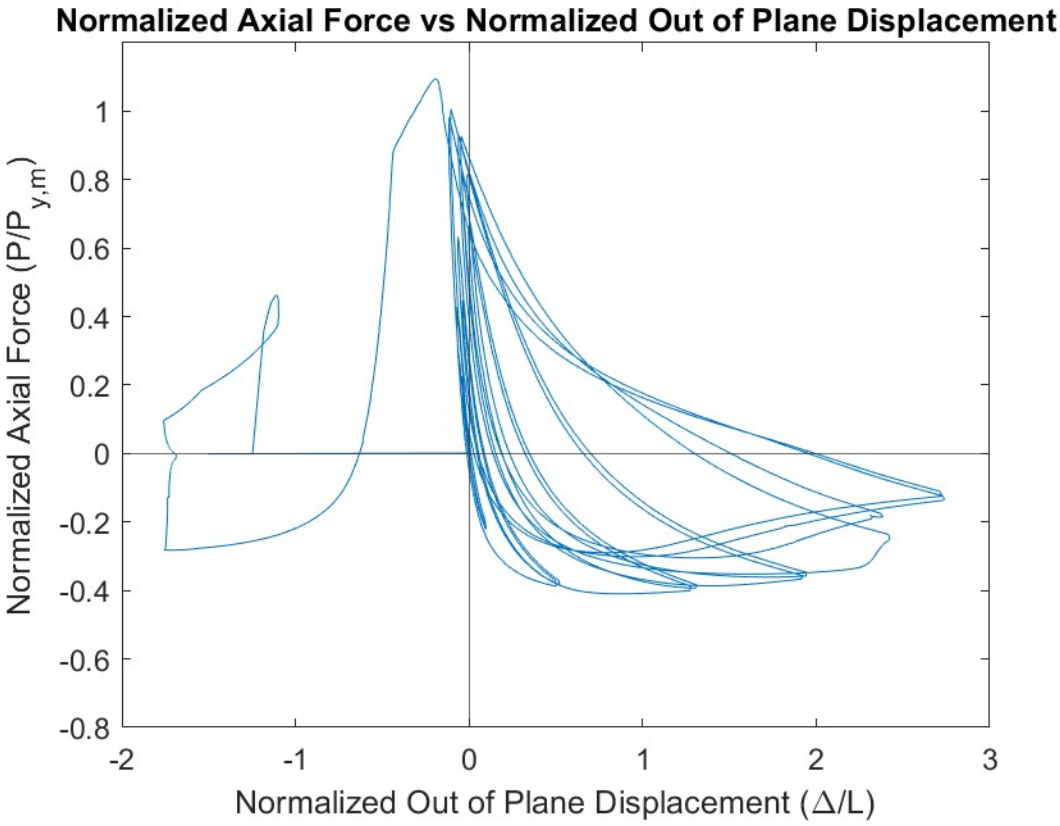

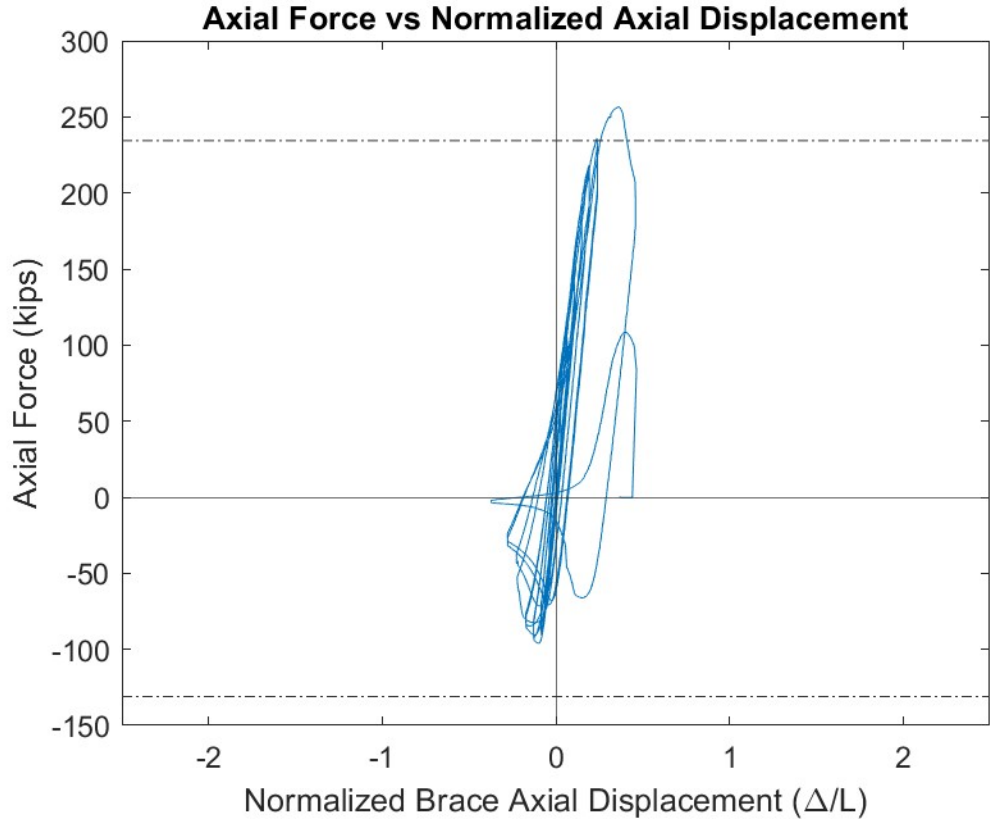

Photos

Peak Out of Plane Displacement - West: 0.693” C2 cycle

Peak Out of Plane Displacement - East: 1.16” C1 cycle

Major Cupping: 0.693” C2 cycle

Brace Fracture: 1.16” T1 cycle

AISC Brace Test Summary

Test Name: 6x6x1/4 A500 Long
Test Date: 8/28/24

Brace Properties

Measured Yield Stress (ksi)	64.7
Measured Ultimate Stress (ksi)	78.6
Measured Yield Load (kips)	339
Critical Buckling Load (kips)	217
Percent Elongation – 2" (%)	31.3
Brace Length (in.)	219.5
Global Slenderness Ratio (L_c/r)	93.8

Area (in^2)	5.24
Moment of Inertia (in^4)	28.6
Thickness – Nominal (in.)	0.233
Thickness – Measured (in.)	0.240
Brace Compactness Ratio (D/t) – Nominal	22.8
Brace Compactness Ratio (D/t) – Measured	25.1

Specimen Damage State

Test Event	Axial Brace Deformation (in.)	Target Displacement Cycle (in.)	Force (kips)	$P / P_{(y/c)}$
Peak Tension Load	1.16	1.62 (T1)	376	1.11 (Y)
B1: Initial Global Buckling	-0.24	0.347 (C1)	-141	0.83 (C)
B2: Moderate Global Buckling	-0.61	0.693 (C1)	-108	0.64 (C)
B3-C: Local Cupping	-1.11	1.16 (C2)	-50	0.30 (C)
B3-T: Striations & Tearing	0.95	1.62 (C2)	271	0.80 (Y)
B4-F: Brace Fracture	1.25	2.08 (T1)	104	0.30 (Y)

Key Observations

Cycle #	Target Displacement (in.)	Observations
11-12	0.693	Bolt slip T1 – North and South Gusset Plate
13-14	1.16	Cupping initiated about 1" north of center (~0.5") C2
15-16	1.62	Bolt slip T1 - South Gusset Plate Major local cupping (~1.3") at C1 peak Marker 15 and 16 not visible at peak due to cupping Partial brace tear – T2 C2, OOP disp. = 14.5"
17-18	2.08	Brace Fracture T1

Test Results

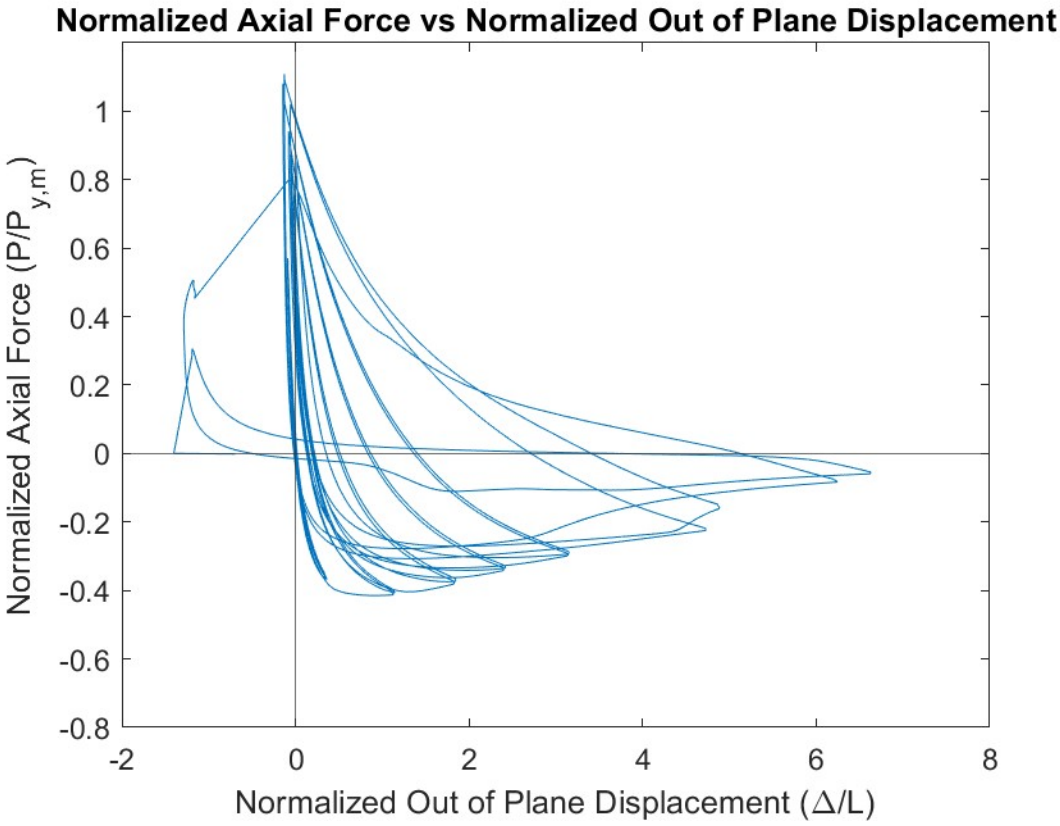

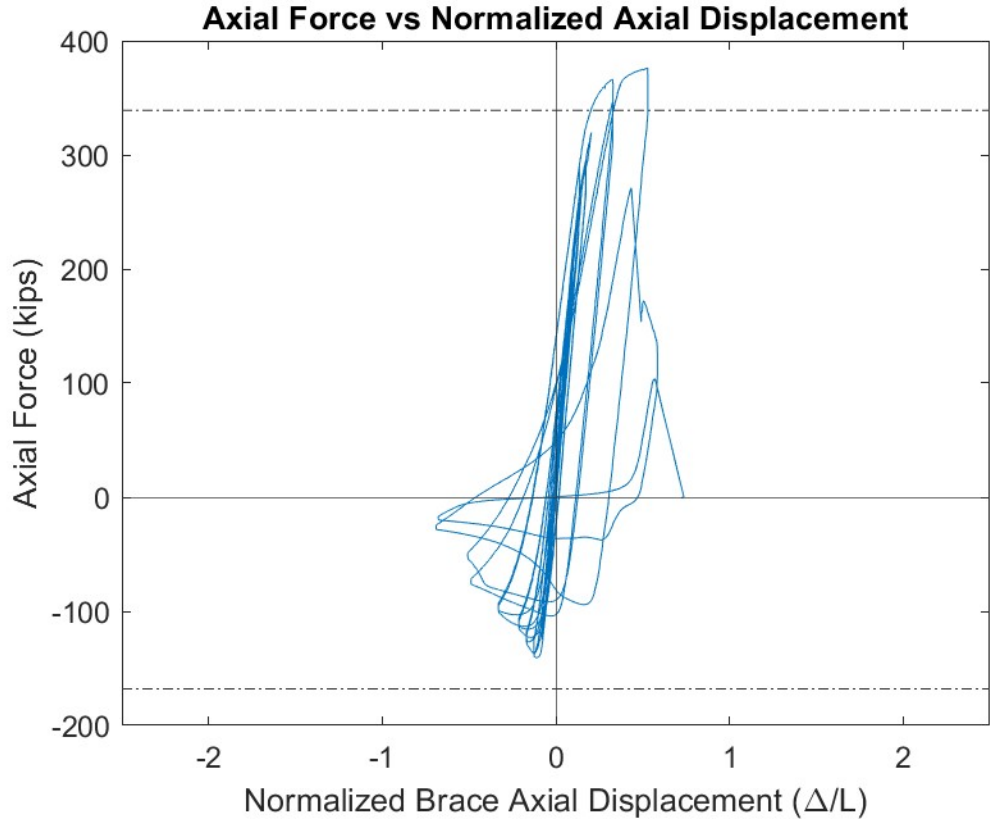

Photos

Peak Out of Plane Displacement: 1.62” C2 cycle

Partial Tear: 1.62” T2 cycle

Major Cupping: 1.62” C2 cycle

Brace Fracture: 2.08” T1 cycle

AISC Brace Test Summary

Test Name: 7x7x1/4 A500 Long
Test Date: 8/29/24

Brace Properties

Measured Yield Stress (ksi)	64.1
Measured Ultimate Stress (ksi)	78.8
Measured Yield Load (kips)	494
Critical Buckling Load (kips)	248
Percent Elongation – 2" (%)	30.3
Brace Length (in.)	219.5
Global Slenderness Ratio (L_c/r)	79.8

Area (in^2)	6.17
Moment of Inertia (in^4)	46.5
Thickness – Nominal (in.)	0.233
Thickness – Measured (in.)	0.239
Brace Compactness Ratio (D/t) – Nominal	27.0
Brace Compactness Ratio (D/t) – Measured	29.4

Specimen Damage State

Test Event	Axial Brace Deformation (in.)	Target Displacement Cycle (in)	Force (kips)	$P / P_{(y/c)}$
Peak Tension Load	0.85	1.16 (T1)	415	0.84 (Y)
B1: Initial Global Buckling	-0.26	0.462 (C1)	-203	0.82 (C)
B2: Moderate Global Buckling	-0.54	1.16 (C2)	-54	0.22 (C)
B3-C: Local Cupping	-0.49	0.578 (C2)	-159	0.64 (C)
B3-T: Striations & Tearing	0.77	1.16 (T2)	328	0.67 (Y)
B4-F: Brace Fracture	0.90	1.62 (T1)	133	0.27 (Y)

Key Observations

Cycle #	Target Displacement (in.)	Observations
9-10	0.578	Large bolt slip T1 – North Gusset Plate Minor local cupping initiated (~0.4") at C2 peak, ~7.5" south of center
11-12	0.693	Bolt slip T1 – South Gusset Plate Major local cupping (~1") at C1 peak Major local cupping (~1.1") at C2 peak
13-14	1.16	Clicking sounds T1 – North and South Gusset Plate Major local cupping (~1.6") at C1 peak Marker 23 and 26 not visible at peak due to cupping Partial brace tear – T2 Brace buckled towards the East after partial tear, OOP disp. = 9.5"
15-16	1.62	Brace Fracture T1

Test Results

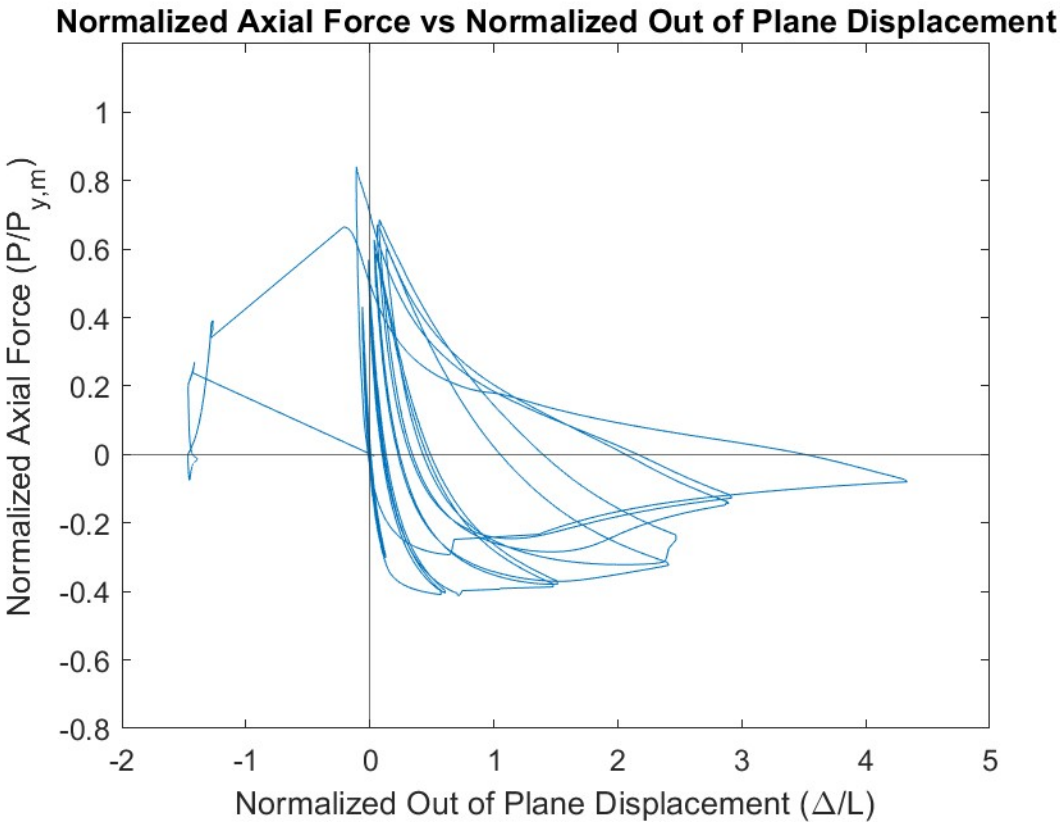

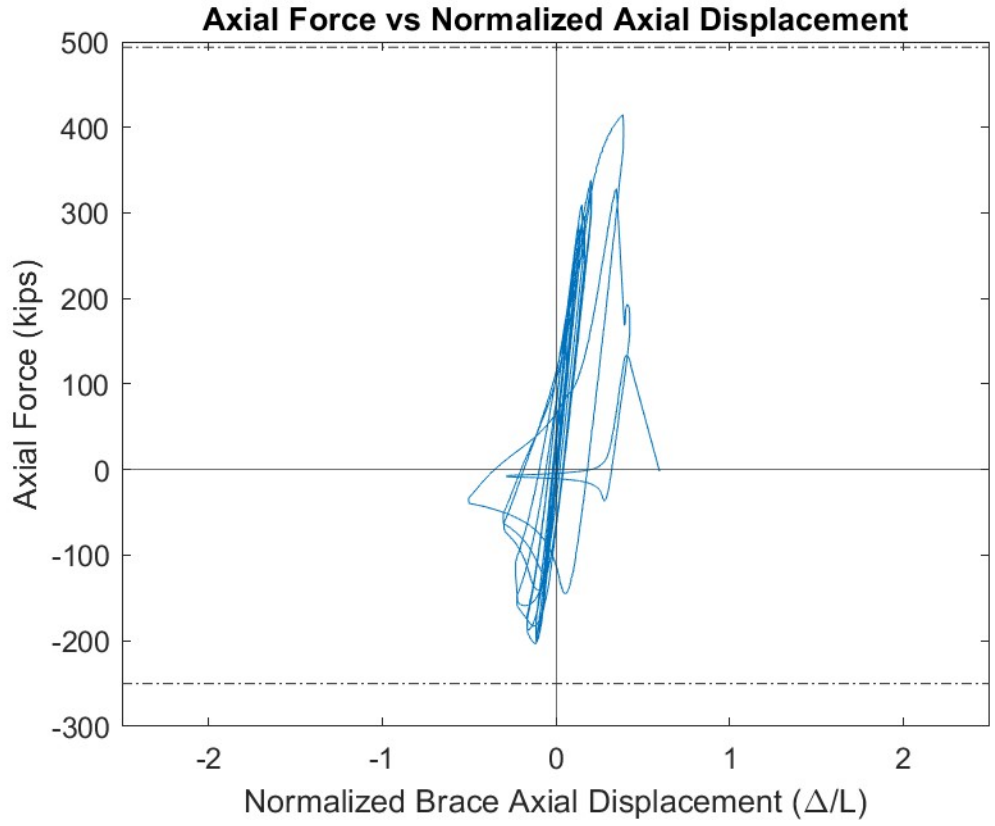

Photos

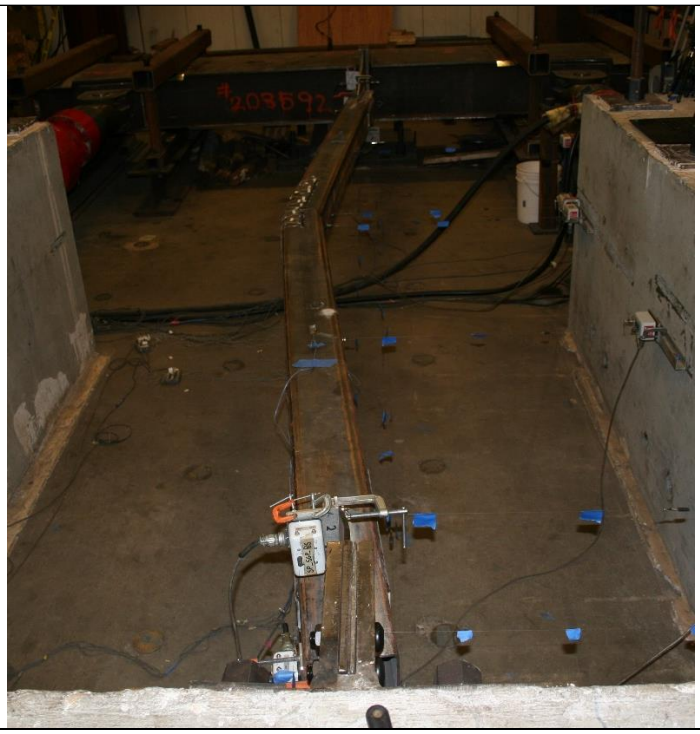

Peak Out of Plane Displacement - West: 1.16” C1 cycle

Peak Out of Plane Displacement - East: 1.16” C2 cycle

Major Cupping: 1.16” C1 cycle

Brace Fracture: 1.62” T1 cycle

AISC Brace Test Summary

Test Name: 8x8x5/16 A500 Long
Test Date: 9/3/24

Brace Properties

Measured Yield Stress (ksi)	64.3
Measured Ultimate Stress (ksi)	75.8
Measured Yield Load (kips)	563
Critical Buckling Load (kips)	405
Percent Elongation – 2" (%)	4.2
Brace Length (in.)	219.5
Global Slenderness Ratio (L_c/r)	70.1

Area (in^2)	8.76
Moment of Inertia (in^4)	85.6
Thickness – Nominal (in.)	0.291
Thickness – Measured (in.)	0.310
Brace Compactness Ratio (D/t) – Nominal	24.5
Brace Compactness Ratio (D/t) – Measured	25.8

Specimen Damage State

Test Event	Axial Brace Deformation (in.)	Target Displacement Cycle (in.)	Force (kips)	$P / P_{(y/c)}$
Peak Tension Load	0.68	1.16 (T1)	557	0.99 (Y)
B1: Initial Global Buckling	-0.31	0.347 (C1)	-316	0.78 (C)
B2: Moderate Global Buckling	-0.89	1.16 (C1)	-120	0.30 (C)
B3-C: Local Cupping	-1.15	1.16 (C1)	-95	0.23 (C)
B3-T: Striations & Tearing	0.73	1.61 (T1)	498	0.88 (Y)
B4-F: Brace Fracture	0.86	1.61 (T1)	278	0.49 (Y)

Key Observations

Cycle #	Target Displacement (in.)	Observations
7-8	0.462	Bolt slip T1 – North and South Gusset Plate Clicking sounds T2 – North and South Gusset Plate
9-10	0.578	Clicking sounds T1 – North and South Gusset Plate
13-14	1.16	Clicking sounds T1 – North and South Gusset Plate Moderate local cupping initiated (~0.9") at C1 peak, ~6" North of center Marker 10 not visible at peak due to cupping Major cupping (~1.5") at C2 peak, OOP disp. = 9.2" Marker 10 and 11 not visible at peak due to cupping
15-16	1.62	Brace Fracture T1

Test Results

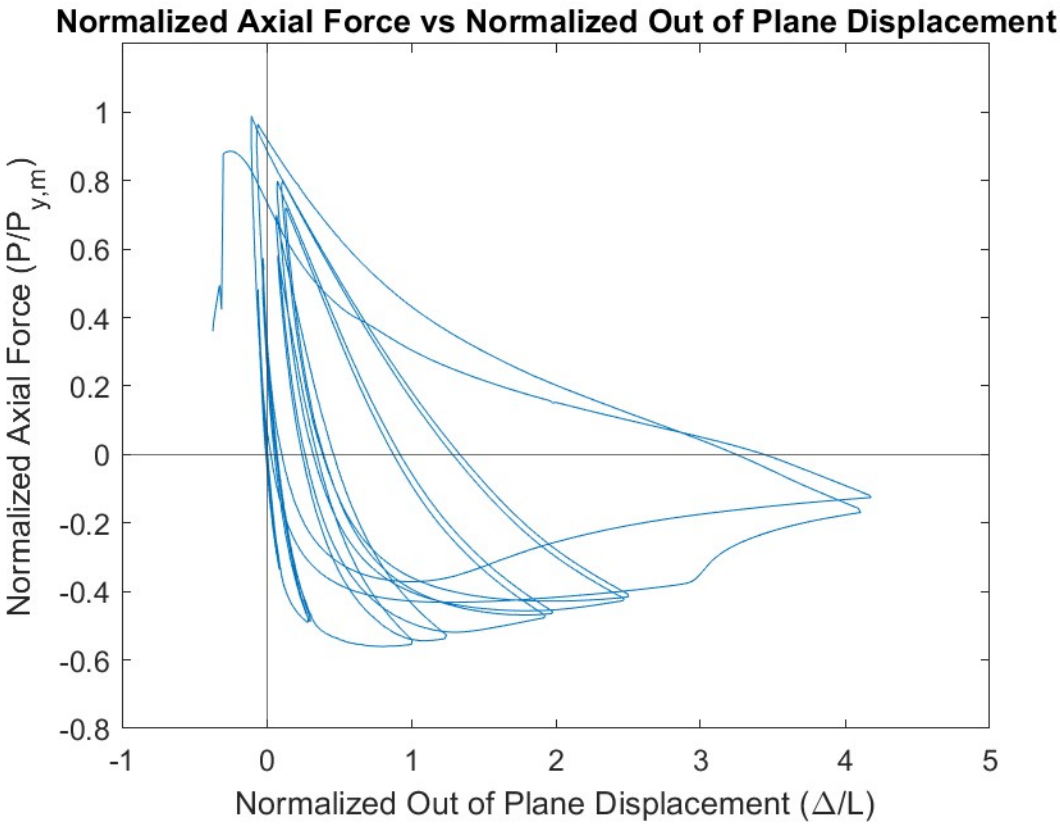

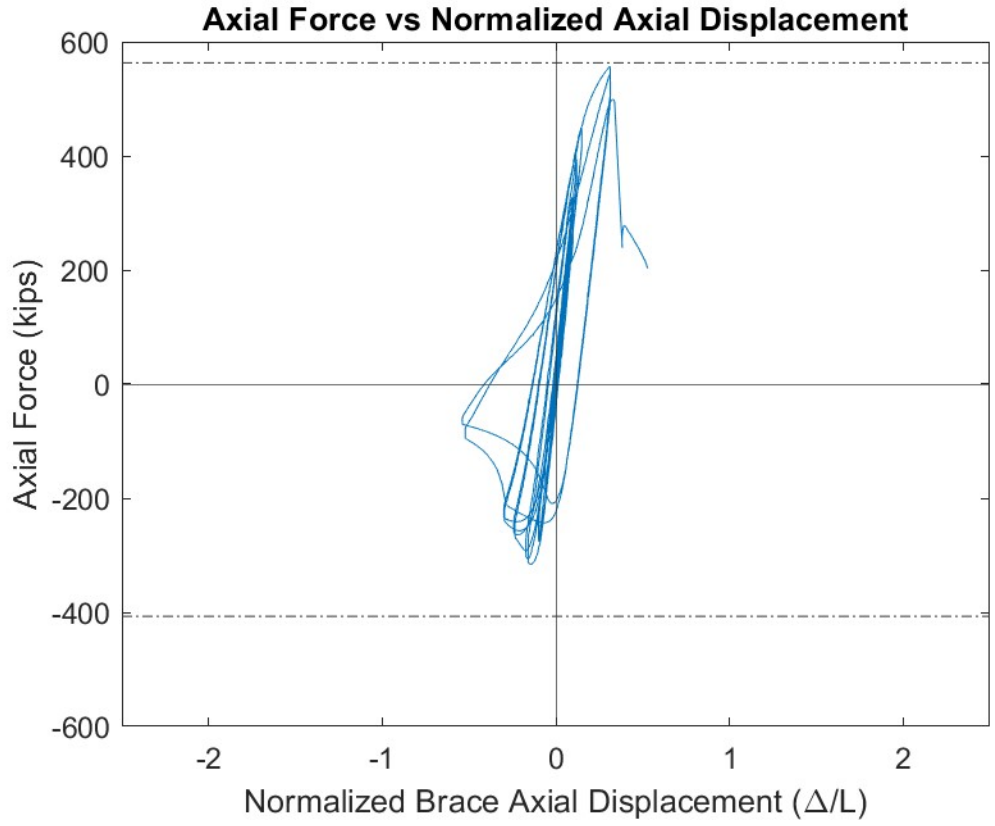

Photos

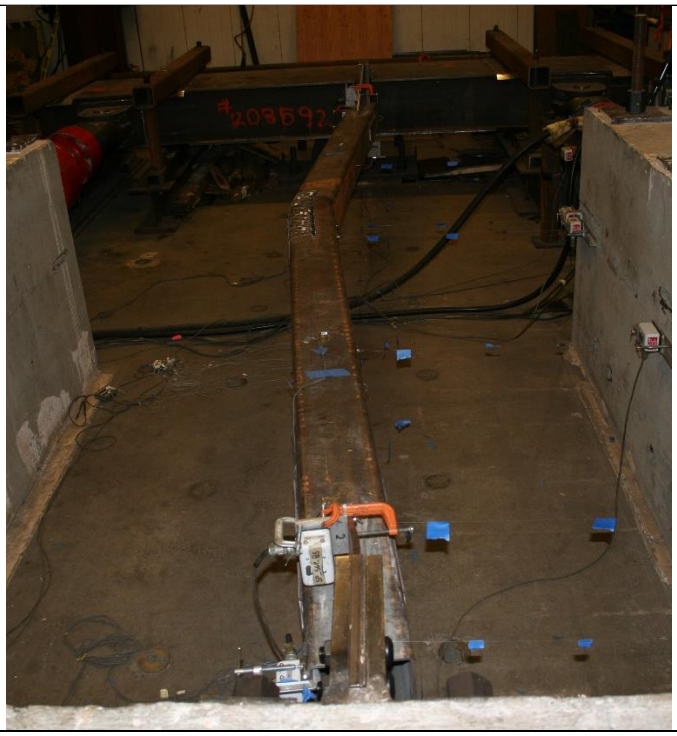

Peak Out of Plane Displacement - West: 1.16” C1 cycle

Initiation of Tearing: 1.62” T1 cycle

Major Cupping: 1.16” C2 cycle

Brace Fracture: 1.62” T1 cycle

AISC Brace Test Summary

Test Name: 6x3/16 A500 Long
Test Date: 8/7/24

Brace Properties

Measured Yield Stress (ksi)	53.6
Measured Ultimate Stress (ksi)	73.4
Measured Yield Load (kips)	189
Critical Buckling Load (kips)	80
Percent Elongation – 2" (%)	33.2
Brace Length (in.)	219.5
Global Slenderness Ratio (L_c/r)	106.6

Area (in^2)	3.53
Moment of Inertia (in^4)	13.5
Thickness – Nominal (in.)	0.174
Thickness – Measured (in.)	0.176
Brace Compactness Ratio (D/t) – Nominal	34.5
Brace Compactness Ratio (D/t) – Measured	34.1

Specimen Damage State

Test Event	Axial Brace Deformation (in.)	Target Displacement Cycle (in.)	Force (kips)	$P / P_{(y/c)}$
Peak Tension Load	2.89	3.00 (T1)	184	0.97 (Y)
B1: Initial Global Buckling	-0.18	0.231 (C1)	-59	0.74 (C)
B2: Moderate Global Buckling	-0.48	0.578 (C1)	-44	0.54 (C)
B3-C: Local Cupping	-2.05	2.54 (C1)	-11	0.13 (C)
B3-T: Striations & Tearing	2.84	3.00 (T2)	155	0.82 (Y)
B4-F : Brace Fracture	2.86	3.47 (T1)	58	0.31 (Y)

Key Observations

Cycle #	Target Displacement (in.)	Observations
19-20	2.54	Minor local cupping (~0.4") initiated at C1 peak ~ 0.5" north of center Moderate local cupping (~0.9") at C2 peak Optotrak marker 15 not visible at C2 peak due to cupping
21-22	3.00	Major local cupping (~1.7") at C1 peak Optotrak marker 15 and 16 not visible at C2 peak due to cupping, OOP disp. = 23.0" Partial brace tear, T2 Brace buckled towards the east after the tear
23	3.47	Brace Fracture T1

Test Results

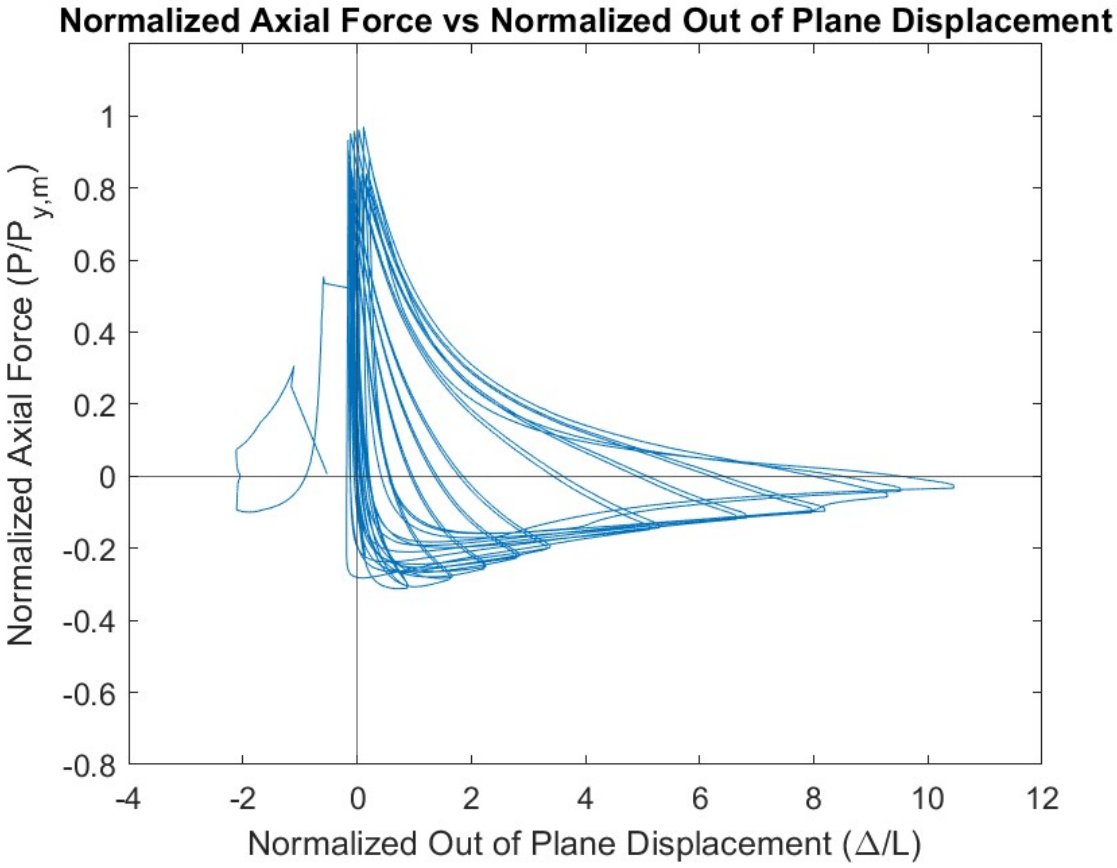

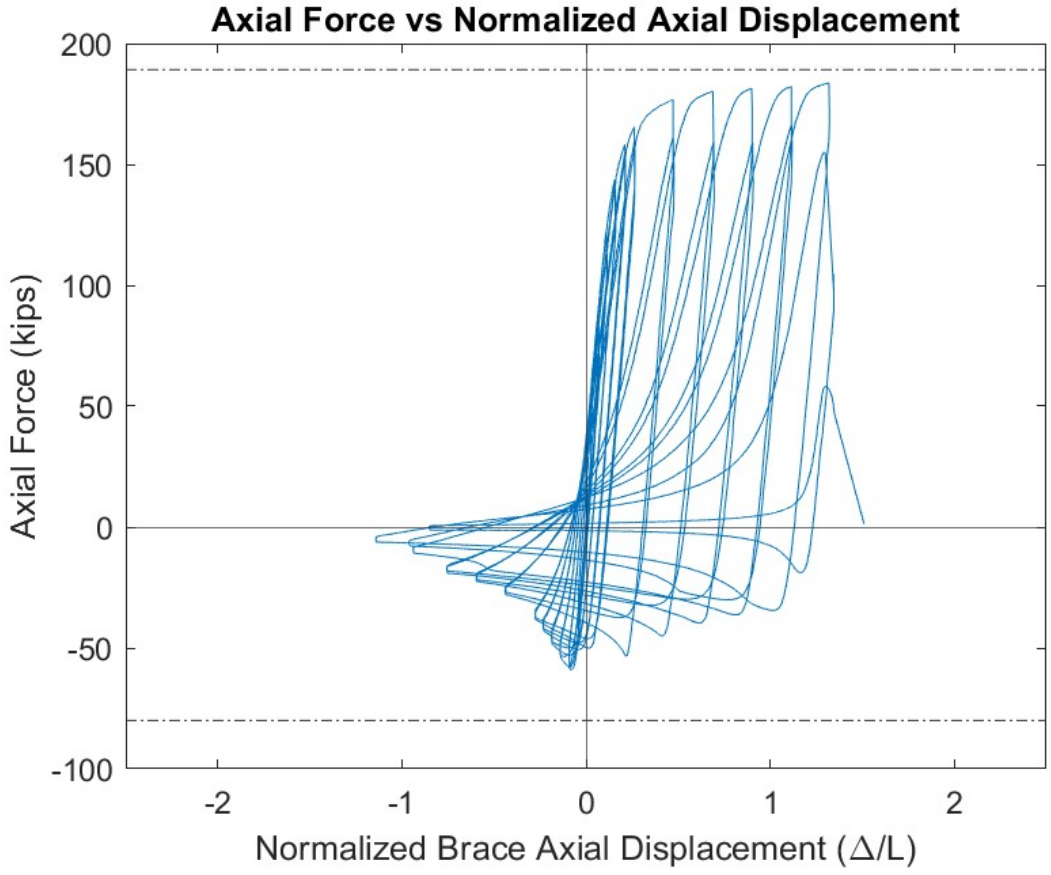

Photos

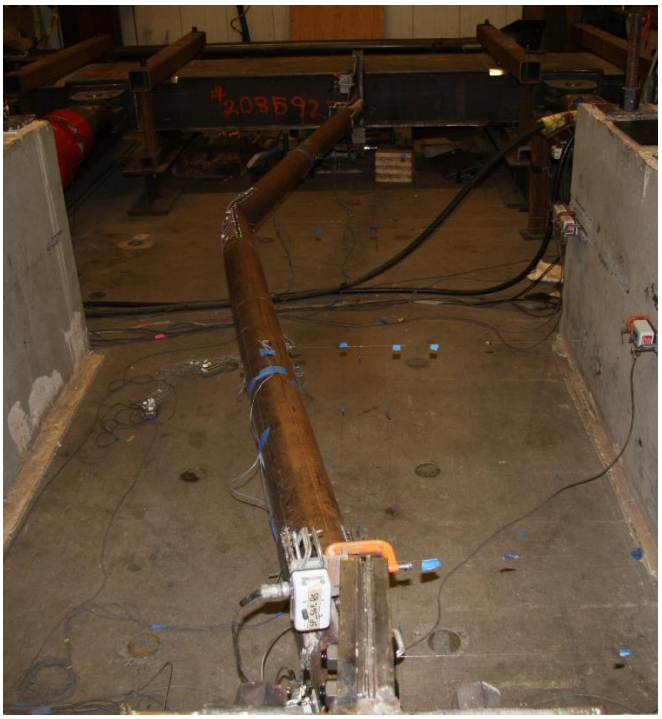

Peak Out of Plane Displacement: 3.00” C1 cycle

Buckling After Partial Tear: 3.00” C2 cycle

Major Cupping: 3.00” C2 cycle

Brace Fracture: 3.47” T1 cycle

AISC Brace Test Summary

Test Name: 6x1/4 A500 Long
Test Date: 8/8/24

Brace Properties

Measured Yield Stress (ksi)	54.2
Measured Ultimate Stress (ksi)	71.6
Measured Yield Load (kips)	229
Critical Buckling Load (kips)	104
Percent Elongation – 2" (%)	40.5
Brace Length (in.)	219.5
Global Slenderness Ratio (L_c/r)	107.6

Area (in^2)	4.22
Moment of Inertia (in^4)	17.6
Thickness – Nominal (in.)	0.233
Thickness – Measured (in.)	0.243
Brace Compactness Ratio (D/t) – Nominal	25.8
Brace Compactness Ratio (D/t) – Measured	24.7

Specimen Damage State

Test Event	Axial Brace Deformation (in.)	Target Displacement Cycle (in.)	Force (kips)	$P / P_{(y/c)}$
Peak Tension Load	3.65	3.93 (T1)	238	1.04 (Y)
B1: Initial Global Buckling	-0.22	0.347 (C1)	-71	0.68 (C)
B2: Moderate Global Buckling	-0.50	0.693 (C1)	-52	0.50 (C)
B3-C: Local Cupping	-2.37	3.47 (C1)	-11	0.10 (C)
B3-T: Striations & Tearing	3.60	3.93 (T2)	133	0.74 (Y)
B4-F: Brace Fracture	3.57	4.39 (T1)	65	0.29 (Y)

Key Observations

Cycle #	Target Displacement (in.)	Observations
7-8	0.462	Clicking sounds – South gusset plate
13-14	1.16	Brace buckled towards the East C1 – Instrumentation was adjusted to accommodate buckling direction
19-20	2.54	Instrumentation adjusted again due to lack of string pot range, C2
23-24	3.47	Minor local cupping (~0.4") initiated at C1 peak Major local cupping (~1") at C2 peak
25-26	3.93	Major local cupping (~1.2") at C1 peak Partial brace fracture T2 Brace buckled back towards the west after partial brace fracture, C2, OOP disp. = 25.9"
27	4.39	Brace Fracture T1

*Minimal optotrak visibility during this test due to buckling direction

Test Results

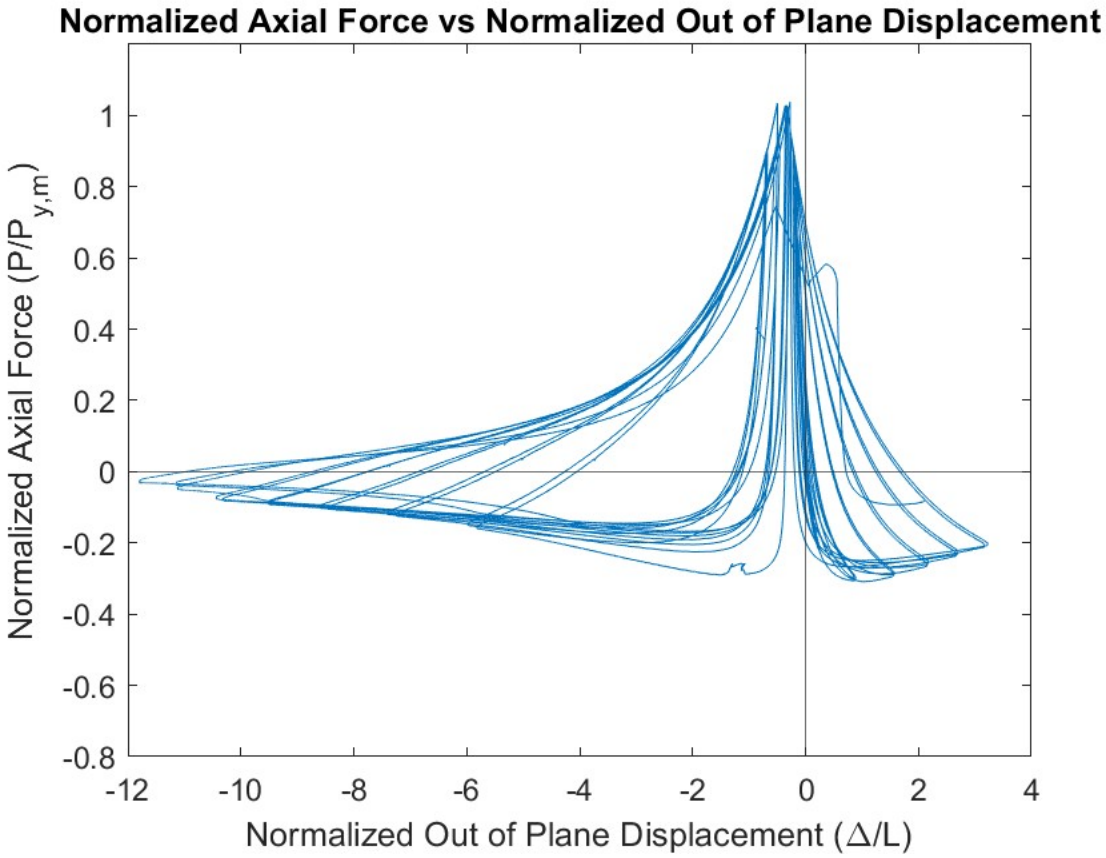

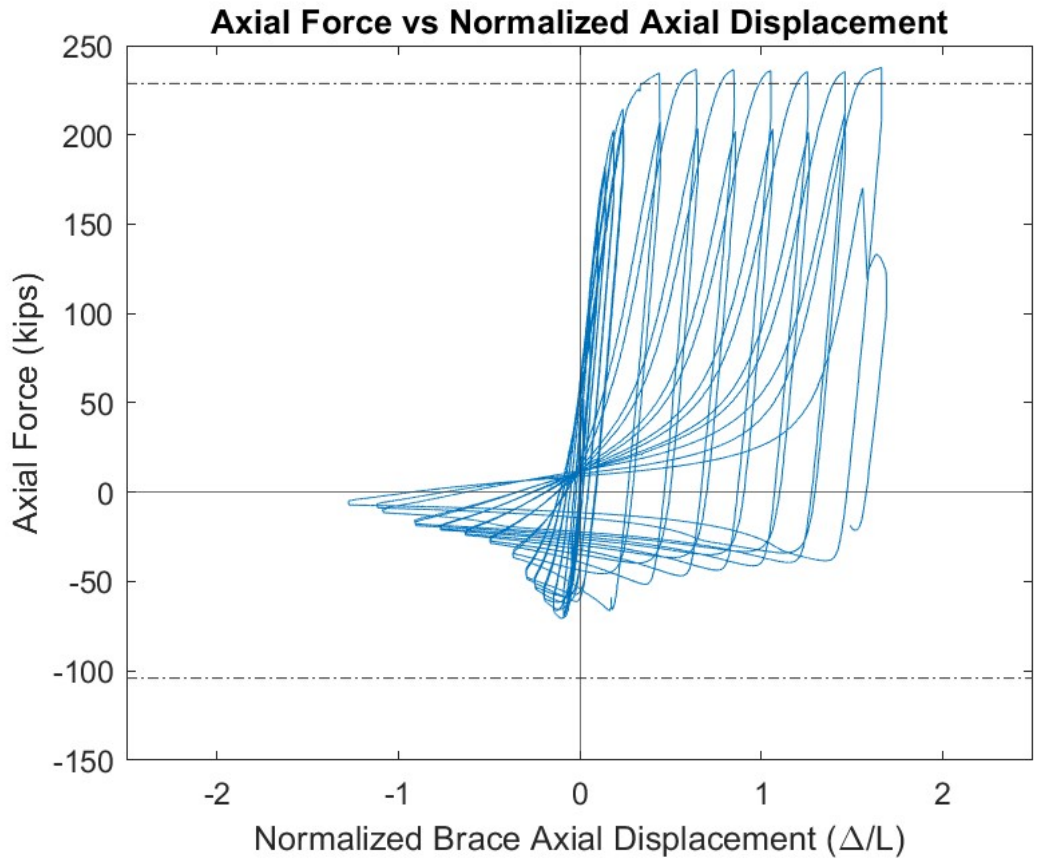

Photos

Peak Out of Plane Displacement: 3.93” C1 cycle

Buckling After Partial Tear: 3.93” C2 cycle

Major Cupping: 3.93” C1 cycle

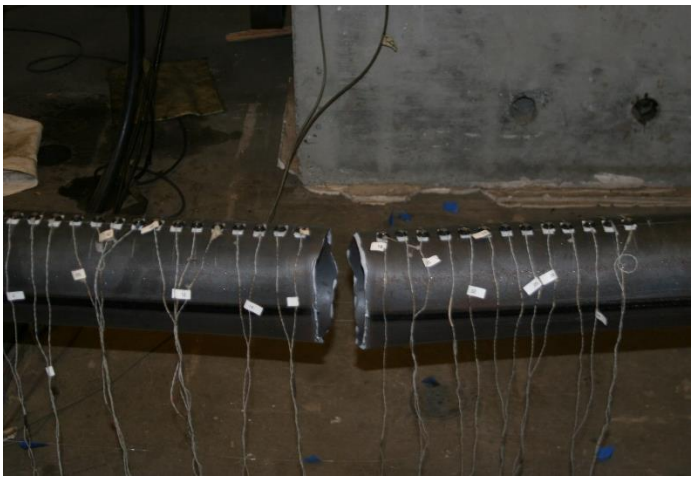

Brace Fracture: 4.39” T1 cycle

AISC Brace Test Summary

Test Name: 6.625x3/16 A500 Long
Test Date: 8/20/24

Brace Properties

Measured Yield Stress (ksi)	56.5
Measured Ultimate Stress (ksi)	76.8
Measured Yield Load (kips)	199
Critical Buckling Load (kips)	106
Percent Elongation – 2" (%)	34.8
Brace Length (in.)	219.5
Global Slenderness Ratio (L_c/r)	96.3

Area (in^2)	3.53
Moment of Inertia (in^4)	18.4
Thickness – Nominal (in.)	0.174
Thickness – Measured (in.)	0.187
Brace Compactness Ratio (D/t) – Nominal	38.1
Brace Compactness Ratio (D/t) – Measured	36.7

Specimen Damage State

Test Event	Axial Brace Deformation (in.)	Target Displacement Cycle (in.)	Force (kips)	$P / P_{(y/c)}$
Peak Tension Load	2.35	2.54 (T1)	206	1.03 (Y)
B1: Initial Global Buckling	-0.22	0.347 (C1)	-73	0.69 (C)
B2: Moderate Global Buckling	-0.58	0.693 (C1)	-53	0.50 (C)
B3-C: Local Cupping	-1.82	2.08 (C1)	-14	0.13 (C)
B3-T: Striations & Tearing	2.35	2.54 (T2)	194	0.97 (Y)
B4-F: Brace Fracture	2.34	3.00 (T1)	98	0.49 (Y)

Key Observations

Cycle #	Target Displacement (in.)	Observations
17-18	2.08	Minor local cupping initiated (~0.3") at C1 peak Moderate local cupping (~0.9") at C2 peak
19-20	2.54	Striations on east face T1 Major local cupping (~1.3") at C1 peak Marker 15 and 16 not visible at compression peak due to cupping Major local cupping (~1.5") at C2 peak, OOP disp. = 20.9" Marker 15 and 16 not visible at compression peak due to cupping
21-22	3.00	Brace Fracture T1

Test Results

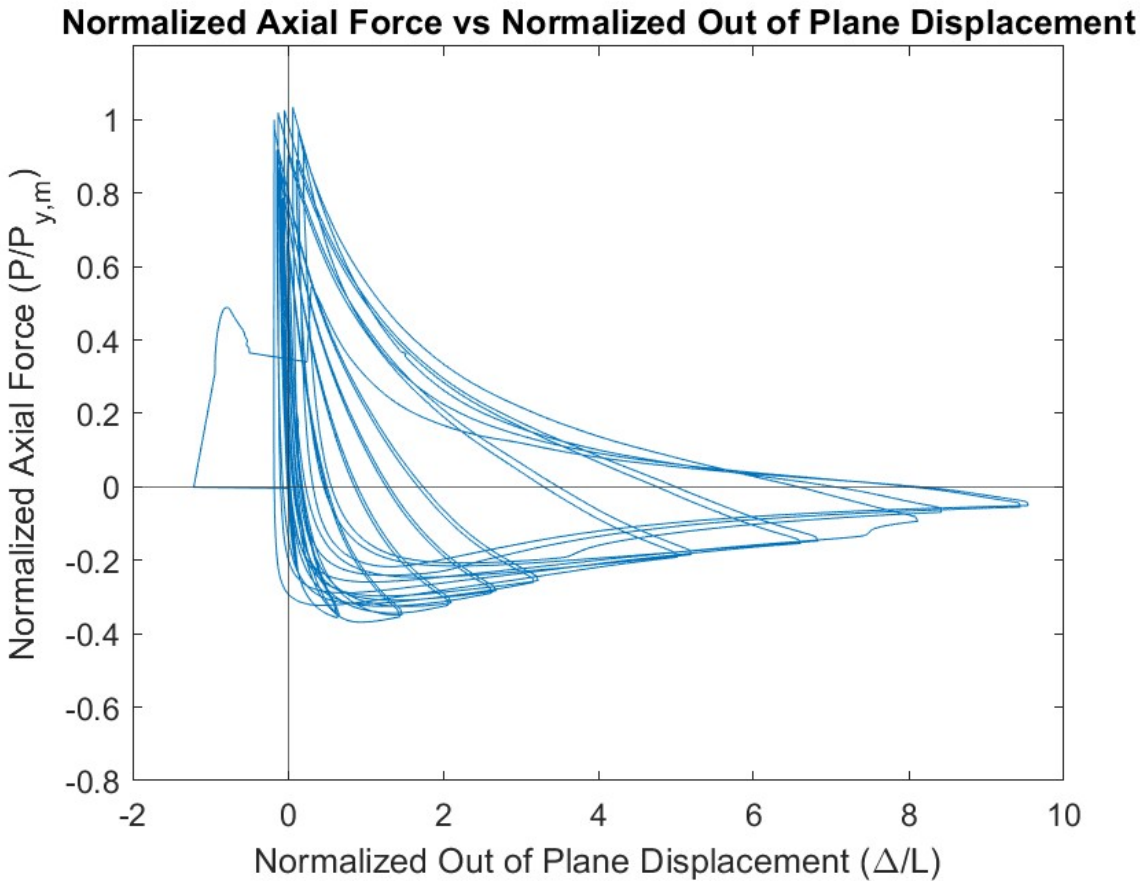

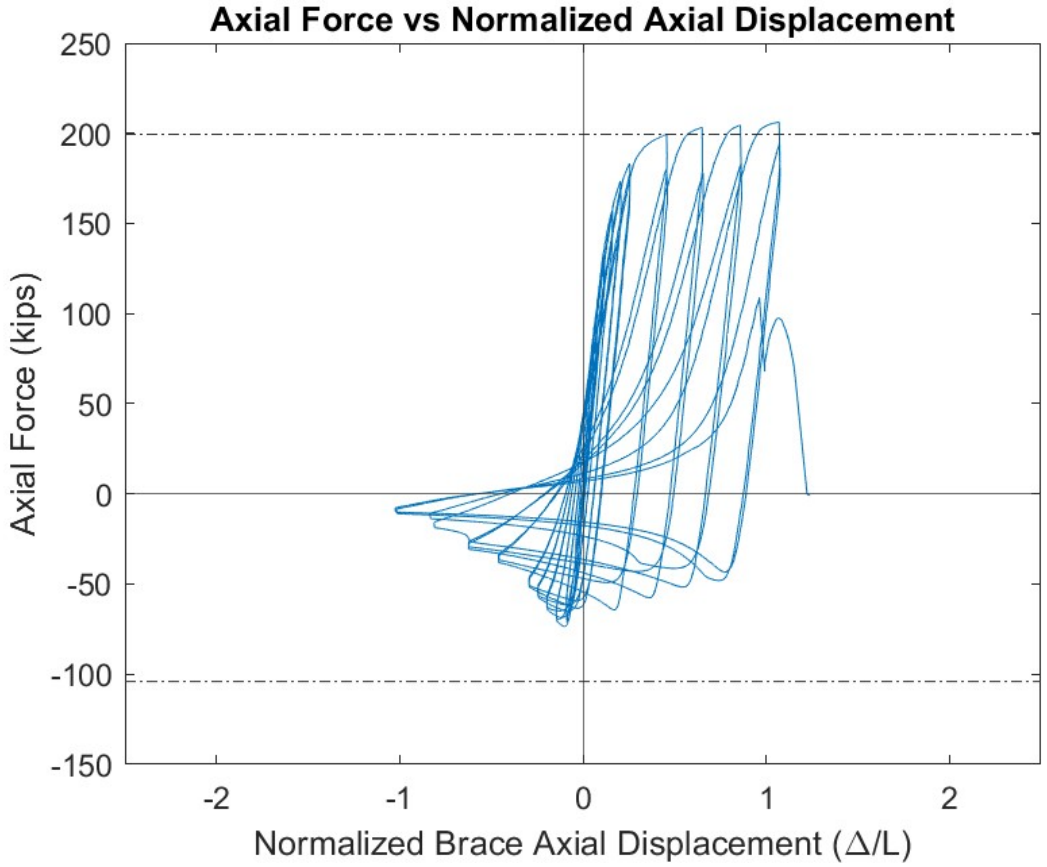

Photos

Peak Out of Plane Displacement: 2.54” C2 cycle

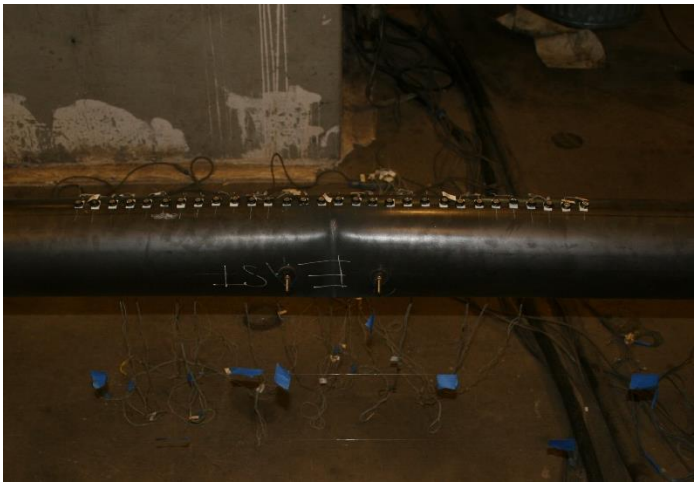

Striations: 2.54” T1 cycle

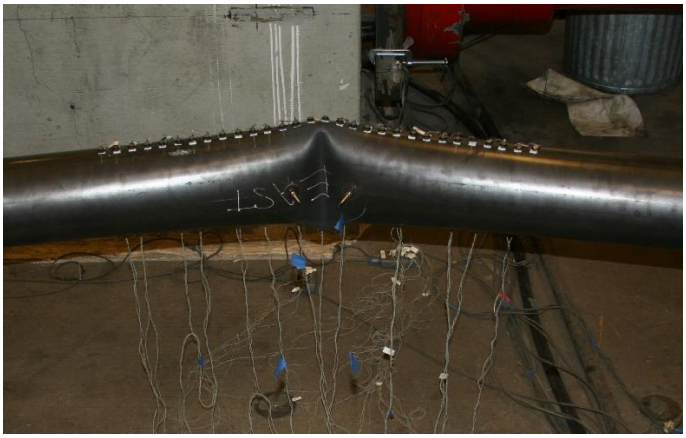

Major Cupping: 2.54” C2 cycle

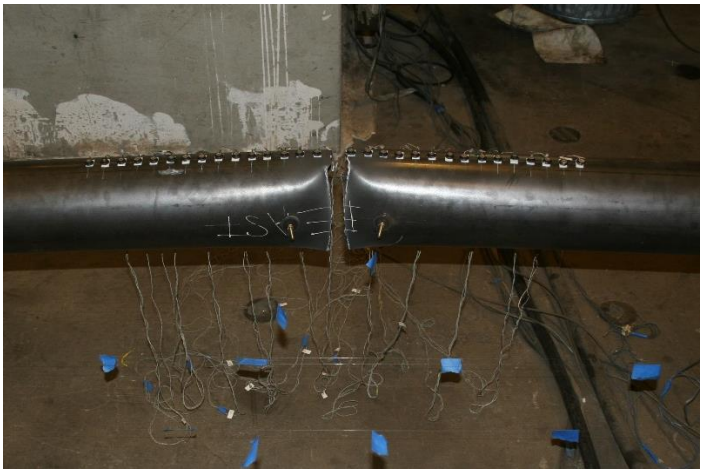

Brace Fracture: 3.00” T1 cycle

AISC Brace Test Summary

Test Name: 6.625x1/4 A500 Long
Test Date: 8/15/24

Brace Properties

Measured Yield Stress (ksi)	59.0
Measured Ultimate Stress (ksi)	74.6
Measured Yield Load (kips)	277
Critical Buckling Load (kips)	140
Percent Elongation – 2" (%)	36.2
Brace Length (in.)	219.5
Global Slenderness Ratio (L_c/r)	97.1

Area (in^2)	4.68
Moment of Inertia (in^4)	23.9
Thickness – Nominal (in.)	0.233
Thickness – Measured (in.)	0.242
Brace Compactness Ratio (D/t) – Nominal	28.4
Brace Compactness Ratio (D/t) – Measured	27.4

Specimen Damage State

Test Event	Axial Brace Deformation (in.)	Target Displacement Cycle (in.)	Force (kips)	$P / P_{(y/c)}$
Peak Tension Load	3.26	3.47 (T1)	283	1.02 (Y)
B1: Initial Global Buckling	-0.19	0.347 (C1)	-114	0.81 (C)
B2: Moderate Global Buckling	-0.62	0.693 (C1)	-73	0.52 (C)
B3-C: Local Cupping	-1.67	2.54 (C2)	-19	0.14 (C)
B3-T: Striations & Tearing	3.26	3.47 (T1)	283	1.02 (Y)
B4-F: Brace Fracture	3.14	3.47 (T2)	104	0.38 (Y)

Key Observations

Cycle #	Target Displacement (in.)	Observations
13-14	1.16	Brace buckled wrong direction (East), C1 – Instrumentation adjusted, see photos
19-20	2.54	Minor local cupping initiated about 1" south of center (~0.5") at C2 peak
21-22	3.00	Major local cupping (~1.3") at C1 peak Major local cupping (~1.6") at C2 peak
23-24	3.47	Striations on east face T1 Major local cupping (~1.8") at C1 peak, OOP disp. = 23.2" Brace Fracture T2

*Minimal optotrak visibility during this test due to buckling direction

Test Results

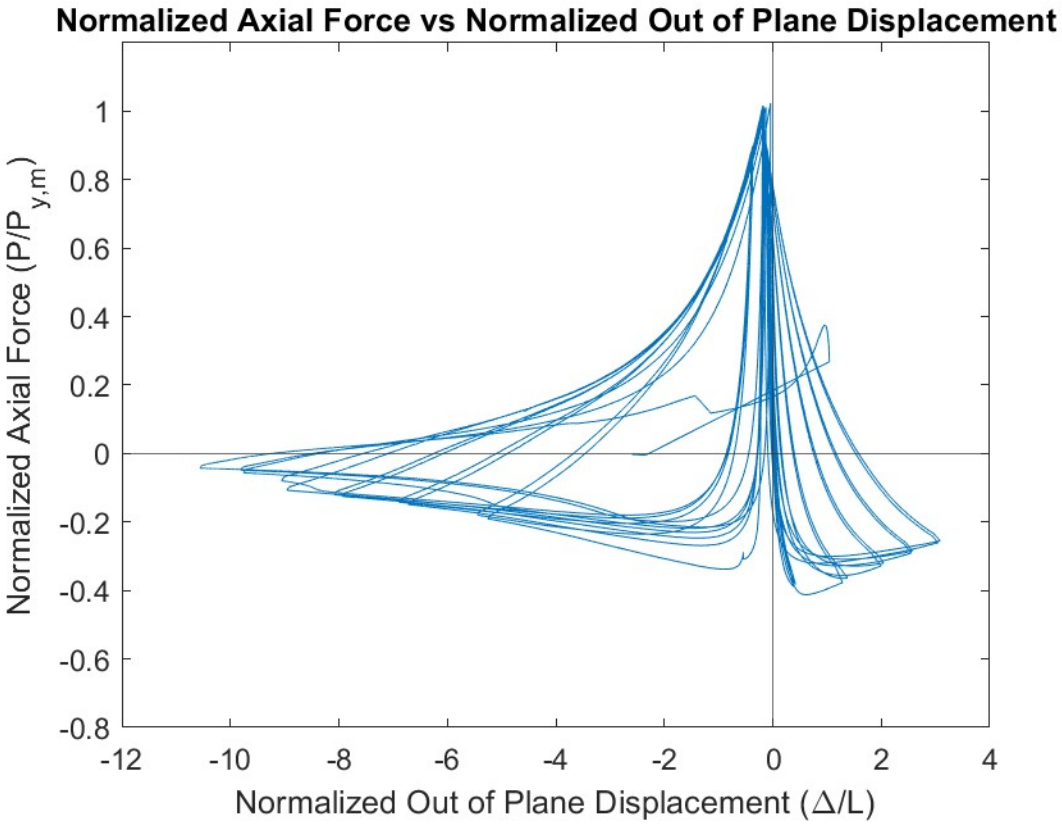

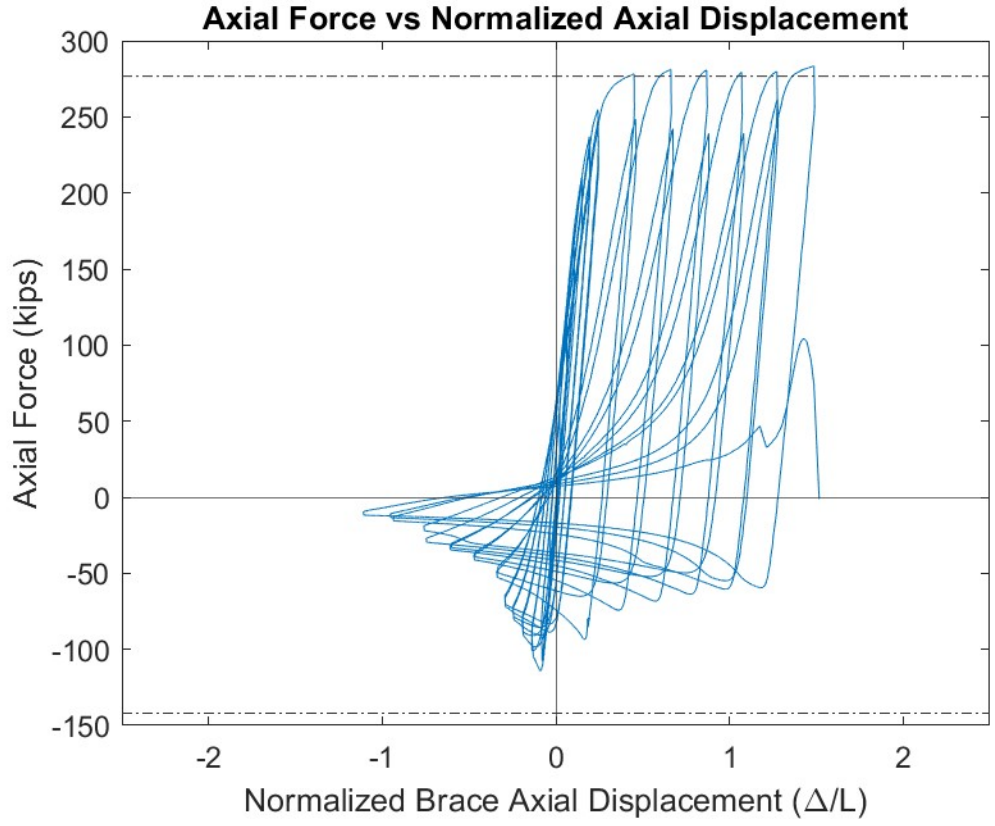

Photos

Peak Out of Plane Displacement (East): 3.47” C1 cycle

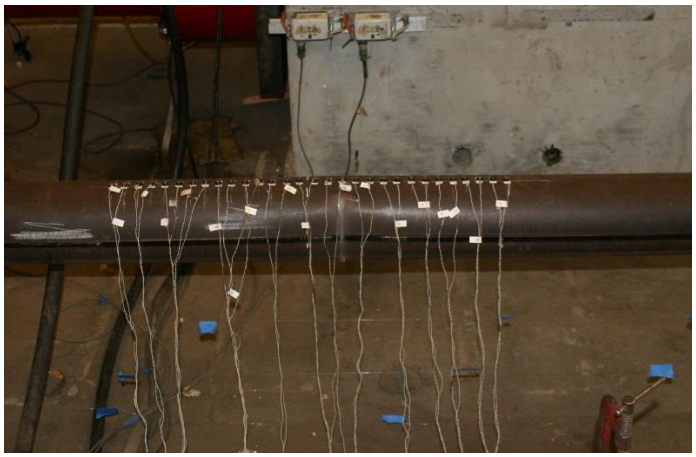

Striations: 3.47” T1 cycle

Major Cupping: 3.47” C1 cycle

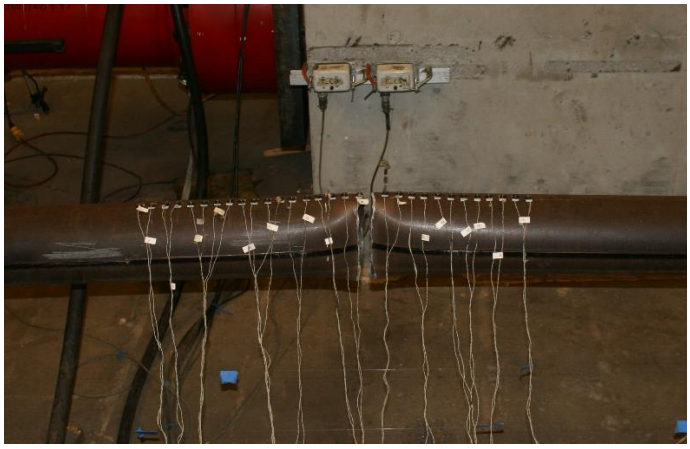

Brace Fracture: 3.47” T2 cycle

AISC Brace Test Summary

Test Name: 6.625x3/8 A500 Long
Test Date: 8/22/24

Brace Properties

Measured Yield Stress (ksi)	58.3
Measured Ultimate Stress (ksi)	63.7
Measured Yield Load (kips)	401
Critical Buckling Load (kips)	199
Percent Elongation – 2" (%)	-
Brace Length (in.)	219.5
Global Slenderness Ratio (L_c/r)	98.9

Area (in^2)	6.88
Moment of Inertia (in^4)	34.0
Thickness – Nominal (in.)	0.349
Thickness – Measured (in.)	0.351
Brace Compactness Ratio (D/t) – Nominal	19.0
Brace Compactness Ratio (D/t) – Measured	18.8

Specimen Damage State

Test Event	Axial Brace Deformation (in.)	Target Displacement Cycle (in.)	Force (kips)	$P / P_{(y/c)}$
Peak Tension Load	1.20	1.62 (T1)	420	1.05 (Y)
B1: Initial Global Buckling	-0.22	0.347 (C1)	-159	0.80 (C)
B2: Moderate Global Buckling	-0.60	0.693 (C1)	-114	0.57 (C)
B3-C: Local Cupping	-2.43	3.00 (C1)	-33	0.17 (C)
B3-T: Striations & Tearing	-3.09	3.47 (T2)	337	0.84 (Y)
B4-F: Brace Fracture	3.31	3.93 (T1)	200	0.50 (Y)

Key Observations

Cycle #	Target Displacement (in.)	Observations
9-10	0.578	Bolt slip south gusset plate – T1
11-12	0.693	Large bolt slip north gusset plate – T1
13-14	1.16	Clicking and bolt slip north and south gusset plate – T1
15-16	1.62	Clicking sounds north gusset plate – T1
21-22	3.00	Minor local cupping initiated (~0.3") at C1 peak about 1" south of center Moderate local cupping (~0.8") at C2 peak
23-24	3.47	Major local cupping (~1.1") at C1 peak Marker 17 and 18 not visible at compression peak due to cupping Striations on east face T2 Major local cupping (~1.3") at C2 peak, OOP disp. = 25.0" Marker 17 and 18 not visible at compression peak due to cupping
25	3.93	Brace Fracture T1

Notes: L_Total String pot zeros out in tension at 0.21"

Test Results

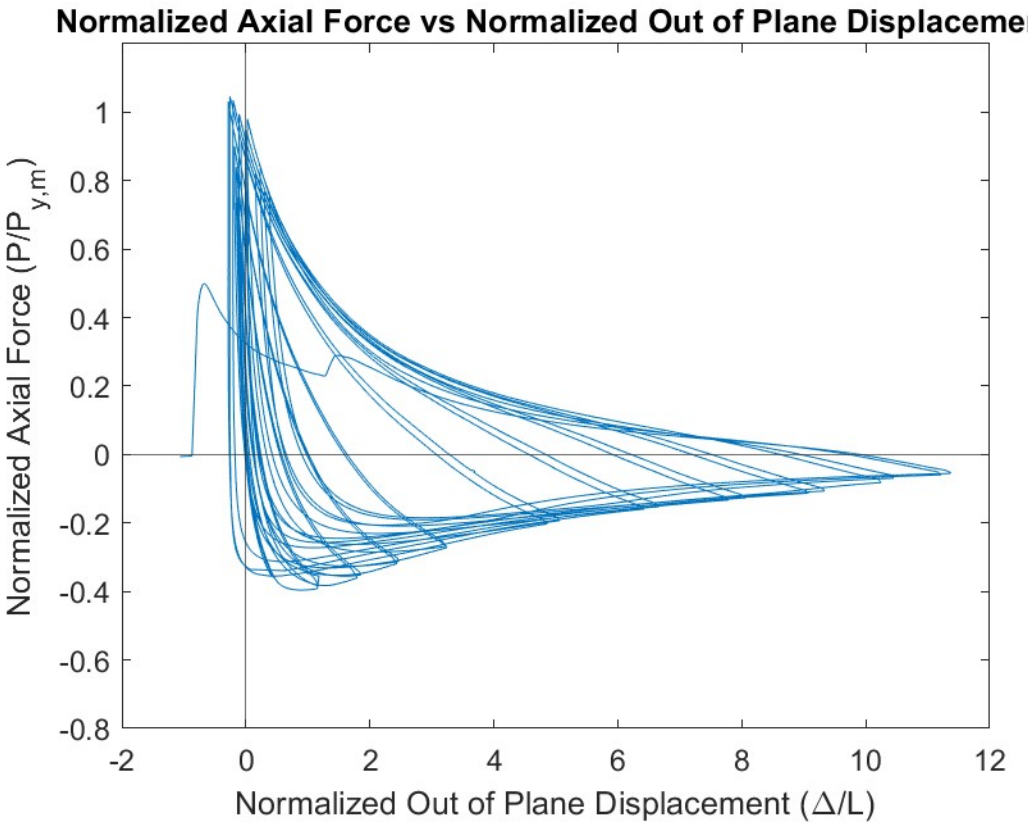

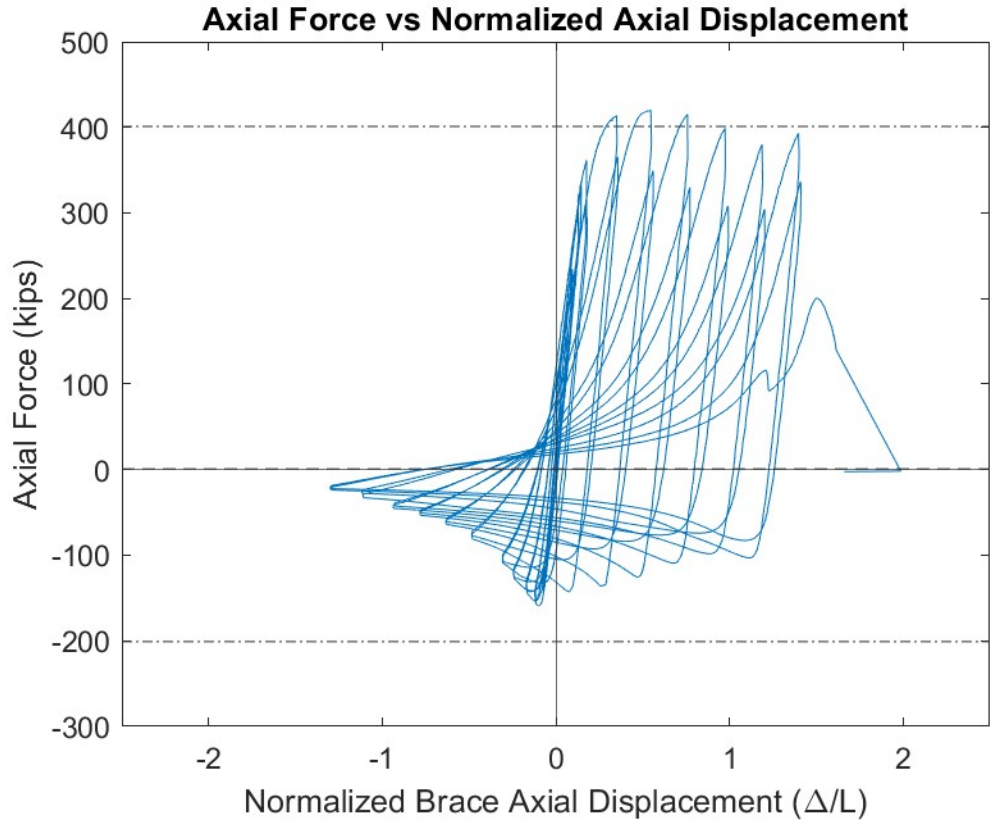

Photos

Peak Out of Plane Displacement: 2.54” C2 cycle

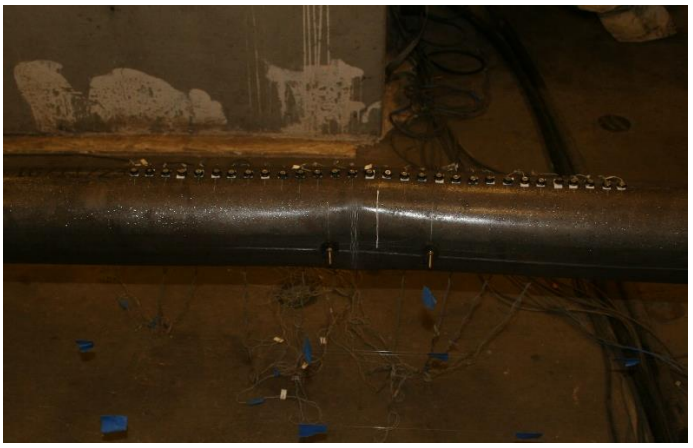

Striations: 2.54” T1 cycle

Major Cupping: 2.54” C2 cycle

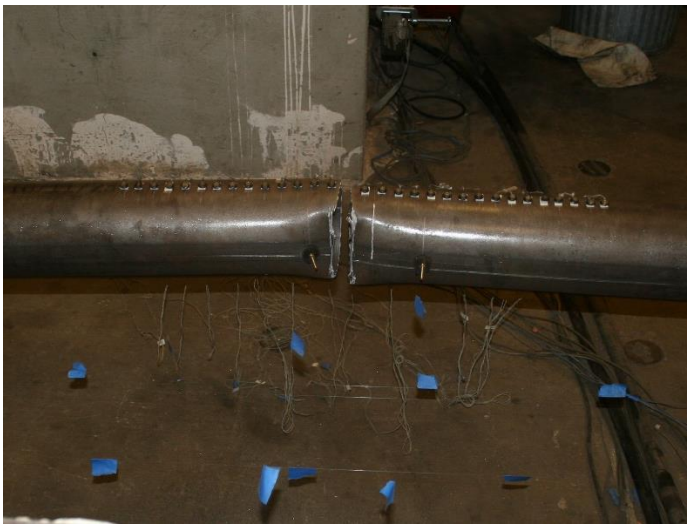

Brace Fracture: 3.00” T1 cycle

AISC Brace Test Summary

Test Name: 6.625x1/2 A500 Long
Test Date: 8/14/24

Brace Properties

Measured Yield Stress (ksi)	63.7
Measured Ultimate Stress (ksi)	66.0
Measured Yield Load (kips)	573
Critical Buckling Load (kips)	254
Percent Elongation – 2" (%)	36.7
Brace Length (in.)	219.5
Global Slenderness Ratio (L_c/r)	100.7

Area (in^2)	9.00
Moment of Inertia (in^4)	42.9
Thickness – Nominal (in.)	0.465
Thickness – Measured (in.)	0.462
Brace Compactness Ratio (D/t) – Nominal	14.2
Brace Compactness Ratio (D/t) – Measured	14.5

Specimen Damage State

Test Event	Axial Brace Deformation (in.)	Target Displacement Cycle (in.)	Force (kips)	$P / P_{(y/c)}$
Peak Tension Load	1.07	1.16 (T1)	522	0.96 (Y)
B1: Initial Global Buckling	-0.13	0.462 (C1)	-244	0.96 (C)
B2: Moderate Global Buckling	-0.40	0.693 (C1)	-164	0.64 (C)
B3-C: Local Cupping	-3.53	4.39 (C1)	-36	0.14 (C)
B3-T: Striations & Tearing	4.37	4.85 (T2)	307	0.53 (Y)
B4-F: Brace Fracture	4.68	5.31 (T1)	224	0.39 (Y)

Key Observations

Cycle #	Target Displacement (in.)	Observations
7-8	0.462	Bolt slip T1 – North and South gusset plate
9-10	0.578	Bolt slip T1 – South gusset plate Clicking T2 – North and South gusset plate
11-12	0.693	Bolt slip T1 – South gusset plate
13-14	1.16	Clicking T1 – North and South gusset plate
21-22	3.00	Transverse string pots checked for remaining line length, C2
23-24	3.47	T_S line adjusted for large compression readings, C1 (* zeros out in tension)
27-28	4.39	Minor local cupping (~0.2") initiated at C1 peak Marker 16 not visible at compression peak Major local cupping (~0.4") at C2 peak Marker 16 and 17 not visible at compression peak
29-30	4.85	Major local cupping (~0.7") at C1 peak Major local cupping (~0.9") at C2 peak, OOP disp = 30.6" Marker 16 and 17 not visible at both compression peaks L_br2 zeroes out during 4.85 compression cycles
31-32	5.31	Partial brace tear T1 Brace Fracture C1

Test Results

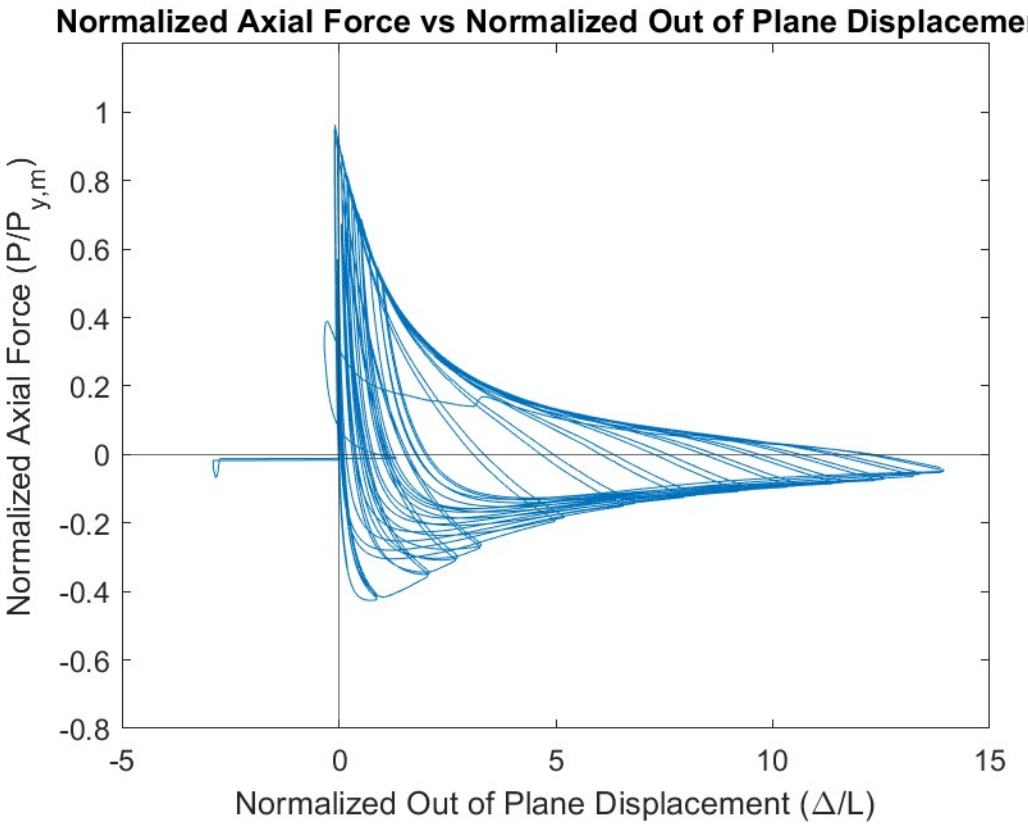

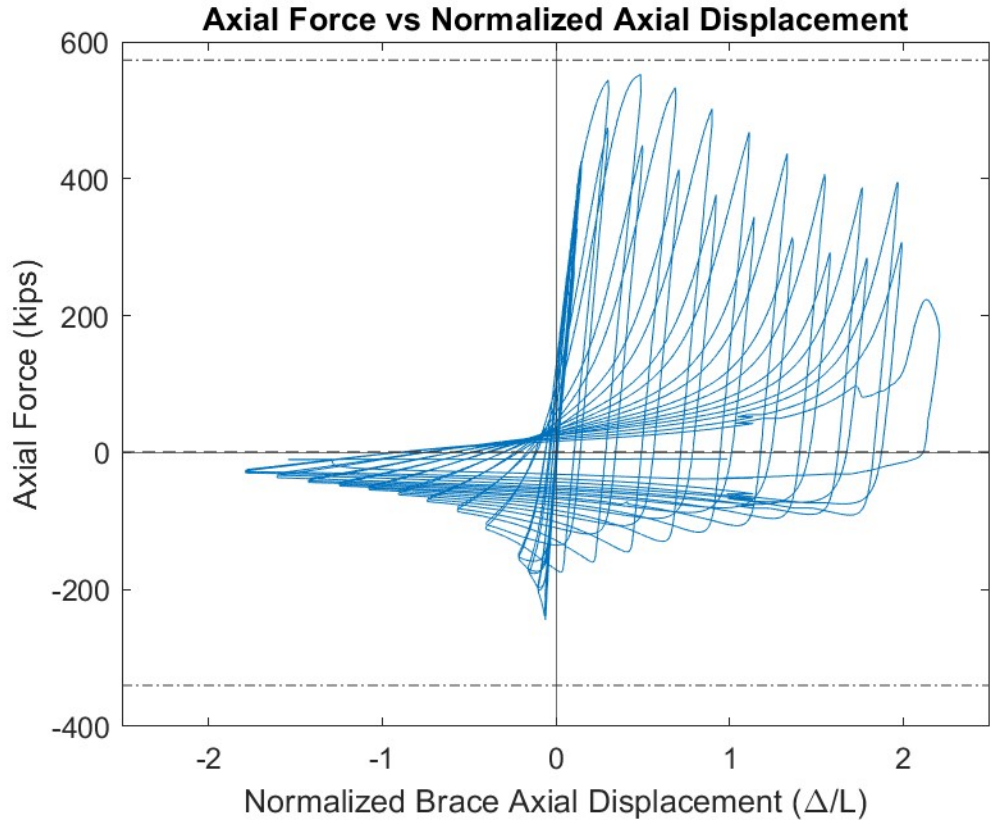

Photos

Peak Out of Plane Displacement: 4.85” C2 cycle

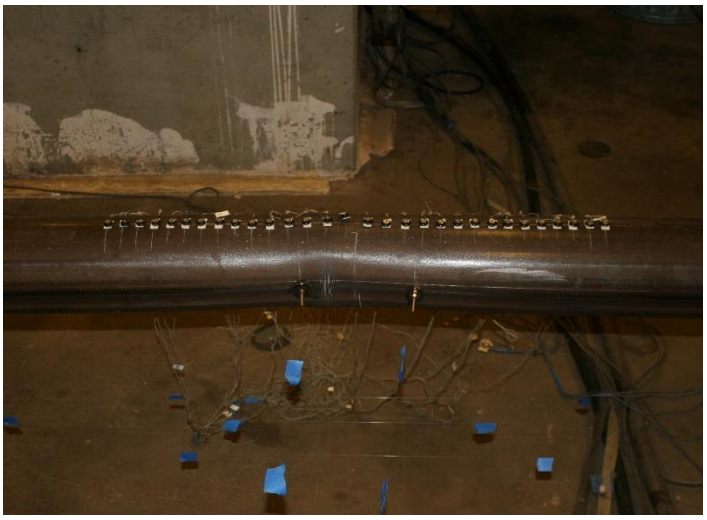

Striations: 4.85” T2 cycle

Major Cupping: 4.85” C2 cycle

Brace Fracture: 5.31” C1 cycle

AISC Brace Test Summary

Test Name: 8.625x3/16 A500 Long
Test Date: 7/10/24

Brace Properties

Measured Yield Stress (ksi)	69.5
Measured Ultimate Stress (ksi)	81.6
Measured Yield Load (kips)	321
Critical Buckling Load (kips)	211
Percent Elongation – 2" (%)	29.5
Brace Length (in.)	219.5
Global Slenderness Ratio (L_c/r)	73.4

Area (in^2)	4.62
Moment of Inertia (in^4)	41.3
Thickness – Nominal (in.)	0.174
Thickness – Measured (in.)	0.199
Brace Compactness Ratio (D/t) – Nominal	49.6
Brace Compactness Ratio (D/t) – Measured	43.4

Specimen Damage State

Test Event	Axial Brace Deformation (in.)	Target Displacement Cycle (in.)	Force (kips)	$P / P_{(y/c)}$
Peak Tension Load	1.55	1.75 (T1)	332	1.03 (Y)
B1: Initial Global Buckling	-0.23	0.375 (C1)	-169	0.80 (C)
B2: Moderate Global Buckling	-0.63	1.25 (C1)	-90	0.43 (C)
B3-C: Local Cupping	-1.01	1.25 (C1)	-57	0.27 (C)
B3-T: Striations & Tearing	1.55	1.75 (T1)	332	1.03 (Y)
B4-F: Brace Fracture	1.37	1.75 (T2)	133	0.41 (Y)

Key Observations

Cycle #	Target Displacement (in.)	Observations
9-10	0.625	Small bolt slip C2 – South gusset plate
11-12	0.75	Very large bolt slip T1 – South gusset plate Clicking sounds T2 – South gusset plate
13-14	1.25	Bolt slip and clicking noises T1 - SGP Minor local cupping (~0.4") initiated approximately 3.5" north of center at C1 peak Small clicking T2 – South gusset plate Major local cupping (~1.1") at C2 peak
15-16	1.75	Striations along east face of brace – T1 Major local cupping (~1.3") at C1 peak, OOP disp. = 15.6" Brace Fracture T2

Test Results

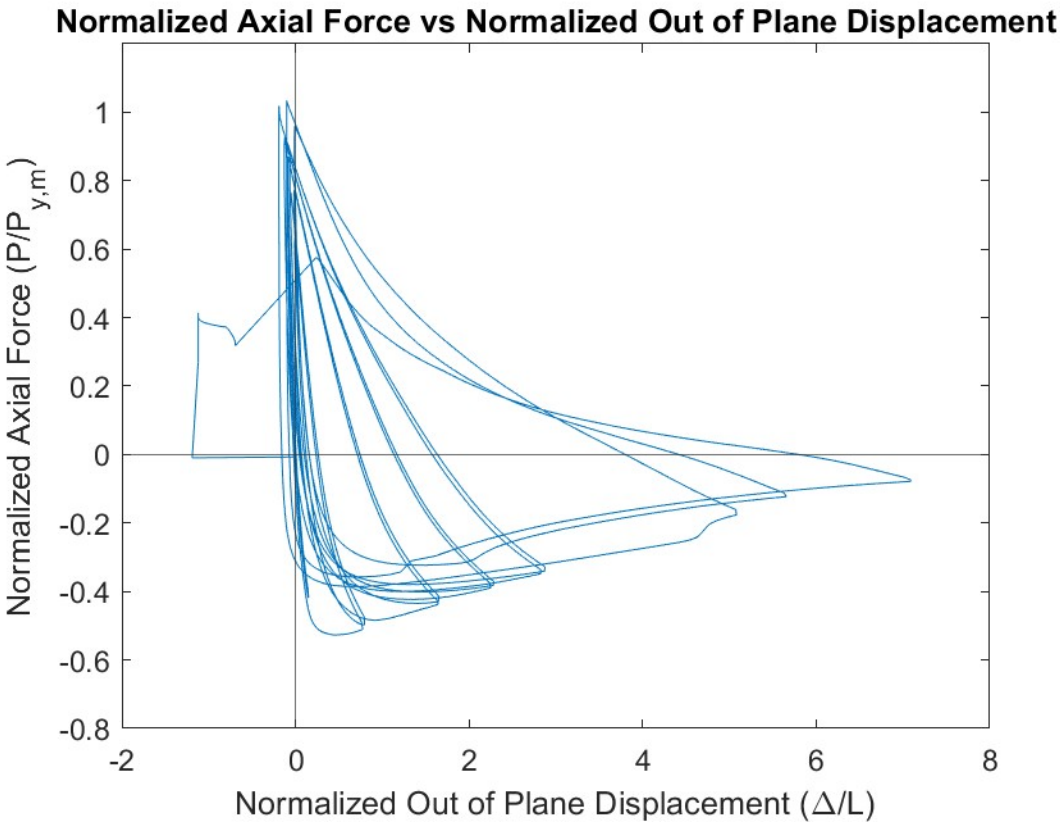

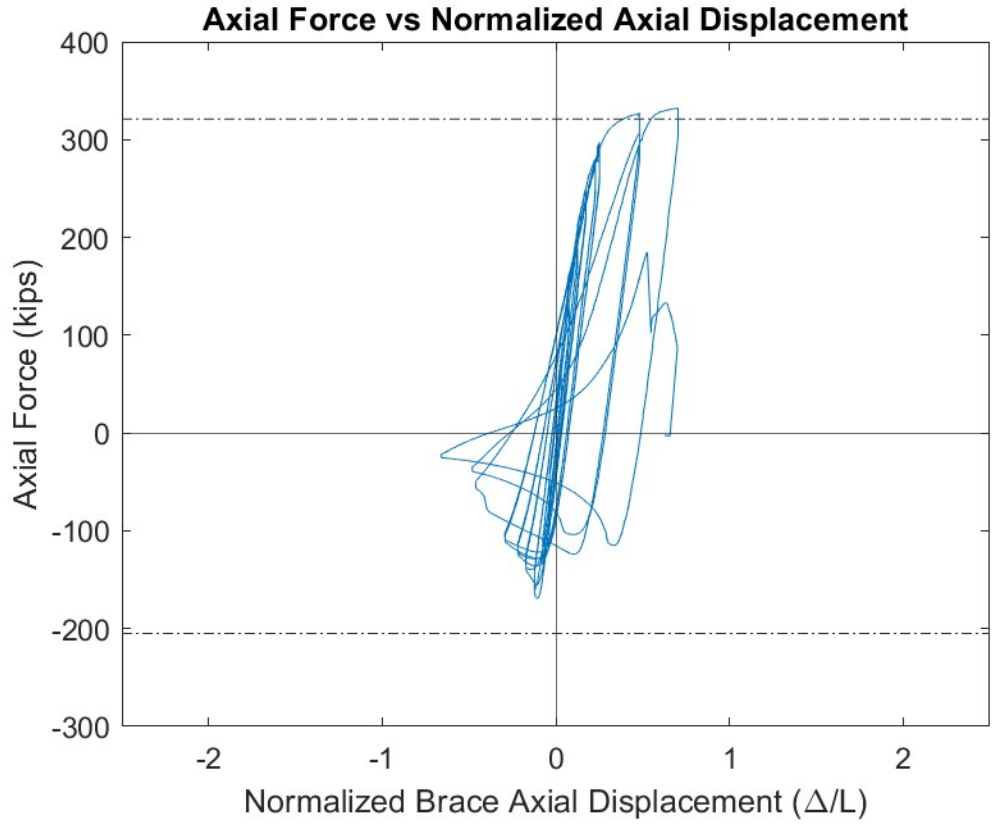

Photos

Peak Out of Plane Displacement: 1.75” Cycles

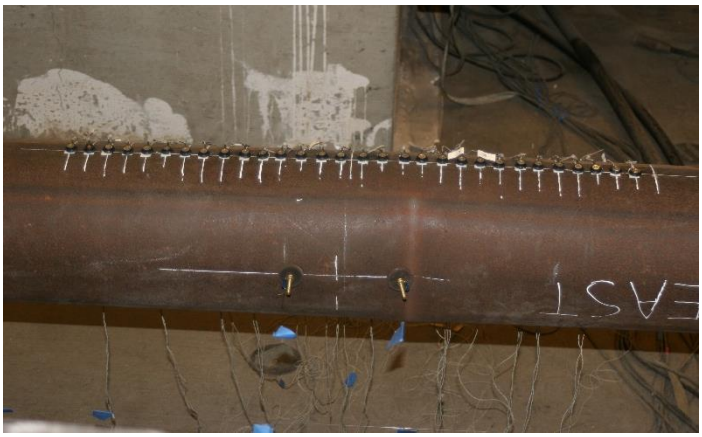

Striations along east face of brace: T1 1.75” cycle

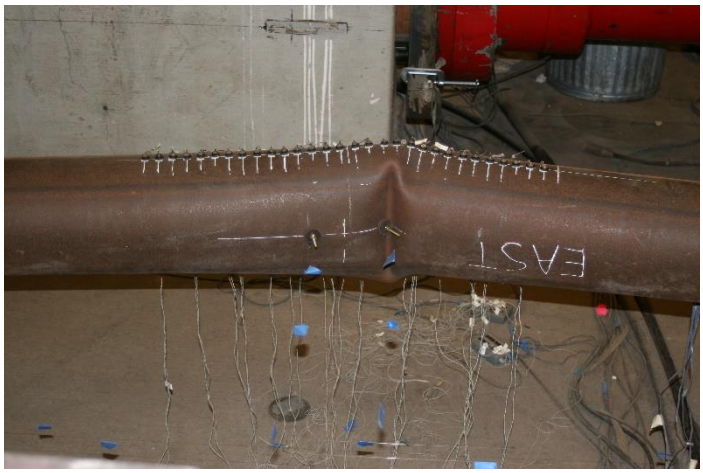

Major Cupping: 1.75” C1 cycle

Brace Fracture: 1.75” T2 cycle

AISC Brace Test Summary

Test Name: 8.625x1/4 A500 Long
Test Date: 7/30/24

Brace Properties

Measured Yield Stress (ksi)	67.0
Measured Ultimate Stress (ksi)	79.5
Measured Yield Load (kips)	411
Critical Buckling Load (kips)	275
Percent Elongation – 2" (%)	30.3
Brace Length (in.)	219.5
Global Slenderness Ratio (L_c/r)	73.9

Area (in^2)	6.14
Moment of Inertia (in^4)	54.1
Thickness – Nominal (in.)	0.233
Thickness – Measured (in.)	0.243
Brace Compactness Ratio (D/t) – Nominal	37.0
Brace Compactness Ratio (D/t) – Measured	35.6

Specimen Damage State

Test Event	Axial Brace Deformation (in.)	Target Displacement Cycle (in.)	Force (kips)	$P / P_{(y/c)}$
Peak Tension Load	1.79	2.25 (T1)	419	1.02 (Y)
B1: Initial Global Buckling	-0.27	0.375 (C1)	-226	0.82 (C)
B2: Moderate Global Buckling	-0.77	1.25 (C1)	-118	0.43 (C)
B3-C: Local Cupping	-1.58	1.75 (C1)	-42	0.15 (C)
B3-T: Striations & Tearing	1.79	2.25 (T1)	419	1.02 (Y)
B4-F: Brace Fracture	1.65	2.25 (T2)	130	0.32 (Y)

Key Observations

Cycle #	Target Displacement (in.)	Observations
5-6	0.375	Small clicking sounds T1 and T2 – South gusset plate
7-8	0.5	Clicking sounds T1 and T2 – South gusset plate
9-10	0.625	Clicking sounds T1 and T2 – South gusset plate
11-12	0.75	Large bolt slip T1 – South gusset plate Clicking sounds T2 – South gusset plate
13-14	1.25	Large bolt slip T1 – North gusset plate Lots of clicking sounds T2 – North and South gusset plate
15-16	1.75	Bolt slip and clicking noises T1 - SGP Major local cupping (~1") initiated approximately 1.5" north of center at C1 peak Optotrak marker 15 not visible at C1 peak due to cupping Major local cupping (~1.2") at C2 peak Optotrak marker 14 and 15 not visible at C1 peak due to cupping
17-18	2.25	Striations along east face of brace – T1 Major local cupping (~1.4") at C1 peak, OOP disp. = 18.4" Brace Fracture T2

Test Results

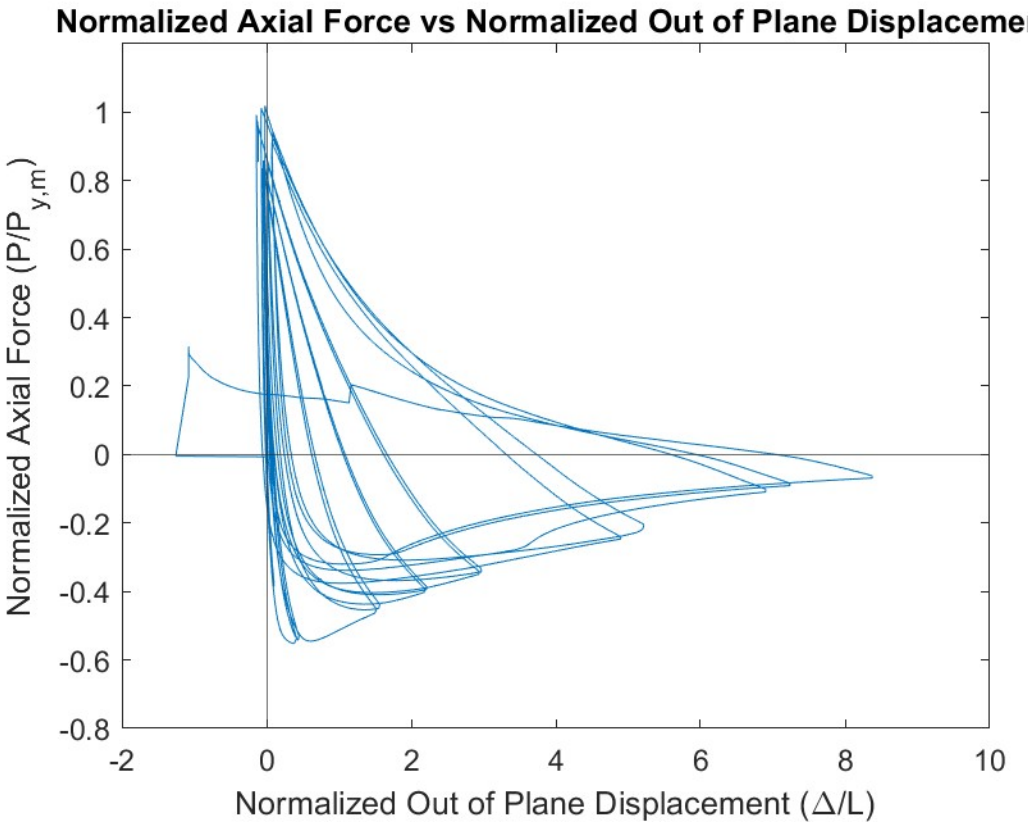

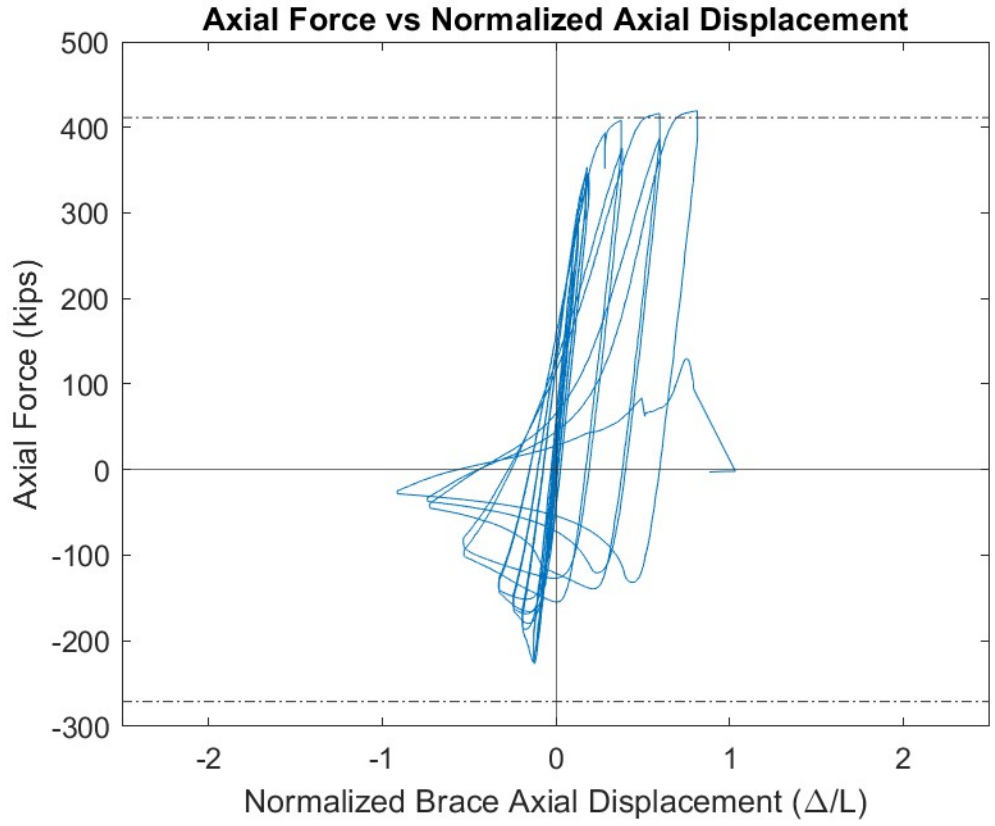

Photos

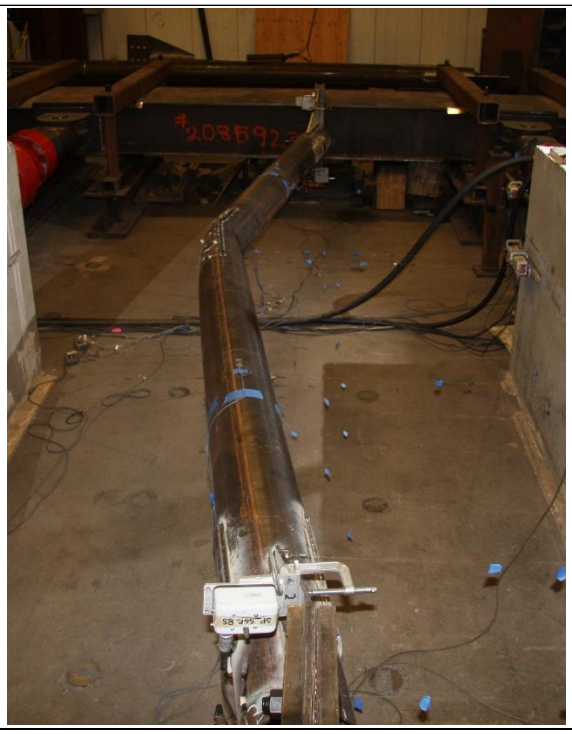

Peak Out of Plane Displacement: 2.25” Cycles

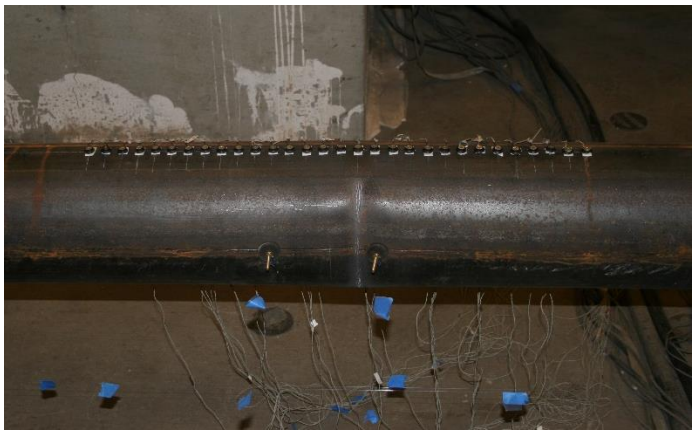

Striations along east face of brace: T1 2.25” cycle

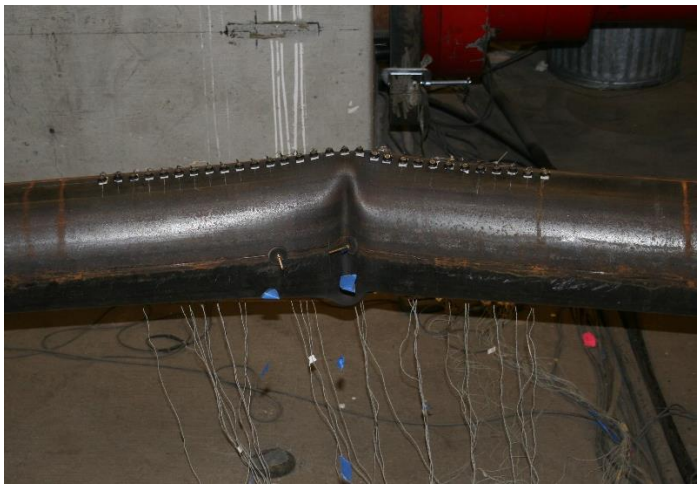

Major Cupping: 2.25” C1 cycle

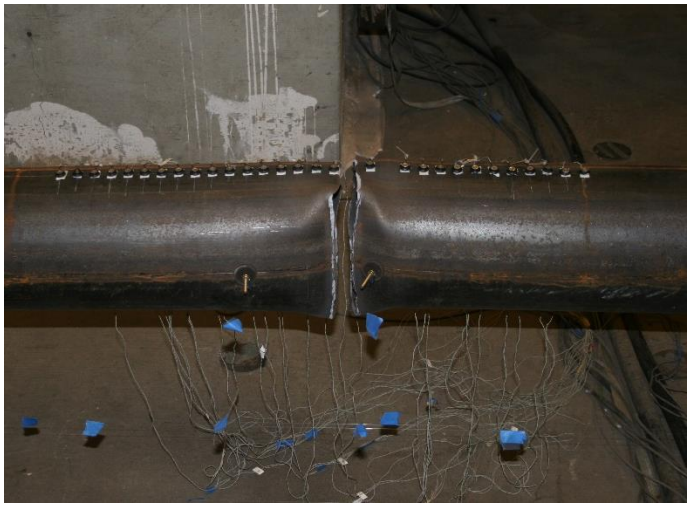

Brace Fracture: 2.25” T2 cycle

AISC Brace Test Summary

Test Name: 8.625x3/8 A500 Long
Test Date: 7/31/24

Brace Properties

Measured Yield Stress (ksi)	65.7
Measured Ultimate Stress (ksi)	75.2
Measured Yield Load (kips)	596
Critical Buckling Load (kips)	396
Percent Elongation – 2" (%)	36.0
Brace Length (in.)	219.5
Global Slenderness Ratio (L_c/r)	74.9

Area (in^2)	9.07
Moment of Inertia (in^4)	77.8
Thickness – Nominal (in.)	0.349
Thickness – Measured (in.)	0.354
Brace Compactness Ratio (D/t) – Nominal	24.7
Brace Compactness Ratio (D/t) – Measured	24.4

Specimen Damage State

Test Event	Axial Brace Deformation (in.)	Target Displacement Cycle (in.)	Force (kips)	$P / P_{(y/c)}$
Peak Tension Load	0.99	2.75 (T1)	579	0.97 (Y)
B1: Initial Global Buckling	-0.29	0.5 (C1)	-311	0.79 (C)
B2: Moderate Global Buckling	-0.91	1.25 (C1)	-165	0.42 (C)
B3-C: Local Cupping	-1.88	2.25 (C1)	-80	0.20 (C)
B3-T: Striations & Tearing	1.99	2.75 (T2)	527	0.88 (Y)
B4-F: Brace Fracture	2.07	3.25 (T1)	212	0.36 (Y)

Key Observations

Cycle #	Target Displacement (in.)	Observations
7-8	0.5	Clicking sounds C1 and C2 – South gusset plate Bolt slip T2 – South gusset plate
9-10	0.625	Large bolt slip T1 – North gusset plate: SP_SGP_BS lessened during slip but was tightened back on when actuators returned to zero displacement Clicking sounds T2 – South and North gusset plate
11-12	0.75	Clicking sounds all cycles – South and North gusset plate
13-14	1.25	Clicking sounds all cycles – South and North gusset plate
15-16	1.75	Clicking sounds all cycles – South and North gusset plate
17-18	2.25	Minor local cupping (~0.1") initiated at C1 peak Moderate local cupping (~0.9") at C2 peak Optotrak marker 15 not visible at C2 peak due to cupping
19-20	2.75	Bolt slip T1 – South gusset plate Major local cupping (~1.4") at C1 peak Optotrak marker 15 not visible at C1 peak due to cupping Striations along east face of brace – T2 Major local cupping (~1.6") at C2 peak, OOP disp. = 21.0" Optotrak marker 15 and 16 not visible at C2 peak due to cupping
21-22	3.25	Brace Fracture T1

Test Results

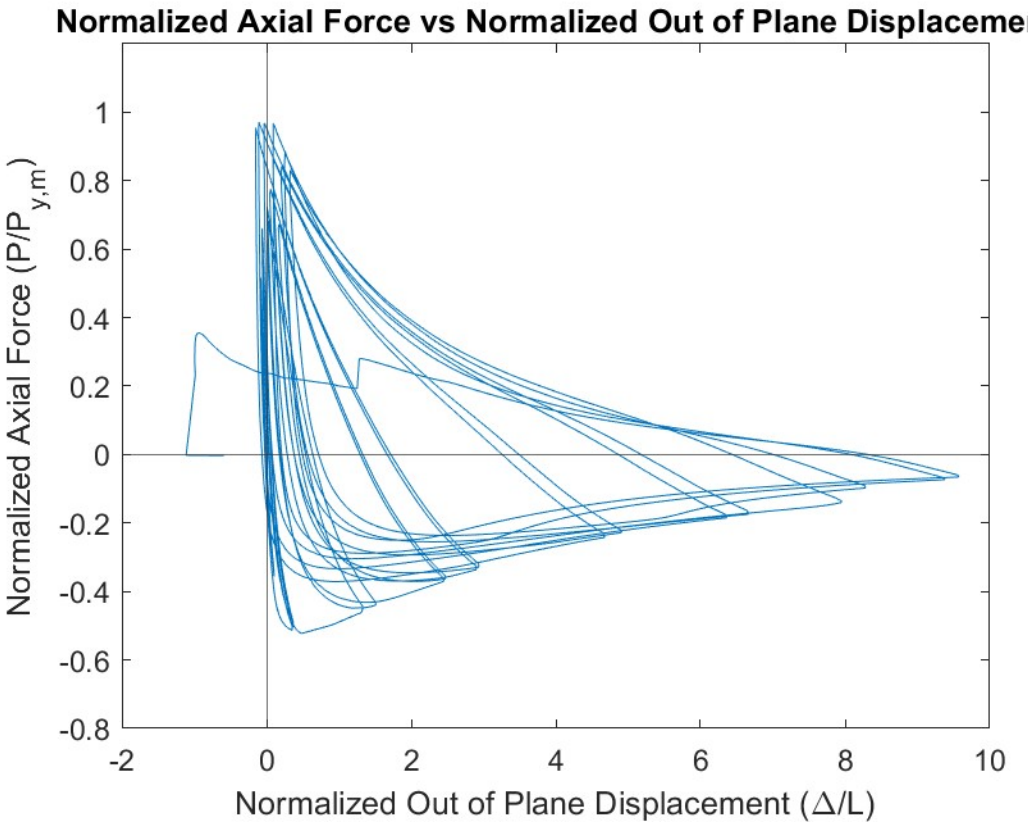

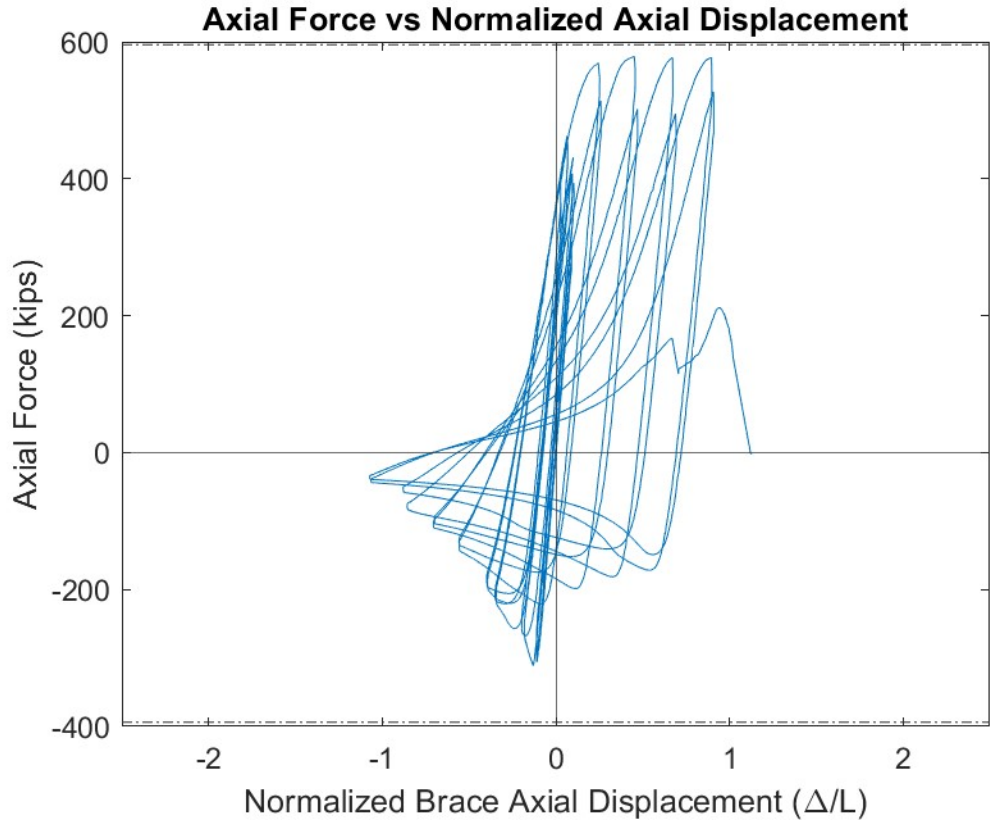

Photos

Peak Out of Plane Displacement: 2.75” Cycles

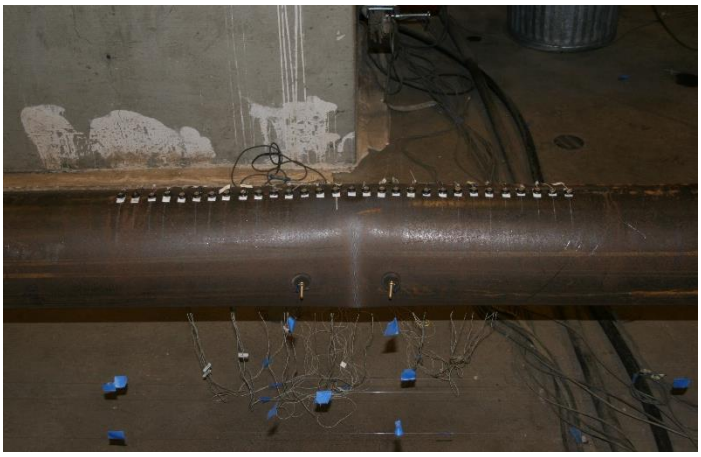

Striations along east face of brace: T2 2.75” cycle

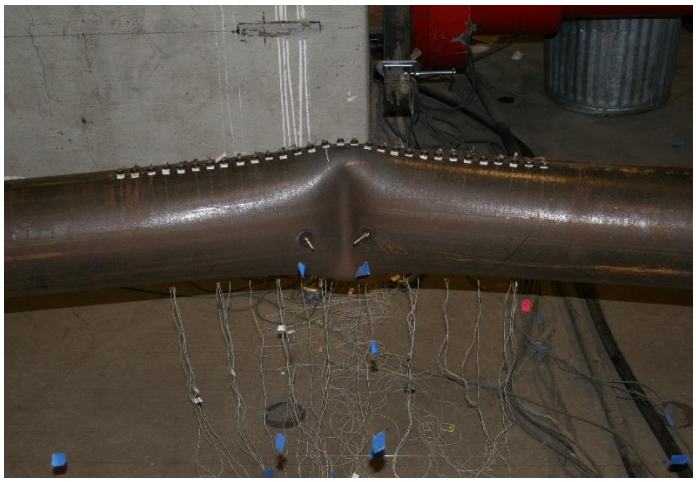

Major Cupping: 2.75” C2 cycle

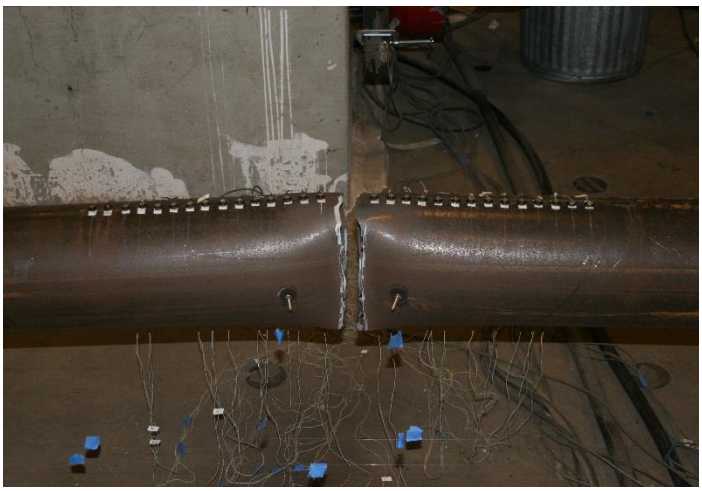

Brace Fracture: 3.25” T1 cycle

AISC Brace Test Summary

Test Name: 10.75x1/4 A500 Long
Test Date: 8/1/24

Brace Properties

Measured Yield Stress (ksi)	62.7
Measured Ultimate Stress (ksi)	74.8
Yield Load (kips)	450
Critical Buckling Load (kips)	400
Percent Elongation – 2" (%)	34.2
Brace Length (in.)	219.5
Global Slenderness Ratio (L_c/r)	59.0

Area (in^2)	7.15
Moment of Inertia (in^4)	85.3
Thickness – Nominal (in.)	0.233
Thickness – Measured (in.)	0.249
Brace Compactness Ratio (D/t) – Nominal	46.1
Brace Compactness Ratio (D/t) – Measured	43.2

Specimen Damage State

Test Event	Axial Brace Deformation (in.)	Target Displacement Cycle (in.)	Force (kips)	$P / P_{(y/c)}$
Peak Tension Load	1.35	1.75 (T1)	468	1.04 (Y)
B1: Initial Global Buckling	-0.24	0.375 (C1)	-268	0.67 (C)
B2: Moderate Global Buckling	-0.80	1.25 (C1)	-84	0.21 (C)
B3-C: Local Cupping	-1.01	1.25 (C1)	-112	0.28 (C)
B3-T: Striations & Tearing	1.21	1.75 (T2)	336	0.75 (Y)
B4-F: Brace Fracture	1.54	2.25 (T1)	130	0.29 (Y)

Key Observations

Cycle #	Target Displacement (in.)	Observations
7-8	0.5	Large bolt slip T1 – North gusset plate Clicking sounds T2 – North gusset plate
9-10	0.625	Bolt slip T1 – South gusset plate Clicking sounds T1 and T2 – North gusset plate
11-12	0.75	Large bolt slip T1 – South gusset plate Clicking sounds all cycles – South and North gusset plate
13-14	1.25	Minor local cupping (~0.4") at C1 peak Major local cupping (~1.1") at C2 peak
15-16	1.75	Striations along east face of brace – T1 Major local cupping (~1.8") at C1 peak Optotrak marker 15 not visible at C1 peak due to cupping Partial Brace Tear T2: L_Br2 came off due to partial brace tear Major local cupping (~1.9") at C2 peak, OOP disp = 16.2" Optotrak marker 15 and 16 not visible at C2 peak due to cupping
17-18	2.25	Brace Fracture T1

Test Results

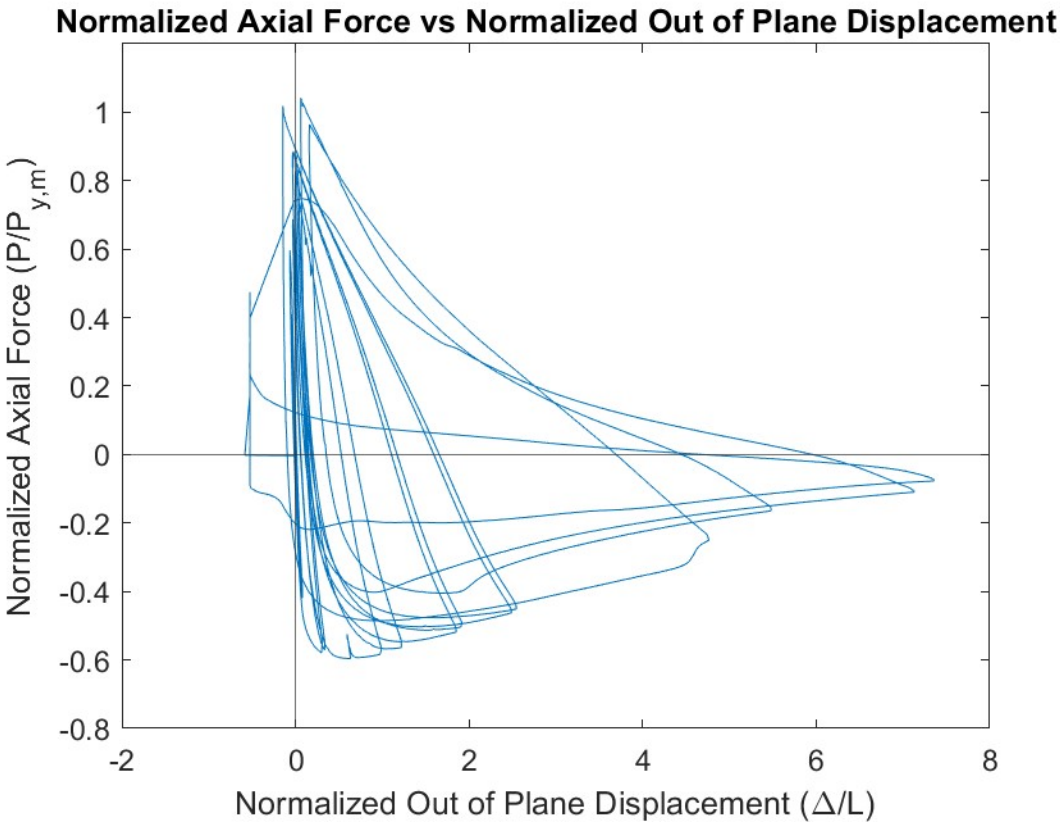

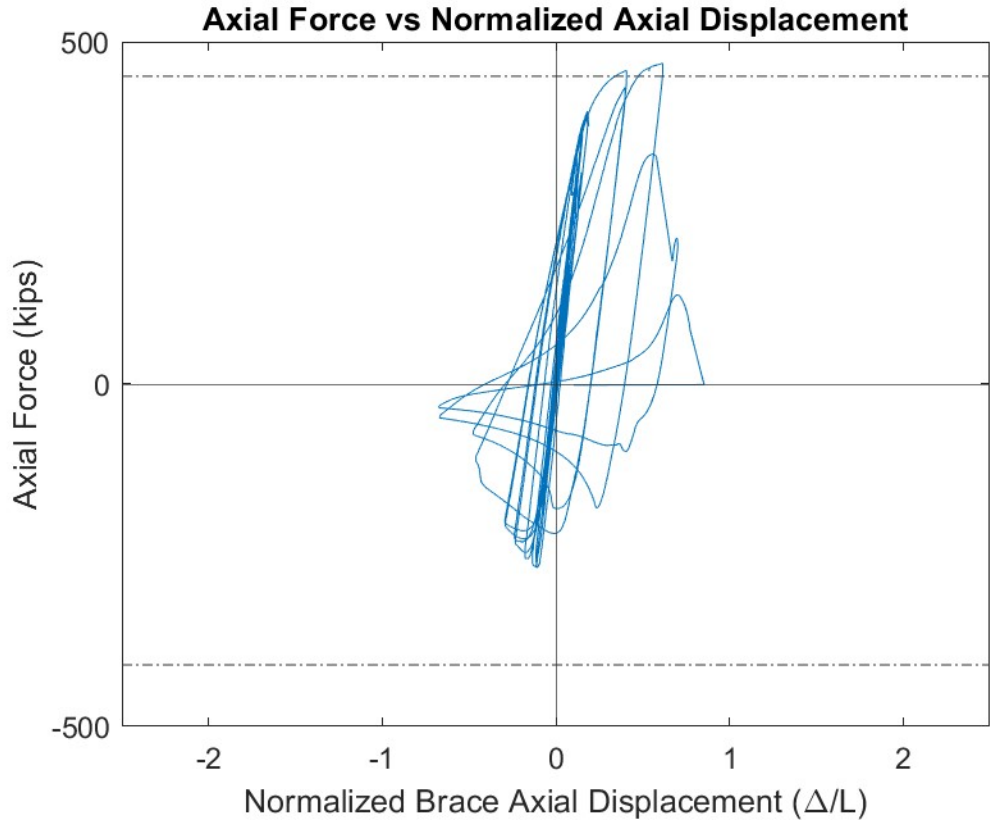

Photos

Peak Out of Plane Displacement: 1.75” Cycles

Partial Brace Tear: T2 1.75” cycle

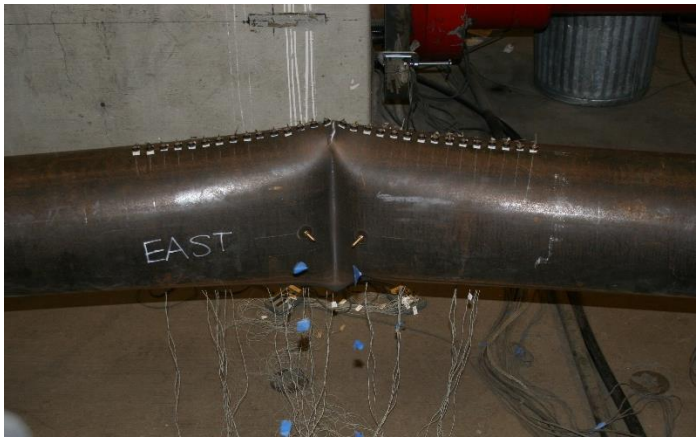

Major Cupping: 1.75” C2 cycle

Brace Fracture: 2.25” T1 cycle

AISC Brace Test Summary

Test Name: 10.75x0.365 A500 Long
Test Date: 8/6/24

Brace Properties

Measured Yield Stress (ksi)	60.4
Measured Ultimate Stress (ksi)	77.0
Measured Yield Load (kips)	670
Critical Buckling Load (kips)	558
Percent Elongation – 2" (%)	35.6
Brace Length (in.)	219.5
Global Slenderness Ratio (L_c/r)	59.6

Area (in^2)	11.1
Moment of Inertia (in^4)	150
Thickness – Nominal (in.)	0.339
Thickness – Measured (in.)	0.349
Brace Compactness Ratio (D/t) – Nominal	31.7
Brace Compactness Ratio (D/t) – Measured	30.8

Specimen Damage State

Test Event	Axial Brace Deformation (in.)	Target Displacement Cycle (in.)	Force (kips)	$P / P_{(y/c)}$
Peak Tension Load	1.75	2.08 (T1)	677	1.01 (Y)
B1: Initial Global Buckling	-0.39	0.462 (C1)	-400	0.72 (C)
B2: Moderate Global Buckling	-1.09	1.62 (C1)	-212	0.38 (C)
B3-C: Local Cupping	-1.43	1.62 (C2)	-123	0.22 (C)
B3-T: Striations & Tearing	1.75	2.08 (T2)	629	0.94 (Y)
B4-F: Brace Fracture	2.08	2.54 (T1)	306	0.46 (Y)

Key Observations

Cycle #	Target Displacement (in.)	Observations
5-6	0.347	Bolt slip C1 – South Gusset Plate
7-8	0.462	Bolt slip all cycles, very noisy – South Gusset plate
9-10	0.578	Bolt slip all cycles, very noisy – South Gusset plate SP_SGP_E fell off due to bolt slip, C1 but was reattached when actuator load = 0
11-12	0.693	SP_NGP_E fell off due to bolt slip, T1 but was reattached when actuator load = 0
13-14	1.16	Lots of clicking sounds all cycles – North and South gusset plate Bolt slip T1 – North gusset plate SP_NGP_E fell off due to bolt slip, T1 but was reattached when actuator load = 0 SP_L_br was loose and tightened back on.
15-16	1.62	Lots of clicking sounds all cycles – North and South gusset plate Bolt slip T1 – South gusset plate Moderate local cupping (~0.7") at C2 peak
17-18	2.08	Major local cupping (~1.5") at C1 peak Optotrak marker 14 and 15 not visible at C2 peak due to cupping Striations along east face of brace – T2 Pumps unexpectantly shut off while the actuators were paused for instrumentation to be adjusted. Actuators sat for 2 hours while pumps were checked. Test resumed Major local cupping (~1.7") at C2 peak, OOP disp. = 17.3" Optotrak marker 15 and 16 not visible at C2 peak due to cupping
19	2.54	Brace Fracture T1

Test Results

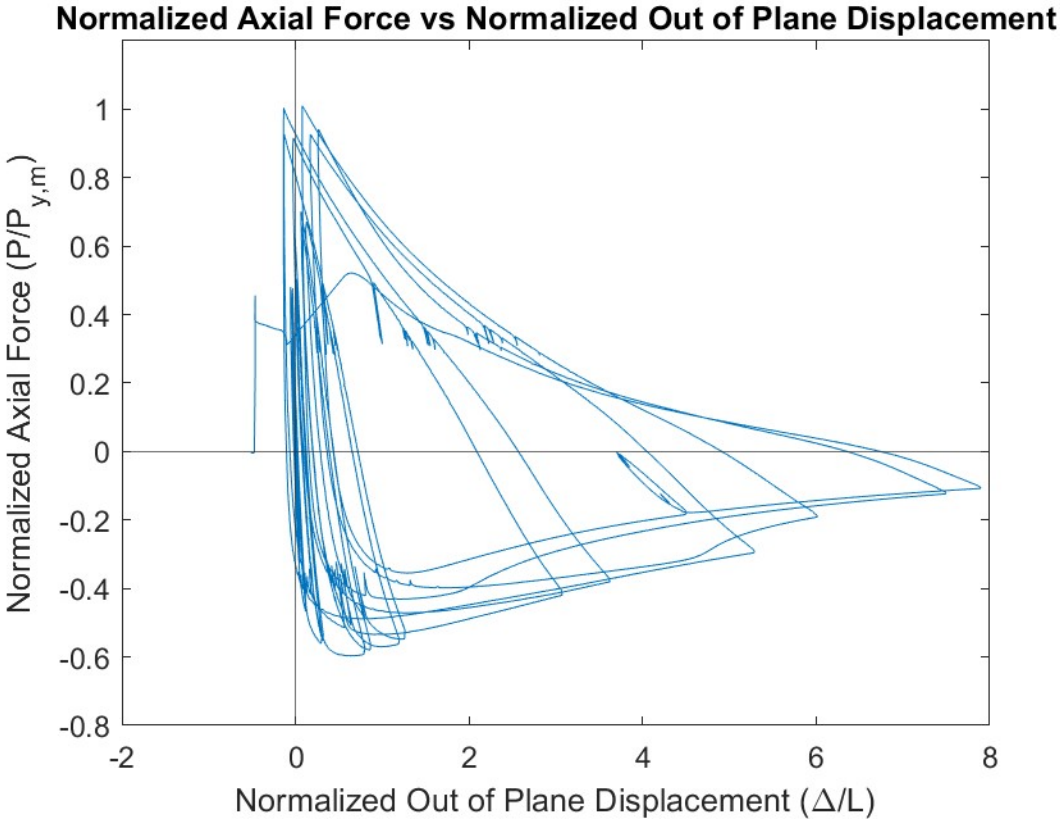

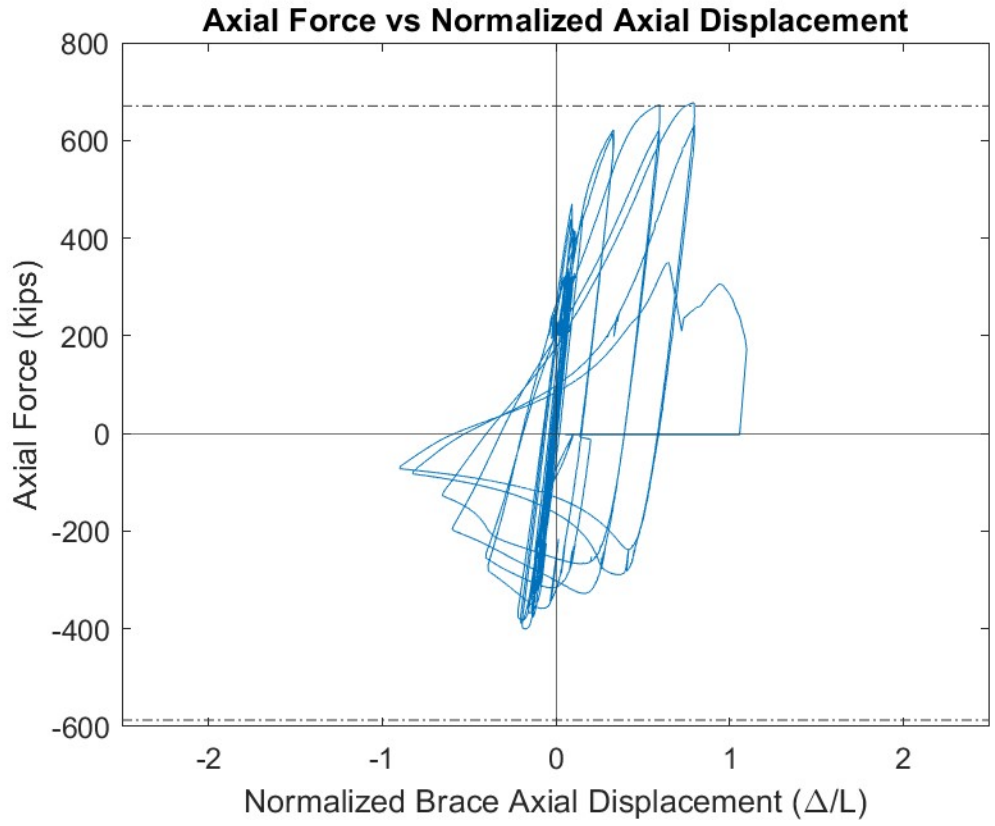

Photos

Peak Out of Plane Displacement: 2.08” Cycles

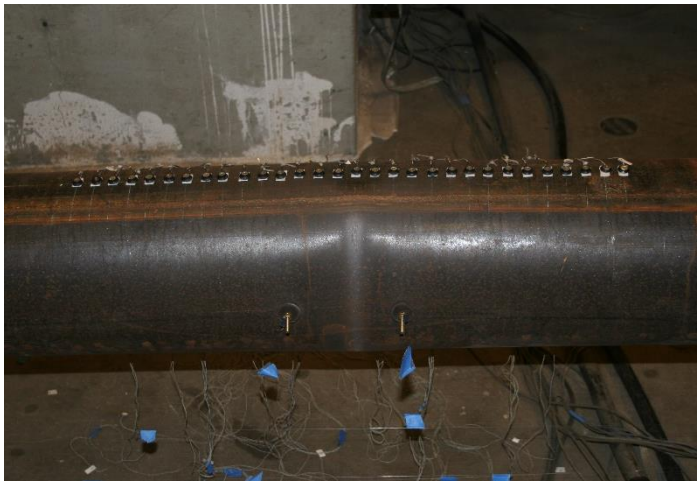

Striations: T2 2.08” cycle

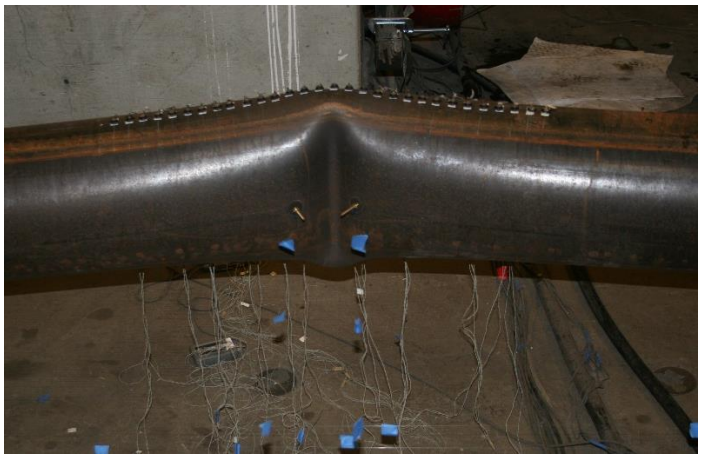

Major Cupping: 2.08” C2 cycle

Brace Fracture: 2.54” T1 cycle